Inelastic Structural Response and FRP Retrofitting of Reinforced Concrete Core Walls

Hamid Arabzadeh

A Thesis
In the Department
of
Building, Civil and Environmental Engineering

Presented in Partial Fulfillment of the Requirements
For the Degree of
Doctor of Philosophy (Civil Engineering) at
Concordia University
Montréal, Québec, Canada

August 2018

CONCORDIA UNIVERSITY

School of Graduate Studies

This is to certify that the thesis prepared

By: Hamid Arabzadeh

Entitled: Inelastic Structural Response and FRP Retrofitting of Reinforced Concrete Core Walls

and submitted in partial fulfillment of the requirements for the degree of

Doctor of Philosophy (Civil Engineering)

complies with the regulations of the university and meets the accepted standards with respect to originality and quality.

Signed by the final examining committee:

______________________ Chair
Dr. Abdel R. Sebak

______________________ External Examiner
Dr. Dan Palermo

______________________ External to Program
Dr. Mehdi Hojjati

______________________ Examiner
Dr. Ashutosh Bagchi

______________________ Examiner
Dr. Lucia Tirca

______________________ Thesis supervisor
Dr. Khaled Galal

Approved by ______________________
Dr. Fariborz Haghighat, Graduate Program Director

____
Thursday 2018-09-13
Dr. Amir Asif, Dean
Faculty of Engineering and Computer Science

ABSTRACT

Inelastic Structural Response and FRP Retrofitting of Reinforced Concrete Core Walls

Hamid Arabzadeh, Ph.D.
Concordia University, 2018

The use of C-shaped reinforced concrete (RC) core walls as the main lateral force resisting system for building structures is a popular choice for medium- to high-rise buildings. These cores are typically closed on three sides (C-shaped) and are either open or partially open on the fourth side. Despite the frequent use of C-shaped RC core walls as the primary seismic force resisting system (SFRS) for multi-story buildings, there are still challenges in estimating their inelastic seismic response, whether they are separate or coupled C-shaped walls. The eccentricity between the centre of mass and the centre of rigidity tends to induce a significant torsional seismic demand on such walls. To address this issue, several design codes have proposed recommendations for evaluating the effect of this eccentricity. Although National Building Code of Canada (NBCC, 2015) specifies provisions to consider the accidental eccentricity and the torsional sensitivity of the structure in the design, there is a gap in the knowledge of the inelastic structural response of C-shaped RC core walls for new buildings. On the other hand, many existing RC C-shaped walls are in need for retrofitting in order to meet current seismic design codes, or to meet increased demands due to change in the use and occupancy of the building, or to retrofit post-earthquake damages. In recent years, application of fibre-reinforced polymer (FRP) composites in retrofitting of RC walls has considerably increased due to its advantages such as high strength to weight ratio and its fast and easy installation.

The objectives of this thesis are to: (i) investigate, numerically, the effectiveness of FRP retrofitting on the seismic performance of RC shear wall systems, (ii) evaluate the deficiency of

seismic design provisions of C-shaped shear wall structures with high torsional sensitivity, (iii) examine, experimentally, the seismic response of FRP-retrofitted C-shaped RC walls to quantify the efficiency of the FRP retrofitting in repairing the RC core walls.

To achieve the first objective, a simplified modelling approach was proposed for analyzing the FRP retrofitted RC walls in order to be used as a simple and efficient method in practice. Nonlinear Incremental Dynamic Analysis (IDA) of a typical twelve story RC building structure, following the FEMA P695 methodology, showed that although the increase of torsional sensitivity has no significant effect on the inter-story drift ratios of the building, it could significantly decrease the Collapse Margin Ratio (CMR).

To achieve the second objective, building structures with different levels of height and torsional sensitivity were studied. Results showed that although response spectrum analysis (RSA) provides consistent predictions for story shear demand in regular buildings, significant underestimation of design forces might be obtained for buildings with a torsional sensitivity of $B \geq 2.0$. Dual Plastic Hinge (DPH) method was found to be an efficient alternative in reducing the story shear demand in structures with high torsional sensitivity, compared to structures designed based on the common Single Plastic Hinge (SPH) method.

To achieve the third objective, a previously tested large-scale C-shaped RC wall was retrofitted using carbon fibre-reinforced polymer (CFRP) composite sheets and was tested under the same condition and loading protocol of the original wall to quantify the efficacy of FRP retrofitting on the wall’s response. Furthermore, multi-directional cyclic tests were conducted in order to evaluate the complete nonlinear response of the FRP retrofitted C-shaped wall up to failure. The assessment was based on experimental measurements and observations in terms of 3D displacements, strains (both from strain gauges and Digital Image Correlation, DIC, system), crack pattern, ductility, curvature profiles and mode of failures. The test showed that the FRP retrofitting scheme used in the current work performed very well by enhancing both the strength and ductility of the retrofitted wall from its damaged state, while holding its stiffness very close, compared to those of the control wall.

Acknowledgements

First and foremost, I would like to thank my supervisor, Professor Khaled Galal for his support, help, and guidance throughout this research study. His continuous encouragement has given me the confidence to focus and proceed. Also, I greatly appreciate our collaborators at École Polytechnique de Montréal, Professor Najib Bouaanani and Mr. Youness Mechmachi, for their collaborations throughout the experimental part of the thesis.

Also, I would like to acknowledge and appreciate the structure laboratory staff at École Polytechnique de Montréal (Martine Leclerc, Patrice Bélanger, Romain Siguier, and Benoît Marleau) for their assistance and technical support during my experimental work.

I will be failing in my duty if I do not mention special thanks to my friends Ali Rezaiefar, Farzad Rouhani, Omer Yagob, Mohammed Albotainy, Nader Ali, Shadman Hosseinzadeh, Ahmed Ashour, Khalid Alotaibi, Layane Hamzeh, and Mohammad Amin Ahadipour for their help, endless support and valuable hints throughout this research study.

I would like to acknowledge the financial support from the Natural Science and Engineering Research Council of Canada (NSERC) as well as the financial support from le Fonds de Recherche du Québec–Nature et Technologies (FRQNT) in the form of a team grant with École Polytechnique de Montréal, and scholarships from the Centre d'études interuniversitaire des structures sous charges extrêmes (CEISCE).

Finally, I would like to thank my main pillars in my life, my parents, without whom, I would not be definitely achieving this success. It is also a rare blessing to have a wife as supportive as Atefeh Nakisa whose love, encouragement, continuous motivation, advises, support, and patience have inspired me to complete this academic journey. Also, I would like to acknowledge my brothers for their invaluable supporting over the past four years throughout my study.

Dedication

To my lovely wife; Atefeh Nakisa,

To my beloved parents,

& To my son; Ryan

Co-Authorship

This thesis has been prepared in accordance with the regulations for a sandwich thesis format. This research presents experimental, numerical, and empirical work carried out solely by Hamid Arabzadeh. Advice and guidance provided for the whole thesis by the academic supervisor Professor Khaled Galal. This thesis consists of the following chapters:

- Chapter 3

  Arabzadeh, H., Goguen, K., Pelletier, K., Bouaanani, N., Galal, K., Léger, P. (2017). "Evaluation of Finite and Fiber Elements RC Models for Nonlinear Cyclic Analysis of U-Shaped Shear Wall", 16th World Conference on Earthquake, Santiago, Chile.

  Arabzadeh, H., and Galal, K. (2015). "Effectiveness of FRP Wraps for Retrofitting of Existing RC Shear Walls", 11th Canadian Conference on Earthquake Engineering, Victoria, BC, Canada.

- Chapter 4

  Arabzadeh, H., and Galal, K. (2017). "Seismic Collapse Risk Assessment and FRP Retrofitting of RC Coupled C-Shaped Core Walls using the FEMA P695 Methodology", ASCE Journal of Structural Engineering, 143(9): 04017096, 1–20.

- Chapter 5

  Arabzadeh, H., and Galal, K. (2018). "Seismic Response Analysis of RC C-Shaped Core Walls Subjected to Combined Flexure, Shear and Torsion," ASCE Journal of Structural Engineering, 144(10): 04018165, 1-17.

- Chapter 6

  Arabzadeh, H., Mechmachi, Y., Galal, K., Bouaanani, N. (2018). "Hybrid Testing of Large Scale FRP Retrofitted C-shaped Walls Subjected to Bi-Directional Ground Motions" to be submitted.

  Arabzadeh, H., Mechmachi, Y., Galal, K., Bouaanani, N. (2018). "Multi-Directional Cyclic Testing of FRP Retrofitted C-shaped Walls" to be submitted.

Table of Contents

List of Figures

List of Tables

CHAPTER 1

Introduction

1.1 Background and Problem Definition

Reinforced concrete (RC) shear walls are frequently selected as the lateral load resisting system for medium- and high-rise buildings. Shear wall resists lateral loads by its flexural and shear deformations. Based on the study by Paulay and Priestley (1992), walls with the height-to-length ratio (h_w/l_w) greater than 3.0 will have a flexural dominant behaviour, whereas RC shear walls with h_w/l_w less than 1.5, often referred to as squat walls, are mainly governed by shear behaviour. The Canadian Concrete Handbook (CSA A23.3, 2014) uses the h_w/l_w ratio of 2 as the delineation between the flexural and shear dominated response for RC wall. There is an increasing tendency on choosing RC shear walls as a Seismic Force Resisting System (SFRS) due to their capability of controlling the inter-story drift ratio. Hence, RC shear wall system was found advantageous in terms of reducing the damages to non-structural elements (Carrillo and Alcocer, 2012).

Most of the research studies on the structural response of RC shear wall systems focused on rectangular cross-section walls. Despite being widely used as an SFRS in buildings, the seismic response of non-planar wall systems, particularly C-shaped walls, did not receive proportionate attention from researchers. Most current design guidelines are developed based on the results of rectangular RC walls, and there are no specific prescriptions for design/analysis of C-shaped RC wall systems. Hence, it is essential to investigate the non-linear seismic behaviour of C-shaped RC walls.

Many existing concrete structures are in need for retrofitting because of different reasons, among which the two main reasons are the loss of required capacity due to ageing/deterioration or damages from the past earthquakes, and the need to withstand higher lateral loads. The latter is often because of continuous advancement of seismic design provisions. Fibre-reinforced polymer (FRP) composite materials are becoming popular in repair, strengthening, retrofitting and upgrading of reinforced concrete structures, while the investigations reported in the literature about their efficiency are limited. Hence, there is a need for more numerical and experimental studies in order to quantify the effectiveness of FRP retrofit systems in the enhancement of structural performance of RC walls. The experimental tests would contribute to calibration/validation of the numerical models.

1.2 Research Significance and Motivation

Klemencic et al. (2007) reported an increasing trend of construction of mid- and high-rise buildings in high seismic regions of Canada and worldwide. RC structural walls including C-shaped core walls are common structural systems in the design of these buildings, which need robust and reliable computational tools in practice. Developing numerical models for estimating the nonlinear response, lateral load, and displacement capacity, and failure mechanisms of RC C-shaped walls under earthquake loads was found by Lu (2014) to be of significant interest to both practising engineers and researchers.

An essential step of the seismic design of RC wall buildings is estimating the wall’s complete force-displacement response. However, the nonlinear behaviour of RC walls is often affected by flexure-shear interaction (FSI), which is associated with multi-axial stress states and coupling of nonlinearities of the wall’s constituent components, i.e. concrete and steel reinforcement. Flexure-shear interaction was found to be the most challenging part of the response in numerical simulation of RC wall buildings, and in some cases, it leads to the significant problem of inaccuracy for buildings with coupled wall system. Non-planar walls such as the common RC core walls around the elevator shaft are often subjected to significant FSI, because of which a considerable effect on the nonlinear response of the wall is expected. This is due to the non-uniform response of wall segments when the three-dimensional (3D) deformations occur in a non-planar wall.

Moreover, load-displacement response estimation is challenging when a cyclic multi-axial loading representative of earthquake excitations is applied. A series of experimental tests by Oesterle et al. (1976) have shown that the load history can notably affect the lateral load-deformation response in terms of capacity and strength degradation. These findings were recently supported by Lu (2014) where it was shown that the influence of loading history is especially important in analysis of non-planar walls, during which the stress-strain state in a section of the non-planar wall can change significantly depending on the angle and direction of load application. In seismic analysis of buildings with RC wall systems, this can result in significant underestimation/overestimation of lateral load and deformation capacity.

Another critical step of the design of RC walls is identifying the most likely failure mode and estimating the wall's cyclic strength and deformation capacity accordingly. Moreover, identifying different failure modes of RC wall systems is essential for retrofitting purposes. Hence, considering the limited studies conducted on C-shaped core walls, it is important to investigate their failure modes during the seismic excitations.

Nonlinear deformations in cantilever walls occur preferably in flexure in regions defined as plastic hinges, which are generally selected to develop at the base of the walls. Significant inelastic deformation and large shear forces at the maximum considered earthquake (MCE) level were observed in recent studies by Calugaru (2013) and Calugaru and Panagiotou (2014), by assessing RC walls in high-rise buildings. This increases the damage potential of RC walls, especially the failure of walls under eccentric loads (e.g. torsionally sensitive buildings) which cannot be captured by using simplified beam-column elements available in common numerical tools such as ETABS, SAP2000 and SeismoStruct. This has been barely investigated in the literature.

As previously mentioned, some of the existing RC wall structures (C-shaped core walls included) need retrofitting during their lifespan. Among different retrofitting techniques, FRP retrofitting has proven to be an efficient alternative for seismic retrofitting of RC wall structures. There is, however, no study on retrofitting of C-shaped RC walls reported in the literature, which necessitates investigating the efficiency of FRP retrofitting solutions for enhancing the seismic response of these types of walls.

In summary, an accurate modelling approach capable is required in order to investigate the three-dimensional inelastic structural response of reinforced concrete core wall buildings. Moreover, due to non-uniform response of C-shaped RC wall segments compared to that of planar walls, both intact and FRP retrofitted C-shaped RC walls need to be further investigated, especially under eccentric loading conditions. The aim of the current study is to address the aforementioned research significances by using both numerical analyses as well as by conducting experimental tests.

1.3 Objectives and Scope of Work

The objectives of this thesis are to: (i) investigate, numerically, the effectiveness of FRP retrofitting on the seismic performance of RC shear wall systems, (ii) evaluate the deficiency of seismic design provisions of C-shaped shear wall structures with high torsional sensitivity, (iii) examine, experimentally, the seismic response of FRP-retrofitted C-shaped RC walls to quantify the efficiency of the FRP retrofitting in repairing the RC core walls. In order to achieve the objectives of this research, the scope of research is as follows:

- Developing and validating a precise modelling approach to reliably predict the nonlinear response of FRP retrofitted RC walls
- Evaluating different FRP retrofitting schemes for enhancing the performance of coupled C-shaped RC walls
- Conducting incremental dynamic analysis (IDA) and seismic assessment of FRP retrofitted RC walls using the proposed method by FEMA P695 (2009)
- Evaluating the seismic response of C-shaped RC wall systems with different torsional sensitivity subjected to combined loading

- Hybrid testing of FRP-retrofitted C-shaped RC core wall system subjected to bi-directional earthquake ground motions
- Cyclic testing of FRP-retrofitted C-shaped RC core wall under multi-directional loading protocol

1.4 Thesis Layout

The thesis is divided into seven chapters as followings:

- Chapter 1 consists of introduction; research significance and motivation; objectives and scope of work; including a brief literature review.
- Chapter 2 includes the literature review including the failure modes of RC shear walls, different retrofit techniques used for RC walls, and the numerical micro and macro models proposed for the simulation of the seismic behaviour of RC walls.
- Chapter 3 consists of numerical investigation of the effectiveness of FRP wraps for retrofitting of existing RC shear walls. First, finite and fibre element RC models for nonlinear cyclic analysis of C-shaped shear wall are evaluated. Results of different modelling approaches are compared to highlight advantages/disadvantages of each method. Then, investigation on the effectiveness of FRP wraps for retrofitting of existing RC shear walls are performed using finite element analysis.
- Chapter 4 investigates the "Seismic Collapse Risk Assessment and FRP Retrofitting of RC Coupled C-Shaped Core Walls using the FEMA P695 Methodology". The proposed numerical macro-model of the RC core walls is described in this chapter.
- Chapter 5 consists of "Seismic Response Analysis of RC C-Shaped Core Walls Subjected to Combined Flexure, Shear and Torsion". Evaluation of seismic force demand in different levels of torsional sensitivity and effectiveness of using the dual plastic hinge method in controlling the seismic shear force demand of RC C-Shaped core walls are described in this chapter.

- Chapter 6 describes the details of the experimental tests and the results including the test setup, wall specimen design and construction, and the FRP-rehabilitation scheme used. A comparison of the results of the FRP retrofitted wall and the original wall is presented to show the efficiency of the FRP retrofitting method in enhancing the structural response of the C-shaped RC wall.
- Chapter 7 includes the summary of the research project, the main contributions and conclusions, and the recommendations for future work.

CHAPTER 2

Literature Review

2.1 Background

Shear walls is a common seismic force resisting system (SFRS) in many RC office/residential buildings in North America that use flat plate / flat slab system for gravity loads. They are also used in industrial buildings and nuclear power plant facilities. The behaviour of RC walls is a complex phenomenon, especially when considering the cyclic and dynamic nature of lateral loads that they resist. Several factors affect the seismic behaviour and ductility of an RC shear wall, particularly its shear span-to-depth ratio and its shear capacity in relation to the wall's flexural capacity. Although the term "shear wall" implies that response is shear-dominated, the desired response is ductile flexural behaviour, with shear controlled by capacity design measures.

Rectangular RC structural walls provide high in-plane stiffness for the structural system, which helps to decrease the structural damage by limiting the drift during seismic events. Many researchers (e.g. Paulay, 1988; and Fintel, 1995) have reported the efficient earthquake performance of shear wall building structures in the literature. Observations from post-earthquake investigations such as in Chile 1985 (Wyllie et al., 1986) showed that the shear wall structures constructed in Chile performed extremely well, with little to no apparent damage in the majority of buildings. Reinforced concrete shear walls have the advantage of withstanding severe earthquakes while minimizing the damage to non-structural elements, compared to frame-type structures that undergo large drift because of their lower stiffness. Conversely, some other investigations by Kim (2004) on the past earthquakes showed that RC walls governed by shear failure have performed poorly due to probable brittle-type failures with low ductility. Fig. 2.1 shows sample failures of RC shear walls in the past earthquakes.

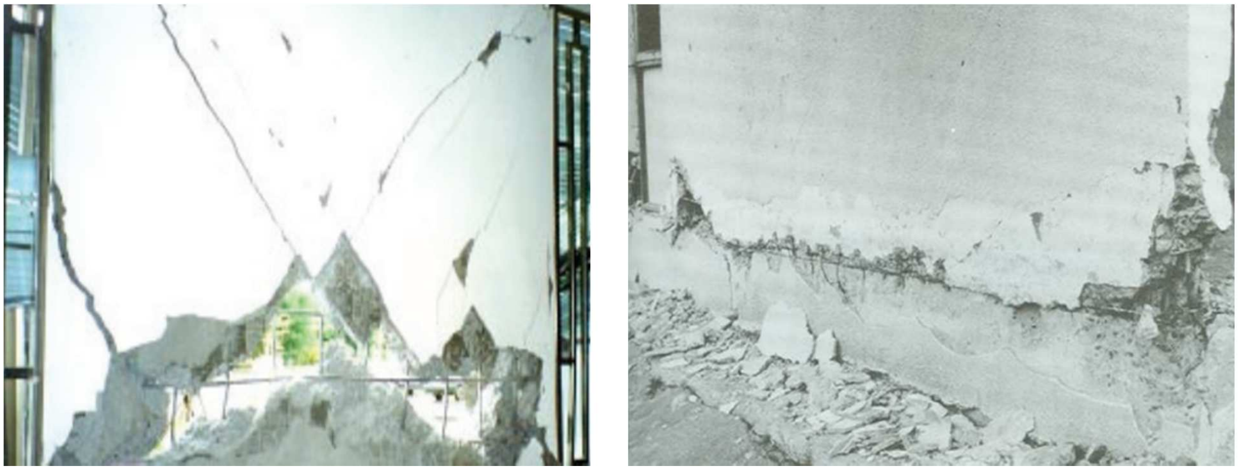
(a) **(b)**

Fig. 2.1. Failure of RC shear walls in: a) Taiwan earthquake 1999 (Yin, 2000), b) Chilean earthquake of 1985 (Wyllie et al., 1986)

In terms of structural behaviour, RC shear walls are typically designed to respond in an elastic manner for insignificant excitations, be it from the wind or small frequent earthquakes. RC shear walls are preferred to be designed in the way that ensures flexural failure mechanism and precludes all brittle mechanisms during larger less frequent earthquakes while resisting lateral loads. According to Paulay and Priestly (1992), RC shear walls also perform better in terms of dissipating the seismic energy imparted by the earthquake if designed to be ductile.

Design of ductile RC shear wall systems should ensure a desirable ductility in the wall's lateral response, mainly provided when the structure's response is dominated by inelastic flexural yielding. This is crucial to minimize the loss of strength in buildings. In other words, structures must be capable of sustaining a high proportion of their initial strength under large deformations that may be beyond elastic deformations. Ductility is a characterizing property of structures subjected to reversed cyclic loads. Priestly et al. (2007) characterized the ductility as the ability of the structure to sustain large inelastic deformations and dissipate the input energy by its hysteretic behaviour.

Increasing ductility can be by limiting strength degradations associated with large deformations, which highly corresponds to the mechanical properties of materials used in the structural element and their detailing. Therefore, precautions have to be considered to ensure that the materials that are supplied are of the correct quality specification. Moreover, carefully detailed plastic hinge zones should be considered, where other non-ductile failure modes have to be inhibited (e.g. diagonal tension or compression failure, sliding failure, and bond failure of reinforcement in lap splices).

Canadian design code CSA A23.3 (2014) states that reinforced concrete shear walls shall be designed to respond with various ductility levels by ensuring that, for all ductility levels, the failure mode at ultimate limit state is dominated by flexure failure; due to yielding of the flexural steel reinforcement, prior to shear failure. This structure is expected to undergo reversed cyclic inelastic deformations without significant loss of strength and is detailed to develop the appropriate level of ductility while remaining structurally stable.

2.2 Common Failure Modes of RC Shear Walls

Paulay and Priestley (1992) categorized the common failure modes of a cantilever RC shear wall system subjected to lateral loads (Fig. 2.2.a) into two categories as the followings:

i. Flexure-dominated failure modes

   This group of failures includes axial-flexural concrete crushing, longitudinal steel bar fracture, longitudinal steel bar buckling and longitudinal steel bar pull-out (Fig. 2.2.b). A combination of these failure modes may also happen at a certain load/displacement (Fig. 2.2.e).

ii. Shear-dominated failure modes

   Failure modes dominated by shear are quite common in squat shear walls, which have the height to length ratio (h_w/l_w) less than 1.5. Diagonal-tension failure (Fig. 2.2.c), diagonal-compression failure, and sliding shear failure (Fig. 2.2.d) are included in this category.

The principal source of energy dissipation in a laterally loaded cantilever wall must be the yielding of the flexural reinforcement in the plastic hinge regions. In an RC wall with undesirable shear dominated response, the major drawback is the steady reduction of strength and ability to energy dissipation capability of the RC wall.

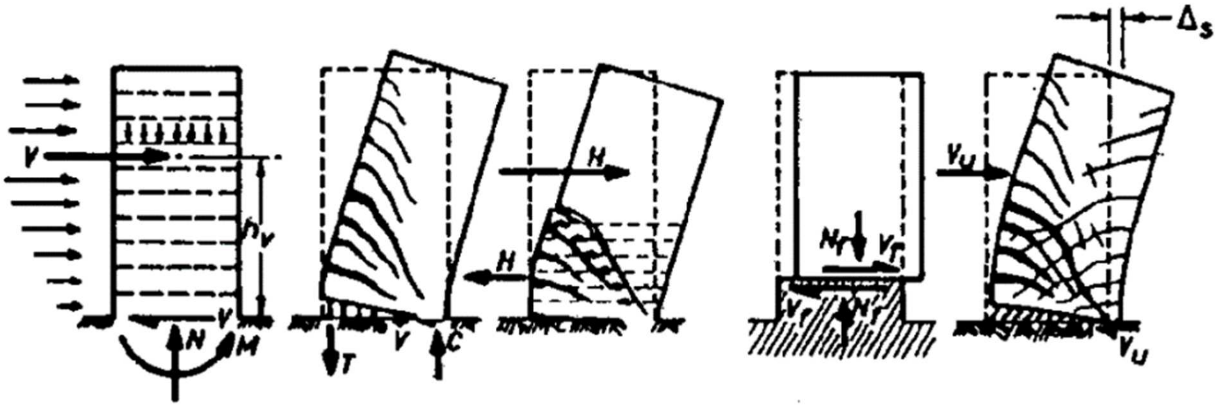

(a) (b) (c) (d) (e)

Fig. 2.2. Common modes of failure in an RC shear wall (Paulay and Priestley, 1992)

2.3 Response Assessment of RC Shear Walls

In order to study the behaviour of shear walls and its failure modes, a review of effective parameters on shear wall behaviour is discussed. Typically, the seismic performance of an RC shear wall can be evaluated experimentally through assessing its hysteretic lateral force-displacement relationships. Many experimental studies have been conducted in the recent decades to investigate the lateral behaviour of RC shear walls (examples shown in Fig. 2.3). Although experimental testing is seen to be the most evident approach to assess the performance of a shear wall, numerical simulation was found to be a valuable tool for parametric studies and collapse assessments of RC shear wall systems in multi-story buildings.

Regarding numerical simulations, investigation of the inelastic response of RC wall systems involves using a reliable modelling approach that is capable of coupling important interactions and response parameters (e.g., nonlinear flexural-shear behaviour, confinement effects, and sliding of cracked surfaces). The layout and parameters of the numerical model require substantial technical expertise, especially when the entire building has to be modelled and analyzed, and not just the structural wall. A variety of software tools are available that conduct non-linear macro- and micro-modelling and analysis of reinforced concrete structural elements.

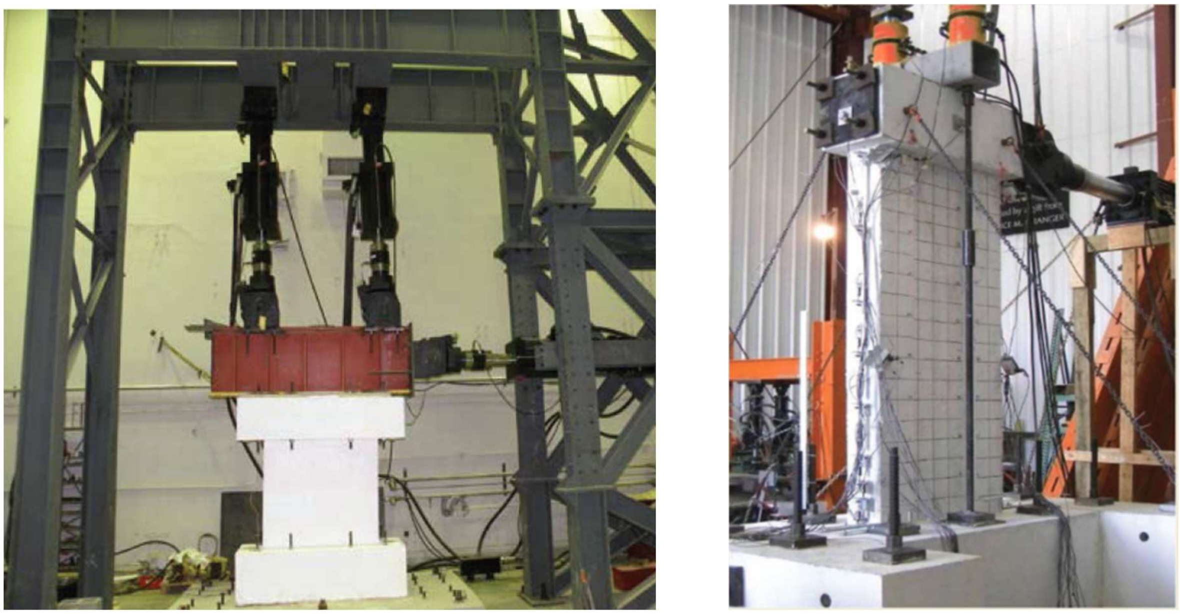

(a) **(b)**

Fig. 2.3. Examples of experimental studies on the lateral response of RC shear walls: a) El-Sokkary and Galal (2013), b) Burgueño et al. (2014)

Detailed solid finite elements (FE) models (i.e. ANSYS, ABAQUS) using built-in constitutive models are able to capture the local stress-strain responses, quantify low cycle fatigue, steel reinforcement bond slip in addition to the global force-displacement responses. These programs require the definition of several material parameters according to the constitutive model and failure envelope used (i.e. smeared vs. discrete steel reinforcement, concrete confinement). Additional parameters to drive the nonlinear solution algorithms to convergence are also of major importance. FE models are also often used to calibrate the nonlinear stiffness and strength properties of macro models (e.g. fibre element models developed by OpenSEES and SeismoStruct) that could be used in a computationally effective way to assess the global nonlinear response of complete building structures (i.e. formation of plastic hinges). The predictions of both FE and fibre element models need to be compared to experimental data to validate their performance for both ductile (flexural) and brittle (shear) failure mechanisms.

The main objective of many recent studies was to develop and validate micro/macro models for reinforced concrete walls subjected to cyclic reversals. Some also developed simplified models that can be used by engineering practitioners. Modelling approaches addressing the required elements and corresponding material constitutive models were explained in detail, and the process for calibration of parameters was highlighted in some cases. As for simulation of RC shear walls, the numerical models have to be able to efficiently track the flexure-shear interactions of the walls. An overview of the common macro models for numerical simulation of RC shear walls is presented in Fig. 2.4.

Comparison of the results from the analysis of the walls subjected to both monotonic and reversed cyclic loading protocols with the corresponding test data assessed the efficiency and limitations of various proposed modelling approaches. Results showed that some models are able to take into the account both stiffness and strength degradations. Moreover, the proposed models are often able to capture the strain histories of the concrete and reinforcement with an acceptable level of accuracy.

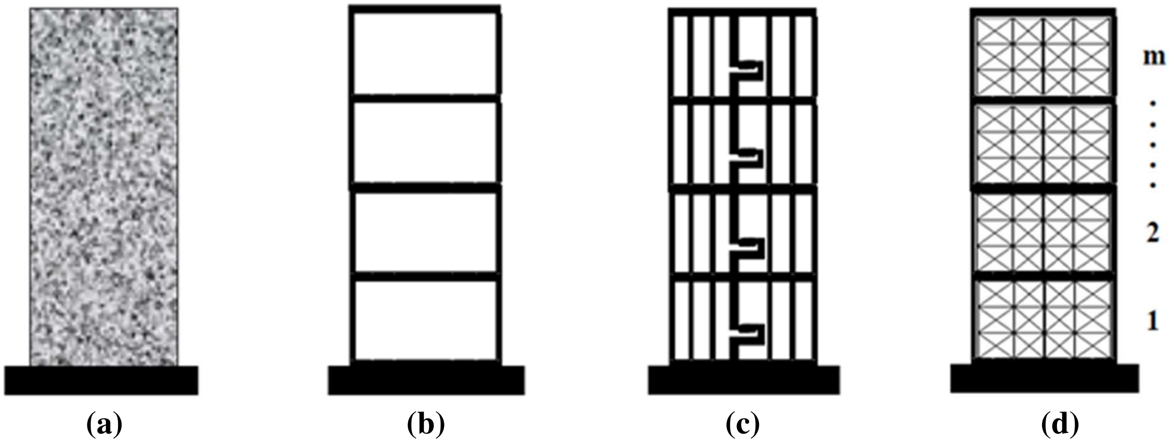

Fig. 2.4. Overview of available macro modelling approaches: a) A typical RC shear wall, b) Wide column model (Millard, 1993), c) Multiple vertical line element model (Vulcano et al., 1988), and d) Truss model (Panagiotou and Restrepo, 2011)

2.4 Structural Response of Non-Planar C-Shaped RC Shear Walls

Despite the frequent use of C-shaped reinforced concrete (RC) cores as the primary force resisting system of multi-story buildings, there are still challenges in estimating their inelastic seismic response, especially when they are used as coupled wall system.

Several researchers have conducted both experimental and analytical investigations to identify the behaviour of coupled rectangular walls and to improve the performance of this system. The C-shaped coupled wall system (i.e. core wall) is one of the simplest and is a popular arrangement used in practice. Despite their popularity, however, there have been relatively few studies on the seismic behaviour of C-shaped RC structures such as the experimental tests by Beyer et al. (2008-a), necessitating research on the seismic performance of C-shaped cores. One of the most important characteristics of these non-planar wall systems is their response when the structure is subjected to torsional efforts due to the eccentricity of lateral forces. Torsional effects become more significant when there is large eccentricity between the centre of mass and centre of rigidity. This type of building configuration is prone to have large torsional response during a severe earthquake. Hart (1975) and Esteva (1987) reported the structural damages due to torsional effects in the past earthquake events. Dizhur et al. (2011) reported more recent observations of damage, which was most likely caused by a "torsionally sensitive response", after the Christchurch earthquake in 2011.

Most of the research studies carried out in the past (Colotti, 1993; Zhang and Xu, 2009; Beyer et al., 2011; Panagiotou and Restrepo, 2011; Fischinger et al., 2012) focused on the behaviour of planar RC walls, and various approaches have been proposed to capture the observed coupling between nonlinear flexural and shear behaviour of walls. These approaches were mostly based on fibre-section elements such as multiple-vertical-line-elements (MVLE) proposed by Vulcano et al. (1988). The biaxial behaviour of concrete material (e.g. modified compression field theory; Vecchio and Collins, 1986) was also considered in some of these approaches.

On the contrary, very little experimental research has been carried out on the performance of non-planar (e.g. C-shaped) RC walls subjected to lateral loads. In one of the first attempts, Ile and Reynouard (2005) examined three full-scale U-shaped RC walls subjected to uniaxial and biaxial cyclic lateral loading. The tests aimed at studying the behaviour of U-shaped walls in uniaxial and biaxial bending and shear, and compared the alternative design requirements of two versions of EC8. Beyer et al. (2008-a) performed bi-directional quasi-static cyclic testing of two

U-shaped walls with different thickness, built at half-scale and designed for high ductility. The tests were performed at the structural engineering laboratories of the ETH Zurich. The tests mainly focused on the flexural behaviour of walls, considering different directions of loading (two orthogonal as well as diagonal). Results showed that the most critical direction was the diagonal one, in which the maximum attained moment was less than what plastic hinge analysis would predict. Moreover, the displacement capacity of the wall in diagonal direction was found to be smaller than the other two orthogonal directions.

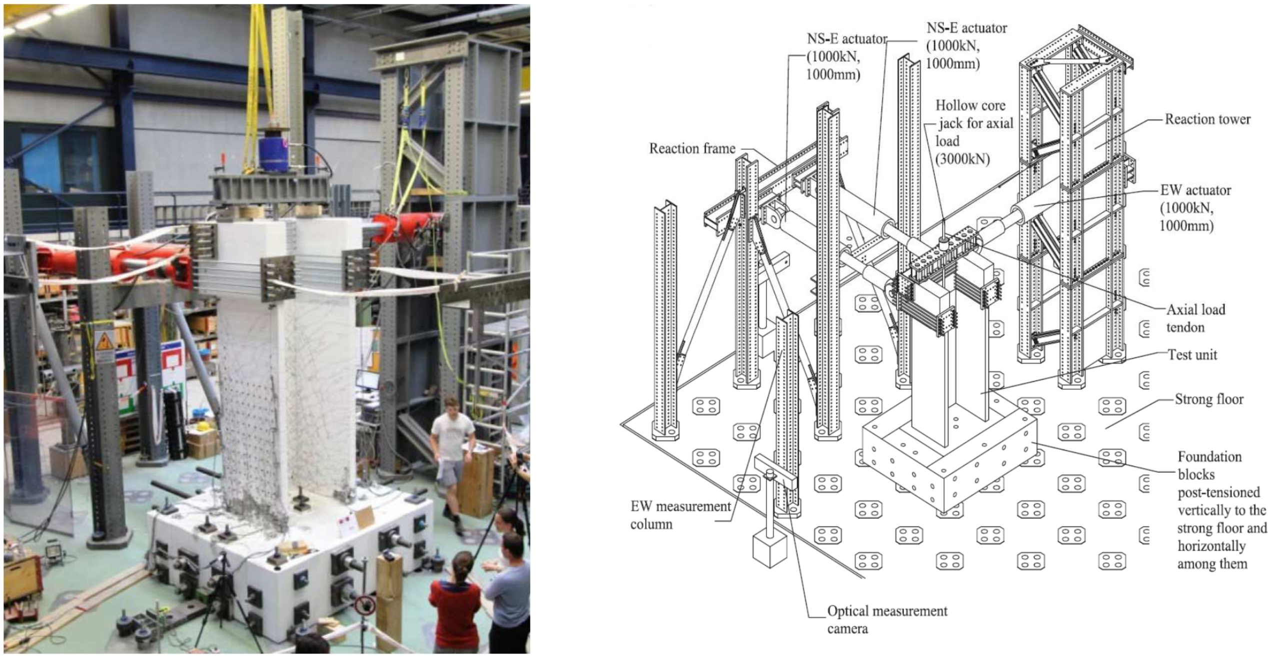

(a) (b)

Fig. 2.5. Experimental tests on C-shaped RC walls (Beyer et al., 2008)

A simplified numerical model was also developed by Beyer et al. (2008-b) including practical recommendations for setting up wide-column models of U-shaped walls subjected to large inelastic deformations (Fig. 2.6). The approach has been shown to produce a reasonable estimation of the ratio between shear and flexural deformations for slender walls. Constantin and Beyer (2012) used a 3D multilayered shell element model for U-shaped walls to capture their local as well as the global behaviour under diagonal loading. The model was developed using the software VecTor4 developed by Wong and Vecchio (2003) at University of Toronto, and was

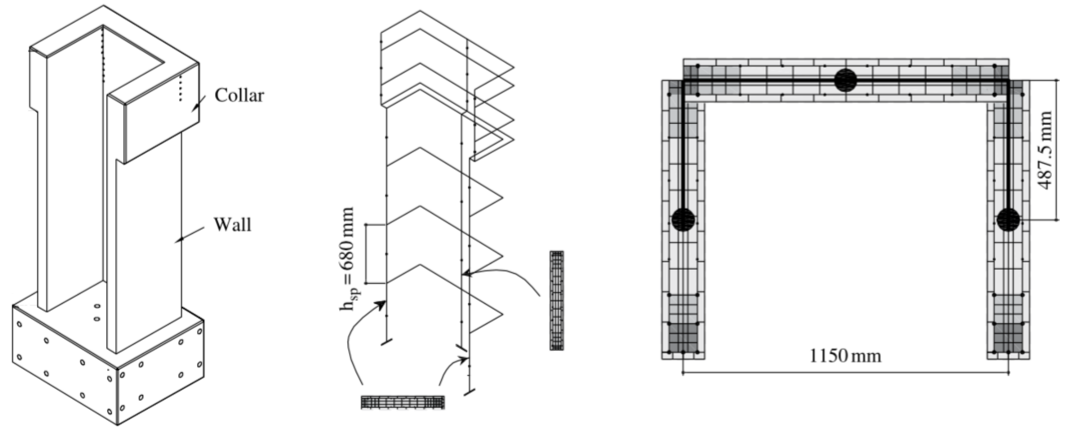

(a) **(b)** **(c)**

Fig. 2.6. Simplified wide column model proposed by Beyer et al. (2008-b)

found to be accurate in terms of loading capacity of the wall, but not for its displacement ductility.

Lowes et al. (2013) examined three 1/3 scale C-shaped wall specimens, representing a part of a coupled RC core system, under biaxial loading protocols (Fig. 2.7). Results of cyclic tests showed that bidirectional loading significantly affected the response for displacement cycles in excess of the yield displacement. At these displacement levels, bidirectional loading resulted in a significant reduction in the stiffness of the wall in the direction parallel to the web of the wall (loading activating strong-axis bending).

Recently, Lu and Panagiotou (2013) presented a three-dimensional (3D) cyclic model for non-planar RC walls, based on beam-truss analogy. The model was able to predict the effects of flexure-shear interaction, considering the biaxial behaviour of concrete, and account for mesh-size effects. Although the proposed model has been revised several times and was validated for three reinforced concrete T-shaped, C-shaped, and I-shaped section wall configurations, a study by Kolozvari (2013) showed that the modelling approach is complicated in terms of calibration of truss members and material properties. The results were also sensitive for achieving accurate displacement responses over a broad range of response amplitudes.

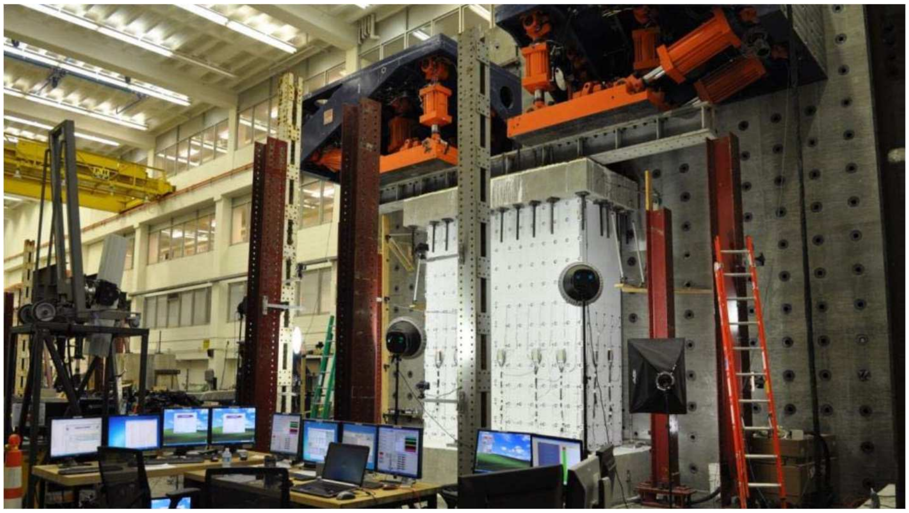

Fig. 2.7. Experimental tests on C-shaped RC walls (Lowes et al., 2013)

2.5 Design Provisions for RC Shear Walls

In the design of RC shear walls, the fundamental design equations are mainly based on the assumption that plane sections remain plane, where shear lag effects associated with flexure and warping torsion are not captured. These effects may be significant in non-planar (C-, I- or T-shaped) wall configurations, and might affect the response of the structural system in seismic excitations. A study by Boivin and Paultre (2010) assessing the seismic performance of multi-story ductile RC shear walls designed according to the 2005 NBCC and the CSA Standard A23.3-04 found that the wall's shear demand can be largely underestimated, especially at the wall base. The issue would result from a deficiency of the current capacity design methods in accounting for the higher mode amplification effects. Based on the investigations by Adebar et al. (2014), in the evaluation of the story force demands, contributions of the higher modes in the seismic response of the structure should be taken into account.

In the seismic design of a multi-story ductile RC wall, this can produce design strength envelopes that largely underestimate the seismic force demand. Hence, more studies need to be conducted on the seismic performance of C-shaped RC shear wall systems and the effectiveness of available retrofitting methods, both of which were investigated in the current study. A recent research by Pelletier and Léger (2017) showed that the dynamic shear amplification factor introduced in recent CSA A23.3-14 allows a more realistic seismic shear force demand to be obtained for RC shear walls. This factor should be applied to prevent brittle shear failure and to account for the inelastic effects of higher modes.

Planar and non-planar RC shear walls represent the typical seismic force resisting systems (SFRSs) associated with RC building structure. These walls should be located in the plan of the building in the way that creates no excessive torsional flexibility of the structure. Fig. 2.8 shows the 3D view of a numerical model developed by Penneton et al. (2006) for analyzing an eight-story RC wall building with unsymmetric plan located in Montreal, Canada. According to the National Building Code of Canada (NBCC, 2015), buildings can be considered torsionally sensitive when the largest ratio of the maximum displacement to the average of the displacements at the extreme points of the structure, among all the stories, exceeds 1.7. According to the NBCC 2015, for torsionally sensitive building structures, design forces resulted from the static analysis are not valid, and a dynamic analysis is required. Buildings with unsymmetric distribution of the elements of the lateral load resisting system, such as the building structure presented in Fig. 2.8 are more prone to higher torsional sensitivity levels.

Moreover, although most ductile cantilever RC wall structures are designed to develop a single plastic hinge at the base of the wall, a dual plastic hinge method can be employed to design RC walls with a second plastic hinge in the mid-height of the wall. Based on the method developed by Panagiotou and Restrepo (2009), a study on the effect of the dual plastic hinge system on controlling the story forces in an RC wall structure is presented in Chapter 5 of the current work.

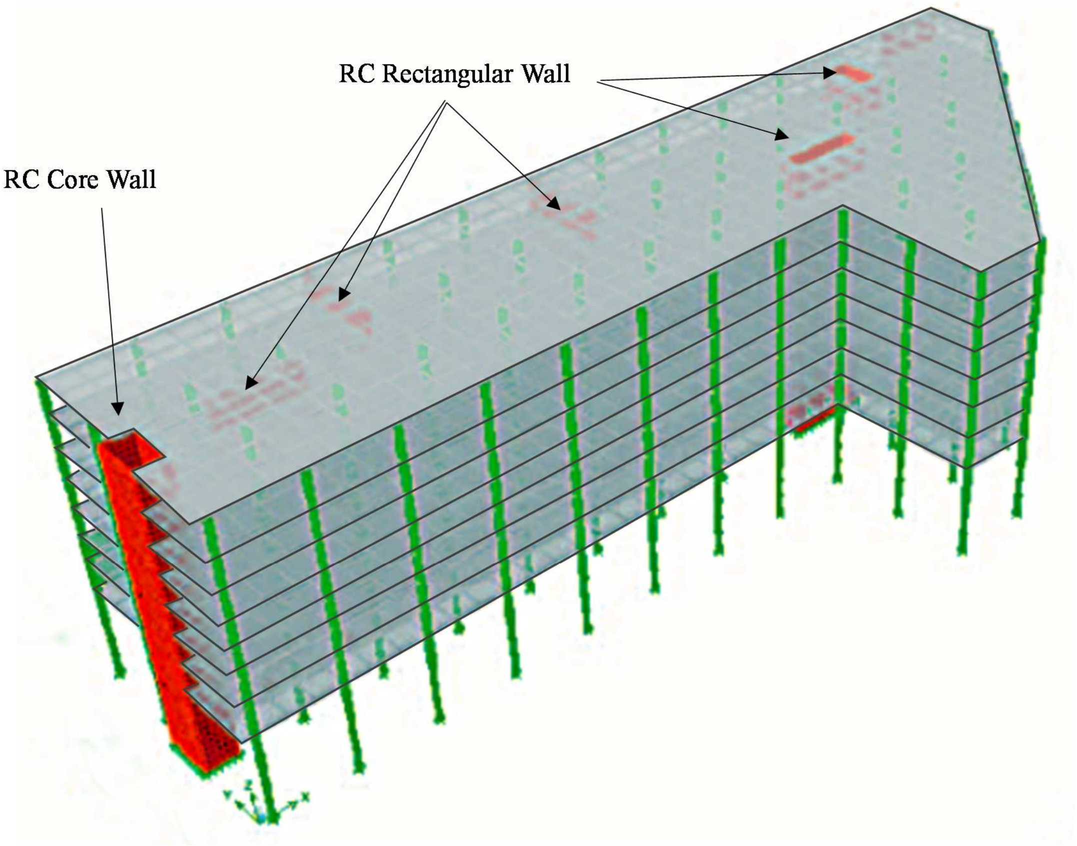

Fig. 2.8. Layout of the numerical model of an eight-story reinforced concrete building with an unsymmetric plan (Penneton et al., 2006)

2.6 Strengthening and Rehabilitation of RC Shear Wall Structures

Last decades witnessed the development of several retrofitting methods for deficient RC shear walls towards improving their seismic performance in terms of the overall strength, ductility, and energy dissipation capacities. Among these, fibre-reinforced polymer (FRP) composite materials have received increasing attention in the past few years as an effective material for retrofitting of existing RC structures.

FRP composite materials offer various forms of products for structural applications where high strength-to-weight and stiffness-to-weight ratios are required. According to a study by Meier (1987), the use of FRP composites for the rehabilitation of beams and slabs started in the 1980s with the pioneering research performed at the Swiss Federal Laboratories for Materials

Testing and Research, or EMPA. Afterwards, FRP materials have been widely used as a solution to enhance the ductility of beam members in RC structures. Because of the high cost of FRP materials in the past, most applications of these materials were for rehabilitation purposes and externally bonding of members in RC structures. However, due to the increase in using of FRP materials, the costs dropped significantly, which led to more applications in constructions and rehabilitation projects.

The use of externally bonded fibre-reinforced polymers (FRPs) has been receiving particular attention in the past decades due to the recognized advantages of low weight/strength ratio, relatively low invasiveness in terms of geometric modification of the existing structure, corrosion protection, and more simplified installation processes. Table 2.1 shows a summary of selected experimental studies on the FRP retrofitting of RC walls. FRP composites were used in different configurations and retrofitting schemes such as vertical strips, horizontal strips, horizontal wrapping and bi-axial FRP sheets.

Successful enhancements of the wall's structural response by using FRP composites were reported by the researchers in the literature. Compared to the results of the original RC walls (i.e. control specimens), improvements were observed in both the strength and ductility of the walls. As it can be seen in Table 2.1, RC walls with different aspect ratios have been tested and the extensive results highlight the efficiency of FRP composites in retrofitting of RC walls with different configurations. However, there has been no research work examining the efficiency of FRP retrofitting on the structural response of C-shaped RC walls. Hence, in the current work, a series of hybrid and cyclic tests were conducted to quantify the effect of FRP retrofitting in the enhancement of the seismic response of C-shaped RC walls.

Though FRP materials have gained much acceptance from both the research community and the industry as a retrofit method of RC structures and various research efforts reported in the literature in proposing different FRP-retrofitting methods for existing RC shear walls, there is still a need to thoroughly investigate the effect of major design parameters. These include the material properties, geometry, the arrangement of reinforcement bars and additional external reinforcement on the overall seismic performance of the system.

Table 2.1. Selected experimental works on the FRP retrofitting of RC walls

	Research study	**Wall aspect ratio**	**FRP retrofitting configuration**
1	Lombard et al. (2000)	1.33	Horizontal and vertical and FRP sheets on both cracked and intact specimens
2	Antoniades et al. (2003)	1	Vertical strips and FRP jacketing on heavily cracked walls as well as one intact specimen
3	Peterson and Mitchell (2003)	2.7 to 3.1	Horizontal FRP strips wrapped around the wall
4	Hiotakis et al. (2004)	1.33	Horizontal and vertical and FRP sheets on both cracked and intact specimens
5	Hwang et al. (2004)	0.43	Vertical only and a combination of horizontal and vertical FRP sheets
6	Ghobara and Khalil (2005)	1.1	Bi-axial FRP sheets on both sides and horizontal uni-axial FRP layers around boundary regions
7	Haroun et al. (2005)	1	Single/Dual layer FRP wraps as well as Horizontal FRP strips
8	Kobayashi (2005)	0.4	Using FRP bands for repair of cracked RC walls
9	Elnady (2008)	1.1	Bi-axial FRP sheets on both sides and horizontal uni-axial FRP layers around boundary regions
10	Li and Lim (2010)	1.125 and 1.75	FRP sheets on the surface and U-shaped wrapping of the boundary elements
11	El-Sokkary et al. (2012)	6.43	Vertical FRP strips at the boundary regions and horizontal FRP wrapping
12	El-Sokkary and Galal (2013)	0.87	Vertical FRP strips and horizontal FRP wrapping as well as X-FRP bracing
13	Nguyen et al. (2014)	0.67 and 2.5	Vertical and horizontal FRP strips
14	Luccio et al. (2017)	2.5	Vertical and horizontal FRP strips
15	Woods et al. (2017)	1.2	Horizontal and vertical and FRP sheets on both sides
16	Todut et al. (2017)	0.66 with opening	Vertical and horizontal FRP strips, as well as short strips at the corners

Chapter 3 of the current work includes a parametric study on the effectiveness of using FRP wraps for retrofitting of rectangular RC walls. The efficacy of FRP retrofitting method in enhancing the seismic response of RC shear walls was recently proved by some researchers, both numerically and experimentally. Experimental tests conducted by El-Sokkary and Galal (2013) showed improvement in lateral load resistance of retrofitted walls, both in terms of strength and ductility (Fig. 2.9). Moreover, experimental tests by El-Sokkary et al. (2012) showed that the FRP rehabilitation could lead to notable improvement in the seismic response of multi-story walls (Fig. 2.10).

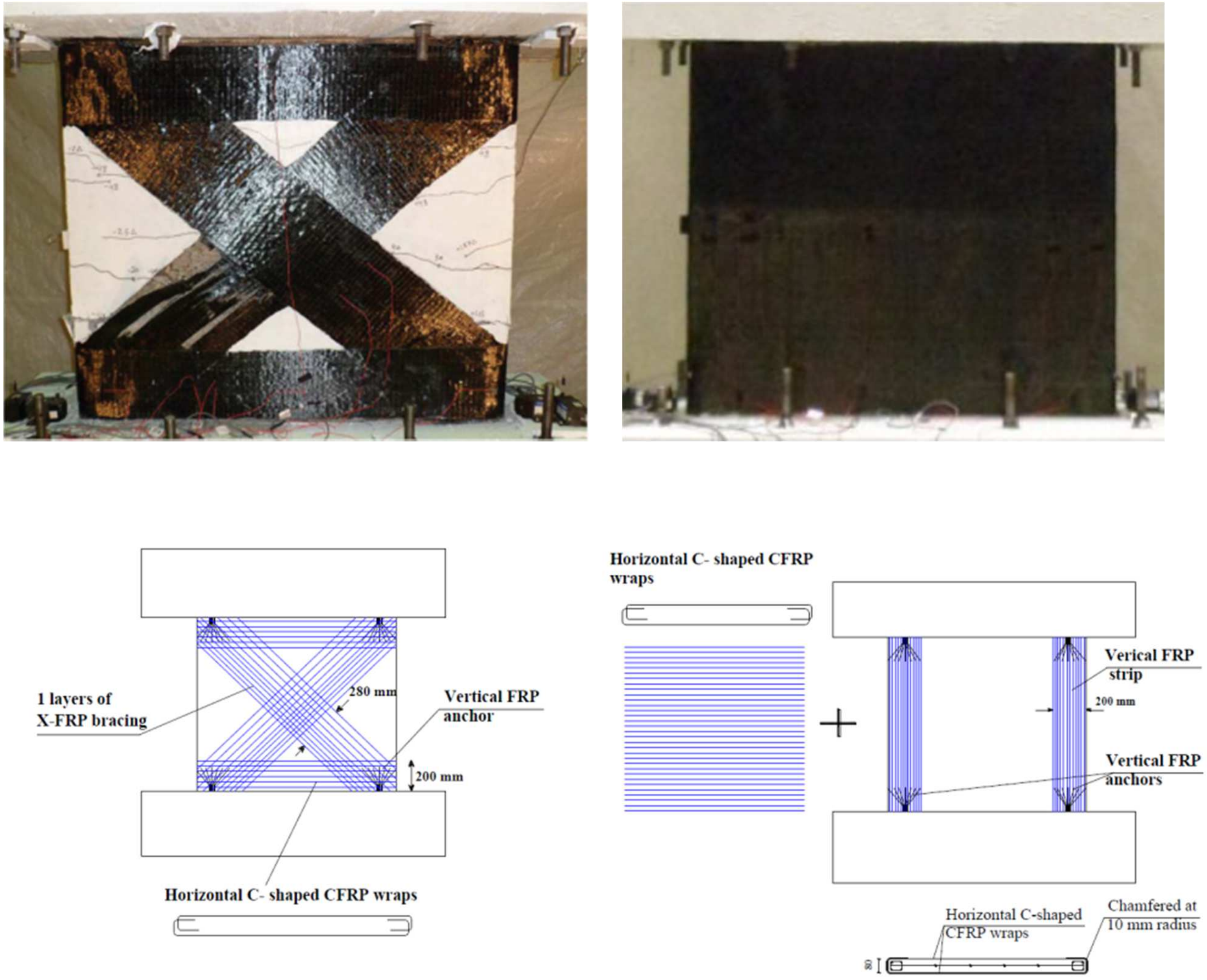

(a) **(b)**

Fig. 2.9. Experimental tests on FRP strengthened RC shear walls (El-Sokkary and Galal, 2013)

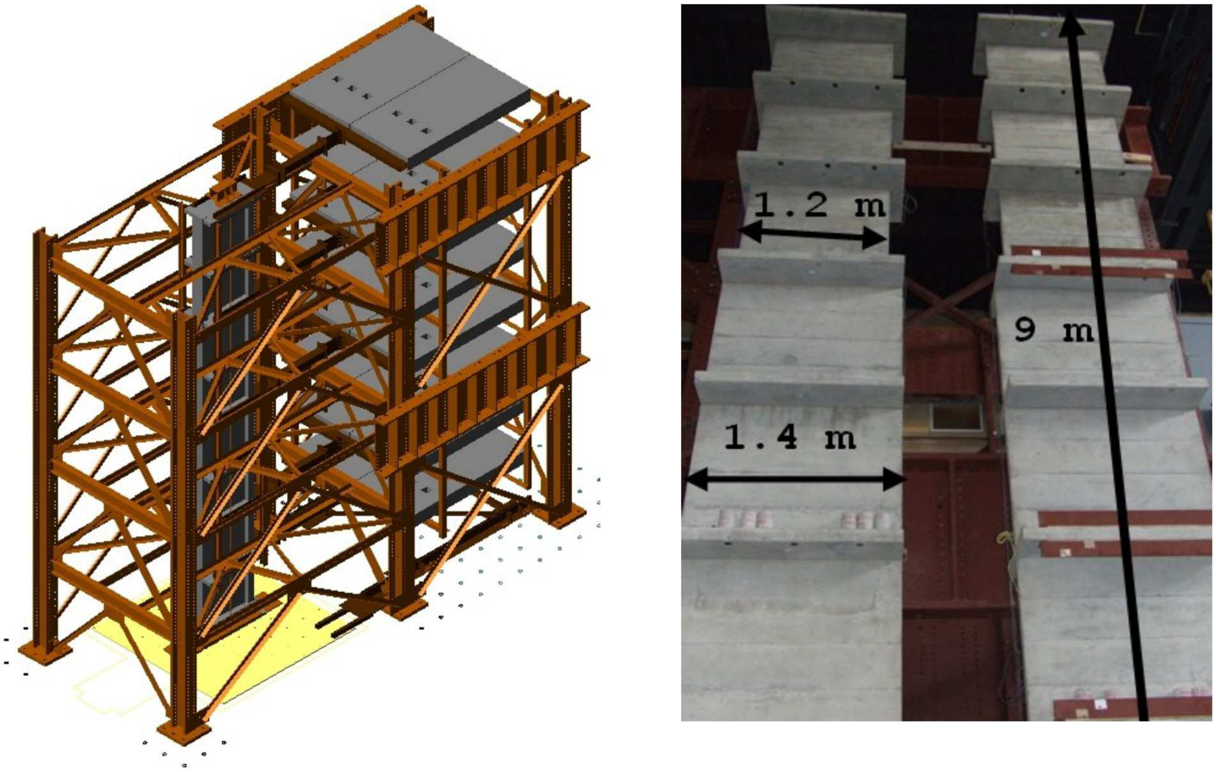

(a) **(b)**

Fig. 2.10. Details of the test assembly on the shake table of École Polytechnique de Montreal and the rehabilitated 8-story walls tested in El-Sokkary et al. (2012)

Alternatively, some researchers developed numerical models to investigate the effectiveness of FRP retrofitting on the structural response of RC walls. Different modeling approaches were proposed by the researchers using macro- and micro- modeling techniques, examples of which are shown in the Figures 2.11 and 2.12. Table 2.2 shows a summary of selected numerical works on the FRP retrofitting of RC wall. As it can be seen from Table 2.2, numerical investigations on the FRP retrofitting of RC walls included rectangular walls only and, to best of authors' knowledge, FRP retrofitting of non-planar walls (e.g. C-shaped walls) has never been studied by other researchers.

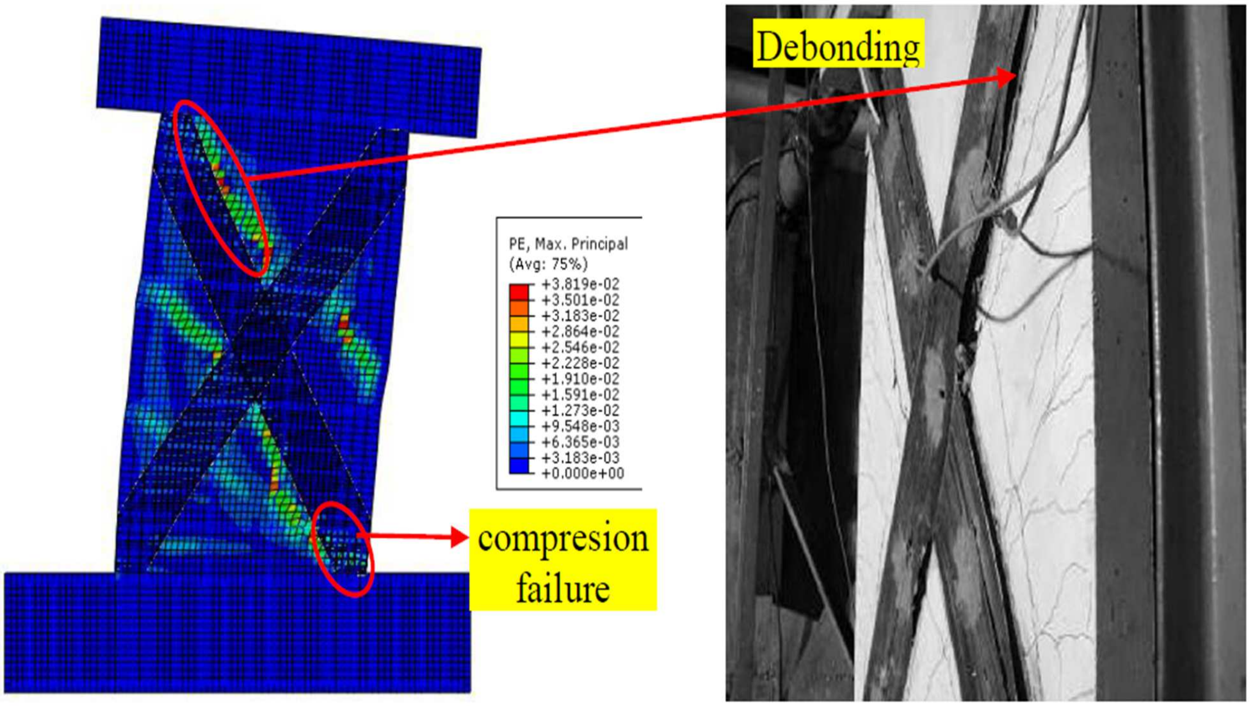

Fig. 2.11. Finite element model developed by El-khoriby et al. (2016)

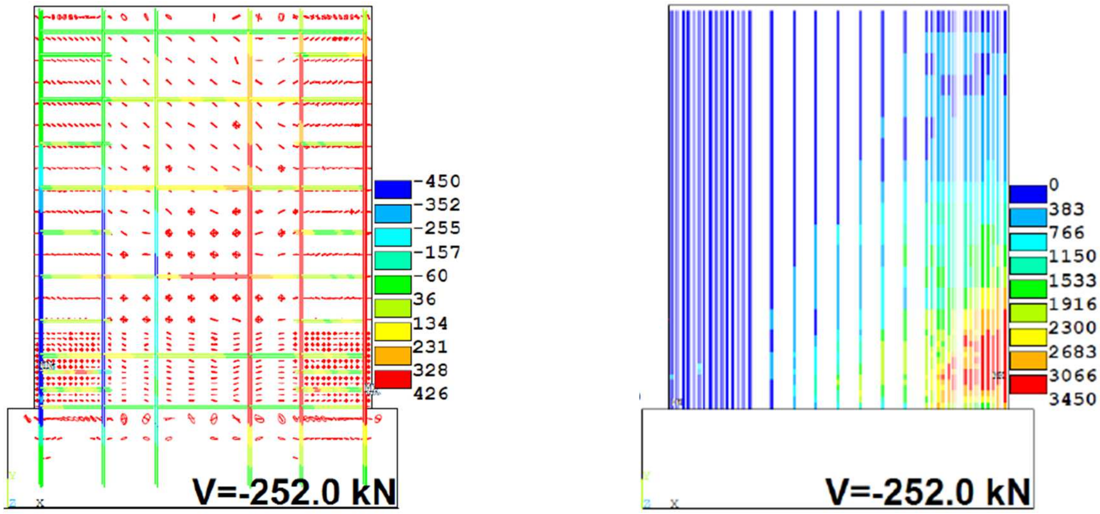

(a) (b)

Fig. 2.12. Finite element model developed by Rezaiefar (2013): a) stress distribution in the steel reinforcement, b) stress distribution in the FRP strips

Table 2.2. Selected numerical works on the FRP retrofitting of RC walls

	Research study	Wall aspect ratio	Numerical model
1	Elnady (2008)	1.1	Macro modeling of FRP retrofitted rectangular RC walls using IDARC and OpenSEES
2	Cortés-Puentes & Palermo (2011)	1.2 and 2	Micro modeling of FRP retrofitted rectangular RC walls using Vector2
3	Cortés-Puentes & Palermo (2011)	2.4	Micro modeling of FRP retrofitted rectangular RC walls using Vector2
4	Mostofinejad and Anaei (2012)	1.37 and 7.49	Micro modeling of FRP retrofitted rectangular RC walls using ABAQUS
5	Rezaiefar (2013)	1 and 1.73	Micro modeling of FRP retrofitted rectangular RC walls using ANSYS
6	Nguyen et al. (2014)	0.67 and 2.5	Micro modeling of FRP retrofitted rectangular RC walls by developing 3D cracking models for concrete
7	Saher et al. (2016)	1.5	Micro modeling of rectangular RC walls retrofitted with FRP X-bracing using ABAQUS
8	Risan et al. (2017)	1	Micro modeling of FRP retrofitted rectangular RC walls with opening using ABAQUS
9	Behfarnia and Shirneshana (2017)	1	Micro modeling of FRP retrofitted rectangular RC walls with opening using ABAQUS
10	Aslani and Kohnehpooshi (2018)	1.27	Micro modeling of FRP retrofitted rectangular RC walls with opening using ABAQUS

In the current work, considering the different FRP retrofitting schemes proposed by El-Sokkary and Galal (2013), seismic collapse risk assessment of RC coupled C-shaped core walls retrofitted with different FRP retrofitting schemes was conducted and the results are presented in Chapter 4 of the current work. The methodology proposed by FEMA P695 was employed for the seismic collapse risk assessment using 44 ground motion records. Moreover, experimental tests were conducted on a C-shaped RC wall retrofitted with FRP composites. Results of the experimental tests are presented in Chapter 6.

2.7 Summary

RC shear walls are best known as efficient lateral resisting systems in buildings because of their high stiffness and their high flexural and shear capacities. Many studies have been carried out to investigate the structural response of RC wall systems with different geometries. However, since the majority of the tests were conducted on planar (rectangular) RC walls, investigation of the nonlinear response of non-planar RC walls is still necessary. Moreover, continuous advancements in seismic design codes and regulations and the ageing and deterioration of existing RC structures are two major reasons for the necessity of seismic strengthening and retrofitting of shear wall structures. In this respect, different retrofitting methods have been proposed, but reliable means of estimating the behaviour of RC shear walls are required to choose the most effective retrofit method. Therefore numerical and experimental studies need to be conducted to propose the required design equations and the most efficient strengthening scheme. FRP retrofitted C-shaped RC walls have never been tested by other researchers in the literature. In Chapter 6 of the current work, hybrid time-history, characterization and cyclic tests are conducted on a C-shaped FRP retrofitted RC wall.

CHAPTER 3

Numerical Investigation on Effectiveness of FRP Wraps for Retrofitting of Existing RC Shear Walls

3.1 Evaluation of Finite and Fiber Elements RC Models for Nonlinear Cyclic Analysis of C-Shaped Shear Wall

3.1.1 Abstract

Reinforced concrete (RC) shear wall buildings are a very common type of construction worldwide. Nonlinear dynamic analyses of this type of structural systems are used more and more by the engineering profession in the context of performance-based design or safety assessment of existing buildings designed using older codes/standards. Researchers are also working to improve advanced RC cyclic constitutive models especially under three dimensional (3D) excitations involving axial, moment, shear and torsional interactions. Several computer programs are available to perform nonlinear seismic analysis of reinforced concrete structures. Detailed solid finite elements (FE) models (i.e. ANSYS, ABAQUS) using built-in constitutive models are able to capture the local stress-strain responses, quantify low cycle fatigue, steel reinforcement bond slip in addition to the global force-displacement responses. These programs require the definition of several material parameters according to the constitutive model and failure envelope used (i.e. smeared vs discrete steel reinforcement, concrete confinement). Additional parameters to drive the nonlinear solution algorithms to convergence are also of major importance. FE models are also often used to calibrate the nonlinear stiffness and strength properties of fibre elements (i.e. OpenSees, SeismoStruct) that could be used in a computationally effective way to assess the global nonlinear response of a complete building structure (i.e. formation of plastic hinges). The predictions of both FE and fibre elements models

need to be compared to experimental data to validate their performance for both ductile (flexural) and brittle (shear) failure mechanisms.

This section describes the developments of FE (ANSYS, ABAQUS) and fibre element (OpenSees, SeismoStruct, SAP2000) models of C-shaped shear walls (2.72m high, 1.30m x 1.05m footprint and 100 mm thick) tested by other researchers under axial and reversed cyclic bi-directional flexural loading. Guidelines are provided for a proper definition of the FE and fibre elements modelling parameters using five different computer programs to satisfactorily reproduce the given experimental results, up to a drift percentage of 2.5%. The capabilities of the different models to predict failure mechanisms are also investigated. The advantages and limitations of the different computational tools are discussed. The results of this study are very useful for researchers and practitioners working in the field of seismic safety evaluation of RC shear wall buildings using predictive computational tools.

3.1.2 Introduction

In a Reinforced Concrete (RC) building, the seismic-force-resisting system is often concentrated in relatively few walls that are distributed around floors, or within non-planar RC wall systems, to provide desirable shear resistance and limit lateral deformations of the building to acceptable levels. Coupled RC U-shaped walls (hereinafter referred to as core walls) can efficiently resist the majority of seismic lateral forces and improve the design flexibility of RC buildings. Substantial lateral strength and stiffness, in addition to deformation capacity, to meet the demands of strong seismic excitations, make core walls a desired option for seismic force-resisting system of RC buildings. In general, structural walls are designed to prevent collapse and loss of life under severe earthquakes. The reason for adopting such a strategy is that it is extremely expensive to design structures to respond elastically under such severe events, which may not occur during their expected life; therefore, inelastic wall deformations are expected.

The seismic behaviour of shear walls in buildings can be affected by many variables such as shear span ratio, interacting nonlinear axial-shear-flexural behaviour, boundary elements, and the interaction with other structural members. Since structural walls are the primary, and in some cases the only, seismic-force resisting elements, robust analytical tools for nonlinear analysis of multi-story buildings are essential for reliable seismic performance design or assessment. These tools must include models capable of estimating the global seismic demands of the building and capturing the hysteretic behaviour of structural walls. Moreover, multi-storey core walls are sensitive to 3D seismic effects, thus requiring modelling tools that can account for these phenomena while providing results with an acceptable accuracy and within a reasonable computational time (Sedgh et al., 2015).

A large number of computer programs have been developed for nonlinear modelling and analysis of building structures. These tools are becoming more and more popular in engineering offices thanks to the growing performance of material constitutive laws and efficiency of numerical formulations. Different modelling approaches can be used, ranging from macro-scale models such as concentrated inelasticity, multi-axial spring models, truss models and combined models, up to micro-models such as finite element (FE) models and fibre models.

Although RC micro modelling using solid FE models (e.g. ANSYS, ABAQUS) can generally provide more detailed and precise results, the relevant expertise required to build such models and to ensure analysis convergence and good quality of the results is still rather highly specialized. In addition, micro modelling is practically inapplicable to large building systems. The need for implementing several material parameters required by selected constitutive laws and/or failure envelopes can be another limitation imposed by built-in material laws in many of the tools available for nonlinear analyses of RC buildings. Understanding of these limitations is crucial for critical assessment of the results of numerical calculations, especially for the cyclic response of the structure.

Macro modelling is more convenient and generally easier than micro modelling and also has rather less calculation process. However, the efficiency of both FE and fibre element models needs to be validated against the experimental data to ensure their reliability for predicting both the global and local behaviour of RC shear walls. Clough et al. (1965) proposed the first nonlinear macro model for numerical modelling of RC elements. Afterward, the first application of the finite element method of analysis in RC elements was proposed Ngo and Scordelis (1967). Since then several advancements were done in the area of modelling of RC elements including shear walls.

In comparison with planar walls, very little experimental research has been carried out on the performance of C-shaped RC walls subjected to lateral loads. In one of the first attempts, Ile and Reynouard (2005) examined three full-scale U-shaped RC walls subjected to uniaxial and biaxial cyclic lateral loading. The tests aimed at studying the behaviour of U-shaped wall in uniaxial and biaxial bending and shear, and compared the alternative design requirements of two versions of EC8. Beyer et al. (2008-a) performed bi-directional quasi-static cyclic testing of two U-shaped walls with different thickness, built at half-scale and designed for high ductility. The tests mainly focused on the flexural behaviour of walls, considering different directions of loading (two orthogonal as well as diagonal). Results showed that the most critical direction was the diagonal one, in which the maximum attained moment was less than what plastic hinge analysis would predict. Moreover, the displacement capacity of the wall in the diagonal direction is smaller than the other two orthogonal directions.

In this study, numerical models of an RC core wall are developed using different micro and macro modelling approaches, including fibre element-based concentrated and distributed inelasticity models, as well as finite elements. Different computer programs implementing these approaches are used to model a C-shaped shear wall tested by Constantin and Beyer (2016) under axial and reversed cyclic bi-directional flexural loading. The predictions of the numerical models are compared to available experimental data to highlight the advantages and disadvantages of each modelling approach.

3.1.3 Review of numerical approaches for seismic safety assessment of RC shear walls

3.1.3.1 Concentrated and distributed inelasticity models

Concentrated inelasticity models, i.e. lumped plastic hinges, are among the simplest and earliest nonlinear formulations for building seismic analyses (Clough et al., 1965). They assume that most significant inelastic deformations occur at the critical zones, such as the ends of beam-column members, while the other parts of the structure remain elastic. Plastic hinges can be accounted for through discrete- or fibre-based formulations (Scott and Fenves, 2006). The fibre-based approach, generally considered as more accurate, is used herein. It consists of using fibre elements which are beams composed of multiple fibres discretized within a certain number of integration sections located along the whole length of a structural member. When applied in a concentrated inelasticity model, this approach directly takes account of the geometry of the structure and material properties. The length of the plastic hinge and its position should be determined prior to analysis (Bae and Bayrak, 2008). Fibre-based formulations can be split into: displacement-based (DB) or force-based (FB) techniques (Neuenhofer and Filippou, 1997). A DB-based simulation uses an interpolation of displacements or curvatures along each fibre element, which may fail to adequately represent highly nonlinear behaviour. DB solutions can be improved by increasing the mesh density but at the expense of higher computational cost. The FB approach is generally preferred as it uses interpolation functions that are chosen to correspond to the exact solution of the internal forces in the elements (Calabrese et al., 2010). It is then possible to represent a structural member using a single FB element without the need for refinement, except for the number of integration sections which can enhance convergence and solution quality. However, FB simulation assumes that plane sections remain plane, which prevents from appropriately accounting for the effects of shear deformations and flexure-shear interactions.

As opposed to concentrated inelasticity models, distributed inelasticity models do not localize inelastic deformations in critical zones, but rather account for their spreading along beam-column members (Soleimani et al., 1979). In this work, the distributed inelasticity approach is combined with the Wide Column Model (WCM) Analogy (Beyer et al., 2008-a) to simulate the nonlinear response of the core wall. As for lumped hinges, fibre-based elements are available either as DB or FB formulations. Due to the multiple segments of the WCM of the studied core wall, only DB elements are used to avoid localization effects, i.e. strong dependence of the obtained nonlinear response on finer mesh discretization and does not converge into one single solution (Calabrese et al., 2010). The same limitations of fibre elements discussed above apply to the WCM, i.e. fibre elements are infinitely rigid in shear and torsion as they account only for compression and flexure. To attenuate this limitation and partially account for the effect of horizontal steel rebars on the shear resistance of the core wall, springs with rigidities determined in a way to simulate shear deformations at these locations, can be assigned between the multiple members of the WCM.

3.1.3.2 Finite elements

In FE analysis of RC shear walls, both shell and solid elements can be used in combination with nonlinear material constitutive laws available in the numerical tool. The main benefits of shell elements are relatively accurate consideration of 3D stress states and internal forces, simplicity and low computational costs. In some cases, however, shell finite elements do not allow adequate consideration of steel rebars in RC structures. Modelling such structures using 3D-solid finite elements is more straightforward, and detailed models of the rebars can be developed regardless of the bar geometry and direction (e.g. longitudinal bars, hoops, and transverse bars in an RC wall). This can lead to more accurate account of local effects such as rebar buckling. However, the associated computational cost can be prohibitive for large-scale problems. Convergence of the analysis is always an issue that needs to be addressed appropriately in FE analysis of concrete members. Static and Dynamic/Implicit or Explicit analyses can be used depending on the software and type of loading applied (ANSYS, 2010; Hibbit, 2007). Implicit static and dynamic analyses sometimes suffer from the low rate of convergence because of contact or material complexities, resulting in a large number of iterations. This is one of the most drawbacks of these FE analyses, which usually happens in nonlinear analysis of RC members with large inelastic displacements corresponding to the concrete cracking (Hibbit, 2007).

3.1.4 RC constitutive models and used software

3.1.4.1 Software used for concentrated and distributed inelasticity models

Three software packages were used to build the concentrated and distributed inelasticity models: SeismoStruct (Seismosoft, 2014), SAP2000 (CSI, 2015) and OpenSees (Mazzoni et al., 2006). SeismoStruct is a fibre element-based software, allowing both DB or FB modelling approaches, as well as concentrated or distributed inelasticity modelling (Seismosoft, 2014). Gauss-Legendre and Gauss-Lobatto numerical integration quadrature rules are used for DB and FB elements, respectively. Four concrete and four steel constitutive laws are available, e.g. Trilinear constitutive law and Mander et al. (1988) for concrete, and bilinear and Menegotto-Pinto (1973) for steel rebars.

SAP2000 (CSI, 2015) is widely used for the design and analysis of any kind of structures, such as buildings and bridges. It is particularly suited for linear analyses, but can also account for geometric nonlinearity through P-delta effects and for material nonlinearity by using plastic hinges or nonlinear link elements (CSI, 2015). Gauss-Legendre numerical integration quadrature is used. Stress-strain curves can be defined as Simple and Park models for steel rebars, and Simple and Mander models for concrete material (CSI, 2015; Mander et al., 1988). Hysteresis types for nonlinear cyclic analysis are somewhat limited as only a select few are available in the software, including kinematic (CSI, 2015) for steel rebars and Takeda (Takeda et al., 1970) for concrete material.

OpenSees is an open source program for seismic response analysis of structural and geotechnical problems (Mazzoni et al., 2006). Both DB and FB formulations are available for fibre-based beam-column elements. The default numerical integration quadrature rules are Gauss-Legendre and Gauss-Lobatto for DB and FB elements, respectively. A wide range of uniaxial materials and section models are available for beam-columns, such as bilinear and

Giuffré-Menegotto-Pinto (1973) for steel rebars, and Kent-Scott-Park (Mazzoni et al., 2006) and Linear Tension Softening (Mazzoni et al., 2006) for concrete material.

3.1.4.2 Finite Elements

Finite element modelling is carried out herein using two software packages: ANSYS (2010) and ABAQUS (Hibbit, 2007). ANSYS offers a specific solid element for RC members, i.e. SOLID65, which is an eight-noded solid element capable of modelling cracking in tension and crushing in compression and it is well suited for the 3D modelling of solids with or without reinforcement materials (ANSYS, 2010). Cracking is supported at any surface along any direction by means of the angle between the normal of the crack surface to the global directions. Steel reinforcement can be considered as smeared throughout the concrete element or using discrete steel rebar elements bonded to the concrete elements. The material constitutive law provided in ANSYS for considering the cyclic response of the concrete medium include smeared cracking and crushing model to add a certain cracking and crushing limit under tensile and compressive stresses respectively. Also, shear transfer coefficients β_t and β_c are provided for crack openings and closures respectively, which represent the shear strength reduction factors for those subsequent loads which induce sliding (shear) across the crack face. These parameters can have significant effects on the cyclic response of RC members subjected to severe shear demands.

ABAQUS has a variety of elements that can be used to model concrete, including both continuum and structural elements. Three different constitutive laws for the concrete material including Brittle Cracking (BC), Smeared Cracking (SC) and Concrete Damage Plasticity (CDP) can be employed. The latter appears to be the most comprehensive model for RC structures, as it can represent all compressive crushing, tensile cracking and tension stiffening behaviours. Moreover, CDP is the only constitutive model that can be used in both Implicit and Explicit analysis. Though the SC constitutive model in ABAQUS uses the same theory as ANSYS does, there is no feature available in ABAQUS to consider the shear reduction because of crack opening/closing. As for the steel reinforcement, there is no smeared reinforcement option provided in the solid elements in ABAQUS. However, discretized reinforcement modelled using truss or beam elements can be effortlessly embedded into the concrete medium.

Although the ABAQUS/Explicit is the usual choice for a seismic analysis, it can be used for certain static or quasi-static problems. Typically, these are problems that would be solved with ABAQUS/Standard but may have difficulty converging, making them computationally expensive. ABAQUS/Explicit determines the solution without iterating by explicitly advancing the kinematic state from the previous increment (Hibbit, 2007), results in a more efficient analysis depending on the case. Substantial disk space and memory savings of ABAQUS/Explicit are other advantages which make it more practical. However, specific considerations such as smooth stepping and loading rate should be taken into account to achieve reasonable results using the Explicit solver.

3.1.5 Experimental data for comparisons of RC constitutive models

To evaluate the performance of RC models, validation of numerical predictions against the data from experimental tests by Constantin and Beyer (2016) are performed. For the sake of brevity, only an overview of these tests is provided herein, detailed information can be found in Constantin and Beyer (2016). The tests were carried to evaluate the lateral capacity of RC core walls subjected to bi-directional loading. One of the tested C-shaped RC core walls, denoted as TUC, is considered here for validation of the numerical approaches described above. Three actuators, two acting along the NS (flanges) direction, and one along the EW (web) direction, were attached to the collar at the top of the wall. Three types of steel rebars, i.e. D6, D8 and D12, having 6, 8 and 12 mm diameters, respectively, were used. To assess the effects of reinforcement distribution on the response, the vertical reinforcement of one flange was uniformly distributed, while it was concentrated in the boundary elements of the other flange. The core wall was subjected to an axial load kept constant during cyclic tests, and to various protocols of bidirectional loads applied through cycles corresponding to different drift ratios from 0.1% to 3.0%.

3.1.6 Hysteretic cyclic responses

The numerical strategies presented in the previous sections are applied next to evaluate the response of the core wall tested by Constantin and Beyer (2016). The results obtained are compared to their experimental findings to highlight the advantages and limitations of each modelling approach.

3.1.6.1 Predictions using concentrated inelasticity models

This section describes the concentrated inelasticity models developed using SeismoStruct and SAP2000. The core wall is modelled as a single beam element with a plastic hinge located at the base. The length of the plastic hinge is determined as proposed in the Canadian code CSA A23.3-14 (2014):

$$L_p = 0.5L_w + 0.1h \tag{1.1}$$

where L_w denotes the length of the wall in the studied direction and h the total height of the building in the studied direction, considered as the distance between the base of the wall and the location of the actuators in the present case. Eq. (1.1) yields plastic hinge lengths of 985 mm and 820 mm along the EW and NS directions, respectively, obtained using L_w = 1.3 m and h = 3.35 m in the EW direction, and L_w = 1.05 m and h = 2.95 m in the NS direction. For the sake of simplicity, a mean value of 900 mm is used as plastic hinge length. The collar is modelled using elastic elements that also serve to connect the actuators to the wall. Considering that only concentrated loads are applied to the core wall, internal forces are interpolated linearly in the FB elements.

Sensitivity analysis was performed to adjust the discretization level of the section in SeismoStruct. Moreover, in the current version of SeismoStruct, it is not possible to model steel rebars with different mechanical properties in a single section. To circumvent this limitation, the mechanical properties of the rebars are defined in proportion to the actual quantity of each rebar type in the section. The constitutive laws of Menegotto-Pinto (1973) and Mander et al. (1988) are used to model steel and concrete, respectively. For practical purposes, the NS actuators are merged into a single one. The cyclic displacements imposed by actuators are applied to the wall through a static time history analysis.

In SAP2000, each rebar is assigned its own mechanical properties, including a nonlinear stress-strain curve with kinematic hardening, including an elastic, a perfectly plastic (which has been removed in our case), an empirical strain hardening, and a softening region. Mander et al. (1988) and Park constitutive laws are used respectively for the concrete and the steel materials. The hysteresis behaviours used for the materials are Takeda et al. (1970) for concrete and kinematic for steel since they are the only ones available that are nonlinear. Confinement has been added manually to the section of the model. Cyclic displacements are applied as a Nonlinear Direct Integration History load case. No mass is assigned to the model and a small stiffness proportional damping is considered to enhance convergence. The Hilber-Hughes-Taylor method (1977) with the parameters $\gamma=0.5$, $\beta=0.25$ and $\alpha= -0.0005$ is used with time increments of 10 s.

Figure 3.1.a illustrates the concentrated inelasticity models built using SeismoStruct and SAP2000. The fibre discretization of the wall cross-section using SeismoStruct is presented in Fig. 3.1.b, as well as the directions used for the bidirectional cyclic loading protocol.

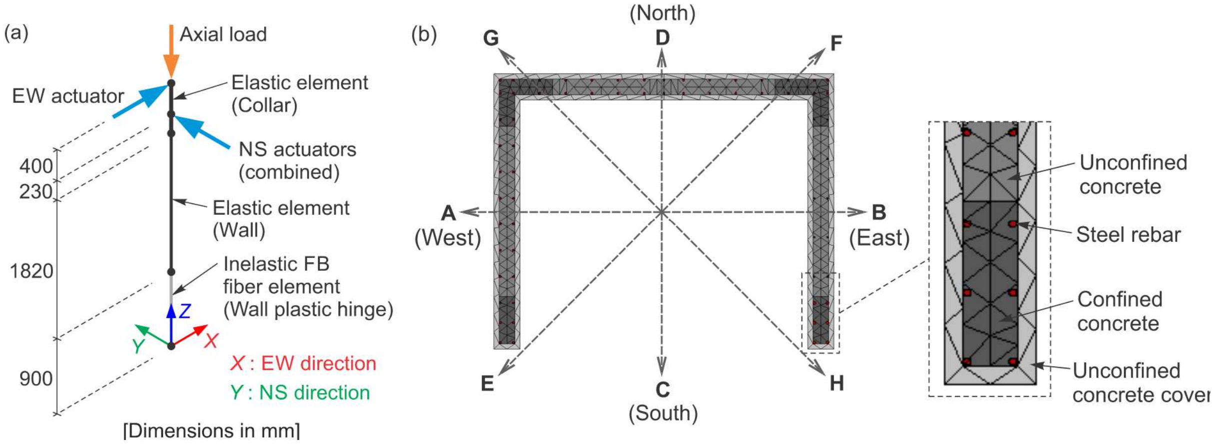

Fig. 3.1. Concentrated inelasticity model: (a) Model components in SeismoStruct and SAP2000; (b) Fiber discretization of the wall cross-section using SeismoStruct.

The hysteretic cyclic response of the core wall along E-F direction (Positions E and F) obtained using concentrated inelasticity models in SeismoStruct (Seismosoft, 2014) and SAP2000 (CSI, 2015) are illustrated in Fig. 3.2 along with experimental data from Constantin and Beyer (2016). A smoothing technique was applied to the SAP2000 results to reduce jagged effects on the graph data. The initial stiffness predicted by SeismoStruct is slightly higher than measured, which can be attributed to shear deformations not being fully accounted for in the model. This effect could be attenuated partially by using link elements assigned a stiffness corresponding to the shear stiffness of the wall along each direction. However, this would increase the computational effort and lessen the attractive feature of using a single FB element per structural member. This procedure is also limited depending on the plastic hinge length since the hinge can only be placed on a single member.

The model seems to reproduce the slight strength-hardening observed in experimental results. However, it does not account for 3D local behaviour along the wall cross-section, i.e. warping effects, which might contribute to the predicted overstrength of the wall, especially at position E along both principal directions. Two other reasons for the discrepancies between predictions and experimental results in. Fig. 3.2.a & b are: (i) that a single set of mean mechanical properties had to be used to represent the three different steel rebars, i.e. D6, D8 and D12, and (ii) that confinement zones had to be predefined as being equal for certain regions of the wall section which is not always the case in the actual wall. Moreover, the model was not able to accurately capture the failure mechanism of the tested C-shaped RC wall.

For the SAP2000 model, a similar behaviour to the SeismoStruct predictions is observed, but in a more amplified way; i.e. the initial stiffness is too high, and an increased overstrength is observed for both directions (Fig. 3.2.c & d) compared to the predictions of SeismoStruct and experimental data. Many of the same discrepancies are observed as in the SeismoStruct model, but in a more amplified way; i.e. the initial stiffness is too high, and an increased overstrength is observed for both directions (Fig. 3.2.c & d). Reasons such as material definitions, somehow limited in the program, and the use of the Section Designer module (along with confined concrete) could explain part of these differences. Numerical tests have shown slight differences between pushover analyses between a square RC column using the Section Designer module and the standard module in the program. The in-cycle strength degradation observed are mainly caused by the smoothing technique used along both EW and NS actuators and is not considered as a discrepancy. The in-cycle strength degradation observed is mainly caused by the smoothing technique used along both EW and NS actuators.

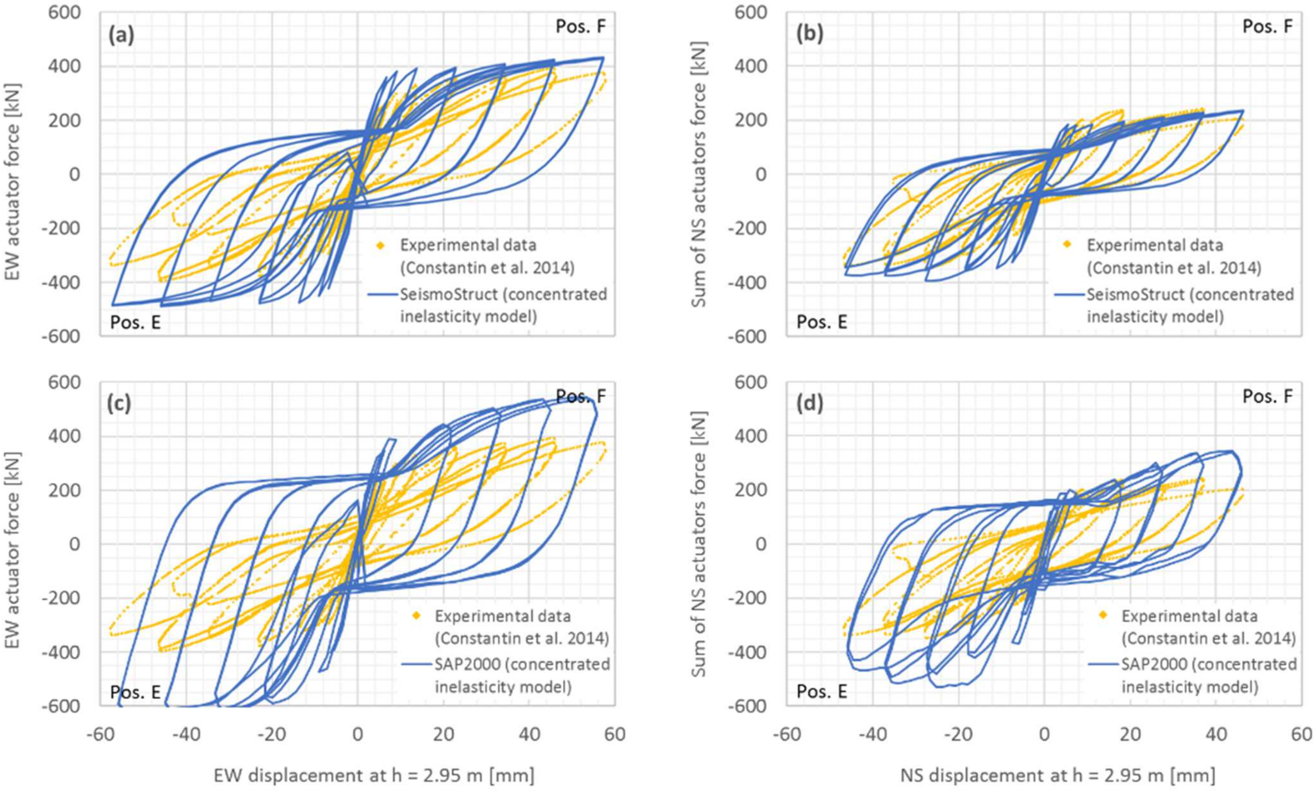

Fig. 3.2. Predictions of the hysteretic cyclic response of the core wall along E-F direction using concentrated inelasticity models vs experimental data: (a) and (b) SeismoStruct; (c) and (d) SAP2000.

3.1.6.2 Predictions using distributed inelasticity models

The distributed inelasticity models are built using SeismoStruct and OpenSees (Fig. 3.3). In both cases, the wall is modelled according to the Wide Column Model Analogy (WCM) proposed by Beyer et al. (2008-a) and steel and concrete materials are modelled using Menegotto-Pinto (1973) and Mander et al. (1988), respectively. In SeismoStruct, the mechanical properties of the rebars are defined in proportion to the actual quantity of each rebar type in a given cross-section as previously, while these properties are assigned individually to each rebar in OpenSees. The vertical elements defining each wall panel are modelled using inelastic DB fibre elements. The collar is modelled using elastic elements as before. Zero-length link elements with elastic concrete properties corresponding to a fraction of the gross section of the wall are used between every two vertical elements to approximately account for shear deformations of the wall (Beyer et al., 2008-a). Horizontal link elements are included to connect the three wall panels. These elements have elastic concrete properties of a fraction of the wall gross section and are only flexible in torsion and out-of-plane flexure (Beyer et al., 2008-a; Pelletier and Leger, 2017)). The collar and wall parts of the model are connected using rigid links located at the three top nodes of the core wall. The cyclic displacements imposed by actuators are applied to the wall through a static time history analysis. The analysis is run as a static analysis. The algorithm used is Krylov-Newton (Scott and Fenves, 2010). The hysteretic cyclic response of the core wall along E-F direction obtained using a Wide Column Model approach with distributed inelasticity models in SeismoStruct (Seismosoft, 2014) and OpenSees (Mazzoni et al., 2006) are illustrated in Fig. 3.4 along with experimental data from Constantin and Beyer (2016).

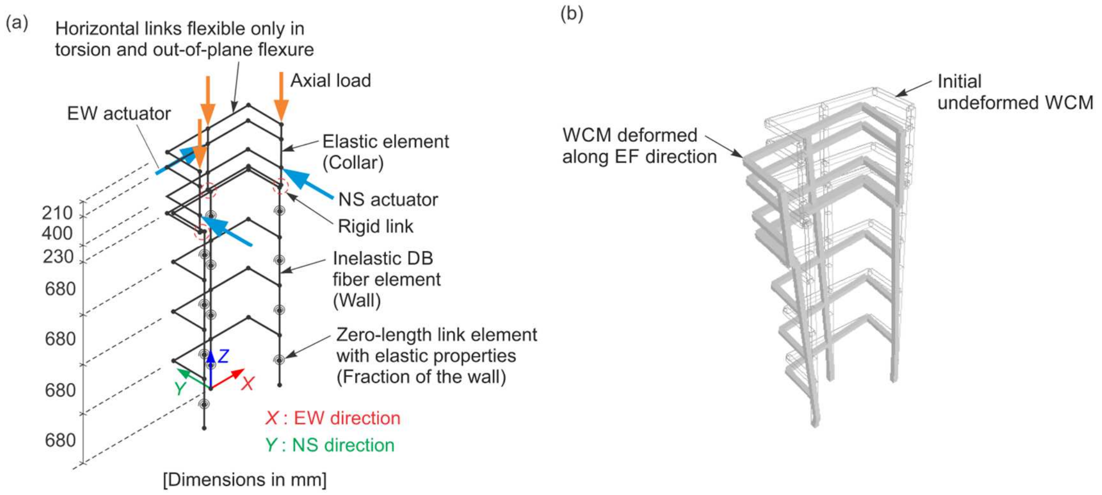

Fig. 3.3. Fibre element-based WCM model: (a) Components of the WCM used in SeismoStruct and OpenSees; (b) Undeformed WCM and deformed configuration along EF direction obtained using SeismoStruct.

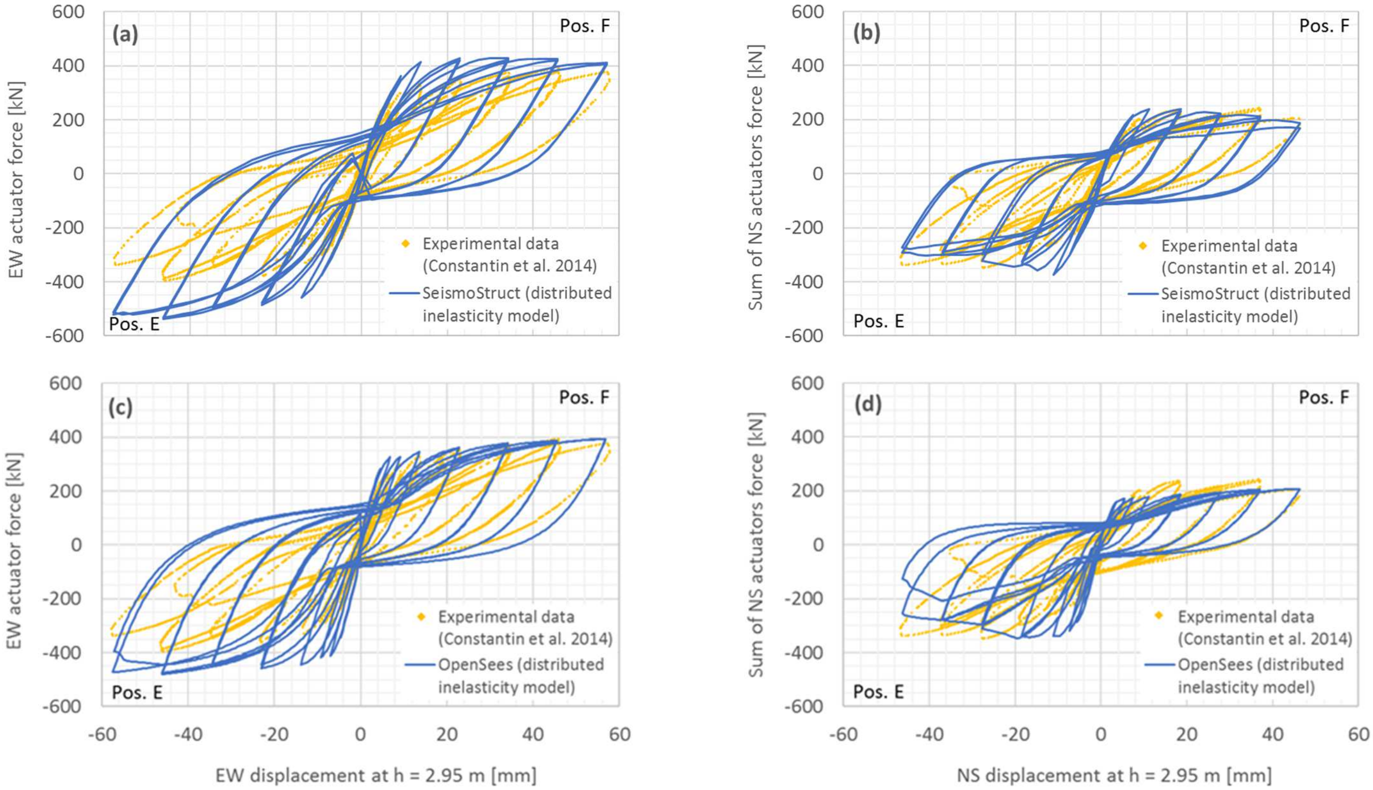

Fig. 3.4. Predictions of the hysteretic cyclic response of the core wall along E-F direction using distributed inelasticity elements and wide column models vs experimental data: (a) and (b) SeismoStruct; (c) and (d) OpenSees.

Fig. 3.4.a & b show that the initial stiffness is well predicted by the SeismoStruct distributed inelasticity elements models. The initial overstrength at the E position on the graph for both actuators can be at least partly explained by the fact that a mean value of mechanical properties had to be used for the west flange (composed of 3 different rebar sizes). Still, the general behaviour is somewhat well represented by the model.

For the EW direction, a slight hardening is observed in later stages of the nonlinear cycles at the E position. This behaviour can be attributed to multiple factors, such as definitions of materials and confinement areas, i.e. they must be specified as symmetric in rectangular shapes in SeismoStruct and a compromise has to be made. In-cycle strength degradation and cyclic strength degradation seem to describe better the behaviour of the core wall in NS direction. This kind of response can happen because of concrete crushing at the ends of the flanges. As was the case in the EW direction, approximations of confinement regions could play a role in this behaviour. The OpenSees models seem to give reasonable results for the F position, while the prediction in the E position is again less accurate. Definitions of the mechanical properties and confinement regions are more precise in this case. The results seem to confirm the overstrength in the E position, but it is less obvious than predicted by SeismoStruct model. The model globally reproduces the behaviour of the wall relatively well. Limited in-cycle strength degradation and cyclic strength degradation are also observed for the E position along the NS direction.

3.1.6.3 Predictions using finite element models

Figure 3.5 shows 3D views of FE mesh used in ANSYS and ABAQUS models. In ANSYS, SOLID65 elements are used to model the concrete, while BEAM188 elements are used to model discretized steel rebars. Smeared Cracking (SC) model and a plastic regime with isotropic hardening are assigned for concrete and steel materials, respectively. Similar configurations are used for model implementation in ABAQUS, i.e. C3D8R solids and beam elements, except the SC model, which is replaced by CDP model. Full bond interaction between the concrete and steel rebars is considered in the numerical models. Mesh sensitivity analysis are performed to adjust the mesh size in the FE models, and same sizes are used in both ANSYS and ABAQUS for comparison purposes. The deformed shape of the core wall FE models and the stress distributions are presented in Fig. 3.5.c & d. The force-displacement curves for both NS and EW actuators obtained using FE analyses are compared to experimental results in Fig. 3.6. As it is depicted in the figure, the observed responses from the ANSYS FE model are in acceptable agreement with the test data in both loading and unloading parts of the cycles. The initial stiffness of the curves match well for both NS and EW directions, and the FE models showed a reasonable precision in predicting core wall capacity and maximum displacements at failure. Possible reasons for the observed discrepancies could be the loss of tension stiffening effects under reversed cyclic load conditions, and the degradation in the bond and anchorage of the reinforcement, particularly at the base. Figures 3.6.c & d show that though the ABAQUS FE model closely predicts the initial stiffness in both directions, it fails in reproducing the cyclic response of the core wall. First, the model overestimates the lateral capacity of the wall. Moreover, while the calculated unloading stiffness of the model is close to the elastic stiffness, the degradation of the unloading stiffness could not be captured. In fact, the model is unable to capture sliding between the already cracked concrete surfaces. Little effects on the hysteretic force-displacement response were observed by adjusting the stiffness recovery parameter available in CDP model. The numerical model exhibits fat hysteresis loops with very low pinching, due to the lack of a proper shear reduction algorithm, which induces shear sliding across crack faces. Shear sliding effects at the time of crack closure upon load reversal can significantly affect cyclic loops and lead to pinching effects in the cyclic response of the core wall.

Figures 3.6.e & f present a comparison between the results of pushover analysis of the core wall using both implicit and explicit solvers implemented in ABAQUS. For the explicit analysis, smooth stepping feature in ABAQUS is used to avoid the waving effects in the response of the core wall. A slow loading rate of 0.1 mm/s is also adopted in the explicit analysis to simulate quasi-static loads and satisfy the recommendations in ACI 374.2R (2013). A mass scaling technique is used with a scaling factor of 16 to expedite the computations, after performing sensitivity analyses. Both implicit and explicit analyses result in a reasonable prediction of the monotonic response of the core wall. The observed discrepancies between the numerical and experimental results, specifically at the strength degradation stage, mainly come from cyclic degradation effects which are the fundamental difference between the nature of two loading protocols. The explicit solver decreases computational time up to 60% in the investigated case. This difference can be even higher in cases when a relatively fine mesh and significantly small time increments are required to address convergence difficulties.

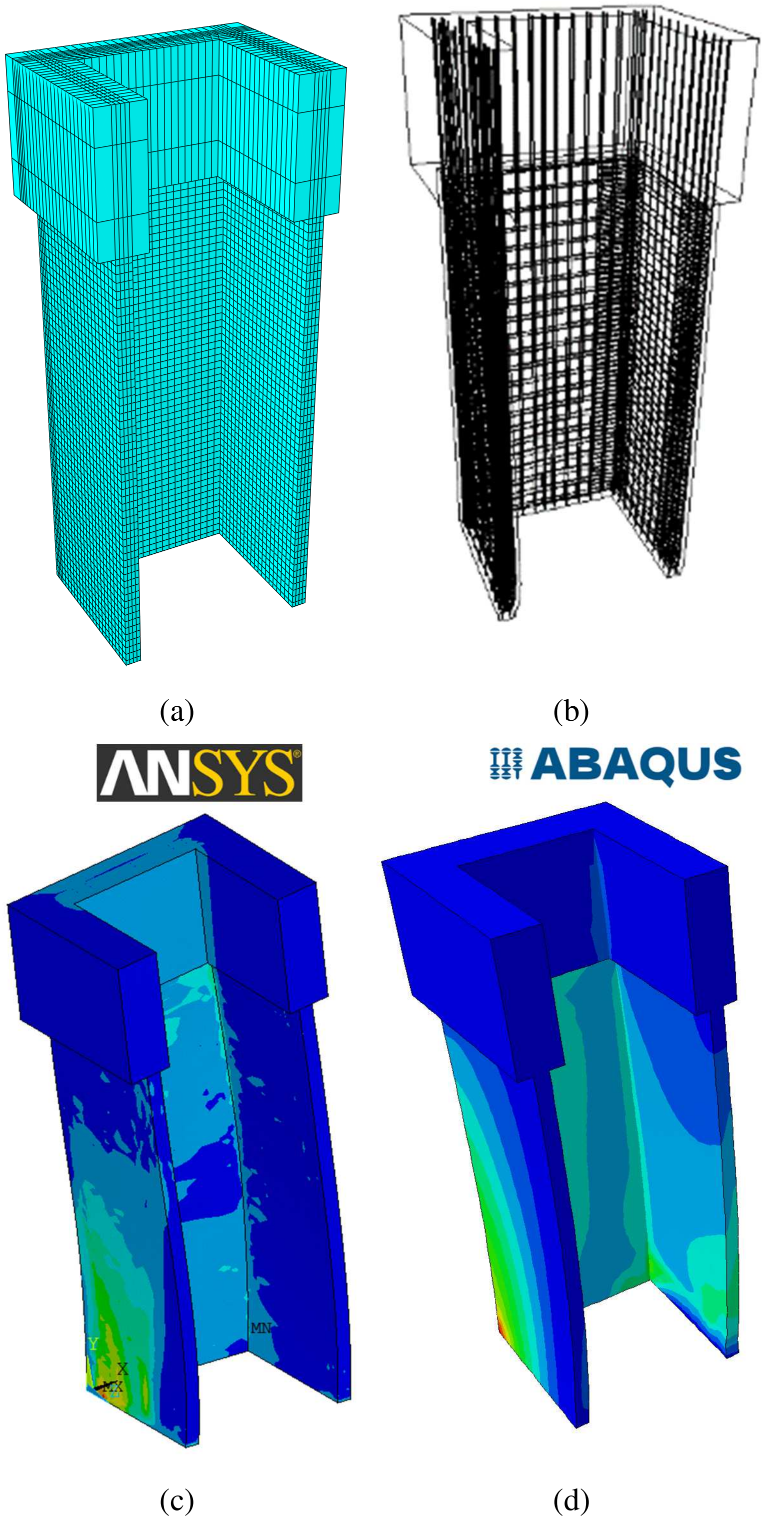

Fig. 3.5. View of the 3D FE models for specimen TUC: (a) FE mesh, (b) Rebars disposition, (c) Deformed shape extracted from ANSYS, (d) Deformed shape extracted from ABAQUS.

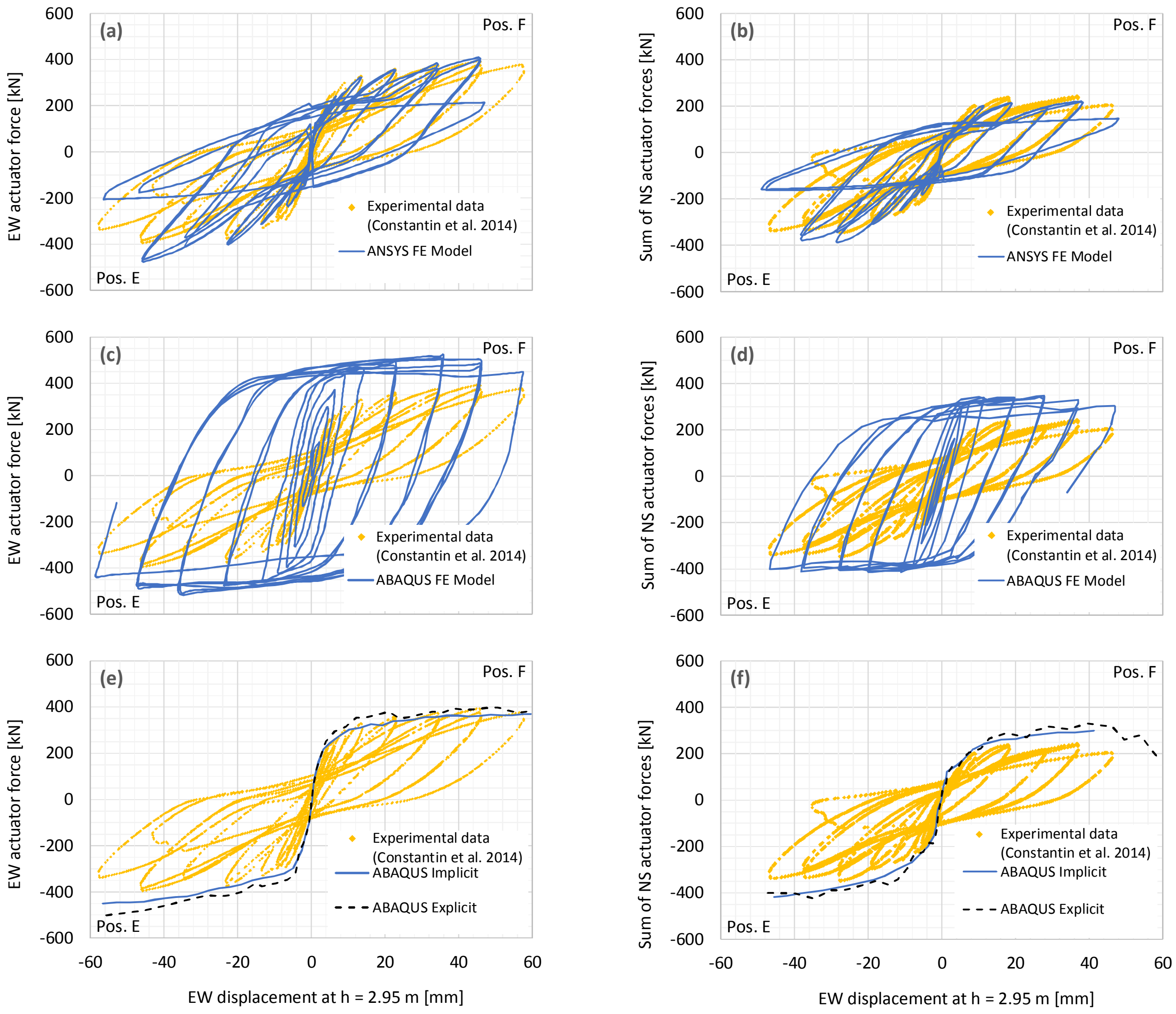

Fig. 3.6. (a) to (d) Hysteretic cyclic response of the FE models: ANSYS and ABAQUS; (e) to (f) Comparison between the monotonic results of ABAQUS/Implicit and ABAQUS/Explicit (EF direction)

3.1.7 Planned experimental testing program – Multiaxial loading of C-shaped walls

An experimental testing program was planned to be conducted at the Structures Laboratory of Polytechnique Montréal. The main objectives of this program were to develop enhanced numerical models to account for 3D seismic effects on C-shaped walls. The results of the tests, obtained from planned cyclic tests of C-shaped walls subjected to multidirectional loads including torsional effects, can be used to validate numerical models for investigating the multi-directional response of RC core walls. High-Performance Multiaxial Loading System available at the Structures Laboratory of Polytechnique Montréal was used for this purpose. The tested core wall was then retrofitted using FRP (Fiber Reinforced Polymers) sheets, and then re-tested under multiaxial cyclic loads. Results of the test specimens (i.e. Original and retrofitted wall) were planned to be compared to quantify the efficiency of the scheduled retrofitting method in strengthening the wall.

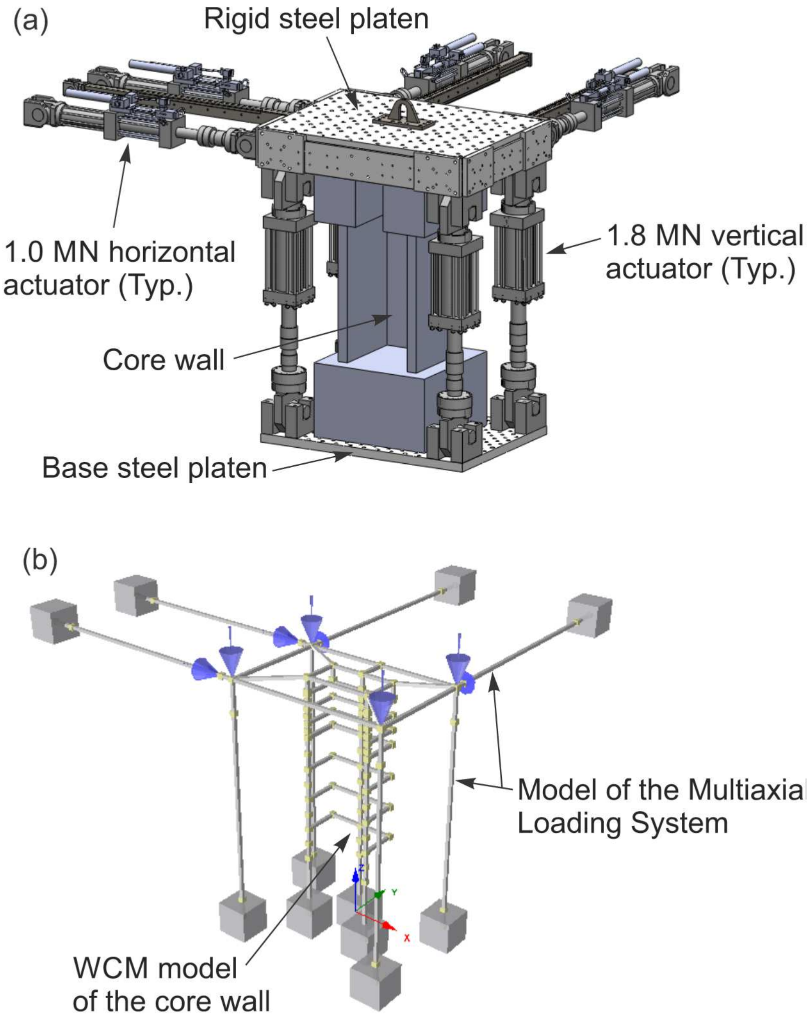

Fig. 3.7. Planned experimental testing program: (a) C-shaped shear wall to be tested using the Multiaxial Loading System available at Polytechnique Montréal, (b) Simulation of the tests using SeismoStruct.

3.1.8 Conclusions

A variety of finite and fibre element RC models for nonlinear cyclic analysis of RC core walls were evaluated in this paper, using different computer programs. The main results are summarized as follows:

- The concentrated plasticity models, created herein using SeismoStruct and SAP2000, have the advantage of being very simple to create. This type of analysis requires a shorter amount of time than the others in terms of building the models and running the analyses. This economy can be to the cost of precision, however; i.e. warping and shear deformations are not taken into account.
- The distributed plasticity models combined with the WCM analogy, created herein using SeismoStruct and OpenSees, are relatively simple to use including features to enhance precision such as shear flexibility.
- FE modelling using the software such as ANSYS and ABAQUS could be as an accurate tool for structural analysis. However, calibration/validation of the results is necessary because of the probable uncertainties.
- By using the shear reduction feature provided by ANSYS, it can perform well in predicting the cyclic behaviour of the RC U-shaped wall, as well as its capacity and the maximum displacement at failure. On the contrary, though it is claimed that CDP model in ABAQUS can capture the cyclic response of RC elements, this seems to be true only in well detailed concrete elements with no pinching. In any case that pinching behaviour is not expected, CDP model can be used.
- In contrast to cyclic loading, results of the CDP model under monotonic loads from both Implicit and Explicit analyses are well in agreement with experimental ones. Hence, Explicit analysis can be successfully used in the quasi-static analysis of RC members.

3.2 Numerical Investigation on Effectiveness of FRP Wraps for Retrofitting of Existing RC Shear Walls

3.2.1 Abstract

Reinforced concrete (RC) shear walls are best known as efficient lateral resisting systems in buildings because of their high stiffness and their high flexural and shear capacities. Continuous advancements in seismic design codes and regulations and the ageing and deterioration of existing RC structures are two major reasons for the necessity of seismic strengthening and retrofitting of shear wall structures. In this respect, different retrofitting methods have been proposed, but reliable means of estimating the behaviour of RC shear walls are required to choose the most effective retrofit method. In this article, the response of FRP-retrofitted RC shear walls subjected to lateral loads is studied using the general-purpose finite element code ABAQUS. The numerical modelling is first validated against available experimental results from the literature, and the numerical results in terms of the load–displacements are in good agreement with experimental data. Squat shear walls and walls with intermediate aspect ratio having different dominant behaviour including flexural, shear and sliding are considered in the study. Geometric and material nonlinearities in the concrete wall, steel rebars and FRP wraps have been taken into consideration. Shear walls with different geometries were modelled in order to study the effectiveness of FRP wraps with different configurations on the wall's behaviour in terms of strength and ductility. It was found that the addition of an external layer of vertical FRP layer results in increased wall's ultimate load bearing capacity without a significant increase in the stiffness in both squat and flexural walls, especially in walls with weak boundary elements. The displacement ductility of squat walls and walls with intermediate aspect ratio are affected differently by the addition of a vertical or horizontal FRP layer.

3.2.2 Introduction

Reinforced concrete (RC) shear walls have been widely used as lateral load resisting systems in buildings. Past earthquakes reconnaissance showed that RC walls governed by shear failure have performed poorly due to probable brittle-type failures with low ductility (Kim, 2004). In past two decades, researchers have performed various investigations to develop proper methods for designing shear walls that have ductile behaviour while providing high shear capacity in proportion to flexural capacity (Mousavi, 2008). On the other hand, many studies focused on strengthening and repairing RC shear walls by using other methods such as steel jacketing and fibre reinforced polymer (FRP) composite wrapping.

Adding vertical FRP layer(s) around the wall's boundary regions was found to be an effective way for improving RC shear walls performance, which can enhance both the ultimate load-bearing capacity and ductility of shear wall system (Khalil and Gobarah, 2005, Mostofinejad and Anaei, 2012, El-Sokkary and Galal, 2013). This retrofit method can be effective for RC shear walls with weak boundary elements (Woods, 2014).

In addition to the vertical FRP layers, using horizontal wraps around the bottom part of a wall system could improve the shear resistance of the wall. As such, local debonding of the vertical FRP layers, as well as the undesirable shear sliding mode of failure, could be prevented.

The present study focuses on investigating the effectiveness of FRP strengthening on the pushover behaviour of RC shear walls using finite element (FE) modelling technique. The FE meshes, boundary conditions, and nonlinearity implementation methods have been calibrated/validated by comparing the predictions of the closest available experimental data. Subsequently, effects from FRP strengthening on the lateral response of RC shear walls were studied. Two groups of walls, known as squat and walls with intermediate aspect ratio according to ASCE-41 (2013), have been selected to investigate the effect of FRP strengthening method on the lateral response of RC shear walls. Geometrical and material nonlinearities in the concrete material, steel reinforcements and also FRP wraps have been taken into consideration. Effects of the variation of FRP covered area of wall on the ultimate load capacity, as well as the ultimate drift, energy dissipation and ductility, have been evaluated.

3.2.3 Numerical Modelling

The software package used for FE modelling in this study was the general-purpose nonlinear finite element package ABAQUS, which offers a comprehensive material constitutive law for simulation of concrete material. This section describes the modelling approach used for the finite element analyses.

3.2.3.1 Geometry and Mesh

Eight-node three-dimensional reduced integration elements with a Gaussian integration point in the element C3D8R have been used for simulating the concrete medium in the numerical model. Using lower integration point can help to reduce the time of analysis. However, using this procedure can cause zero-energy mode called hourglassing, which leads to severe flexibility and no straining at the integration points. ABAQUS uses a small artificial stiffness to prevent this phenomenon (Hibbitt, 2007). Steel reinforcements are modelled using truss elements T3D2 and positioned in the exact locations as in the experimental works. Adjacent nodes have then been coupled using embedment constraint. For simulating the FRP layers, four node reduced-integration shell elements S4R were used with compatible element sizes to avoid convergence issues.

The solid elements located in boundary regions and also in the bottom part of the wall have a dimension of approximately 1% of wall length in all three directions. This leads to a quite fine mesh in concrete. To optimize the computational efforts, a relatively coarser mesh up to 5% percent of the wall length was adapted for the rest of the model. Compatible meshes were also considered for steel reinforcements and FRP layers. Fig. 3.8.a shows the employed mesh in the finite element model.

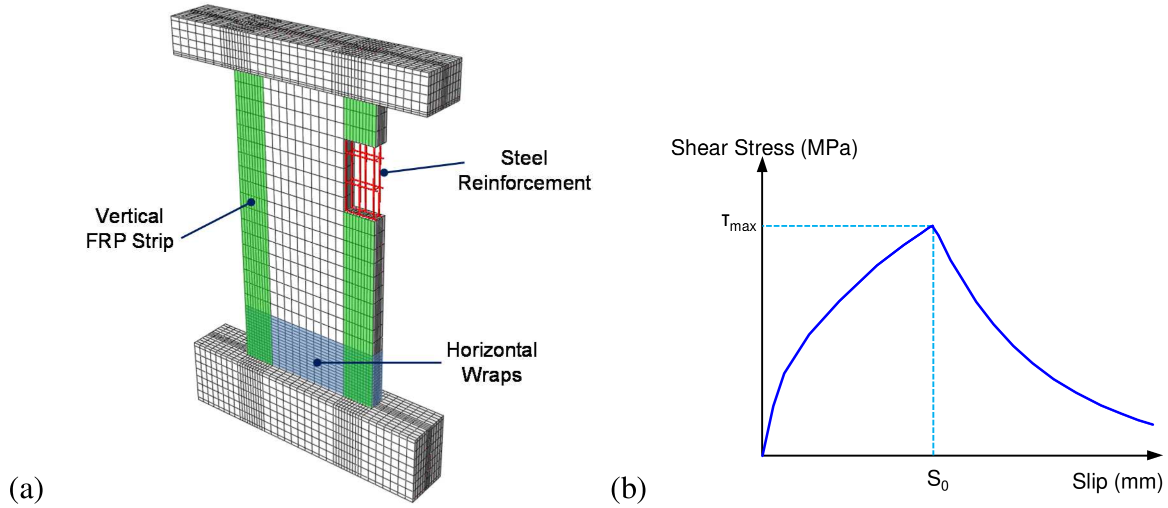

Fig. 3.8. a) Finite element mesh, b) Schematic FRP bond-slip relationship model proposed by Lu et al. (2005)

3.2.3.2 Material Constitutive Laws

There are a number of concrete constitutive models available in the literature based on principles of elasticity, plasticity and continuum damage mechanics. In the current study, Concrete Damage Plasticity (CDP) model was used to define the mechanical properties of concrete in the model. Modified Hognestad equation is used to define the compressive stress-strain behaviour of concrete material. The tensile strength of concrete (f_t) is considered to be equal to 0.3 $fc^{2/3}$ according to the CEO-FIB2010 (fib, 2013). In addition to the user-defined compressive and tensile responses, two other parameters are required to define the yield function for the CDP model. The ratio of initial biaxial compressive yield stress to initial uniaxial compressive yield stress (σ_{b0} / σ_{c0}) was considered equal to 1.16. The ratio of the second deviatoric stress invariant on the tensile meridian to that on the compressive meridian (K_c) was used equal to 0.67 for the analyses (Lubliner et al., 1989). The dilation angle of concrete material was also set equal to 55 degrees as proposed by Dey (2014).

For steel reinforcements, combined hardening plasticity was considered by providing the nonlinear half cycle stress-strain data equal to reported values in the experimental tests.

FRP material is considered orthotropic and transversely isotropic, i.e. the mechanical properties are the same in any direction perpendicular to the fibres. In this study, FRP material was modelled by defining lamina type of elasticity along with failure sub option offered by ABAQUS. Table 3.1 shows the mechanical properties of CFRP wraps used by El-Sokkary and Galal (2013). Same material properties are considered in evaluating the effectiveness of FRP strengthening of shear walls in the next section.

Table 3.1. FRP Material Properties

Parameter	Value
Tensile Strength (MPa)	1062
Elastic Modulus (MPa)	102000
Rupture Strain (%)	1.05

3.2.3.3 FRP-Concrete Interaction

The bond interface between concrete and FRP sheets, which was generated by utilizing a layer of epoxy resin as adhesive material, has a significant effect on the seismic performance of the strengthened shear wall (Rezaiefar, 2013). In some experimental works, mechanical anchorage devices also used to ensure the prevention of de-bonding (Hiotakis et al., 2004), (Ghobarah and Khalil, 2004), (Elnady, 2008). In the simulations of the adherence between FRP layers and the concrete surface, some other researchers (Kezmane et al., 2012) have used a perfect adherence. Some others also used the method of penalizing to model the contact between two surfaces with a coefficient of friction acting between the master surface and slave surface.

In cases where the epoxy resin is the only adhesive medium, debonding failure mechanism should be considered into the model corresponding to the mechanical properties of concrete and FRP material. The bond-slip relationship model proposed by Lu et al. (2005) has been implemented into the model by using nonlinear connector elements in ABAQUS. A schematic of the proposed relationship is depicted in Fig. 3.8.b. Tributary area of adjacent nodes are calculated using a Matlab script. Then, different slip based relationships are defined to couple the adjacent concrete-FRP nodes in the model.

3.2.3.4 Numerical Analysis

To perform a quasi-static pushover analysis, either a static or a dynamic analysis could be used. In order to reduce the convergence issues, Dynamic/Explicit analysis in ABAQUS is used in this study. Sensitivity analysis was done and a total time equal to 10 seconds was found to be long enough to prevent dynamic waving effect in the results. Displacement controlled analysis was defined by applying a smooth stepping mode through the analysis in the way that provides a quasi-static situation for the analysis. This method was also previously employed by other researchers (Rafiei, 2011, Dhanasekar and Haider, 2008) and was found to be able to achieve reasonable results.

3.2.4 Model Validation

In this section, the validation of the proposed model for accurate following of the response of RC shear walls under lateral loads has been performed by comparing the simulation results with available experimental data. Recently, few researchers (Rafiei, 2011, Woods, 2014) validated the capability of ABAQUS to simulate the lateral response of RC shear wall systems subjected to lateral loads.

To ensure the precision of modelling approach, validation of numerical predictions against two experimental tests by Lefas et al. (1990) were performed. The tests were carried out for examining the lateral capacity of RC shear walls with different slenderness ratios. Moreover, to ensure that the strengthened wall response would be also covered by the numerical model, a comparison between the pushover numerical results and test records of an FRP strengthened shear wall by Elsokkary and Galal (2013) was also performed in the second part.

Two wall specimens SW15 and SW22 from the tests by Lefas et al. (1990) with slenderness ratio (i.e. height/shear span) equal to 1 and 2 respectively were selected to be used in the model validation stage. Wall SW15 was an RC shear wall constructed with 40 MPa concrete (cube strength) and 470 MPa and 520 MPa yield strength steel reinforcement for vertical and horizontal reinforcement, respectively. The wall had 750mm height, 750mm length, and 70mm thickness. The wall reinforcement consisted of two layers of reinforcement, d8mm @ 60mm and d6.25mm @ 80mm bars, providing a reinforcement ratio of 2.4% and 1.1% in the vertical and the horizontal directions, respectively. Wall SW22 has 1300mm height, 650mm length, and 65mm thickness, constructed with 50.6 MPa concrete (cube strength). The wall reinforcement consisted of two layers of reinforcement, d8mm @ 62mm and d6.25mm @ 115mm bars, providing a reinforcement ratio of 2.5% and 0.8% in vertical and horizontal direction respectively. Both walls were first subjected to a normalized axial load equal to 0.1, then the lateral load was applied in displacement control situation. These two walls were used as control wall in the current study to investigate the effect of FRP strengthening in the lateral response of RC shear walls.

Wall RW1 was also selected from tests by El-Sokkary and Galal (2013), which had 1200mm height, 1045mm length, and 80mm thickness. The wall was constructed with 37MPa concrete (cylinder) and grade 400, 10M steel bars for the reinforcement. Details of mechanical properties of the materials were presented in the Section 2.2. Normalized axial force equal to 0.02 was acting on the wall during the test.

Modelling approach presented in the previous section was used for simulation and analysis of the aforementioned specimens. Fig. 3.9 illustrates the comparison between numerical predictions and experimental data. As it can be observed in the figure, the numerical model can reasonably predict the lateral response of RC shear walls. For original shear walls SW15 and SW22, very good agreement was observed between the results. Small discrepancies between the results might be because of some uncertainties in material strength and also effect of some residual stresses because of probable imperfections. These effects have not been considered in the numerical model.

Numerical results for strengthened wall RW1 are also presented in Fig. 3.9.b which shows a very reasonable agreement with the experimentally measured response. In fact, although there is a difference between the descending branches of force-deformation curves, the general trends are quite similar. Moreover, the model successfully predicted the initial stiffness, ultimate load and corresponding drift, and ultimate drift of the strengthened wall. Numerical models are then utilized to perform a parametric study on FRP-strengthening of RC shear walls.

3.2.5 Results of Numerical Analysis

3.2.5.1 Wall Strengthening Schemes

Five different levels of FRP strengthening were investigated for both SW15 and SW22 walls in this study, which consist of walls with the area covered by horizontal FRP wraps equal to 10 to 100 percent on each side of the wall. All walls had vertical FRP layers on both sides of their boundary elements with the width equal to 20% of wall length. The strengthening schemes are as follows:

- Original walls with no FRP strengthening
- Walls with vertical layer and 0.1*h* horizontal wraps at bottom
- Walls with vertical layer and 0.1*h* horizontal wraps at bottom and top
- Walls with vertical layer and 0.2*h* horizontal wraps at bottom

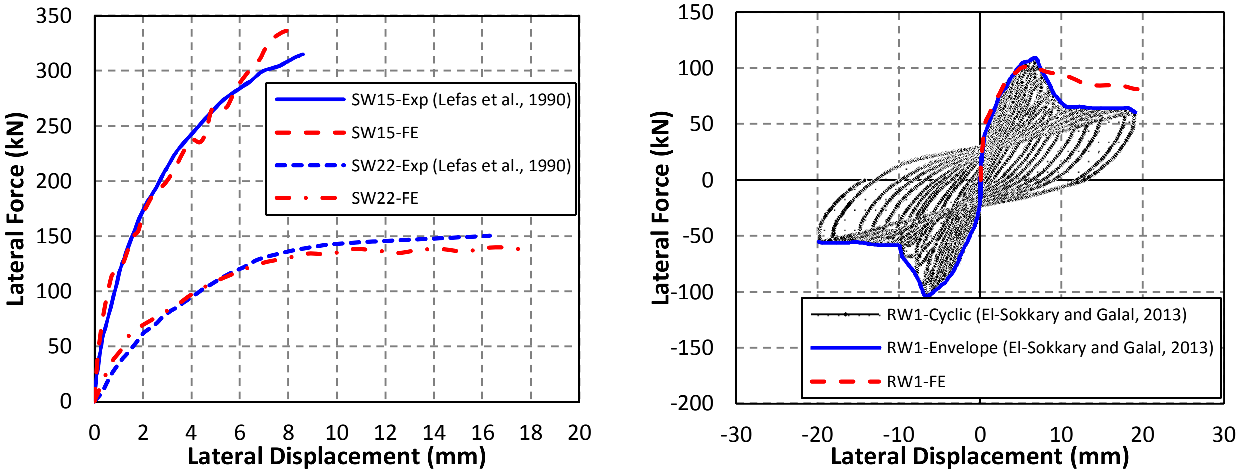

(a) (b)

Fig. 3.9. Verification of Numerical Model, a) Concrete Shear Walls Tested by Lefas et al. (1990), b) Retrofitted Wall Tested by El-Sokkary and Galal (2013)

- Walls with vertical layer and 0.2*h* horizontal wraps at bottom and top
- Walls with vertical layer and horizontal wraps fully covered the wall

where *h* represents the height of the wall. Fig. 3.10 presents a typical strengthening scheme of the wall with vertical and horizontal FRP wraps. It should be mentioned that, for walls with extremely low (or high) geometrical aspect ratio, more than two vertical (or horizontal) FRP layer could be used for strengthening the wall as proposed by Nguyen et al. (2014).

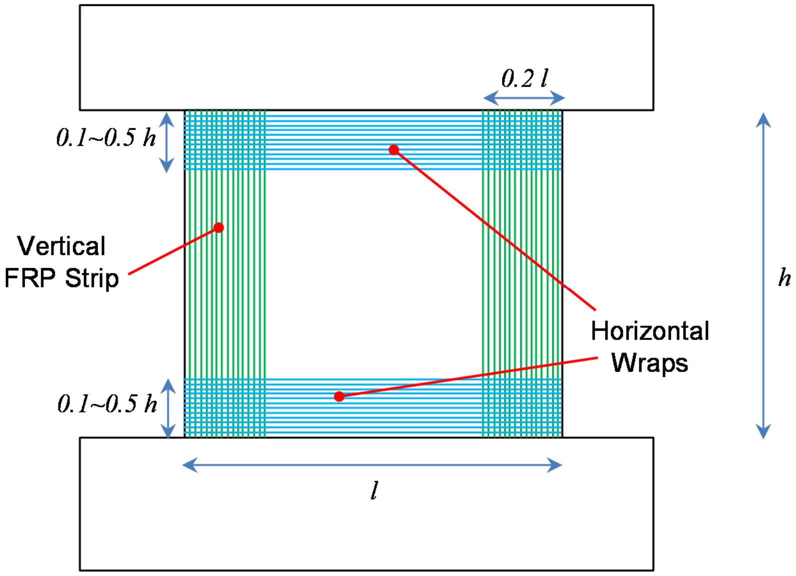

Fig. 3.10. Strengthening Scheme of Walls by using FRP Wraps

3.2.5.2 Pushover Behavior

In this section, lateral responses of the studied walls are retrieved in order to evaluate the effectiveness of FRP strengthening on enhancing the wall lateral resistance. Load-displacement pushover curves for both squat walls and walls with intermediate aspect ratio are presented in Fig. 3.11. In general, the FRP strengthening schemes have enhanced the lateral resistance of walls, but in different levels, as expected. Moreover, similar strengthening configurations led to different improvements in the walls. It should also be noted that although both walls achieved higher resistance, the enhancement in the wall strength seems to be more affected by the vertical FRP strips. As it can be seen, the results obtained from the case of covering 0.1h at the bottom of the wall is so close to the case of covering 0.1h at bottom and top. By increasing the height of horizontal FRP wraps, higher stiffness, as well as higher ultimate drift, are obtained from both walls. However, differences in walls with intermediate aspect ratio are not significant.

A quantitative comparison between results is presented in Table 2. Evaluating the results shows that 7 to 45 percent increase in the ultimate load capacity of the squat wall is achieved by using the studied strengthening schemes. This corresponds to 9 to 41 percent increase in the ultimate drift of squat wall before failure point. In the walls with intermediate aspect ratio, using the studied strengthening schemes improved the ultimate load capacity from 26 to 49 percent in comparison with the original shear wall. Corresponding ultimate drifts were increased by 6 to 13 percent.

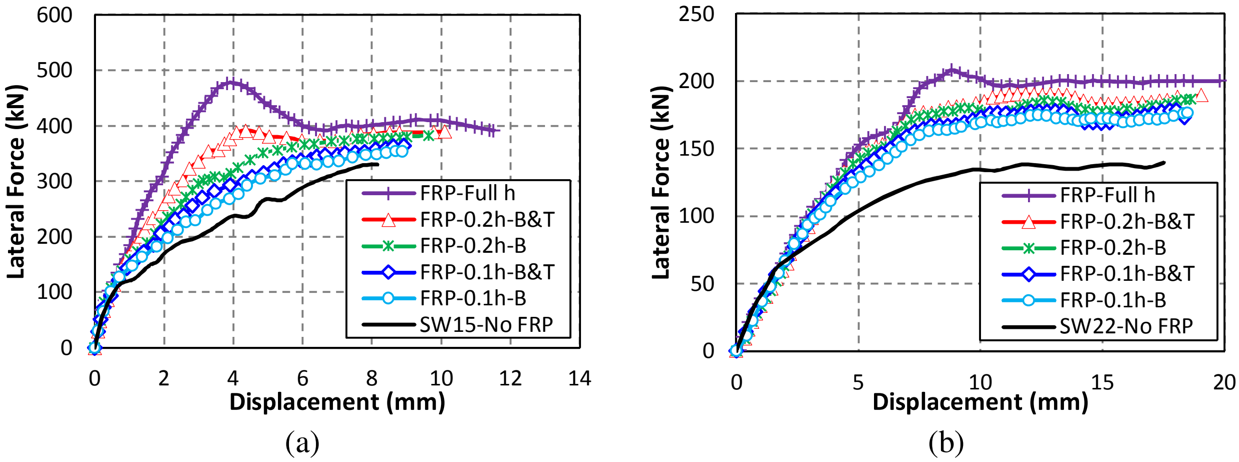

(a) (b)

Fig. 3.11. Pushover Response of Walls, a) Squat Walls, b) Walls with Intermediate Aspect Ratio

In the walls with intermediate aspect ratio, using the proposed strengthening schemes improves the ultimate load capacity by about 26 to 49 percent in comparison with the original shear wall. Corresponding ultimate drifts were increased by 6 to 13 percent. A side-by-side comparison could be done between strengthening schemes “FRP-V&0.1h-Bottom&Top” and “FRP-V&0.2h-Bottom”. Both cases have the same covered area equal to 20%, but the latter presents a better improvement in the wall response in both squat and intermediate aspect ratio mode. This represents the bottom side of the wall as a critical region, especially in squat walls, where a relative increase in the wall capacity (in comparison with the corresponding value in the original wall) is almost 60% higher (i.e. 10% and 16%, respectively).

3.2.5.3 Energy Dissipation

In terms of lateral resisting systems, the energy dissipation during the lateral effort of the system is one of the main characteristics. In this section, a comparison between energy dissipation capabilities of walls is performed through energy-drift curves as presented in Fig. 3.12. As previously observed in the pushover curves, by increasing the area of the wall strengthened by FRP wraps, more energy needs to be dissipated by the wall system at a certain drift level. Highest contribution in energy dissipation results from the specimens fully covered by horizontal FRP wraps, in which 135% and 67% increase in the energy dissipation are observed for squat walls and walls with intermediate aspect ratio respectively. More explicitly, the remarkable influence from horizontal FRP wraps on squat walls is observed.

For presenting the results in a more tangible way, dissipated energy by the walls was categorized in two structural performance levels according to FEMA 356 (2000); Immediate Occupancy (IO) and Life Safety (LS). FEMA 356 recommends drift limits equal to 0.5% and 1% as IO and LS performance levels respectively. These levels are indicated in Fig. 3.12 with red and blue dashed vertical lines respectively. Results are compared for two wall groups in Fig. 3.13.

As shown in Fig. 3.13.a for squat walls, the effectiveness of FRP strengthening on increasing the energy dissipation capability is relatively significant in both IO and LS performance levels, ranging from 2% to 68% and 14% to 65% respectively. A similar comparison is performed for walls with an intermediate aspect ratio in Fig. 3.13.b, in which a lower effectiveness from FRP strengthening can be observed. The increase in energy dissipation capability ranges from 16% to 29% and 23% to 42% in IO and LS performance level respectively.

Table 2 – Results of Pushover Analysis of Walls

Specimen	Strengthening Scheme	FRP Covered Area	Ultimate Load (kN)	Drift at Ultimate Load	Ultimate Drift	Energy Dissipated at IO (kN.m)	Energy Dissipated at LS (kN.m)	Total Energy Dissipated (kN.m)
SW15	No FRP Strengthening	0%	330.1	1.09%	1.09%	315	815	917
	FRP-V&0.1h-Bottom	10%	354.5	1.16%	1.18%	322	932	1170
	FRP-V&0.1h-Bottom&Top	20%	364.5	1.19%	1.19%	350	979	1230
	FRP-V&0.2h-Bottom	20%	383.0	1.29%	1.29%	390	1034	1465
	FRP-V&0.2h-Bottom&Top	40%	390.3	0.58%	1.35%	439	1156	1658
	FRP-V&Full h	100%	477.1	0.51%	1.54%	529	1345	2152
SW22	No FRP Strengthening	0%	139.6	1.35%	1.35%	251	676	76
	V&0.1h-Bottom	10%	176.5	1.42%	1.42%	291	832	100
	FRP-V&0.1h-Bottom&Top	20%	178.4	1.39%	1.41%	297	853	101
	FRP-V&0.2h-Bottom	20%	186.4	1.43%	1.43%	306	879	107
	FRP-V&0.2h-Bottom&Top	40%	190.2	0.89%	1.47%	311	905	113
	FRP-V&Full h	100%	208.2	0.68%	1.52%	323	961	127

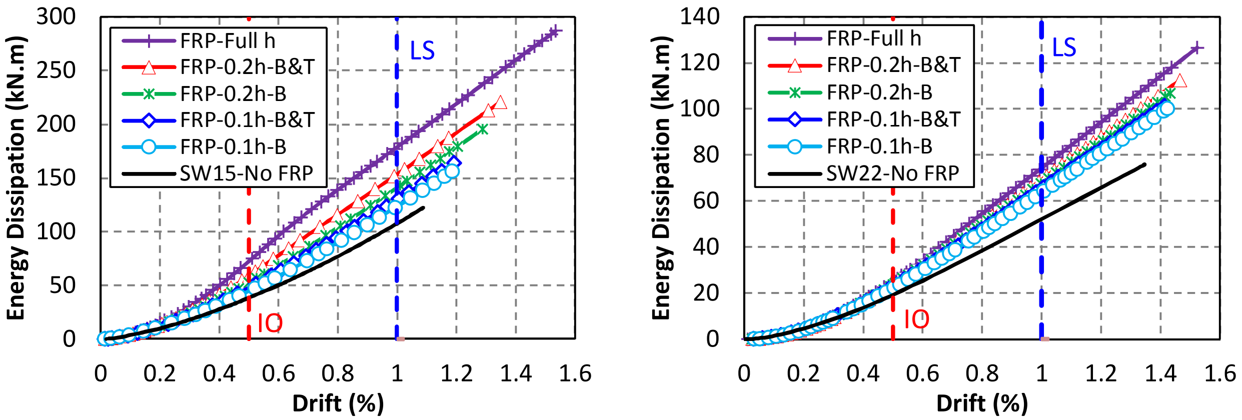

(a) (b)

Fig. 3.12. Energy Dissipation in Walls, a) Squat Walls, b) Walls with Intermediate Aspect Ratio

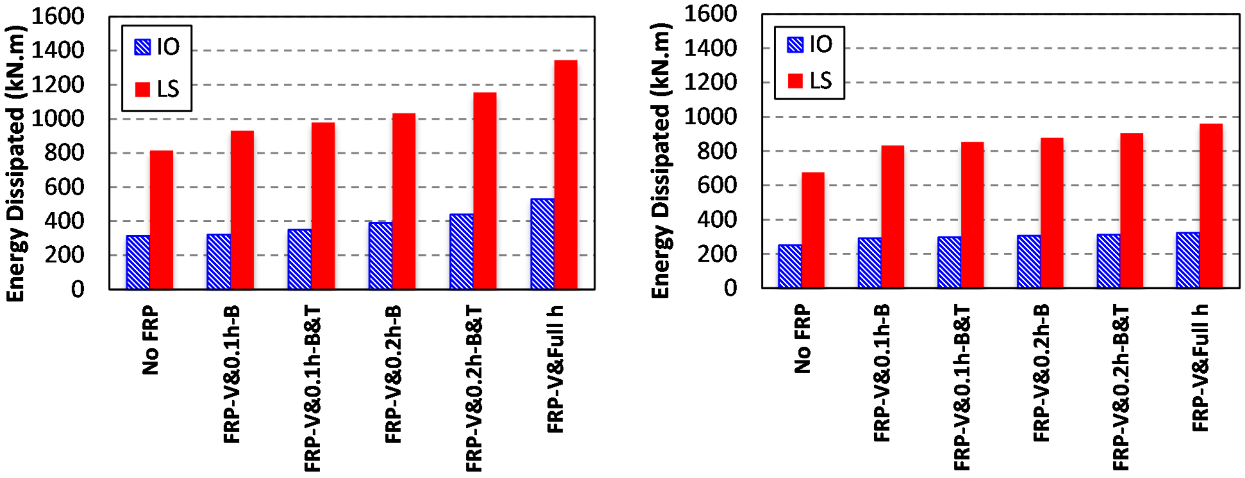

(a) (b)

Fig. 3.13. Energy Dissipated by Walls in Immediate Occupancy and Life Safety levels,
a) Squat Walls, b) Walls with Intermediate Aspect Ratio

3.2.5.4 Evaluating the Ductility of Strengthened Walls

Since the relation between strength and deformation of RC members may not have a well-defined yield point, some approximate levels should be used to define yield and ultimate limits. In the current study, the proposed approach by Carrillo et al. (2014) called $\mu_{0.85}$ method was used to evaluate the ductility of wall specimens. This method defines the ductility ($\mu = \Delta u/\Delta y$) as the ratio between ultimate displacement and the displacement corresponding to 0.85 of maximum load on the ascending branch of the monotonic envelope (Todut et al., 2014). The term Δu

corresponds to drift ratio at the point that horizontal load value falls to 80% of the maximum horizontal force (i.e. 20% degradation).

Fig. 3.14 shows the variation of ductility coefficient of wall specimens. Taking into account only squat wall specimens, it can be concluded that there is a direct relation between the wrapped area of the wall and the wall ductility coefficient; increase in the wrapped area significantly increases the ductility coefficient. This seems to be reasonable since the lateral behaviours of squat shear walls are mainly controlled by shear. This conclusion was also supported by the results of other researchers, such as Kheyroddin and Naderpour (2008).

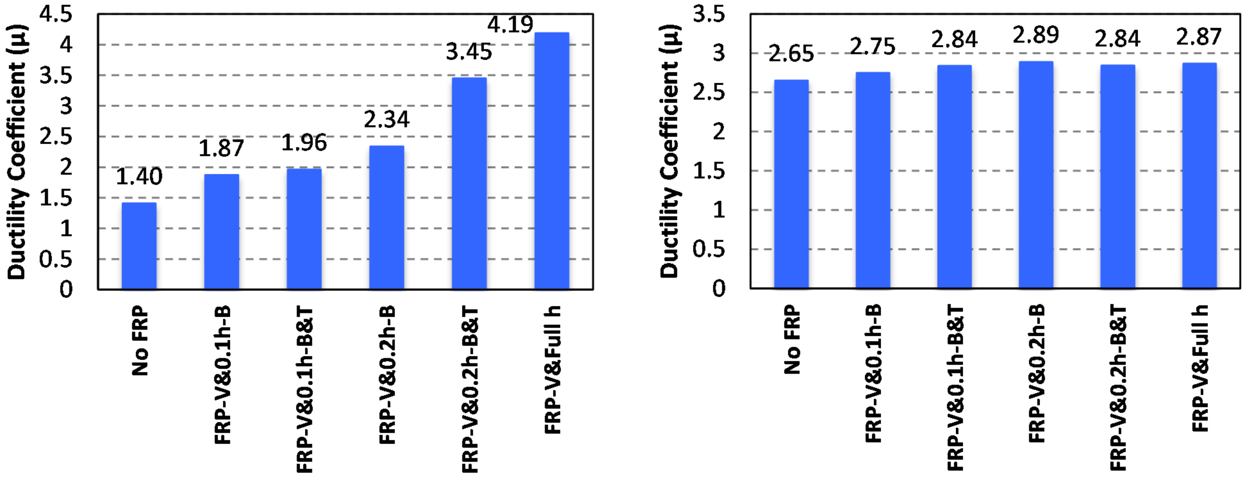

(a) (b)

Fig. 3.14. Evaluating the Displacement Ductility of Walls, a) Squat Walls, b) Walls with Intermediate Aspect Ratio

Results for walls with an intermediate aspect ratio in Fig. 3.14.b demonstrate that FRP strengthening has no significant effect on the ductility of these walls. Moreover, in this case, the wall fully covered by FRP wraps has developed a lower ductility compared to a wall with 20% covered area. Hence, full horizontal FRP wrapping is recommended for squat walls.

A quantitative comparison shows that by using studied FRP strengthening schemes, the ductility of the wall could be raised by up to 198% and 9% in squat walls and walls with intermediate aspect ratio respectively.

3.2.6 Conclusions

The effectiveness of FRP-strengthening on lateral response of RC shear walls was investigated in the current study, using nonlinear FE analyses. Pushover analyses of shear walls were performed, and results showed that:

- FRP strengthening can enhance the lateral performance of RC shear wall by increasing the wall ultimate load capacity up to 49%, as well as the ultimate drift, energy dissipation and ductility.
- Energy dissipation capability of walls improved in both IO and LS performance levels. Total energy dissipation increased up to 135% and 67% for squat walls and walls with intermediate aspect ratio, respectively.
- By using the proposed strengthening schemes, the ductility of squat walls jumped by up to 198% increase, while only 9% increase was observed in walls with intermediate aspect ratio.

- Energy dissipation capability of walls improved in both IO and LS performance levels. Total energy dissipation increased up to 135% and 67% for squat walls and walls with intermediate aspect ratio, respectively.
- By using the proposed strengthening schemes, the ductility of squat walls jumped by up to 198% increase, while only 9% increase was observed in walls with intermediate aspect ratio.

In further studies, the effect of FRP-strengthening on the response of non-planar shear walls with different geometries and rebar configurations can be conducted. Furthermore, the modelling approach can also be used in predicting the behaviour of repaired walls subjected to minor damages during the earthquakes.

CHAPTER 4

Seismic Collapse Risk Assessment and FRP Retrofitting of RC Coupled C-Shaped Core Walls using the FEMA P695 Methodology

4.1 Abstract

Despite the frequent use of C-shaped reinforced concrete (RC) cores as the primary force resisting system of multi-story buildings, there are still challenges in estimating their inelastic seismic response, especially when they are used as coupled wall system. Recent studies showed the inadequacy of old code provisions in predicting the seismic shear demands of these systems. This deems many existing RC cores structurally deficient and needs to be retrofitted. One alternative is to retrofit RC shear walls using FRP composite materials to enhance the capacity and the ductility of the system. The current paper focuses on two aspects of coupled C-shaped RC core systems: (i) seismic collapse of the system for different torsional sensitivities, and (ii) effectiveness of FRP retrofitting on the seismic response of the structure. Modifications were proposed to the wide column model recently proposed by other researchers to accurately capture the inelastic torsional behaviour of RC cores, including different modes of failure. Moreover, a simplified spring model is proposed to consider the effect of Fiber Reinforced Polymer (FRP) retrofitting with vertical strips as well as X-bracing. The proposed modelling approach is validated against available experimental data. Nonlinear Incremental Dynamic Analysis (IDA) of a typical twelve story RC building structure located in Eastern North America was performed using OpenSEES, following the FEMA P695 methodology. It was shown that although the torsional sensitivity has no significant effect on the inter-story drift ratios of the building, it could significantly decrease the Collapse Margin Ratio (CMR). Combined Shear/Flexural failure was found to be the most common failure mode. Observed results also confirmed that the FRP strengthening could be used as an efficient method for enhancing the collapse resistance of RC

core wall systems. By using a proper strengthening scheme with FRP material, more than 60% increase in the CMR can be achieved for the structural system.

4.2 Introduction

Reinforced Concrete (RC) walls are often used as coupled systems in construction of multi-story buildings because of their advantages in comparison with individual walls such as higher lateral stiffness, lower bending moments on each individual wall, and higher energy dissipation because of the inelastic deformations of coupling beams (El Tawil et al., 2010). These elements have been extensively utilized in medium-rise and high-rise building structures within the past decades. Nowadays, RC coupled shear walls are popular lateral force resisting systems, especially in high-risk seismic zones (Farhidzadeh et al., 2013). The reason behind this trend is that RC coupled walls are significantly capable of controlling the inter-story drift ratio, which has been frequently used as a performance indicator in the design of structures (Carrillo and Alcocer, 2012). Similarly, these structural systems are quite efficient in reducing the associated implication of non-structural elements damage.

The expected energy dissipation mechanism of a ductile RC wall system under lateral deformations is flexural yielding (i.e. plastic hinges) at the base of both the cantilever and coupled wall systems, and at both ends of each coupling beam in a coupled wall system (Boivin and Paultre, 2012). Series of design provisions are specified in the current codes to confine the inelastic response at the wall base. These are aimed at ensuring enough strength against undesirable modes of failure like brittle shear failure (Ghorbanirenani et al., 2012).

Many researchers have conducted both experimental and analytical investigations to identify the behaviour of coupled walls and to improve the performance of these systems. The C-shaped coupled wall system (i.e. core wall) is one of the simplest and is a popular arrangement used in practice. Despite their popularity, however, there have been relatively few studies on the seismic behaviour of these RC structures (Beyer et al. 2008), necessitating research on the seismic performance of C-shaped cores. One of the most important characteristics of these nonplanar wall systems is their response when the structure is subjected to torsional efforts due to the eccentricity of lateral forces. This will be more significant when the structural system is asymmetric in the plan regarding the lateral stiffness and strength distribution. Such a configuration in the plan of a building is prone to have large torsional response during a severe earthquake. Reports and field observations after the past earthquakes showed severe structural damages because of torsional effects (Hart, 1975; Esteva, 1987). A recent investigation by Dizhur et al. (2011) reported significant structural damages, which was apparently caused by a “torsionally sensitive response”, after the Christchurch earthquake in 2011.

Most of the researches carried out in the past focused on the behavior of planar RC walls, including various proposed approaches for predicting their nonlinear flexure-shear interaction behavior (Colotti, 1993; Elwood, 2002; Massone et al., 2006 and 2009; Mullapudi and Ayoub, 2009; Zhang and Xu, 2009; Jiang and Kurama, 2010; Beyer et al., 2011; Panagiotou and Restrepo, 2011; Fischinger et al., 2012). These approaches were mostly based on fibre-section elements such as multiple-vertical-line-elements (MVLE) proposed by Vulcano et al. (1988). The biaxial behaviour of concrete material (e.g. modified compression field theory; Vecchio and Collins, 1986) was also considered in some of these approaches.

On the contrary, experimental researches on the performance of non-planar (e.g. C-shaped) RC walls subjected to lateral loads are very limited. In one of the first attempts, Ile and Reynouard (2005) examined three full-scale U-shaped RC walls under cyclic lateral loading. The purpose of the study was to investigate the behaviour of U-shaped walls against uniaxial and biaxial bending and shear and to compare the design provisions required by two versions of Eurocode 8. A shell model was also developed for simulation of non-planar RC walls. Beyer et al. (2008-a) investigated the bi-directional quasi-static cyclic response of ductile U-shaped RC walls by conducting experimental tests on two half-scale specimens with different thicknesses. The tests mainly focused on the flexural behaviour of walls, considering different directions of loading (two orthogonal as well as diagonal). Results showed the diagonal direction as the most critical direction, in which the maximum moment resisted by the wall was less than the corresponding value calculated by the plastic hinge analysis. Moreover, the displacement capacity of the wall in diagonal direction was found to be smaller than the other two orthogonal directions. A simplified numerical model was also developed by Beyer et al. (2008-b), and a practical approach was proposed for implementation and analysis of U-shaped walls. The numerical approach was based on wide-column analogy and has been shown to produce a reasonable estimation of the inelastic displacement response for slender walls. Constantin and Beyer (2012) used a three dimensional (3D) multilayered shell element model for U-shaped walls to capture their local as well as the global behaviour under diagonal loading. The model was developed using the software VecTor4 developed at the University of Toronto (Wong and Vecchio, 2003), and was found to be accurate in terms of loading capacity of the wall, but not for its displacement ductility.

Lowes et al. (2013) examined three 1/3 scale C-shaped wall specimens, representing a part of a coupled RC core system, under biaxial loading protocols. Results of cyclic tests showed that bidirectional loading significantly affected the response for displacement cycles in excess of the yield displacement. At these displacement levels, bidirectional loading resulted in a significant reduction in the stiffness of the wall in the direction parallel to the web of the wall (loading activating strong-axis bending).

Recently, Lu and Panagiotou (2014) presented a three-dimensional (3D) cyclic model for non-planar RC walls, based on beam-truss analogy. The model was able to predict the effects of flexure-shear interaction, considering the biaxial behaviour of the concrete material, and account for mesh-size effects. Although the proposed model has been revised several times and they validated the model for three reinforced concrete T-shaped, C-shaped, and I-shaped section wall specimens, the modelling approach was found to be complicated in terms of calibration of truss members and material properties (Kolozvari, 2013). The results were also sensitive for precisely tracking the displacement responses of walls in a wide-amplitude.

In the design of RC shear walls, the fundamental design equations are mainly based on the "plane sections remain plane" assumption, which is unable to capture the shear lag effects related to flexure and warping torsion. Such effects can be substantial in non-planar (C-, I- or T-shaped) wall configurations, and might affect the response of the structural system in seismic excitations.

A study Boivin and Paultre (2010) was shown that the seismic provisions proposed by NBCC 2005 and the CSA standard A23.3-04 (2014) for the design of ductile RC shear walls buildings could considerably underestimate the shear demand, especially at the base of the shear wall system. This issue would be due to the fact that the amplification effects from the higher modes of vibration cannot be efficiently taken into account by the current capacity design methods. In the seismic design of a multi-story ductile RC wall, this can result in a considerable underestimation of the seismic force demand. Hence, more studies need to be conducted on the seismic performance of these structural systems and effectiveness of available retrofitting methods, both of which were investigated in the current study. A recent research on the seismic design of RC shear walls (Pelletier and Léger, 2017) showed that a more reliable shear force demand can be achieved by using the recently introduced dynamic shear amplification factor by CSA A23.3-14 (2014). This factor should be applied to account for the inelastic effects of higher modes and to prevent brittle failure occurrence. However, RC shear wall systems that are designed based on the CSA A23-04 need to be controlled for shear demands. Moreover, CSA A23.3-14 excludes the coupled and partially coupled walls from the clause specified for "accounting for inelastic effects of higher modes". Furthermore, NBCC 2015 provides a higher mode factor M_v which is equal to 1.0 for coupled shear walls except in very occasional cases, T_a=2.0 seconds and $S_{0.2}/S_5$=65, in which the M_v is equal to 1.03. On the contrary, it was found by Boivin and Paultre (2010) that the shear envelope calculated based on the capacity design method is significantly unconservative in either the cantilever or coupled wall directions. Therefore, more accurate evaluations for the future designs and retrofit options for existing building are essential.

FEMA P695 (FEMA 2009) has proposed a methodology to assess the seismic performance of structures. This methodology provides a rational method for evaluating the adequacy of proposed response parameters, including the response modification factor (R), the system over-strength factor (Ω_0), and deflection amplification factor (C_d) of a seismic force resisting system. Using nonlinear analysis techniques, the methodology combines certain steps to develop and analyze a specific structural model for probabilistic collapse assessment of structure. The methodology explicitly considers uncertainties in selected ground motions, modelling approach, design, and test data.

Due to lack of an extensive database on detailed experimental data for non-planar RC walls in the literature, among the modelling approaches available for predicting the response of these systems, only a few have the capability of tracking the cyclic response of C-shaped RC cores when subjected to modest to significant shear-flexure interaction (SFI). In some models, more studies have to be conducted on the sensitivity of outputs to input parameters (e.g., material properties and modelling assumptions), and more validation against global behaviour (load-displacement) and local responses (rotations, stresses, strains) are needed. Hence, the WCM proposed by Beyer et al. (2008-b), which incorporates coupling effects between axial/flexural and shear responses under cyclic loading conditions, was found to be the most practical modelling approach in this case because of its simplicity of use and the accurate results captured by the model.

The objective of this paper is to quantitatively evaluate the seismic collapse risk of coupled RC core walls with different torsional sensitivity factors and to assess the effectiveness of FRP retrofitting of these structural systems on their seismic responses. This evaluation is done according to the FEMA P695 (FEMA 2009) methodology. A modified wide column model (WCM) was proposed for simulating the nonlinear response of RC cores, considering the torsional effects. A simplified 3D macro model was developed using OpenSEES (Open System of Earthquake Engineering Simulation, McKenna et al. 2013), and subsequently, experimental test data from the literature were used to validate the accuracy of the modelling approach. Moreover, a simplified spring model is proposed to consider the effectiveness of using FRP wrapping, vertical strips and X-bracing for retrofitting purposes. After validating the numerical model, nonlinear Incremental Dynamic Analysis (IDA) of a typical twelve story RC structure located in eastern part of Canada was performed, following the FEMA P695 methodology. A series of 50 artificial ground motions proposed by Atkinson (2009) were used for IDA analyses of the RC core in different levels of torsional sensitivity. The analyses results were compared to determine the dynamic collapse capacity of the structure before and after FRP retrofitting.

4.3 Analysis Methodology

Several analytical models have been developed in the literature to capture the response of shear/core walls. However, when the nonlinear response is of interest, the behaviour of these C-shaped RC cores is significantly affected by the interaction between axial force, flexure, and shear. Precise capturing of these effects has essential difficulties in macro scale numerical modelling (Ile and Reynouard, 2005). Although the adoption of the model according to cyclic material properties (micro-scale modelling) can lead to more accurate results in this case, more numerical effort is a major drawback. Hence, in the current study, macro modelling method was selected for numerical analysis of C-shaped core systems, using the most accurate boundary conditions and constraints. The numerical modelling in this paper is based on a WCM proposed by Beyer et al. (2008-b) for inelastic analysis of C-shaped walls. Though Pelletier and Léger (2017) showed that the accuracy of numerical results could be improved by increasing the number of modules in the WCM, especially for high ductility levels, numerical analysis requires more computational efforts and implementation difficulties. Hence, because of the high number of analysis tend to be done in the current work, specifying only one module appeared to provide reasonable accuracy in the seismic analyses of RC buildings. The modelling approach is explained in detail in this section.

4.3.1 Geometry and configuration of the model

A schematic diagram of the numerical model of the wall is shown in Fig. 4.1.a, including the configuration of nodes and elements. The discretized fibre section of the core wall is also presented in the Fig. 4.1.b.

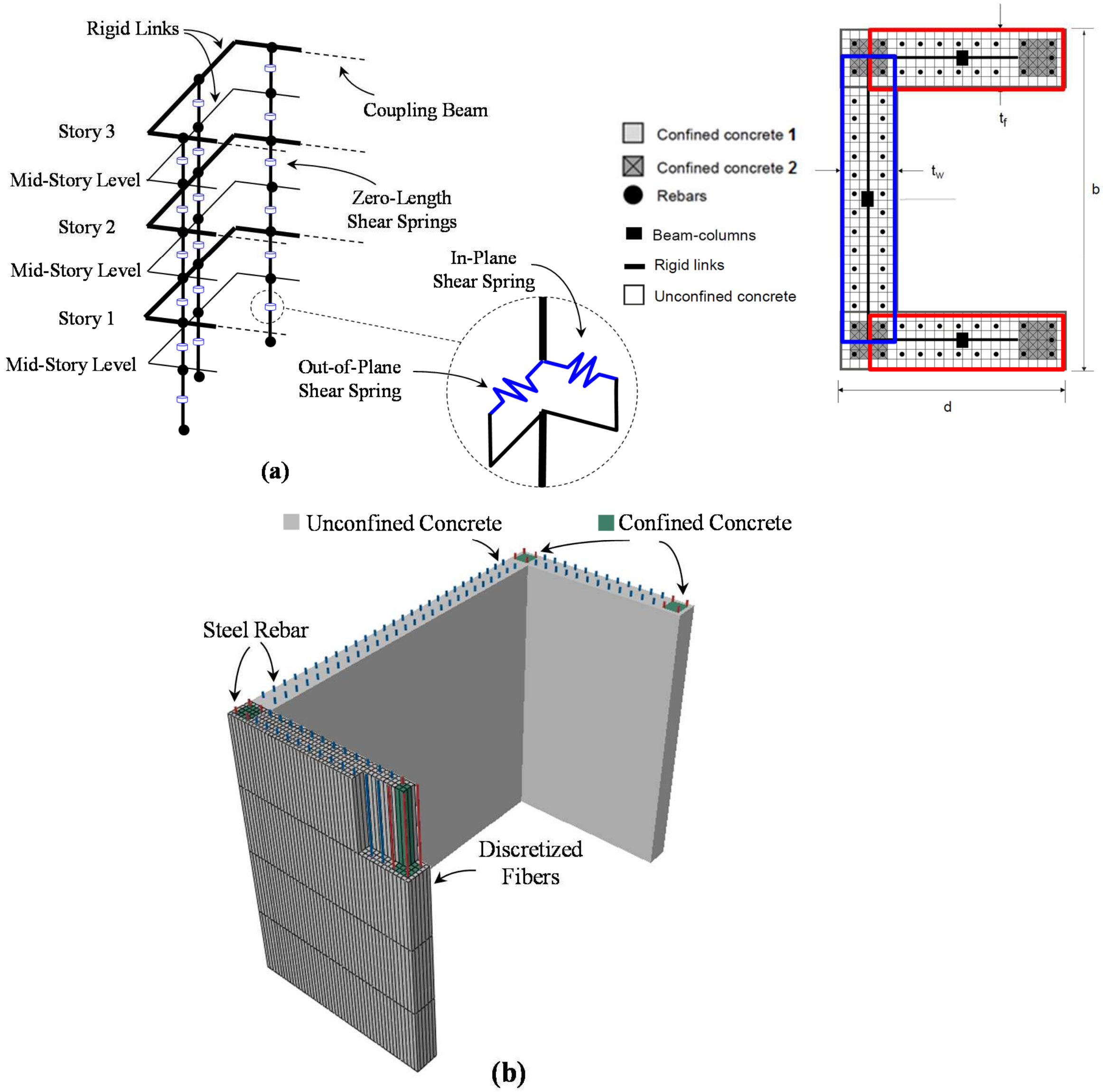

Fig. 4.1. Wide Column Model for the C-shaped core wall, a) isometric view of an RC core elements and position of the wall elements and links, b) subdivision of the fibre cross-section of C-shaped RC core

4.3.1.1 General WCM model

Each C-shaped section of each core wall was separated into three rectangular regions (i.e., two flanges and the web), modelled by vertical elements in their centroid representing each segment. A horizontal link was used along the length of each segment to connect these vertical elements. The corner areas of core section were divided into two and assigned to the web and flange sections. Hence, the bars located in inner corners of the section was assigned two times (web and flange sections) to represent the outer bars as well.

Beam-column elements with displacement-based formulation were used for piers in the model by assuming a constant axial strain and a linear distribution for the curvature. Both the axial elongation and the combined axial load and bending moment interaction of RC sections could be taken into account by using these elements. These effects are of utmost importance in the simulation of C-shaped RC cores in which the variation of axial load in elements is expected when subjected to a bi-directional loading protocol.

Each element was set to have five gauss integration points along its length. Full base fixity was assumed for the walls and no soil-structure interaction was considered based on the results of a study by NIST (2010). However, slippage in the wall-footing intersections was considered which is explained in the next section. The number of concrete and reinforcement fibres was different for the models but was selected to create fine discretization in the section and to provide desirable accuracy. The confinement effect of the concrete materials was considered based on the model proposed by Mander et al. (1988).

As for the displacement-based elements, proper selection of the element length controls undesirable strain localization, in which plastic deformations will start to occur in the first layer of elements at the base of the wall, while the elements in the upper layers are still at the elastic stage (Calabrese 2010). Stafford-Smith and Girgis (1986) suggested limiting the spacing between horizontal links to about 20% of the overall height of the wall. Consequently, in the verification models in the current work, the height of each wall specimen was divided into four equal-length part. Keeping the same aspect ratio approximately, the number of divisions was selected to be equal to two in each story (i.e. two rigid links) in the simulation of the 12-story building.

As for the number of elements between links, Beyer (2008-b) found that a WCM with two elements between successive links suits most engineering studies. Therefore, extra nodes between successive links were introduced to equally divide the available height into two elements (Fig. 4.1.a).

The horizontal links should have common nodes at the corners, and modelled as rigid links, except for a torsional flexibility (Beyer et al., 2008-b; Reynouard and Fardis, 2001). The torsional flexibility (GK_t) assigned to the horizontal links was calculated using the Eq. 4.1 suggested by Xenidis et al. (1993):

$$GK_t = G\frac{h_l\, t_w}{3} \qquad (4.1)$$

where G is the shear modulus of concrete, K_t is the torsional stiffness, h_l is the rigid link spacing, and t_w is the thickness of the wall. Validation of the results against available hysteresis results from the experimental test was conducted to examine the adequacy of the number of elements in the model. The selected number of elements was found to be sufficient for predicting the cyclic response of C-shaped walls, which will be explained in the next sections.

Because of the lack of shear flexibility in the selected type of elements, the two elements defined between successive rigid links were connected by zero-length spring elements to consider shear flexibility of the wall segments. Hence, for both the in-plane and out-of-plane directions, horizontal translational degree of freedom in the zero-length element assigned to have stiffness corresponding to the shear stiffness of the two wall elements connected to the spring element. EqualDOF type constraints were also used to couple the other degrees of freedom of the two nodes. Unlike the moment capacity of walls, estimation of shear capacity of even a rectangular wall comes with large differences between available code provisions or shear models published in the literature. Beyer et al. (2008-b) suggested that, for both the flanges and the web of RC core wall, the shear behaviour can be considered as elastic behaviour, by using the uncracked section shear stiffness (k_s) computed by the Eq. 4.2:

$$k_s = \frac{G\, A_s}{h_l} \qquad (4.2)$$

where A_s was taken as 80 percent of the gross section area of each segment (i.e. flanges and web). This assumption will have a considerable lack of accuracy once a shear mechanism in the wall segment occurs. In this study, a bilinear trend was used instead to consider the shear failure in the wall segment response. Shear strain at yield was set to be equal to 0.0015 based on the study by Massone (2006).

4.3.1.2 P-δ effects

The lateral displacement of the building caused by the seismic (and wind) loads on the lateral resisting system of the structure is usually accompanied by further displacements because of the P-δ effect. In the simulation of the 12-story building (Fig. 4.2), effects of geometrical nonlinearity were also considered in the model by adding a P-δ frame (leaning column analogy). This P-δ frame was located at a distance equal to the typical span length of the building (6 meters) in East-West direction (Fig. 4.2.c). The frame consisted of rigid co-rotational beam-column elements (columns) and horizontal rigid links connecting the columns to the rigid links at the corner of the section web at each story level. Because of the 3D modelling approach used in the study, P-δ frame elements were also connected to the core through diagonal truss elements, to avoid instability of the system. The floor mass was computed at the story levels and was lumped at the corresponding nodal point. The tributary area considered for the P-δ frame at each story level was set as the total floor (or roof) area, out of which the tributary area of the core wall system was excluded. A significant effect was observed on the lateral response of the building due to the P-δ effect, especially for higher lateral displacements.

4.3.1.3 FRP elements

Effects from horizontal FRP wrapping on the behaviour of wall segments were considered through confining the concrete materials and increasing the stiffness of horizontal springs in the way that represent the shear stiffness of FRP wraps and the wall section itself. Guidelines proposed by ACI 440 (2008) for FRP strengthening of reinforced concrete shear walls were considered at this step. Vertical FRP strips and FRP X-bracing were also modelled using uniaxial “elastic-no tension” material object in OpenSEES. Two options were available for implementing the vertical FRP strips: a) fibre based definition of FRP layers into the section of each wall segment, similar to the proposed scheme by ACI 440 (see Fig. 4.3.c), b) using separate spring elements connecting the corresponding nodes on the rigid links. To obtain comparable results with the wall strengthened using X-braced FRP strips, the second option was used in the current study. The elements were defined by connecting the corner nodes, middle nodes, and the nodes created at the end of flanges to define the coupling beams in the model (Fig. 4.3.b). Moreover, vertical FRP wrapping of the coupling beams was considered for all the FRP strengthened models. The schematic drawing of the FRP retrofitting layout is shown in Fig. 4.5.

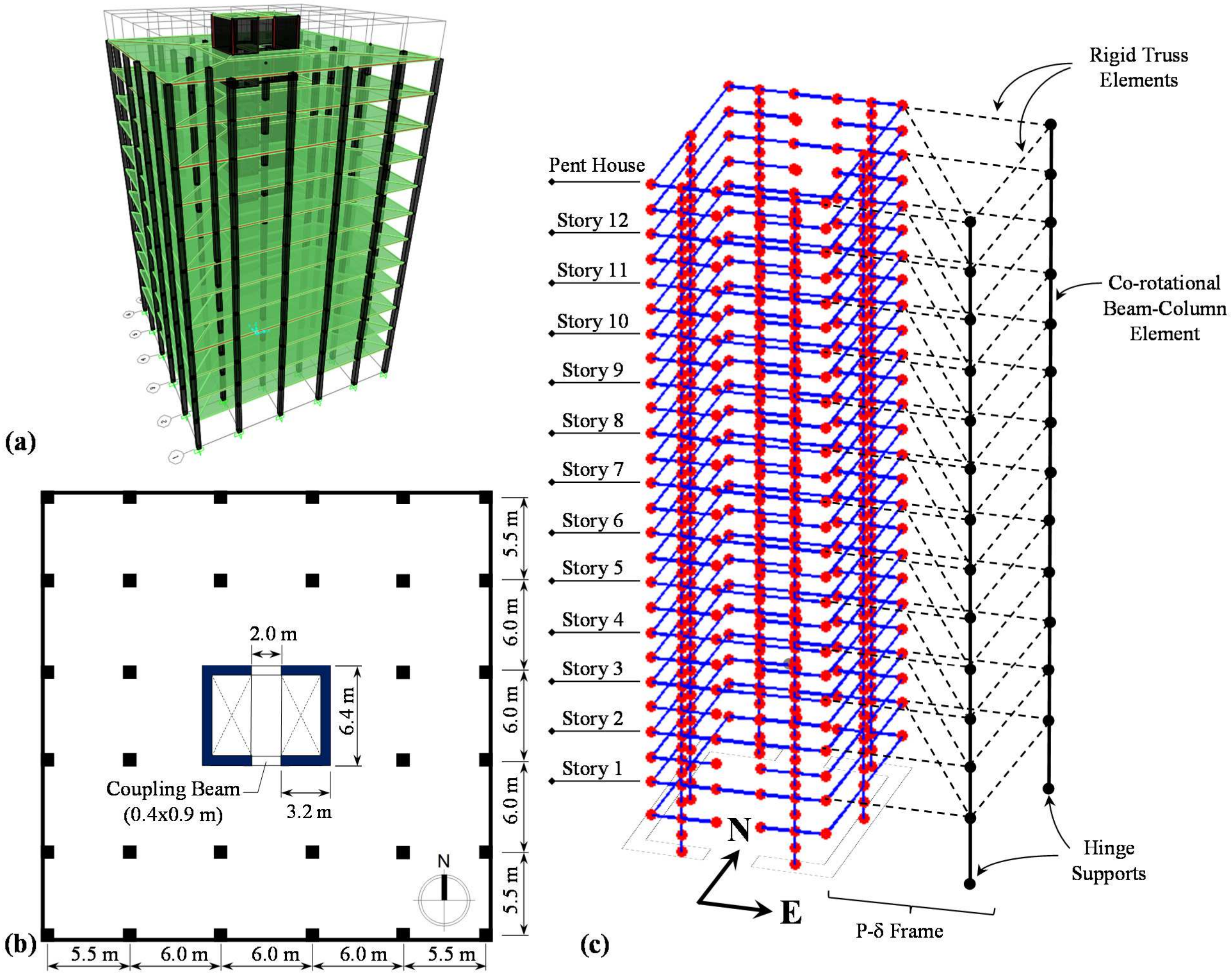

Fig. 4.2. a-b) 3D layout and the plan view of the 12-story building coupled C-shaped RC core, c) Wide Column Model for the 12-story core wall.

Perfect anchoring of FRP strips was assumed at story levels. Moreover, to create a debonding rule in the midstory height, the nodes on the rigid link were duplicated, and the bond-slip relationship model proposed by Lu et al. (2005) was implemented into the model. Tributary areas of FRP strips were calculated, and slip based relationships were defined to couple the nodes in the model. The other degrees of freedom were slaved by using EqualDOF constraints in OpenSEES.

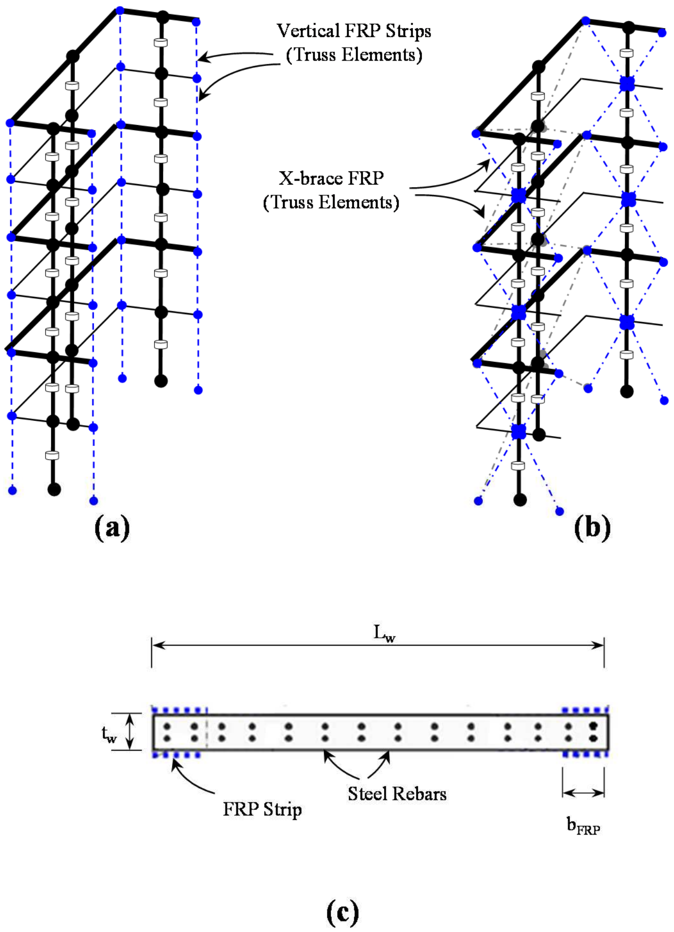

Fig. 4.3. Configuration of FRP elements in the model: a) Vertical FRP strips, b) X-brace FRP strips, c) Typical cross section of core wall segments with vertical FRP strips proposed by ACI 440-2R (2008)

4.3.1.4 Strain penetration effects

In addition to the flexural/shear deformations in RC members, the end rotation due to reinforcement slip has to be captured in the model, which occurs not only at large inelastic stage but also during the elastic response of members (Huang, 2012). This effect, called as strain penetration effect, was shown by experimental observations (Kowalsky et al. 1999) to have a relatively considerable contribution in the total lateral deformation of flexural members

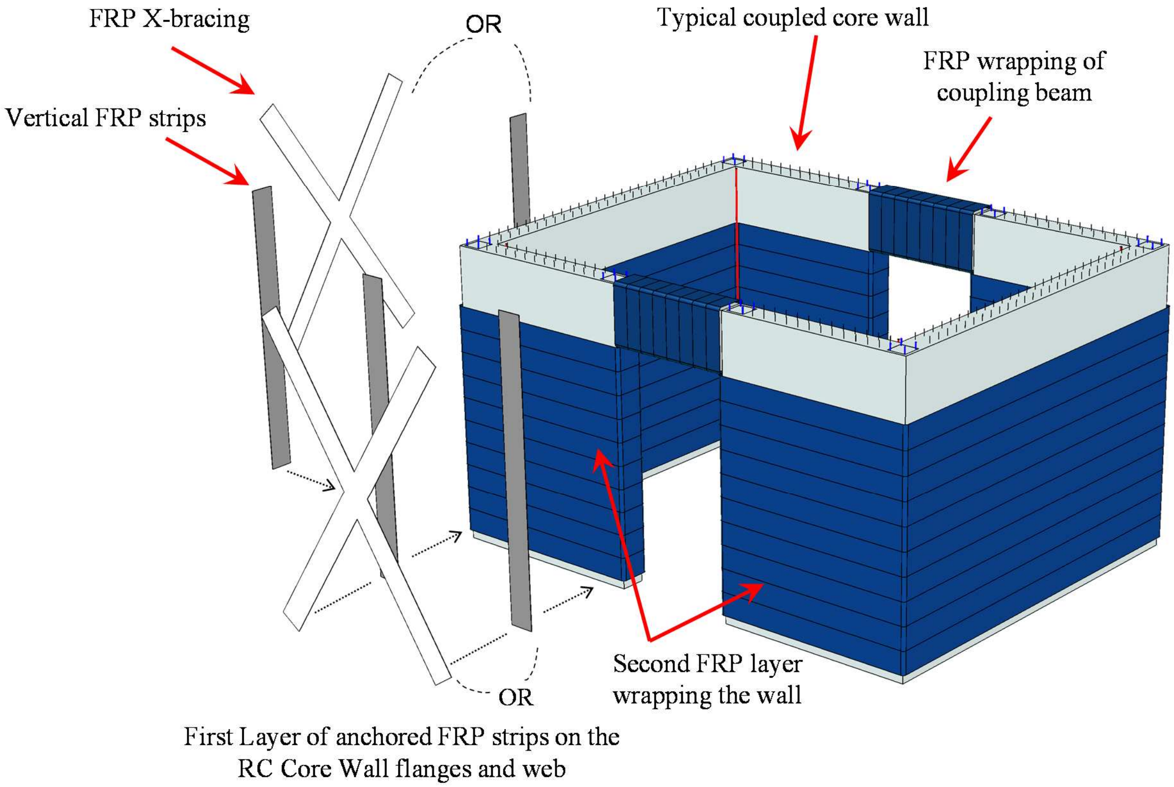

Fig. 4.4. Schematic drawing of the FRP retrofitting layout

This effect should not be ignored in the modelling of RC cores to avoid overestimating the stiffness of RC core, which can lead to underestimating the lateral drift of the core wall. Since the fibre-based modelling approach corresponds to the basic assumption that plane sections remain plane (i.e. perfect bond condition), the strain penetration effect can be considered by utilizing a zero-length element at the base of wall segments. Fig. 4.5 shows the schematic location of a zero-length element at the base of the fibre-based model of the RC core.

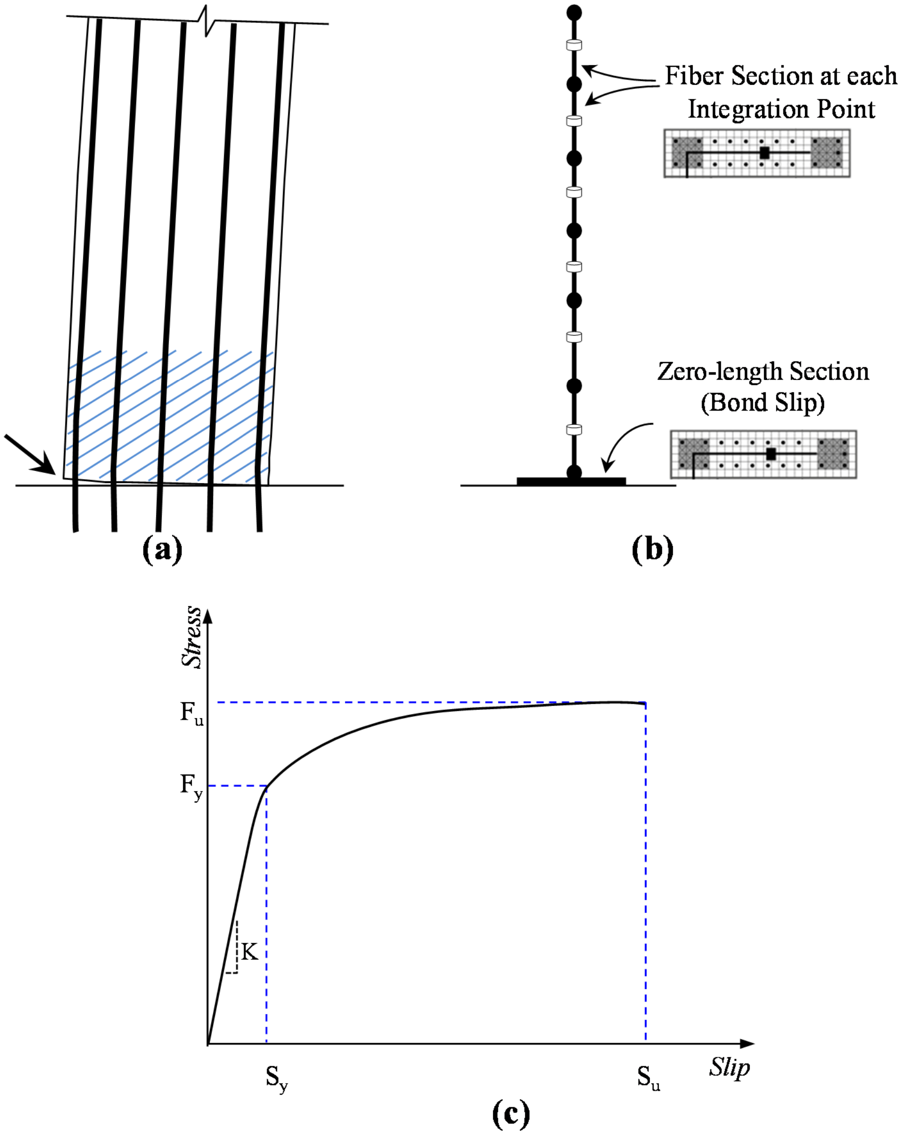

Fig. 4.5. Bond-slip components used to consider the strain penetration effects: a) Schematic drawing, b) Fiber-based model for each core wall segment, c) Stress-displacement relationship developed by Zhao and Sritharan (2007)

In the current work, the stress-slip model proposed by Zhao and Sritharan (2007) was used to take into account the strain penetration effects in the wall to footing intersections. OpenSEES Bond_SP01 material was used to represent the vertical reinforcements. This model considers the total bar slip caused by strain penetration effect as a function of a certain level of stress in the bar (Zhao and Sritharan 2007).

4.3.2 Failure criteria for materials

Mechanical properties of materials were defined based on the reported test data or nominal strength of concrete and steel reinforcement using the available empirical equations. However, confinement effects on the concrete behaviour have also been taken into account. Fig. 4.1.b shows the distribution of different materials in the cross-section of the RC cores simulated in the numerical model.

Modified Kent and Park model (Scott et al, 1982) was used to define the nonlinear constitutive laws for concrete fibres (Concrete02 in OpenSEES). Though the model proposed by Chang and Mander (1994) has few more accurate features such as better simulation of the gradual closure of cracks under cyclic loading and calibration of the stress-strain data resulted from experimental tests (Concrete07 in OpenSEES), the Concrete02 model was used because of its simplicity of calibration. The model offers a reasonable level of accuracy while holds its simplicity, and is extensively used even though some constitutive models developed afterward were proved to be more precise and comprehensive (Orakcal et al., 2006). The monotonic compressive stress-strain ($\sigma_c - \varepsilon_c$) curve can be described by three regions as following (see Fig. 4.6):

$$\sigma_c = Kf_c'\left[2\left(\frac{\varepsilon_c}{\varepsilon_0}\right) - \left(\frac{\varepsilon_c}{\varepsilon_0}\right)^2\right] \qquad ; \varepsilon_c \leq \varepsilon_0 \qquad (4.3)$$

$$\sigma_c = Kf_c'[1 - Z(\varepsilon_c - \varepsilon_0)] \qquad ; \varepsilon_0 < \varepsilon_c \leq \varepsilon_{20} \qquad (4.4)$$

$$\sigma_c = 0.2Kf_c' \qquad ; \varepsilon_c > \varepsilon_{20} \qquad (4.5)$$

The initial tangent moduli (E_c) can be calculated by the following expressions:

$$E_c = 4500\sqrt{f_c'} \text{ (MPa)} \qquad (4.6)$$

In the above equations, ε_0 denotes the strain corresponding to the concrete peak stress under compression, ε_{20} denotes the strain corresponding to 20% of maximum compressive stress, K is the confinement modification factor, f_c' is the concrete compressive strength (unconfined peak stress in cylinder test) in MPa, and Z represents the slope of strain softening. A set of linear stress-strain relations was subsequently proposed by Yassin (1994) to define the hysteretic unloading and reloading rules for the material model (Fig. 4.6). The tensile strength of concrete ($f_t^{'}$) was calculated as following:

$$f_t' = 0.623\sqrt{f_c'} \tag{4.7}$$

where $f_t^{'}$ and $f_c^{'}$ are expressed in MPa. In the current work, a similar form of the stress-strain curve was used for both unconfined and confined concrete. Peak compressive strength for the confined concrete was calculated based on the method proposed by Mander et al. (1988), for different regions of the cross sections, which are depicted in Fig. 4.1.b.

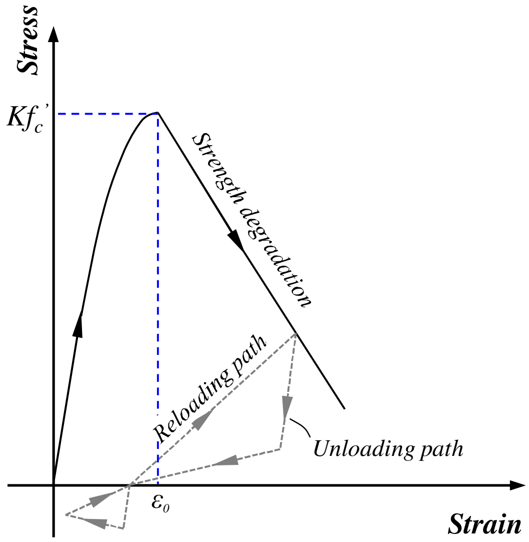

Fig. 4.6. Hysteretic unloading and reloading rules used in the model (Yasin, 1994)

For steel reinforcement, the Giuffré-Menegetto-Pinto hysteretic model (Filippou et al., 1983) with default parameters (Steel02 in OpenSEES) was adopted to represent the nonlinear transition from elastic stage to strain hardening stage for cyclic and pushover analyses. This model defines the steel material objects with isotropic strain hardening. Input data to define this relationship are elastic modulus E_s, yield strength f_y and the coefficient which defines the relationship between the elastic modulus and the slope of tangent after reaching the yield point. In cases that the ultimate strength of the steel bars are not known (e.g. the studied 12-story building in the current work), the hardening ratio equal to 0.5% can be assumed that is suitable for most steel bars. No bond-slip was considered with respect to the surrounding concrete.

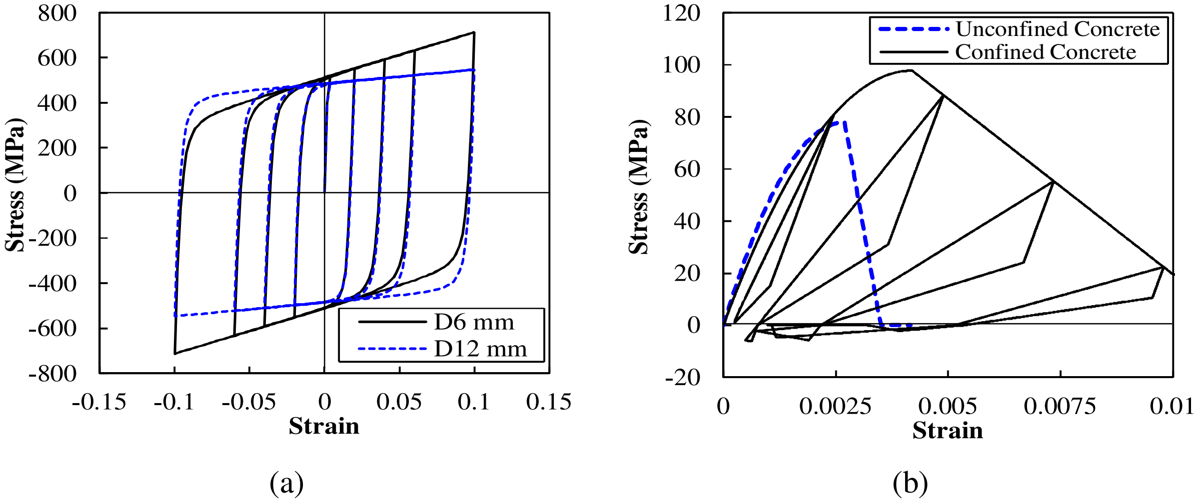

(a) (b)

Fig. 4.7. Sample hysteresis stress-strain behaviour of material assigned in the numerical model: a) Reinforcement, b) Concrete

Table 4.1 shows the sample material parameters adopted for the verification cases as well as the 12-story building. Sample plots of the cyclic material behaviour employed for the steel and concrete fibres in the numerical model of the specimen TUA are depicted in Fig. 4.7. Details and mechanical properties of different FRP layers are shown in Table 4.2. Same FRP materials were used in all the retrofitting schemes.

4.4 Model Validation

In order to validate the modelling approach and the assumed failure criteria, two RC wall specimens from different experimental programs available in the literature were selected to be modelled using the above-explained approach. The results of the numerical simulations were compared with the reported experimental results. The lateral force acting on the wall is normalized to the maximum shear resistance allowed by the ACI 318-14 ($V_n = 0.666A_{cv}\sqrt{f_c'}$).

Table 4.1. Sample material parameters for the OpenSEES model

Specimen	Concrete Material							Steel Material		
	Region	f_c''	e_0	K	f_{cu}	e_u	f_t	Rebar	f_y	f_u
TUA (Beyer et al., 2008-a)	Unconfined region	-77.9	0.0037	1	-15.58	-0.010	5.50	D12mm bars	488	595
	Confined region 1	-87.3	0.0039	1.121	-16.70	-0.010	5.69	D6mm bars	518	681
	Confined region 2	-97.8	0.0042	1.256	-19.57	-0.010	6.16			
Wall8 (Lowes et al., 2013)	Unconfined region	-35.2	0.0025	1	-7.03	-0.010	3.69	#2	531	592
	Confined region 1	-41.5	0.0027	1.18	-8.30	-0.010	4.01	#4	441	630
12-Story Building	Unconfined region	-30.0	0.0023	1	-6.00	-0.010	3.41	10M	400	545
	Confined region 1	-31.2	0.0024	1.0404	-6.24	-0.010	3.48	25M	400	545

Table 4.2. Details and mechanical properties of different FRP layers

FRP Layer	Type	Thickness (mm)	Strip width	Number of layers	f_u (MPa)	E_{FRP} (MPa)	$\varepsilon_{rupture}$ (%)
Horizontal wraps	CFRP	0.2	---	2	1,062	102,000	1.05
Vertical FRP strips	CFRP	0.2	800	1	1,062	102,000	1.05
FRP X-braces	CFRP	0.2	1200	1	1,062	102,000	1.05
Vertical wraps (coupling beams)	CFRP	0.2	---	2	1,062	102,000	1.05

4.4.1 Core walls tested by Beyer et al. (2008-b)

Beyer et al. (2008-b) performed four tests on C-shaped shear walls with different wall thickness and reinforcement configurations to evaluate the performance of this type of wall geometry when subjects to bi-directional loading protocols. The specimen TUA was a C-shaped RC core with 2720 mm height, 150 mm wall thickness, 1300 mm width and 1050 mm depth. The top of the core was attached to a concrete collar with 300 mm thickness, providing joints to be attached to three actuators (two acting on flanges and one on the web). As it is noted in Table 4.1, D6 and D12 type bars were used for steel reinforcement in flanges/web and corner boundary zones, respectively. A high strength concrete material ($f_c^{'}$ = 77.9 MPa) was used for constructing the core. The core was subjected to an axial force equal to 780 kN (core wall self-weight plus the loads applied by experimental equipment). This axial force was kept constant during the cyclic test, and a bidirectional loading protocol with consecutive cycles corresponding to different levels of ductility was applied on the core.

Fig. 4.8.a shows the normalized load-drift data at the top of the wall from the experimental test along with corresponding results from the numerical model. The figure demonstrates a good agreement between the experimental records and the numerical predictions with small discrepancies. The small discrepancies between the test results and numerical predictions, though are acceptable for such a simplified model, might be due to the shear flexibility assigned for rigid links, by which the compatibility of strains between the flange and web section at the corner of the core was violated.

4.4.2 Core walls tested by Lowes et al. (2013)

The experimental work of Lowes et al. (2013) consisted of testing three C-shaped RC core specimens with similar designs representing the bottom three stories of a modern mid-rise building. The objective of their study was to investigate the impact of bidirectional loading on the earthquake performance of isolated C-shaped walls and C-shaped walls in coupled core-wall systems.

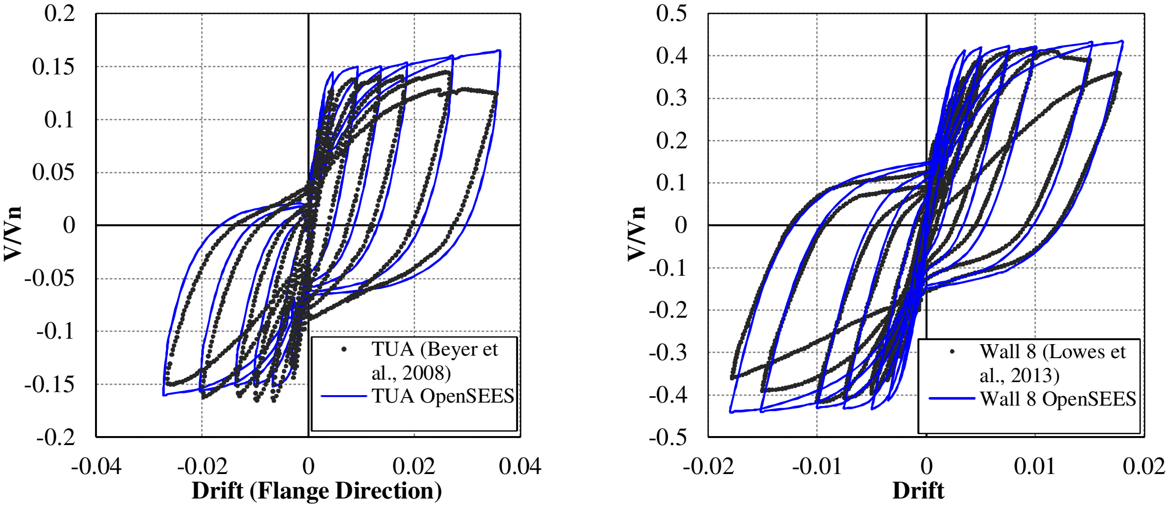

(a) (b)

Fig. 4.8. Comparison of results from the numerical model and the experimental data: a) Specimen TUA tested by Beyer et al (2008-a), b) Specimen Wall8 tested by Lowes et al. (2013)

The specimen Wall8 was a C-shaped RC core with 3660 mm height, 152.4 mm wall thickness, 3048 mm width and 1219.2 mm depth. A wall cap with 457.2 mm height was constructed to apply a cruciform lateral load pattern to the wall specimen. The axial load maintained constant (equal to 5% of the gross axial capacity: $0.5f_c^{''}A_g = 1361$ kN) when the wall was subjected to lateral loading in the strong direction. As can be seen in Fig. 4.8.b, there is a very good correlation between the normalized lateral load-drift curves from the numerical analysis and those from the experimental work of Lowes et al. (2013). As the displacement increases, however, the numerical model shows a bit higher load resistance than the experimental one. The model was able to capture the yielding and failure mode (bar rupture) in the specimen.

Comparisons between the main output results from the numerical models and the experimental works showed satisfactory accuracy of the model in tracking the lateral response of C-shaped RC cores. Peak loads in reversal cycles, as well as the general load-displacement trends, matched well with the experimental observations. Table 4.3 shows the summary of the results from the verification models including the maximum shear capacity of RC cores, V_{max}, lateral rigidity, $K_{initial}^{loading}$, unloading stiffness in the cycle corresponds to approximately 1% drift,

$K_{@1\%drift}^{unloading}$, yield displacement, Δ_y, and the applied shear corresponding to the yield point, V_y. From the comparisons shown, it could be seen that the average error percentage for each set of the compared results shows that the failure criteria, as well as the modelling approach used for the numerical analysis, were acceptable.

The validated model was then used to perform a seismic collapse risk assessment on a typical 12-story building, with different levels of torsional sensitivity.

Table 4.3. Summary of verification results: numerical predictions in comparison to the experimental data

	Numerical to Experimental ratio				
Specimen	V_{max}	$K_{initial}^{loading}$	$K_{@1\%drift}^{unloading}$	Δ_y	V_y
TUA (Beyer et al., 2008-a)	0.98	0.97	1.02	0.92	1.06
Wall 8 (Lowes et al., 2013)	1.06	1.10	1.07	0.94	1.10

4.5 IDA Analysis of a Typical 12-Story Building

A 12-story RC building in Montreal, Canada with subsoil condition class D was selected for seismic collapse risk assessment of the structure using the FEMA P695 methodology. The building design was initially provided by Concrete Design Handbook (2004), according to the National Building Code of Canada (NBCC, 2005) and the CSA A23.3-04 (2004).

Each floor consisted of 5.5 m end spans and three 6 m interior spans in both horizontal directions, resulting in outside to outside plan dimension of 29.75 m. Considering the penthouse on the roof, the total height was 48.65 m; consisted of a 4.85 m high first story and typical story height equal to 3.65 m. The 3D view and the plan of the building were presented in Fig. 4.2. The gravity system consisted of flat plate slabs with 200 mm thickness, supported by 550 mm square columns. The core wall measured 6.4 m by 8.4 m, outside to outside of the walls, consisted of two C-shaped RC core with 400 mm thickness and connected through 900-mm-deep coupling beams, which was positioned centrally in the plan of the building. The reinforcement layout at the end of flanges and at the web-flange junctions was considered as 4-25M bars, while 10M vertical and horizontal bars with 200 mm spacing were considered as the distributed reinforcement. The reinforcement for coupling beams was considered as 8-20M diagonal bars. Geometrical details of the coupled RC core wall is shown in Fig. 4.9. The building was designed to be built using 30 MPa strength concrete and 400 MPa strength steel reinforcement. The structural damping was considered by means of mass and stiffness proportional Rayleigh damping.

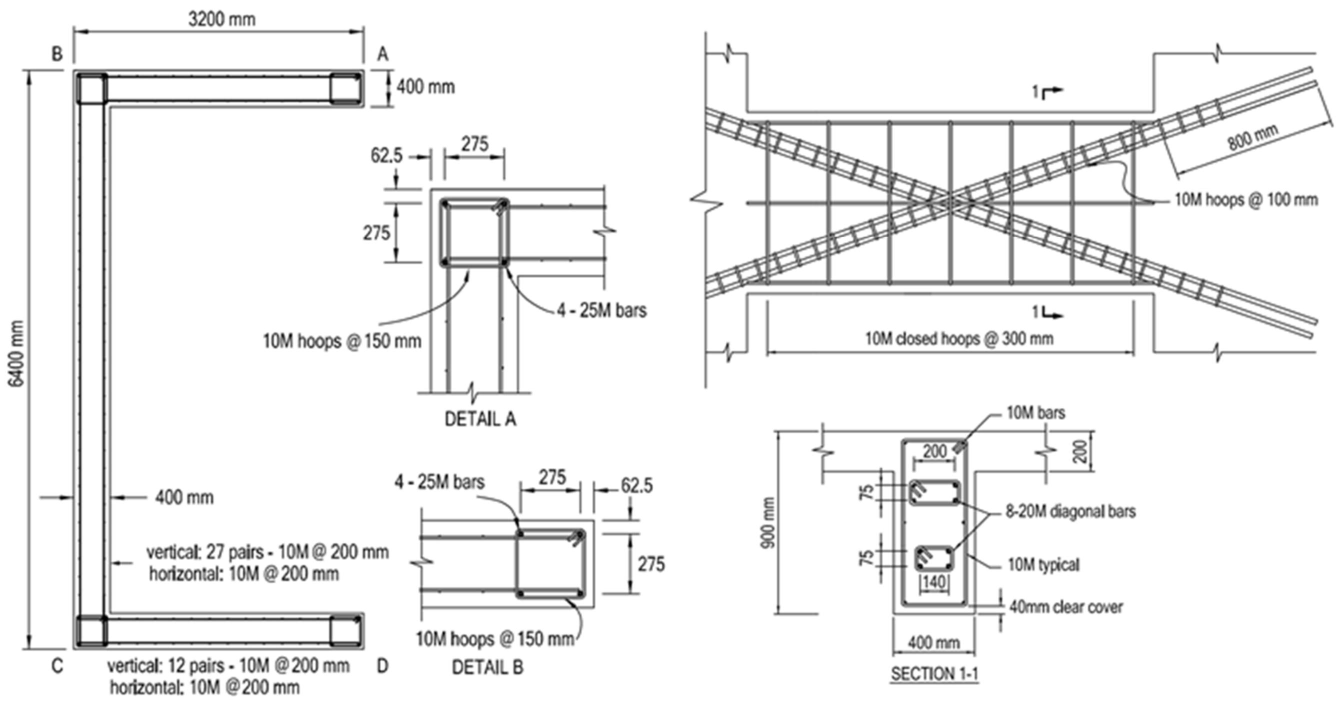

Fig. 4.9. Geometrical and reinforcement configuration of the coupled RC core wall: a) C-shaped walls, b) Coupling beams (CSA A23.3-04, 2004)

A damping ratio of 5%, which is a typical value for RC buildings, was assigned to the first two modes of the structure. Although the Rayleigh damping feature in OpenSEES can formulate the damping matrix using the initial, current, or last committed stiffness matrix, only the initial stiffness matrix was used in the current work. However, the rigid truss elements that link the frame and the leaning columns were excluded.

4.5.1 Torsional sensitivity

Both Canadian and American design codes present limits for classifying "torsional sensitivity" of building structures. Torsional sensitivity in a building is defined as the maximum value B, among floors, where B_x computed at level x is $B_x = \delta_{max}/\delta_{ave}$. In the aforementioned expression, δ_{max} is the maximum story displacement, calculated at level x considering %10 accidental torsion, at one end of the structure, and δ_{ave} is the corresponding average displacement for the two endpoints of the structure. According to NBCC 2015, when the value of B exceeds 1.7 and $I_EF_aS_a(0.2) > 0.35$, the building is considered torsionally sensitive. In this case, results from static analysis are not adequate anymore, and a 3D dynamic analysis is required for evaluating the response of structure. In the current work, since the building selected for the collapse assessment was designed according to the Canadian standards, the NBCC 2015 limit was used to classify torsional irregularities. The IDA results first collected for three different levels of torsional sensitivity (B=1.0, 1.7 and 2.5). The torsional flexibility of the building was increased by providing an inherent mass eccentricity e_x through artificial shifting of the centre of mass (CM) from the centre of rigidity (CR). This amount of e_x was obtained based on an iterative procedure by analyzing the structure against the design level earthquake. Moreover, the accidental torsion equal to 5% was taken into account. Subsequently, the model with B = 1.7 was analyzed with different FRP strengthening schemes, including horizontal FRP wrapping, using vertical FRP strips, and X-bracing with FRP strips.

4.5.2 Ground motion selection

According to FEMA P58-1 (2012), "a minimum of 7 ground motion records is recommended because of extremely poor prediction of record-to-record variability obtained in small suite of ground motions" (Michaud and Léger, 2014), regardless of the spectral matching efficiency. Moreover, using more than 44 ground motion records for seismic collapse risk assessment of buildings is recommended by FEMA P695 (2009) to achieve more reliable results. However, high computational effort is always a drawback. Since the considered building was located on Site Class D in Montreal, and due to the lack of real seismic wave data from the past in Canada, in the current work, 50 spectrum-compatible artificial accelerograms were used for IDA analysis of the building. These records were divided into two groups: a) "Near-Fault" includes ground motions of magnitudes (M) between 5.5 and 6.5 with closest distance to fault, R_{fault}, from 0 km to 15 km; b) "Far-Field" consists of ground motions of magnitudes (M) between 6.75 and 7.25 with R_{fault} from 10 km to 90 km. These accelerograms were developed by Atkinson (2009) for the esign of structures in Montreal, and their characteristics including magnitude M, closest distance to fault R_{fault}, peak ground acceleration PGA, and max velocity to max acceleration ratio v/a are presented in Table 4.4. As it is shown, records in the group (a) produce higher v/a ratio which confirms the expected response of structures under the near-fault excitations.

It should be noted that there are no specific provisions in NBCC 2015 regarding scaling of ground motions. However, it is indicated that scale factors should be applied for all selected ground motions to match the Uniform Hazard Spectrum (UHS) at the first mode period of the structure. Moreover, scaled ground motions should match or have larger intensity than the UHS at all the points representing the period of higher modes. On the other hand, ASCE/SEI-7 (2010) states that the mean of the 5% damped response spectra for a group of seven or more ground motions should fit or be above the UHS in all the points within the range of $0.2T1 - 1.5T1$.

Table 4.4. Unscaled selected ground motions with magnitude (*M*), closest distance to fault (R_{fault}), peak ground acceleration (PGA), and max velocity to max acceleration ratio (*v/a*)

Near-fault records					Far-field records				
Event	*M*	R_{fault} (km)	PGA (*g*)	*v/a*	Event	*M*	R_{fault} (km)	PGA (*g*)	*v/a*
east6d1.1	6	12.8	0.707	0.0663	east7d1.1	7	13.8	0.627	0.0802
east6d1.2	6	12.8	0.523	0.0496	east7d1.2	7	13.8	0.623	0.1150
east6d1.3	6	12.8	0.591	0.0276	east7d1.3	7	13.8	0.764	0.0594
east6d1.4	6	12.5	0.671	0.0559	east7d1.4	7	15.3	0.767	0.0832
east6d1.5	6	12.5	0.471	0.0448	east7d1.5	7	15.3	1.183	0.0781
east6d1.6	6	12.5	0.678	0.0415	east7d1.6	7	15.3	0.866	0.0533
east6d1.7	6	12.8	0.491	0.0686	east7d1.7	7	14.2	0.840	0.0909
east6d1.8	6	12.8	0.593	0.0443	east7d1.8	7	14.2	0.813	0.0706
east6d1.9	6	12.8	0.370	0.0413	east7d1.9	7	14.2	1.152	0.0919
east6d1.10	6	12.8	0.366	0.0483	east7d1.10	7	14.9	0.968	0.0795
east6d1.11	6	12.8	0.410	0.0502	east7d1.11	7	14.9	0.997	0.0522
east6d1.12	6	12.8	0.515	0.0404	east7d1.12	7	14.9	0.902	0.1139
east6d1.13	6	10.7	0.570	0.0419	east7d1.13	7	14.8	0.950	0.0702
east6d1.14	6	10.7	0.568	0.0362	east7d1.14	7	14.8	0.944	0.0714
east6d1.15	6	10.7	0.941	0.0318	east7d1.15	7	14.8	0.928	0.0935
east6d1.16	6	13.6	0.606	0.0596	east7d1.16	7	20.6	0.635	0.0833
east6d1.17	6	13.6	0.461	0.0416	east7d1.17	7	20.6	0.606	0.0496
east6d1.18	6	13.6	0.609	0.0540	east7d1.18	7	20.6	0.403	0.1003
east6d1.19	6	14.4	0.510	0.0483	east7d1.19	7	20.1	0.668	0.0817
east6d1.20	6	14.4	0.433	0.0798	east7d1.20	7	20.1	0.487	0.0609
east6d1.21	6	14.4	0.484	0.0491	east7d1.21	7	20.1	0.655	0.0754
east6d1.22	6	14.4	0.452	0.0357	east7d1.22	7	14.3	0.960	0.0732
east6d1.23	6	14.4	0.557	0.0333	east7d1.23	7	14.3	0.768	0.0853
east6d1.24	6	14.4	0.649	0.0507	east7d1.24	7	14.3	1.101	0.0787
east6d1.25	6	14.4	0.535	0.0448	east7d1.25	7	19.6	0.538	0.0804
Average	6	13.1	0.550	0.0474	*Average*	7	16.1	0.806	0.0789

Considering the ASCE/SEI 7-10 (ASCE 2010) standard requirements, all selected records were scaled to reach a mean spectrum that matches the design spectrum over the interval of $0.2T_1 - 1.5T_1$, where T_1 is the first mode period of vibration obtained by conducting a modal analysis in OpenSEES. Fig. 4.10 shows the response spectra of the scaled ground motions together with the mean spectrum and the design spectrum proposed by NBCC for Montreal.

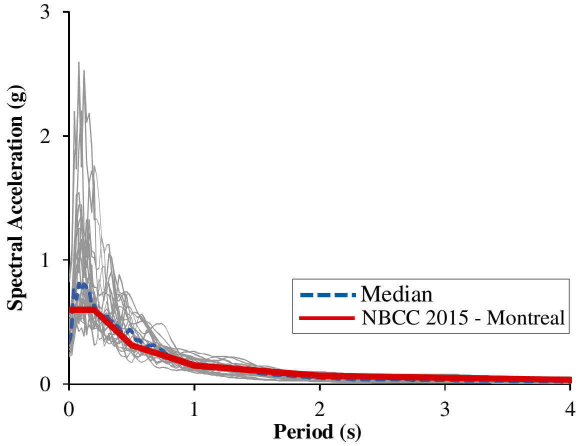

Fig. 4.10. Response spectra for 50 scaled artificial ground motion records for Montreal

4.5.3 Nonlinear structural analysis

4.5.3.1 Building configurations

Dynamic time history analyses were performed to evaluate the collapse capacity of the building in the East-West direction, which is the direction that the RC core wall acts as coupled wall system. As mentioned, the 12-story RC core system was analyzed in six different configurations as followings:

- Original structure with torsional sensitivity value B ≈ 1.0;
- Original structure with torsional sensitivity value B = 1.7;
- Original structure with torsional sensitivity value B = 2.5;
- Structure with B = 1.7 and RC wall strengthened with horizontal FRP wrapping (H-FRP);
- Structure with B = 1.7 and RC wall strengthened with horizontal wrapping and vertical FRP strips (H&V-FRP);

- Structure with B = 1.7 and RC wall strengthened with horizontal wrapping and X-brace FRP strips (H&X-FRP).

Each structure was analyzed for 50 ground motion records and with at least 16 different intensity factors. Hence, 2400 time history analyses were conducted in total. The number of analysis steps and the time-step of the analysis should be specified properly to execute the dynamic time history analysis. The time-step used in time history analysis must be less than or equal to the sampling rate of the input ground motion. In the current work, the time-step of each analysis was specified to $\Delta t = 0.01$ sec, which is half of the sampling rate of the input ground motions.

4.5.3.2 Analytical failure modes

Despite the several failure criteria adapted for the material behaviour in the model, some failure modes could not be directly simulated in the numerical model because of some limitations in OpenSEES. These failure modes have to be assessed through post-processing of the recorded data. Considering the criteria proposed by Gogus and Wallace (2015), the following failure modes were tracked in the model outputs:

- Steel buckling/fracturing: Though the MinMax feature in OpenSEES was used to limit the strain capacity of steel bars, failure of a single row of rebars (wall thickness direction) was found to be insufficient to cause collapse (Thomsen and Wallace, 1995). Thus, buckling or fracture of the reinforcement positioned at approximately one-quarter length of each segment of the core wall was considered as the collapse point (Fig. 4.11.a).
- Concrete crushing: Similar criteria established for concrete crushing, in which the failure corresponds to reaching the crushing strain for concrete fibres positioned at approximately one-quarter length of the wall segment, in the unconfined region. As for the confined region, crushing strain at the innermost confined concrete fibre was tracked to find the crushing point (Fig. 4.11.b, c).

- Axial failure: 5% drift limit at axial failure was selected for a 12-story archetype, based on the model developed by Wallace et al. (2008) for lightly reinforced wall piers, and considering the details published by GCR 10-917-8 (NIST 2010).
- Shear/flexural failure of the wall: By developing the cracks in the tension wall in a coupled shear wall system, penetration of the flexural cracks near the compression edge is expected. As a result, more contribution of the dowel action of the vertical reinforcement is expected for resisting the sliding shear failure. This increases the probability of the shear sliding failure in the wall (Pauly and Priestly, 1992). This was captured by applying the corresponding limits on the horizontal springs representing the shear behaviour of the wall segments.

Failure of the coupling beams was not considered as a collapse mechanism for the system. In fact, the coupling beams act as a fuse in ductile coupled shear walls, dissipating most of the seismic energy input. However, as a second energy-absorbing line of defence, the walls should also be detailed to accommodate plastic hinging at the base without excessive loss of strength to avoid a collapse after all the coupling beams have yielded (Honarparast and Chaallal, 2015).

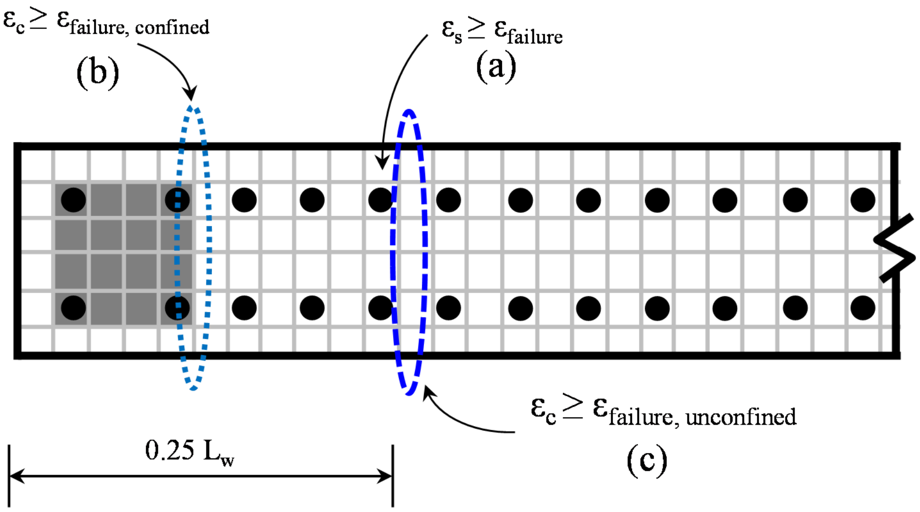

Fig. 4.11. Reinforcing steel and concrete failure mode criteria: a) steel rebar failure; b) concrete crushing in confined region; c) concrete crushing in unconfined region

It is worth mentioning that once a failure mode happens at a certain time of the analysis ($t_{failure}$), the estimated redistribution of forces after $t_{failure}$ would not be reliable. However, in the current work, $t_{failure}$ was considered as failure moment and the results afterward were excluded from the analysis data. This post-processing procedure helps in minimizing the effects of the observed errors in capturing the post-peak strength degradation (i.e. discrepancies in the results of verification models) on the collapse assessment.

4.6 Results and Discussion

The impact of dynamic loads and higher modes on the performance of the structures designed based on the old CSA A23.3-04 was investigated using incremental dynamic analyses (Vamvatsikos et al. 2002), before and after the FRP retrofitting. IDA analyses were conducted on each archetype according to the FEMA P695 methodology. After post-processing the data using the aforementioned criteria, IDA response plots were created. Fig. 4.12 presents the IDA response plot of the structure in different configurations.

4.6.1 Collapse fragility of the structures

A collapse fragility function was developed for each case by cumulative distribution of the results obtained from the IDA analyses. The selected Intensity Measure (IM) selected in the current study was the 5% damped spectral acceleration at the fundamental period of the structure [$Sa(T_1,5\%)$]. The fragility curve presents the intensity of the ground motion versus the collapse probability (Ibarra et al., 2002). Though the scaling was performed for different IM levels in the IDA analysis, the fragility function fitting method proposed by Baker (2015) was used to derive the fragility function.

The collapse probability of 50% for the structure, called as median collapse capacity (S_{CT}), and the collapse margin ratio (CMR) were calculated from the IDA results. Fig. 4.13 depicts a sample fragility curve obtained from the results of IDA analyses using the function fitting method proposed by Baker (2015). The sample set of data used in the development of the fragility curve (Fig. 4.13) is presented in Table 4.5, in which the term “Fraction Causing Collapse” is simply the ratio of the collapsed cases to the total number of analyses for each IM level. The term “Theoretical Fragility Function” corresponding to each IM level was calculated through a normal distribution for the specified median and standard deviation. The median and dispersion for the data set were calculated using the proposed method by Baker (2015).

The CMR, as a primary parameter for characterizing the collapse safety of structures, could be calculated as S_{CT}/S_{MT}, where S_{MT} is the maximum considered earthquake (MCE) intensity corresponding to the fundamental period T, and S_{CT} is the median collapse intensity from the IDA results. It is worth mentioning that the fundamental period (T) used in the FEMA P695 (2009) methodology is the strength-based period which is presented in the Section 12.8 of ASCE/SEI 7-10 (2010).

Fig. 4.14 compares the fragility curves obtained from IDA analyses of building structures. As it can be seen from Fig. 4.14.a, the torsional sensitivity can dramatically affect the fragility function of the building in the IDA analyses. The median collapse capacity (S_{CT}) of the RC core system decreased about 8% by reaching the torsional sensitivity of $B = 1.7$. As for the structure with $B = 2.5$, the reduction in the mean failure capacity was more than 36% in comparison with the one with $B \approx 1.0$. The fragility function was also very steep for the case with $B = 2.5$.

As for the strengthened RC cores, the structure strengthened with horizontal FRP wrapping showed an increase in the collapse capacity up to 17% (Fig. 4.14.b), while more significant improvement obtained by H&V-FRP and H&X-FRP configurations showing 44% and 63% increase respectively (Fig. 4.14.c-d). Moreover, FRP strengthened walls were found to obtain flatter fragility response in comparison with original walls. Table 4.6 shows the summary of collapse assessment results of RC cores evaluated in the current study.

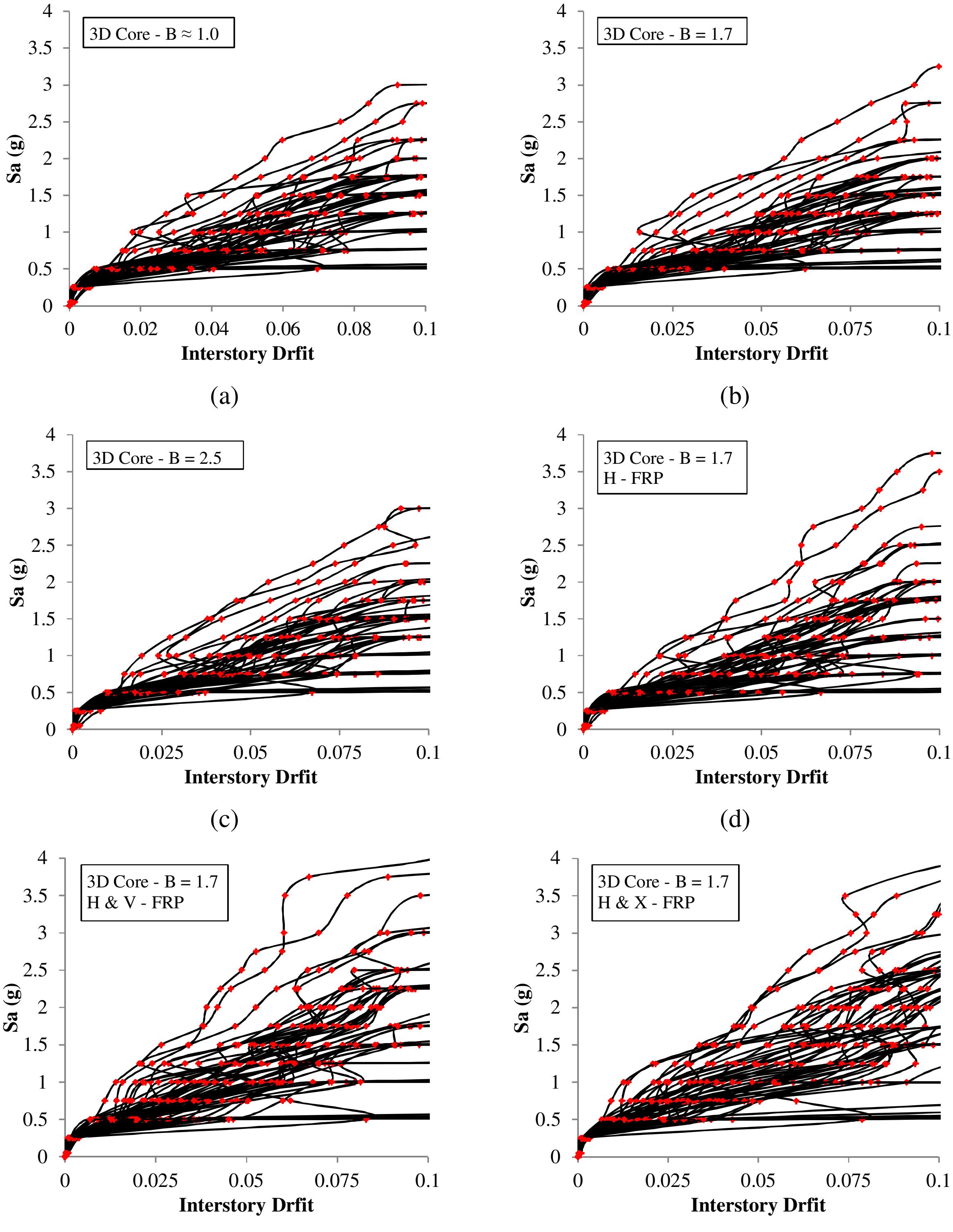

(a) (b) (c) (d) (e) (f)

Fig. 4.12. Incremental dynamic analysis (IDA) response plot of 12-story building: a) B ≈ 1.0, b) B = 1.7, c) B = 2.5, d) B = 1.7 (strengthened with horizontal FRP wrapping), e) B = 1.7 (strengthened with horizontal and vertical FRP), f) B = 1.7 (strengthened with horizontal and X-brace FRP).

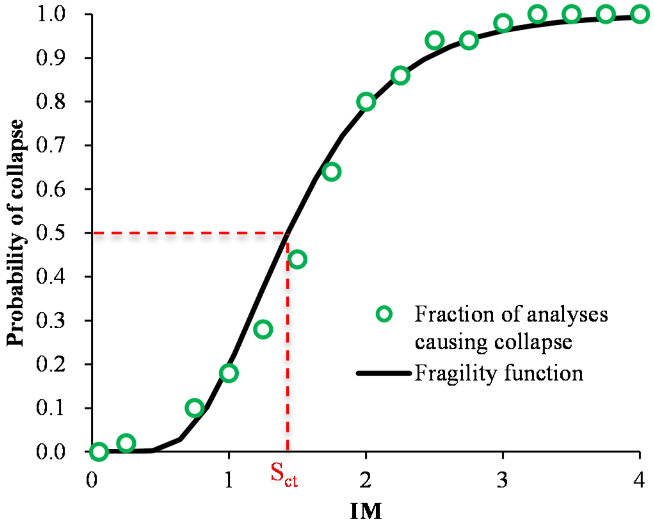

Fig. 4.13. Sample fragility function fitting for the results of IDA analyses

Table 4.5. Sample data set used in the development of the sample fragility curve

IM	Number of analyses	Number of collapses	Fraction causing collapse	Theoretical fragility function
0.05	50	0	0.00	0.00
0.25	50	0	0.00	0.00
0.75	50	6	0.12	0.05
1	50	11	0.22	0.18
1.25	50	15	0.30	0.34
1.5	50	21	0.42	0.51
1.75	50	26	0.52	0.65
2	50	37	0.74	0.76
2.25	50	43	0.86	0.84
2.5	50	46	0.92	0.89
2.75	50	48	0.96	0.93
3	50	48	0.96	0.95
3.25	50	48	0.96	0.97
3.5	50	49	0.98	0.98
3.75	50	50	1.00	0.99

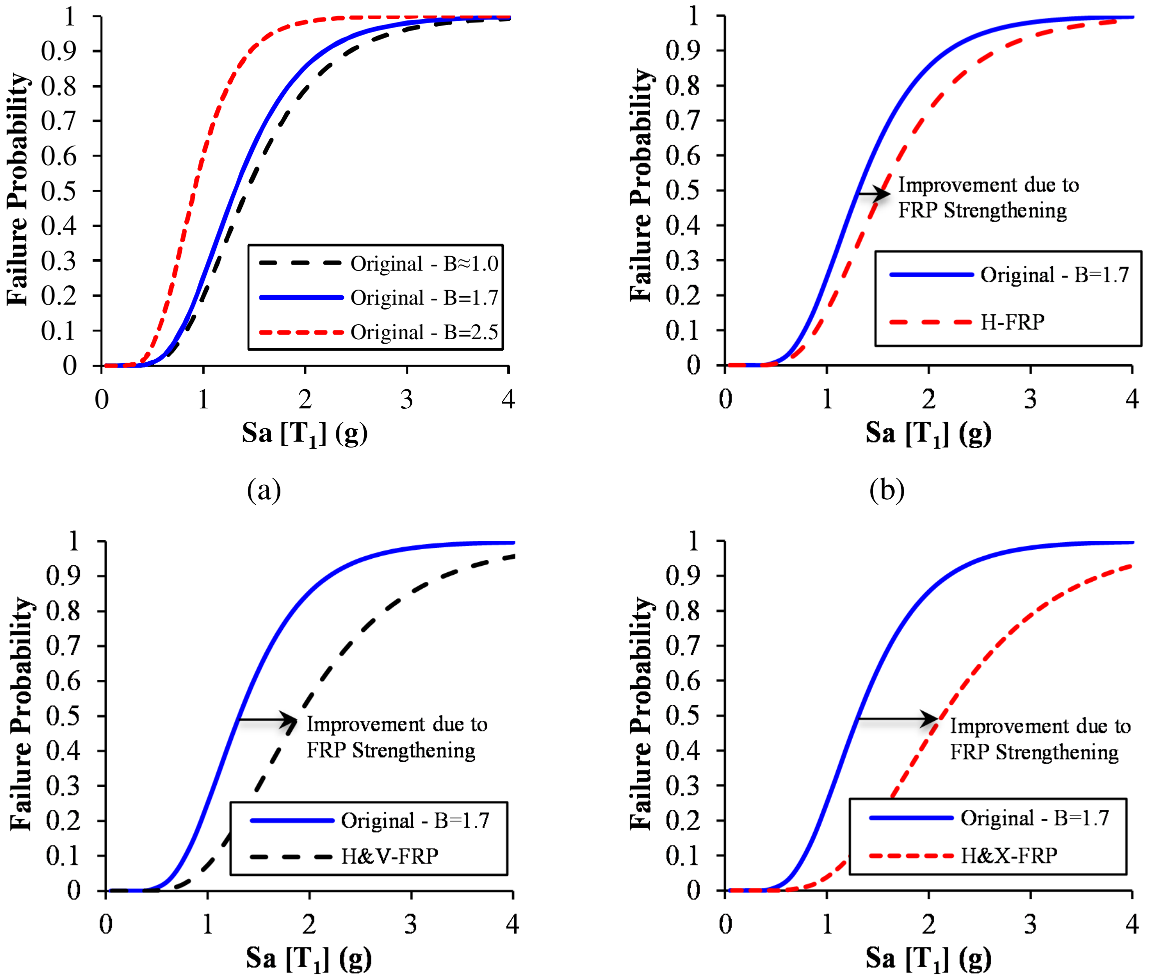

(a) (b)

(c) (d)

Fig. 4.14. Fragility curves of original and strengthened buildings: a) Original RC core with different torsional sensitivity, b) Strengthening with horizontal FRP wrapping, c) Strengthening with horizontal FRP wrapping and vertical FRP strips, d) Strengthening with horizontal FRP wrapping and X-brace FRP strips

Table 4.6. Summary of collapse assessment results for RC cores

Archetype ID	Configuration	Strengthening Scheme	B	S_{MT} [T] (g)	S_{CT} [T] (g)	CMR
O1	Original	----	B ≈ 1.0	0.174	0.910	5.2
O2	Original	----	B = 1.7	0.174	1.310	7.5
O3	Original	----	B = 2.5	0.174	1.429	8.2
S1	Strengthened	Horizontal FRP	B = 1.7	0.174	1.544	8.9
S2	Strengthened	Horizontal and Vertical FRP	B = 1.7	0.174	1.889	10.9
S3	Strengthened	Horizontal and X-brace FRP	B = 1.7	0.174	2.136	12.3

4.6.2 Fragility curves at different performance levels

Based on the results by Carrillo and Alcocer (2012), although the available drift limits for the performance levels defined by FEMA-356 (2000) and ASCE41-13 (2013) are not safe for the non-ductile structures, these acceptance levels can be conservatively used for ductile structures. It should be acknowledged here, however, that damage states after retrofitting of the buildings will be shifting in terms of inter-story drift ratio depending on the retrofitting method used. For the sake of comparison, in the current work, damage states was kept constant correspond to the proposed performance levels by ASCE41-13, and fragility curves for different configurations of the structure were developed accordingly. Immediate Occupancy (IO), Life Safety (LS) and Collapse Prevention (CP) performance limits were considered for the seismic collapse assessment. Fig. 4.15 presents the results of collapse probability for different buildings. A comparison between the median collapse capacities is presented in Table 4.7 for different limit states. As it can be seen, though the mean collapse capacities were similar for the original structures with different torsional sensitivities in IO level, structures with higher torsional sensitivities resulted in 20~25% less failure capacity in the LS and CP levels, respectively. Close results were obtained for the retrofitted structures at the IO level, while up to 15% and 20% increases were observed for the failure capacities in the LS and CP levels, respectively. These drift based results for the structures retrofitted with H-FRP and H&V-FRP were relatively close, while a significant enhancement was obtained by using H&X-FRP retrofitting.

4.6.3 Inter-story drift ratio

Since the inter-story drift is an important indicator of structural behaviour in the performance-based seismic analysis, this section presents the variation of maximum inter-story drift during the IDA analysis. For each building configuration, post-processing was performed on the statistical data resulted from the IDA analysis. The results are presented in terms of box plots in Fig. 4.16, in which, for each story, the black solid line shows the range of variation from the lower bond to the upper bond. The green box presents the inter-quartile range (Q3-Q1), which starts from the lower quartile and finishes at the upper quartile, and the vertical solid line inside the box indicates the median. As it is shown, the lower bond and the upper bond for the maximum inter-story drift ratios of the original structures were approximately 0.5% and 1.4% respectively. Although the median of the drift data for each story fluctuates along this range, it peaks at 0.89%, 0.82% and 0.79% for the structures with $B \approx 1.0$, $B=1.7$, and $B=2.5$ respectively. This shows a decrease up to 12% in the peak median by increasing the torsional sensitivity of the structure.

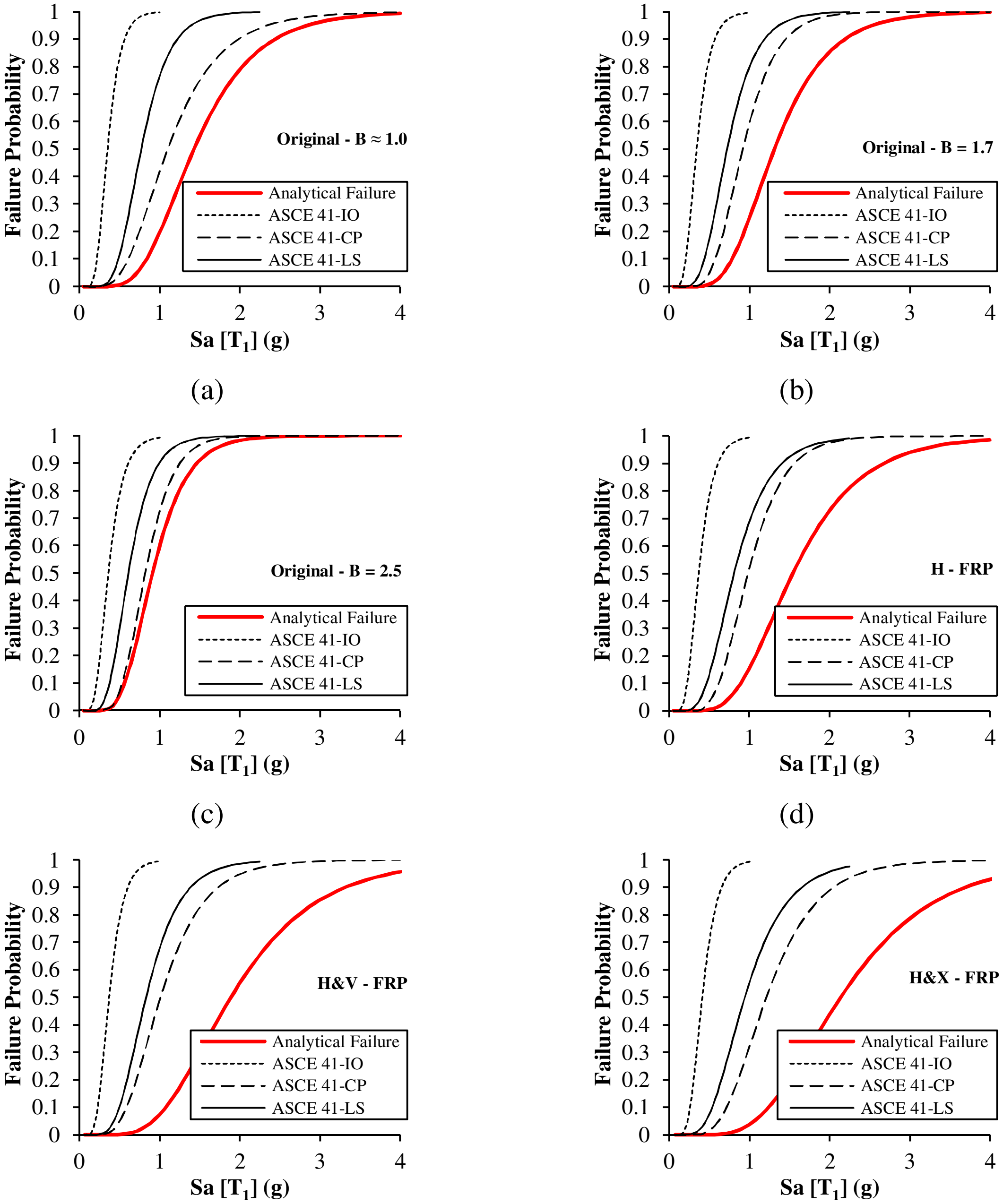

(a) (b)

(c) (d)

(e) (f)

Fig. 4.15. Fragility curves for different performance levels of original and strengthened buildings

Table 4.7. Median structural capacity associated with the drift limit proposed by ASCE41-13

Archetype ID	Description	Limit state		
		IO	LS	CP
O1	Original - B ≈1.0	0.35	0.77	1.1
O2	Original - B = 1.7	0.34	0.72	0.92
O3	Original - B = 2.5	0.36	0.61	0.82
S1	H - FRP	0.37	0.81	0.99
S2	H & V - FRP	0.37	0.83	1.01
S3	H & X - FRP	0.41	0.94	1.21

Though the torsional irregularity created efforts in terms of torsion on the structural system, however, inter-story drift components of the system were not influenced significantly. This is because the contribution of torsional degree of freedom in the drifts of the structure is too small in comparison with translational movements.

As for the FRP strengthened structures, the peak medians obtained were equal to 0.71%, 0.68% and 0.57% for the cases H-FRP, H&V-FRP, and H&X-FRP respectively. It was found that the FRP retrofitting performed well in controlling the maximum inter-story drift ratio during ground motions at the design level. A significant decrease in the peak median was observed in comparison with the original structure with B=1.7, starting from 14% decrease in the H-FRP structure and peaking at 31% decrease in the case of H&X-FRP. This can be justified by the effect of FRP composites on increasing the shear strength of original walls and coupling beams through wrapping the members. Increasing the shear strength can alter the failure mode of each part to a more ductile mode with higher energy dissipation. Subsequently, it limits the inter-story drift ratio of the RC core wall, which leads to a more ductile behaviour. Nevertheless, the investigated retrofitted schemes can postpone the stiffness deteriorations, which points out a better damage and drift control upon retrofitting. Moreover, the interquartile range (Q3-Q1) was found to be smaller in the FRP strengthened structure in comparison to the original structures.

For instance, this can be clearly observed in Fig. 4.16.f for the case H&X-FRP. Results of initial pushover analyses showed the FRP retrofitting using FRP X-braces to be the most efficient method, capable of enhancing both the strength and the ductility of RC walls. Similar results were observed by El-Sokkary et al. (2012), and El-Sokkary and Galal (2013).

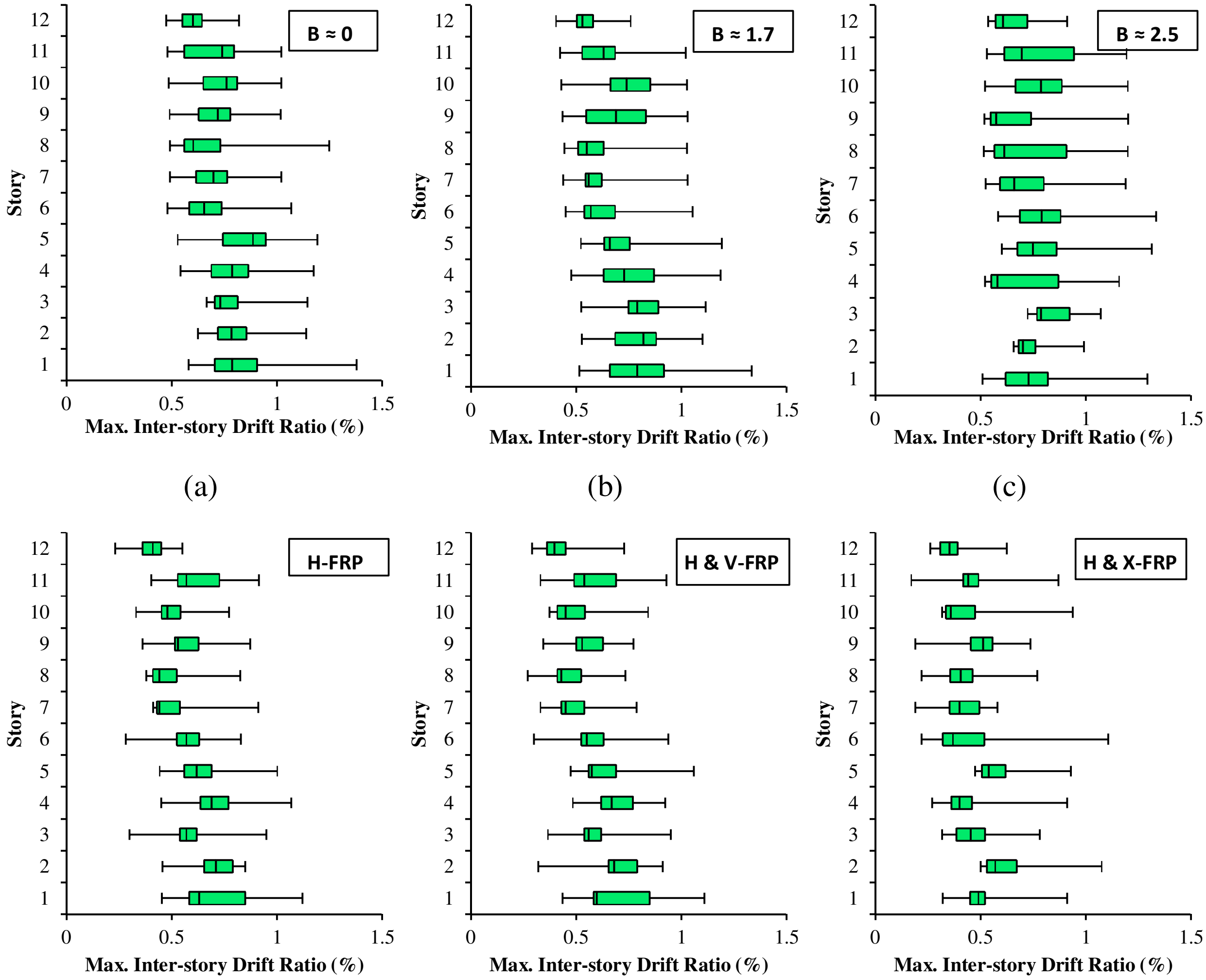

(a) (b) (c)

(d) (e) (f)

Fig. 4.16. Inter-story drifts of 12-story buildings for all 50 records at design levels

4.6.4 Story shear demand envelope

The effect of torsional sensitivity on the story shear demand of the building is investigated in the current study. As it is shown in Fig. 4.17.a, the story shear force profiles over building height is shifted rightward by increasing the torsional sensitivity of the structure. The story shear was normalized by the peak base shear in the case with B≈1.0. The maximum base shears were increased by 34% and 63% for the case of B=1.7 and B=2.5 respectively.

As for the effectiveness of FRP strengthening, the strengthened structures were also investigated and the results are shown in Fig. 4.17.b. By normalizing the results by the peak base shear in the case B=1.7, it was found that FRP retrofitting with horizontal wrapping increased the base shear by 7%, while the H&V-FRP retrofitting resulted in an increase of 8%. The peak base shear in the H&X-FRP retrofitted structure was increased by 23%.

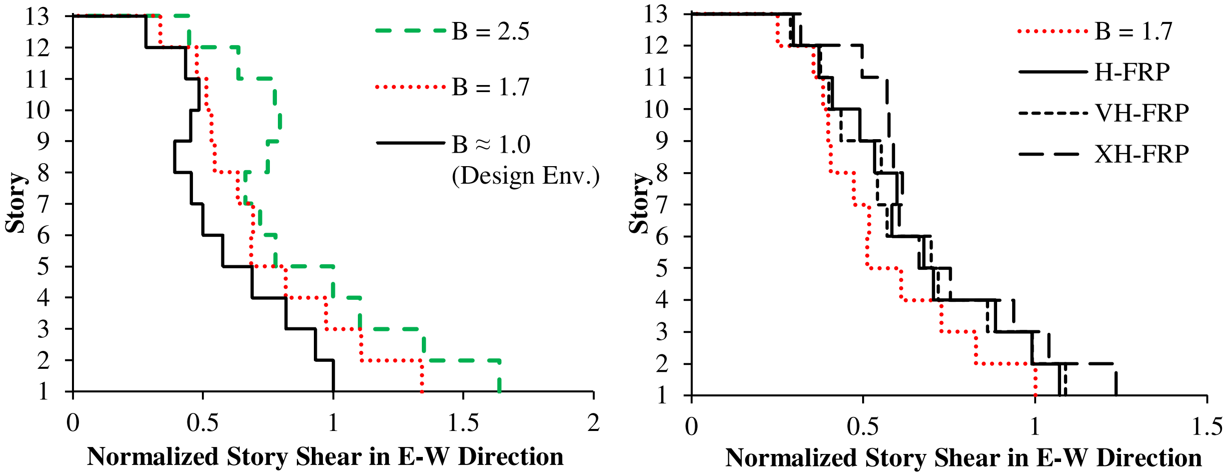

(a) (b)

Fig. 4.17. Story shear force profiles over building height in E-W direction.

Regarding the increase in the base shear demand of the structure, FRP retrofitting targeted enhancing both the strength and ductility of the RC core wall system without a noticeable increase in the initial stiffness of the structure. Increasing the strength, however, makes an offset in stiffness degradation of the wall system, and leads to a stiffer response in the hardening region (between the yield point and the peak strength). Hence, while the retrofitting increases the capacity of the system, it increases the shear demand as well.

4.6.5 Failure modes

Different failure modes previously mentioned were considered during the dynamic analyses, and afterward in post-processing, to find the most common failures and the most critical regions in the investigated buildings. The failure mechanisms were considered in four different groups including the shear/flexural failure, confined concrete crushing, unconfined concrete crushing and steel rebar buckling/fracturing. The axial failure was excluded since it was found to be dominant in none of the models in the current work.

Fig. 4.18 presents the results of failure distribution over the building height. As it can be seen, shear failure of the wall usually happened in the first story of the building, while the concrete crushing failures were distributed between the base and the 3rd floor. The story level of steel rebar buckling/fracture failure mode was ranging from the first floor up to the 7th floor of the building. Formation of the failure along the height of the building demonstrates the contribution of higher modes on the seismic response of the buildings under selected ground motion records. It confirms the findings of Boivin and Paultre (2010) and highlights the influence of recently introduced dynamic shear amplification factor by CSA A23.3-14 to account for inelastic effects due to higher modes.

Such effects from the higher modes of multi-story structures can lead to increase the shear forces beyond the design level in the different stories. Hence, shear forces and bending moments in the upper floors may exceed the calculated design levels, and inelastic rotation can consequently occur in a region with no properly implemented ductile detailing. Therefore, some failure modes might not necessarily occur at the base of the structure. Similar results were observed by Tremblay et al. (2008).

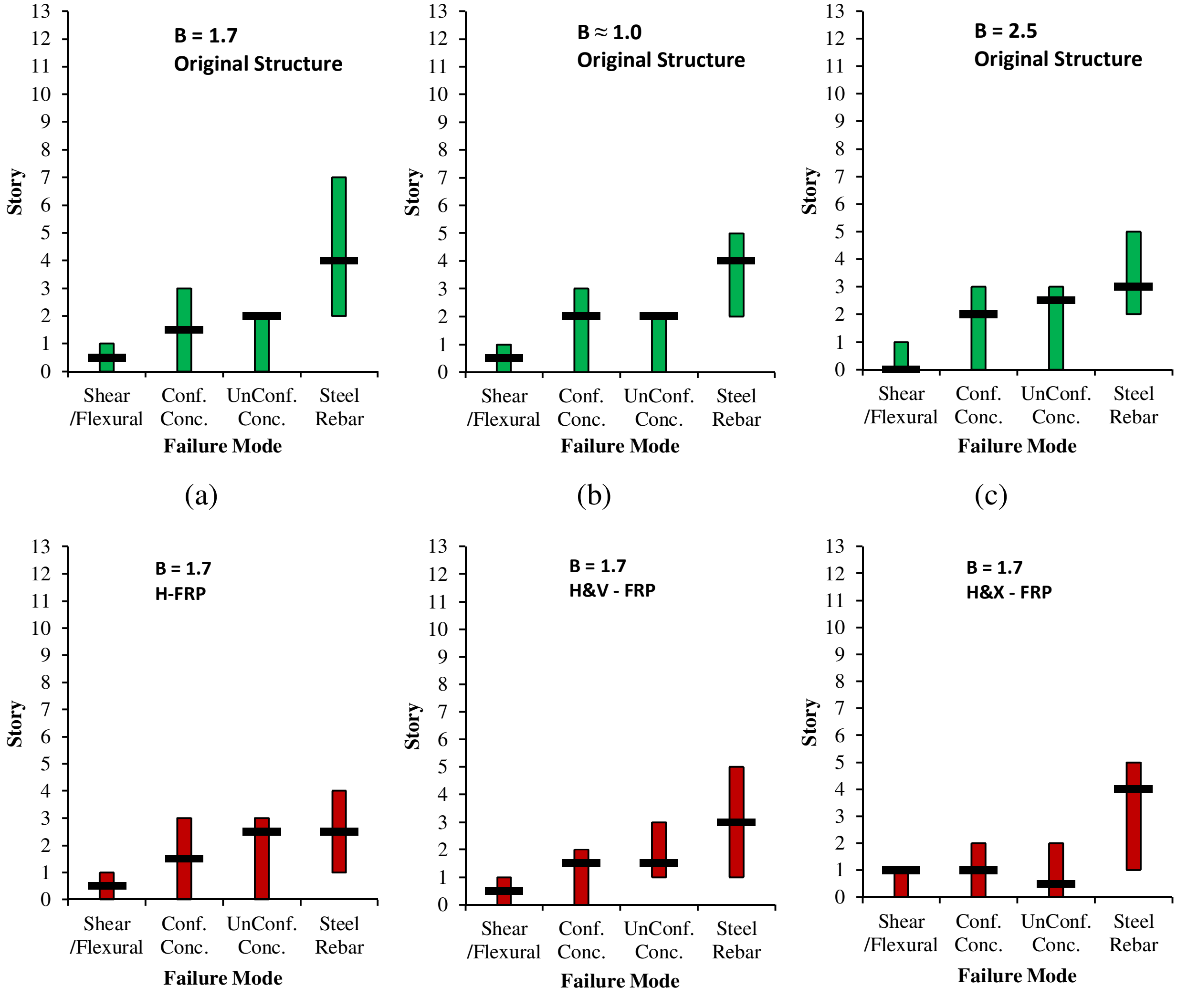

(a) (b) (c)

(d) (e) (f)

Fig. 4.18. Failure distribution over building height

The variations of the story level of mechanisms for different failure modes are summarized in Table 4.8. According to the tabulated data, the distribution of different failure modes over the building height was quite similar in the buildings with different torsional sensitivity. As for the strengthened building, however, the FRP retrofitting led to shifting the concrete crushing failures downward to the first story. Moreover, the shear/flexural failures were slightly shifted upward to the top of the first story after retrofitting with H&X-FRP.

Table 4.8. Variations of the story level of mechanisms for different failure modes

Archetype ID	Description	Median Story Level of the Failure			
		Shear/Flexural	Conf. Conc.	UnConf. Conc.	Steel Rebar
O1	B ≈ 1.0	0.5	2	2	4
O2	B = 1.7	0.5	1.5	2	4
O3	B = 2.5	0	2	2.5	3
S1	H-FRP	0.5	1.5	2.5	2.5
S2	H&V-FRP	0.5	1.5	1.5	3
S3	H&X-FRP	1	1	0.5	4

Fig. 4.19 shows the distribution of each predicted collapse mechanism of the 12-story coupled core wall system in whole the models. As it is clearly depicted in the figure, the most common failure mode was the shear/flexural failure (55% median), and the least common one was the steel rebar failure (8% median). Table 4.9 presents the tabulated data for different building configurations, in which similar trends for all the buildings can be seen. The proportion of the shear/flexural failure was increased in buildings with higher torsional sensitivities, ranging from 56% to 68% in the buildings with B≈1.0 and B=2.5 respectively. A slight decrease in the proportion of shear/flexural failure was also observed, from 54% in the buildings with H-FRP and H&V-FRP to 50% in the building with H&X-FRP.

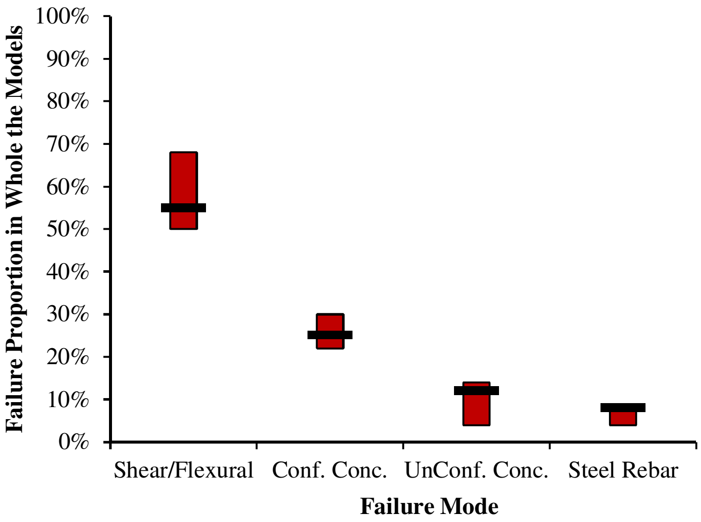

Fig. 4.19. Distribution of different failure modes among the models

Table 4.9. Predicted collapse mechanism of the 12-story coupled core wall system

Archetype ID	Description	Failure Type Distribution			
		Shear	Conf. Conc.	UnConf. Conc.	Steel Rebar
O1	B ≈ 1.0	56%	22%	14%	8%
O2	B = 1.7	58%	22%	12%	8%
O3	B = 2.5	68%	24%	4%	4%
S1	H-FRP	54%	30%	12%	4%
S2	H&V-FRP	54%	26%	12%	8%
S3	H&X-FRP	50%	28%	14%	8%

Certain limitations must be recognized in evaluating the results of this study, which offer suggestions for future studies. Firstly, IDA analyses were conducted in East-West direction (couple direction of the wall) only, and the effects of bi-directional seismic excitations were not considered in the study. Moreover, the modelling approach used here was not able to accurately capture the post-peak strength degradation of wall specimens. Furthermore, perfect anchoring for the FRP strips was assumed and failure of FRP connections was not considered in the study. The results of the study were limited to a building designed and analyzed for Montreal, Canada only. This needs to be extended to other seismic regions in order to generalize the findings.

4.7 Conclusions

This study provides results from IDA analysis of coupled RC core walls using a nonlinear macro-modelling approach to investigate the collapse capacity of coupled RC cores. The modelling approach was initially developed by other researchers. However, modifications were proposed in the current study to consider the effectiveness of FRP strengthening on the collapse response of RC core systems. Using a set of 50 artificial ground motion records, more than 2400 time history analyses were conducted on nonlinear 3D models of 12-story buildings with different torsional irregularities and strengthening schemes. Results showed that:

- Based on the good agreement between the results of FE analysis and the experimentally tested C-shaped RC shear walls reported in the literature, the elements and modelling considerations adopted in this paper proved to be capable of simulating the behaviour of this type of shear walls under cyclic loading. The maximum error percentage for the prediction of lateral load capacity and lateral stiffness using the approach in this paper were 6% and 10% respectively. Moreover, the numerical model performed well in predicting the unloading stiffness of simulated wall with a maximum error of 7%.
- The case study assessed in the current study showed a CMR of more than 5 for the original structure, which passes the acceptable collapse margin ratio (ACMR) proposed by FEMA P695 (2009). However, by using a proper strengthening scheme with FRP material, an improvement of up to CMR = 12.3 with flatter fragility functions can be achieved for the structural system. Results are in agreement with the work recently published by Gogus and Wallace (2015).

- The torsional sensitivity has a significant effect on the collapse capacity of the building, resulting in up to 8% and 36% decrease by reaching the torsional sensitivities of B = 1.7 and B 2.5, respectively. Steeper fragility functions were also observed by increasing the torsional sensitivity.
- FRP retrofitting was found to be an efficient method for improving the collapse capacity of coupled C-shaped RC cores. Three different strengthening schemes were evaluated and X-bracing of walls with FRP strips found to be the most efficient strengthening layout. These results were previously confirmed by experimental tests on planar RC shear walls by El-Sokkary and Galal (2013).
- The torsional sensitivity of the structure has no significant influence on inter-story drift components of the system. FRP retrofitting, however, performed well in reduction of the inter-story drifts (14% to 31%) and in the enhancement of the system performance. Moreover, the fluctuation of the drift ratios was lower than the corresponding values in the original structures.
- Shear/flexural failure was the most common failure mode and the steel rebar failure was the least common one. The proportion of the shear/flexural failure was increased up to 21% in buildings with higher torsional sensitivities.

4.8 Appendix: Bond-slip model for concrete/FRP interface

Three different bond-slip models were proposed by Lu et al. (2005) to consider the concrete/FRP interface. Because of its simplicity among the aforementioned models, the bi-linear bond-slip model was adopted in the current work to create a debonding rule for the interaction between the concrete and FRP strips. The model proposes a set of equations for calculating the relation between the local bond stress τ and the local slip s, described by the following equations:

$$\tau = \tau_{max} \frac{s}{s_0} \qquad \text{if } s \le s_0 \tag{4.8a}$$

$$\tau = \tau_{max} \frac{s_f - s}{s_f - s_0} \qquad \text{if } s_0 < s \le s_f \tag{4.8b}$$

$$\tau = 0 \qquad \text{if } s > s_f \tag{4.8c}$$

where τ_{max} is the maximal local bond stress, s_0 is local slip at τ_{max}, and s_f is local slip when bond stress τ reduces to zero. These parameters can be calculated by the following equations:

$$\tau_{max} = \alpha_1 \beta_w f_t \tag{4.9}$$

$$s_0 = 0.0195 \beta_w f_t \tag{4.10}$$

$$s_f = 2G_f / \tau_{max} \tag{4.11}$$

where

$$G_f = 0.308 \beta_w^2 \sqrt{f_c'} \tag{4.12}$$

$$\beta_w = \sqrt{\frac{2.25 - b_f/b_c}{1.25 + b_f/b_c}} \tag{4.13}$$

In the above equations, $\alpha_1 = 1.5$ is a coefficient in the proposed bond–slip models determined by the iterative procedure, β_w is the width ratio factor, b_f is the width of FRP strip and b_c is the width of the concrete segment which was taken equal to the tributary area of each FRP strip.

CHAPTER 5

Seismic Response Analysis of RC C-Shaped Core Walls Subjected to Combined Flexure, Shear and Torsion

5.1 Abstract

Although dynamic torsional responses are often regarded as secondary effects in the seismic design of symmetric-plan buildings, torsional effects arising from plan asymmetry can be substantial in some cases. In Reinforced Concrete (RC) wall buildings, a combination of flexural, shear and torsion dictates the type of failure, which needs to be addressed in the design of RC walls. The current study investigates two aspects of building structures with C-shaped RC walls: (i) evaluation of seismic force demand in different levels of torsional sensitivity, and (ii) effectiveness of using the dual plastic hinge method in controlling the seismic shear force demand. A macro-scale modelling approach using the wide column analogy was used to capture the inelastic response of C-shaped RC wall buildings, including torsional effects. The numerical model of the wall was validated against available experimental data. Nonlinear time history analyses of typical multi-story buildings located in Eastern North America (8, 12 and 16-story) were performed using OpenSEES. Using the 2015 National Building Code of Canada, four different levels of torsional sensitivity ($B = 1.3$, $B = 1.7$, $B = 2.0$ and $B = 2.5$) were considered for each building configuration. It was shown that although the studied range of torsional sensitivity has no substantial effect on the bending moment envelope of the building, it significantly increases the story shear force demand during an earthquake. The shear force envelopes in torsionally sensitive buildings ($B > 1.7$) exceeded the capacity design envelope predicted by the response spectrum analysis of a major number of selected ground motions. Afterward, the dual plastic hinge design method recently proposed by other researchers was adopted and it was found to be an efficient method, resulting in lower shear force demand along the height of the structure, especially when high torsional flexibility is expected.

5.2 Introduction

The capacity design method is the base for the seismic design of shear walls in many countries such as Canada and New Zealand. Though current civil engineering practice prefers to use the nonlinear static procedure because of its simplicity and consistency in the design process, dynamic time history or response spectrum analyses are inevitable in some case. According to NBCC 2015, dynamic analysis is mandatory if the torsional sensitivity (irregularity) of the building, B, exceeds the limit of 1.7 (NBCC, 2015). Torsional sensitivity in a building is determined based on the maximum value B, among all floors, where B_x computed at floor level x is $B_x = \delta_{max}/\delta_{ave}$. Similar classification is specified by ASCE/SEI 07-16 (ASCE, 2016). However, ASCE 07-16 includes two levels of torsional irregularities for torsionally sensitive buildings, definition of which is slightly different than the NBCC 2015 definition. According to ASCE 07-16, torsional sensitivity is the ratio of maximum to average story drift in a story, and “torsional irregularity” corresponds to the buildings in which this ratio exceeds 1.2 but not more than 1.4 which is categorized as the limit for “extreme torsional irregularity” It should be noted that the aforementioned limits are specified for non-flexible diaphragms only (ASCE, 2016). Fig. 5.1 shows a schematic view of asymmetry in building plan as well as the torsional sensitivity according to the NBCC 2015.

Though the code does not prescribe a specific type of dynamic analysis, response spectrum analysis (RSA) method is the most preferable technique to predict the seismic response of structures. As for shear wall structures, this technique provides an accurate and adequate estimation of response parameters when the wall behaves within the linear range. The linear behaviour, however, is not the realistic response of the wall in many cases, and fluctuation of both the flexural and shear stiffness is expected when the structure is subjected to a severe earthquake (Luu et al., 2013). The code simply applies some reduction factors to the predicted force demand from an elastic analysis to consider the response nonlinearity in the design.

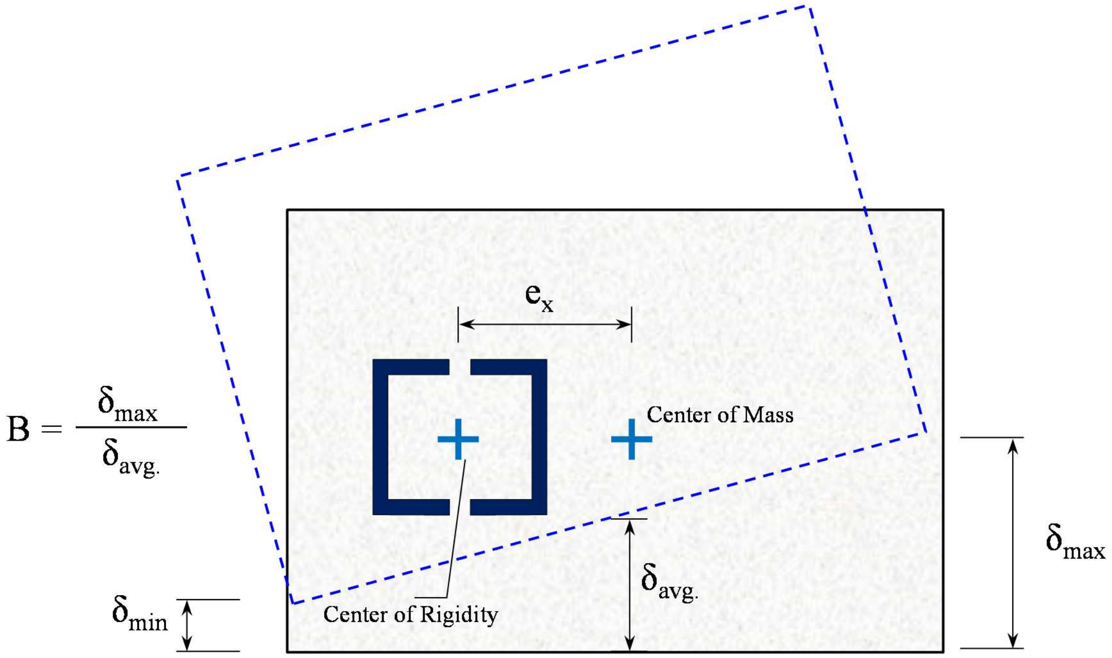

Fig. 5.1. Schematic view of an asymmetric building plan

Since the force redistribution upon the nonlinear actions in the wall cannot be captured by the elastic modal analysis, unrealistic effects from the higher modes will be induced, and consequent inaccuracies may occur in the seismic response predictions of the RC wall (Paulay and Priestley 1992; Luu et al., 2013).

In the seismic analysis of RC wall structures, higher mode effects can significantly amplify the force demands (bending moments and story shears) over the height of the RC wall system, potentially leading to unexpected damage or possibly failure (Wiebe, Christopoulos, 2009). As a result of the early New Zealand investigations (Blakeley et al. 1975), a simple dynamic shear amplification factor was introduced in the 1982 New Zealand Design Standard (NZS 3101, 1982), to account for the higher modes effects on the design forces of the structure. Accordingly, a new clause (21.5.2.2.7) was added in the recent version of the Canadian code CSA A23.3-14, in which a dynamic shear amplification factor, ω_v, was introduced to account for the inelastic effects of higher modes in the RC walls, except for coupled and partially coupled wall structures. This exception can be explained in part by the fact that, unlike cantilever walls which deform entirely in a flexure mode, the deformation of coupled walls includes a significant shear (sway) mode due to the deformation of the coupling beams. On the contrary, despite the several observations reported in the literature, codes in the United States have not yet considered the significant effect of higher modes on the seismic demands in buildings with a cantilever RC wall system.

In the seismic design of RC wall structures, story shear force demands can be of special interest as an important response parameter. As mentioned previously, the shear increase due to inelastic effects of higher modes was not considered in the 2004 version of CSA A23.3-04 (Boivin and Paultre, 2010). A recent study by Pelletier and Léger (2017) showed that the new dynamic shear amplification factor prescribed by CSA A23.3-14 results in a more realistic seismic shear force demand compared to nonlinear time history results. However, an increase in the shear force demand was reported by increasing the torsional sensitivity of the building. Since the results of the nonlinear time history analysis (NTHA) are subjective to several parameters such as the building configuration and the ground motion selection, more studies need to be conducted to highlight the effect of the high torsional sensitivity of the building in its seismic response.

Realistic estimation of seismic force demand is more essential when high torsional effects in the seismic response of the structure are expected. There is little information of studies on how torsional effects can affect the seismic force distribution in building structures. Fajfar et al. (2005) found that inelastic torsional effects in the seismic response of the structure depend on the ductility demand and thus on the intensity of selected ground motion. A substantial contribution from torsional effect can be expected in some cases, which generally decreases with increasing plastic deformations, and leads to significant variations in the seismic force demand of the structure. A study by Dubey and Sangamnerkar (2011) on seismic behaviour of asymmetric RC buildings showed that torsional analysis of buildings should not be considered as a secondary analysis only. Structural damages during the past wind storms and earthquakes reveal that torsion is the most critical factor in some cases, leading to major damage or complete collapse of buildings. A research was conducted by Herrera et al. (2013) subsequent to the collapse of a commercial and a school building categorized as structures with high torsional risk and discontinuity in diaphragms during the earthquake of Cariaco, Venezuela (1997). Seismic response and torsional effects of RC structure with irregular plant and variations in diaphragms, designed with Venezuelan codes were investigated. As expected, the observed internal forces due to torsional effects on the columns located in the core of the building were less than the corresponding force for the columns of the outer axis, which confirmed the design presumption for reducing the stress concentration in those structural members.

The objective of this paper is to quantitatively evaluate the seismic response of C-shaped RC core walls with different torsional sensitivity factors and to assess the performance of the dynamic shear amplification factor prescribed by CSA A23.3-14 in predicting the story shear force demand of buildings with a high level of torsional sensitivity. This evaluation is done by comparing the seismic response prediction from the RSA with the results of NTHA. A three-dimensional macro model was developed using OpenSEES (McKenna et al. 2013) based on the modified wide column model (WCM) proposed by Arabzadeh and Galal (2017) for simulating the nonlinear response of RC cores, including shear deformations nonlinearity. The model was originally proposed by Beyer et al. (2008) and was extended by Pelletier and Léger (2017). The accuracy of the modelling approach was evaluated against the available experimental test data from the literature. The validated numerical model was then used to investigate the seismic response of 8, 12 and 16-story RC building structures located in Eastern North America using NTHA. A group of 48 artificial records proposed by Atkinson (2009), including near-distance and far-distance ground motions with different magnitudes, were used for NTHA of the RC core in different levels of torsional sensitivity. The story shear force envelopes from individual ground motions were compared afterward with the corresponding story shear resistance, V_r, resulted from the seismic design based on RSA.

The capacity design proposed for design of cantilever walls in the Canadian design code (CSA A23.3-14), as well as the Eurocode (EC8) and the New Zealand seismic standard (NZS-3101), is based on a plastic hinge at the base of the wall and assumes an elastic response along the rest of the wall height. Though these codes consider a linear variation for the flexural design envelope to take higher mode effects into account, studies by Panneton et al. (2006) and Priestley et al. (2007) showed that such an assumption is subjective. In other words, this assumption does not always preclude the spread of plasticity into the upper regions, and subsequently, sufficient protection against yielding in the upper portions of the walls cannot be provided. A bilinear flexural design envelope was proposed afterward by Priestley et al. (2007) to address this issue.

Based on the results of a statistical study, Wiebe and Christopoulos (2009) found that providing multiple plastic hinges along the height of the walls (acting as nonlinear fuses) would be advantageous. Hence, with no noticeable increase in the maximum displacement, the peak flexural demand can be limited and this will prevent it from exceeding the design envelope. Considering this, a dual plastic hinge (DPH) design approach useful for the design of high-rise RC structural walls was proposed by Panagiotou and Restrepo (2009). A general layout of DPH model for RC walls is presented in Fig. 5.2. The approach introduced a second hinge at an intermediate height of the cantilever wall, which was intended to reduce the effects of higher modes of response in buildings. Moreover, the SPH design approach requires large amounts of longitudinal reinforcement in the intermediate portion of the walls and this is associated with significant congestion and higher cost (Panagiotou and Restrepo, 2009).

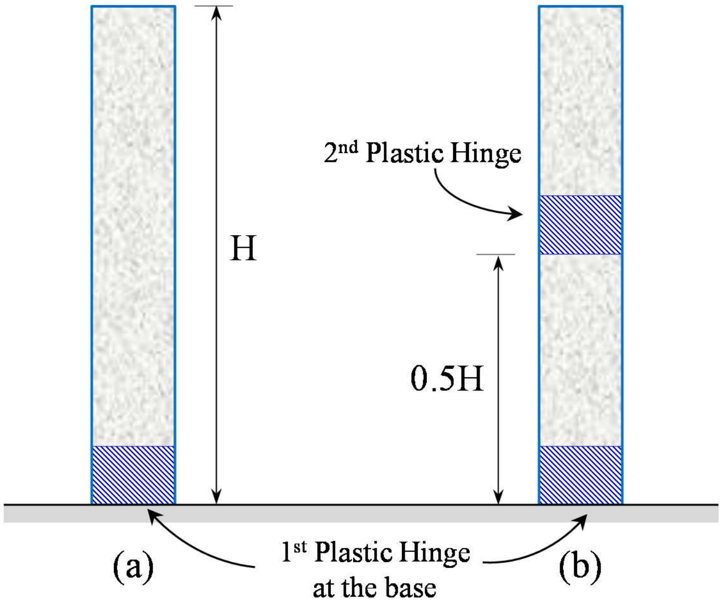

Fig. 5.2. General layout of SPH and DPH model for RC walls

Hence, in the current work, a DPH configuration was adopted to evaluate the effectiveness of the proposed method in controlling the story shear demand in torsionally sensitive structures. Results of the analysis of the 8, 12 and 16-story buildings adopted with SPH and DPH approach are compared in the following sections.

5.3 Analysis Methodology

Among the various simulation techniques proposed in the literature for predicting the response of shear/core walls, the WCM modelling approach proposed by Beyer et al. (2008-b) was found to be one the most robust and efficient ones. In the current study, the proposed WCM was modified according to Arabzadeh and Galal (2017). The number of modules in each segment of the C-shaped wall section, however, was increased to two to provide higher accuracy as proposed by Pelletier and Léger (2017). The modelling approach is briefly explained in this section. Details of the modelling approach can be found in Arabzadeh and Galal (2017).

5.3.1 Geometry of the models

Fig. 5.3 shows a schematic diagram of the wall model, including the configuration of nodes and elements. Based on the recommendations of Pelletier and Léger (2017), each C-shaped part of the core section was subdivided into three rectangular sections (i.e., the web and two flanges), modelled by displacement-based beam-column elements as piers.

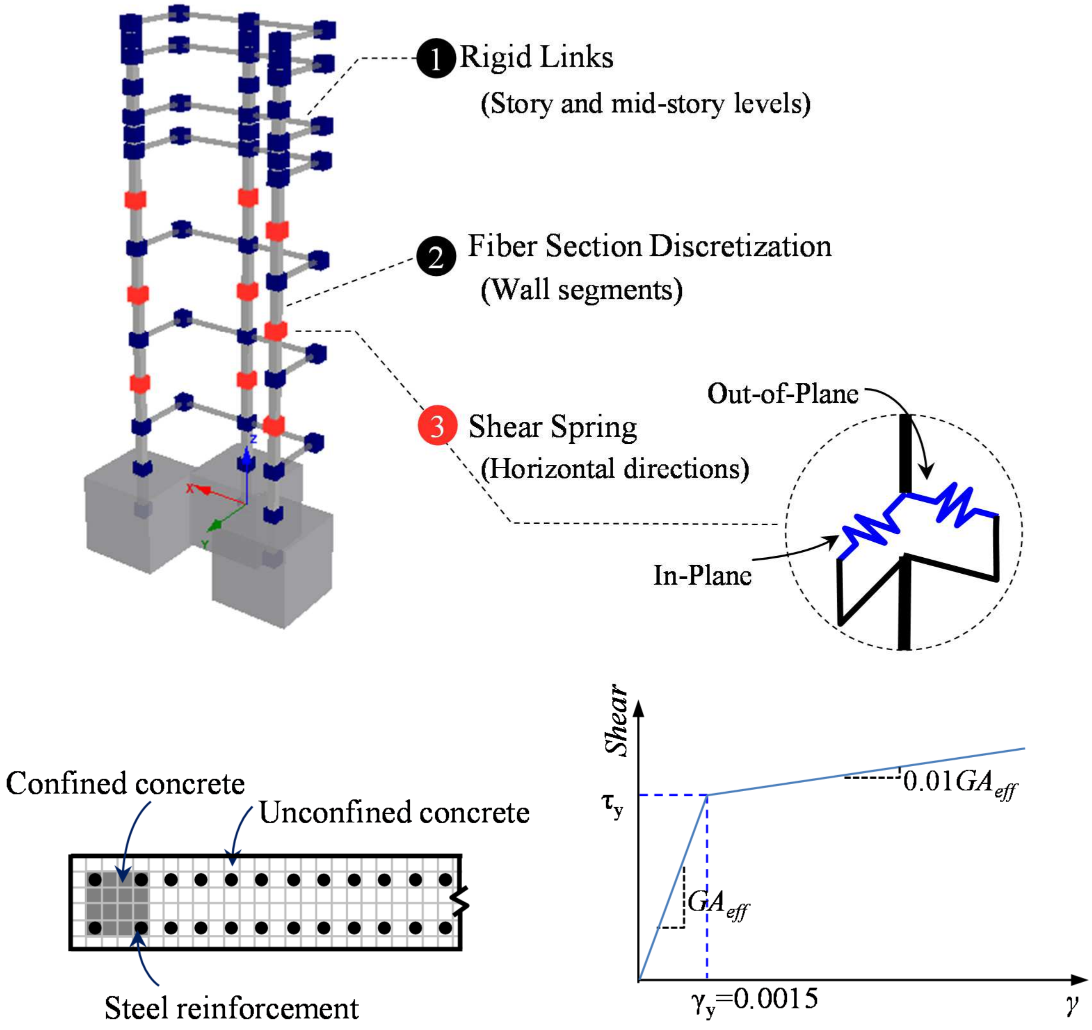

Fig. 5.3. Model configuration of the RC core wall

The ability to capture the axial load-bending moment interaction in these elements makes them an ideal choice for simulation of RC walls, in which the axial load in each individual element might vary throughout the cyclic excitation. As for the nonlinear time history analyses, structural elements (i.e. wall segments and columns) were modelled using the fibre section feature in OpenSEES corresponding to the gross section properties of elements, and a fine discretization was selected for each fibre section in the model. Horizontal links running along the weak axis of the sections were used to connect these vertical elements at story and mid-story levels. Full base fixity was assumed for the walls and the soil-structure interaction was neglected.

The slippage in the wall-footing intersections (strain penetration effect), however, was considered by utilizing zero-length element at the base of wall segments. The stress-slip model proposed by Zhao and Sritharan (2007) was assigned to the vertical reinforcement, represented by the Bond_SP01 material model in OpenSEES.

As suggested by Stafford-Smith and Girgis (1986), the spacing of the horizontal links was set such that provide two rigid links in each story (i.e. four pier elements along the height of the story). In-plane and out-of-plane shear flexibility of the wall segments were considered by defining zero-length elements between the nodes at mid-height of consecutive links. Corresponding stiffness for each translational degree of freedom was assigned, and all other degrees of freedom of the two nodes were slaved using EqualDOF constraints. A bilinear trend was considered for the shear behaviour of horizontal zero-length springs in each wall segment (Fig. 5.3.b). Fig. 5.4 shows a comparison between the backbone curve for the load-displacement response of RC walls proposed by ASCE/SEI 41-17 (2017) and the assumptions considered in the current study. A typical hysteresis load-displacement curve for an RC shear wall is also presented in Fig. 5.4.b. Shear strain at yield was taken as 0.0015 based on test results by Massone (2006) which has a good agreement with the proposed values by ASCE 41-17. Moreover, the ultimate drift of 0.0075 considered in the current study was the same as the limit proposed by ASCE 41-17.

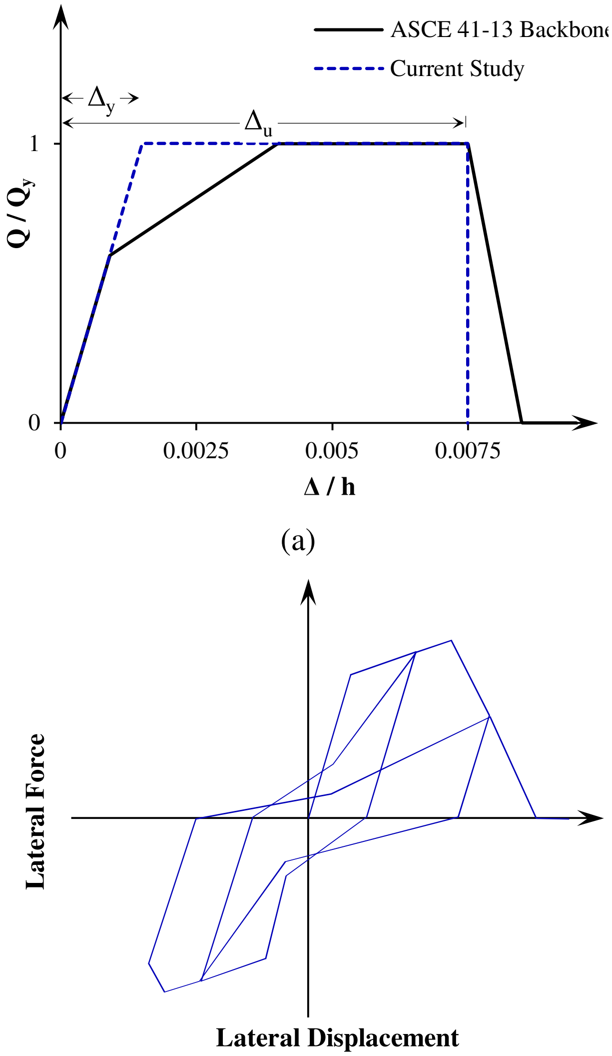

(a)

(b)

Fig. 5.4. Reinforced concrete wall response: a) Backbone curve comparison, b) A typical hysteresis load-displacement curve

5.3.2 Failure criteria for materials

Nominal strengths of concrete and steel reinforcement were used in the numerical modelling using the available empirical equations. Modified Kent and Park model (Scott et al, 1982) was used to define the nonlinear constitutive laws for concrete fibres (Concrete02 in OpenSEES). The equations proposed by Mander et al. (1988) was used to consider the confinement effects on the stress-strain behaviour of the concrete. The maximum tensile strength of concrete was assumed to be equal to $f_t^{'} = 0.623\sqrt{f_c^{'}}$ (Yassin, 1994).

For steel reinforcement, the Giuffré-Menegetto-Pinto hysteretic model (Filippou et al., 1983) with default parameters (Steel02 in OpenSEES) was adopted to represent nonlinear behaviour of steel bars. No bond-slip was considered with respect to the surrounding concrete.

Table 5.1 shows the sample material parameters adopted for the verification cases as well as the multi-story buildings. Examples of the cyclic material laws employed for the concrete and steel fibres in the numerical model of the specimen MEM-4 (Chen et al., 2016) are depicted in Fig. 5.5.

Table 5.1. Sample material parameters for the OpenSEES model

Specimen			U-shaped beam (Krpan and Collins, 1981)		MEM-4 (Chen et al, 2016)		Multi-story Buildings	
			Unconfined region	Confined region 1	Unconfined region	Confined region 1	Unconfined region	Confined region 1
Concrete Material	$f_c^{'}$	(MPa)	-52.00	-59.85	-40.92	-46.40	-30.00	-31.20
	e_0	---	0.0030	0.0033	0.0027	0.0029	0.0023	0.0024
	K	---	1	1.151	1	1.134	1	1.040
	f_{cu}	(MPa)	-10.40	-11.97	-8.18	-9.28	-6.00	-6.24
	e_u	---	-0.01	-0.01	-0.01	-0.01	-0.01	-0.01
	f_t	(MPa)	4.49	4.82	3.99	4.24	3.41	3.48
			#2	#5	$\phi 6$	$\phi 8$	10M	25M
Steel Material	f_y	(MPa)	362	348	277	353	400	400
	f_u	(MPa)	490	475	447	573	545	545
	E_s	(GPa)	203	194	200	200	200	200

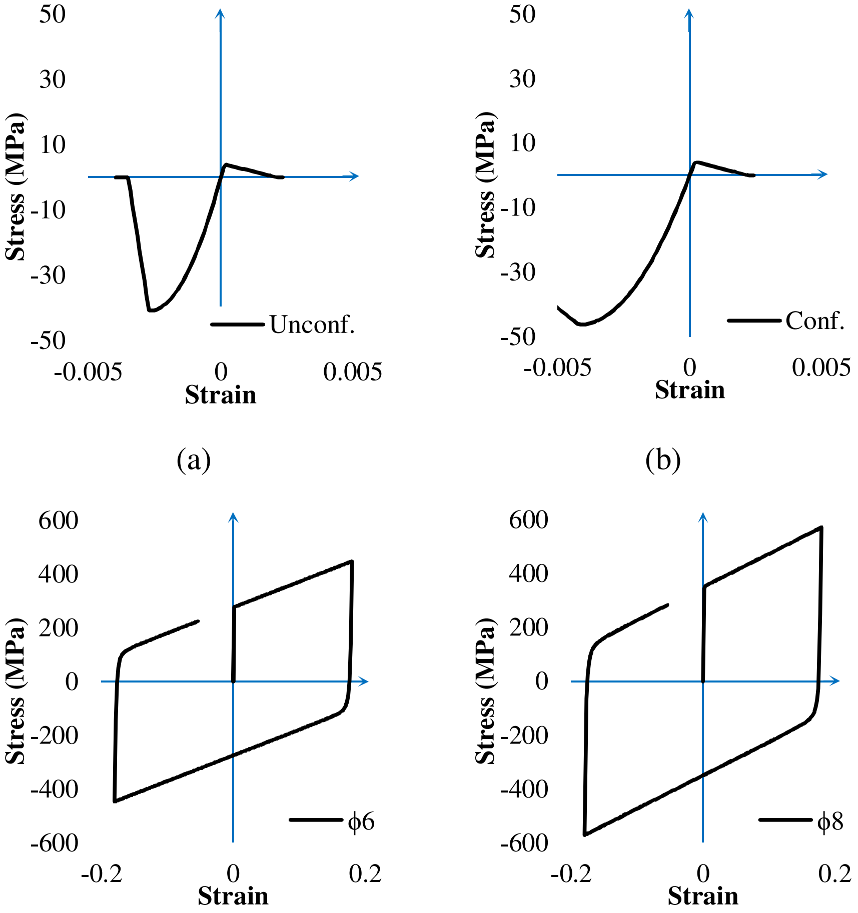

(a) (b)

(c) (d)

Fig. 5.5. Sample hysteresis stress-strain behaviour of material assigned in the numerical model for specimen MEM-4 (Chen et al., 2016): Concrete (a, b); Steel (c, d)

5.4 Model Validation

In order to validate the capability of the numerical model developed in this study, results of the numerical analysis of two RC specimens subjected to torsional loads were compared to the reported experimental results. A brief summary of each experimental program is presented in this section.

5.4.1 Thin-walled C-shaped RC specimen tested by Krpan and Collins (1981)

Krpan and Collins (1981) tested a thin-walled RC channel beam loaded in pure torsion at mid-span. These thin-walled section beams have similar warping behaviour to the RC cores subjected to torsion, and hence was selected as an appropriate case for validating the accuracy of the numerical model. Fig. 5.6.a shows the test setup of the experiment. The beam was a 6400 mm long C-shaped section, torsionally restrained at both ends using rigid concrete blocks and had a 200 mm thick rigid diaphragm located at mid-span. Two actuators were acting on this diaphragm to create the required torque by applying two equal and opposite forces using a steel loading frame. The beam cross section was 75 mm thick, 840 mm wide and 650 mm high. The beam reinforcement was designed to avoid brittle shear failures. Steel bars #5 was used as longitudinal reinforcement and the transverse reinforcement was #2 stirrups at 76 mm.

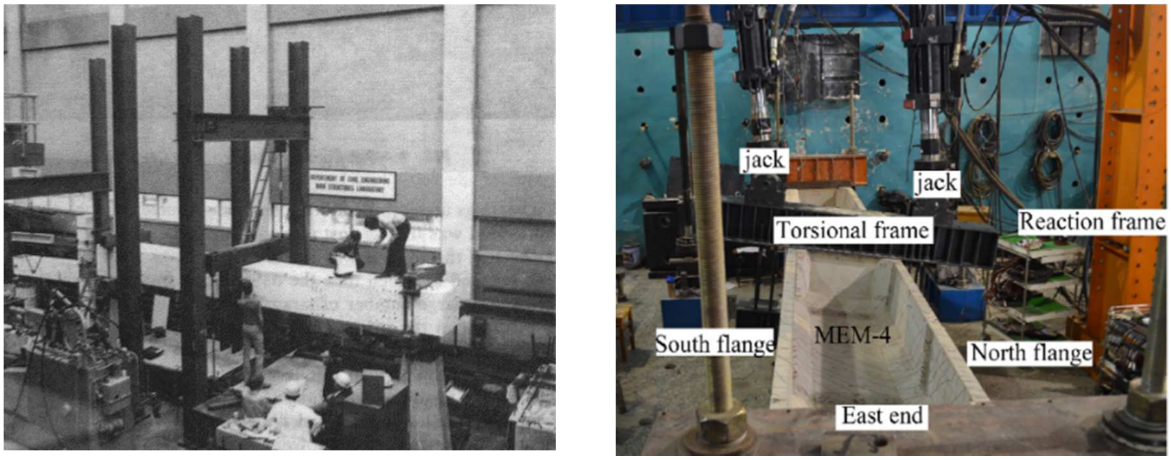

(a) (b)

Fig. 5.6. Experimental test setup: a) Krpan and Collins (1981), b) Chen et al. (2013)

The first observed cracks during the experiment were the vertical flexural type cracks, occurred at mid-span, at the bottom of the flange. The cracks were initiated at the torque level of approximately 23 kN.m. Moreover, yielding of the longitudinal steel bar was first observed at the applied torque of 191 kN.m. Post-processing of the data recorded from the numerical model (fibre section forces) showed the same trend of crack initiation at the torque level of 36 kN.m. The numerical model captured the first yielding of the steel bars to be at the applied torque of 199 kN.m. The final failure of the specimen from the numerical model does not fully match the test results due to the anchorage failure of longitudinal steel during the test. In the numerical model, the steel bars was assumed to be perfectly anchored.

Fig. 5.8-a shows the torque-rotation data from the experimental test along with corresponding results from the numerical model. The figure demonstrates a good agreement between the experimental records and the numerical predictions prior to longitudinal reinforcement yielding, after which the model was found to have more flexibility than what was observed from the experimental test. The small discrepancies between the test results and numerical predictions might be due to the variation of concrete material properties in small-scale specimens and possible measurement errors for the concentrated forces.

5.4.2 Thin-walled C-shaped RC specimen tested by Chen et al. (2016)

The experimental work of Chen et al. (2016) consisted of testing four C-shaped thin-walled RC members, 1:4 reduced scale, under pure torsion. Considering the thin-walled feature, the thickness of both the flanges and the web was designed for 70 mm. The specimens were 6650 mm long with the height of the flanges and the web width equal to 500 mm and 900 mm, respectively, aimed to provide the length to thickness ratio of almost 7. The specimens were lengthened by 350 mm on both ends to fix a fastening device which provided a fully anchored situation during the loading process. The specimen MEM-4 selected for the verification purpose in this study was made of a 40.92 MPa strength concrete, and was reinforced with 8 mm longitudinal bars (F_y=353.3 MPa) and 6 mm stirrups at 70 mm distances (F_y=276.7 MPa). The test setup is presented in Fig. 5.6.b and the shear flow in the section in presented in Fig. 5.7. Several steel plates were also embedded in both support ends to prevent local failure. A chamfer with the scale of 1:1.125 was considered on the inner side of the connection between flanges and web, to reduce the probable stress concentrations. Similar to the work by Krpan and Collins

(1981), the torsional load was applied through two opposite and equal forces from two actuators acting on a loading frame, which was fixed on a strengthened diaphragm plate at mid-span.

Flexural vertical cracks were first observed at support and mid-span when the torque was almost 17 kN.m, while first yielding of the steel bars was measured at the torque level of 85 kN.m. The numerical predictions followed a similar trend achieving the corresponding torque values of 15 kN.m and 93 kN.m, respectively. The numerical model was found to be able to capture the final failure of the specimen as it was observed in the experimental test. The specimen ultimately failed because of the yielding of the longitudinal tensile bar and the crush of compressive concrete as a consequence. As can be seen in Fig. 5.8-b, there is a very good correlation between the torque-rotation curves from the numerical analysis and those from the experimental work of Chen et al. (2016). It can be observed that in larger rotations, the numerical model showed a bit higher twisting resistance than the experimental one, especially in the post-peak region of the curves.

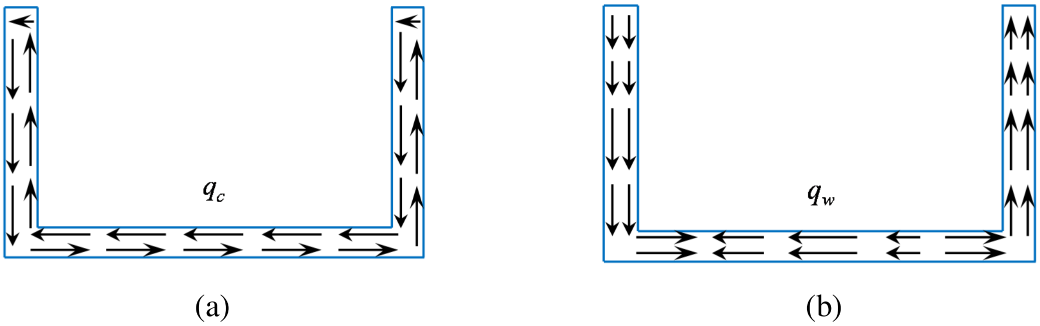

Fig. 5.7. Shear flow diagrams of a C-shaped section: a) circulatory torsion, b) warping torsion

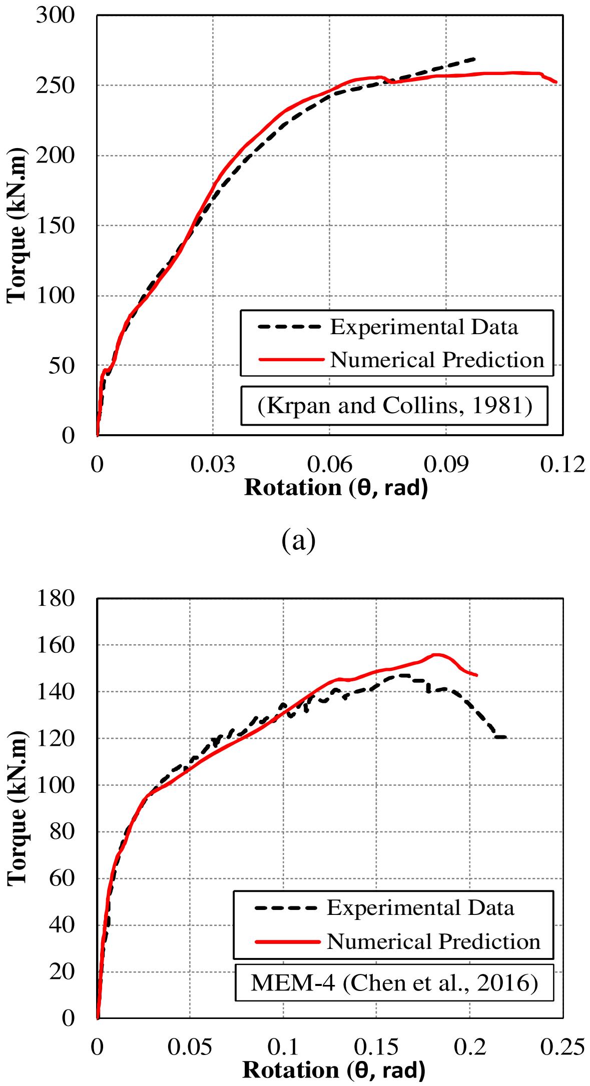

(a)

(b)

Fig. 5.8. Comparison of results from the numerical model and the experimental data: a) Specimen tested by Krpan and Collins (1981), b) Specimen MEM-4 tested by Chen et al. (2013)

To evaluate the capability of the numerical model in tracking the torsional response of C-shaped open section RC members, a quantitative comparison was conducted between the output data resulted from the numerical models and the experimental data. Table 5.2 shows the summary of the results from the verification models including the torque corresponding to the first yield in the longitudinal reinforcement, and maximum torque capacity of the specimen. In general, the inelastic torsional responses were well captured. After the yielding point in both validation cases, yielding of both the longitudinal and transverse reinforcements were observed, from which the load transferred to the reinforcements after the crack initiation can be revealed. Hence, the numerical model was found to be capable of tracking the inelastic behaviour of thin-walled open section RC walls subjected to torsional forces. The validated model was then used to perform a parametric study on C-shaped RC wall buildings, in different levels of torsional irregularity.

Table 5.2. Summary of verification results

Specimen	Results	Long. Reinf. Yield (kN.m)	Error (%)	Ultimate Capacity (kN.m)	Error (%)
(Krpan and Collins, 1981)	Experimental	190	---	268.5	---
	Numerical	186.1	-2%	258.7	-4%
MEM-4 (Chen et al., 2016)	Experimental	95	---	146.9	---
	Numerical	99.1	4%	155.8	6%

5.5 Seismic Analysis of Multi-Story Buildings

Nonlinear time history analyses of the buildings under a group of ground motions were conducted using the macro model developed in OpenSEES. Configurations of the studies buildings and the selected ground motions are presented in this section. Moreover, a comparison of the results of NTHA with the data from the Response Spectrum analysis for each building configuration is presented.

5.5.1 Building configurations

RC core wall buildings with different number of stories including 8, 12, and 16 stories were analyzed using the nonlinear time history method. The buildings were considered for site class C in Montreal, Canada, and were designed according to the National Building Code of Canada (NBCC, 2015) and the CSA A23.3-14 (2014). NBCC 2015 classifies the site class C for ground profiles consisted of very dense soils and soft rocks with 360 to 760 m/s average shear wave velocity, average standard penetration resistance higher than 50, and soil undrained shear strength above 100 kPa.

To evaluate the effectiveness of the torsional loads on the seismic response of the building, each building structure was analyzed in four different levels of torsional sensitivity, including B=1.3, 1.7, 2.0, and 2.5. For the sake of consistency in all the building configurations, the accidental torsion was considered by shifting the CM from the CR by a distance equal to $\pm 0.05Dnx$. Torsional sensitivity (irregularity) of the building structures is classified in both Canadian and American design codes. According to NBCC 2015, torsional sensitivity of building structures is defined as the largest ratio of the maximum storey displacement at the extreme points of the structure to the average of the displacements at the extreme points in each floor when the structure is subjected to an eccentric equivalent static force with eccentricity of $\pm 0.1D_{nx}$ from the centre of mass. A building with $B > 1.7$ is classified as a torsionally sensitive building, and in such a case, the response of the structure cannot be evaluated based on the results of static analysis only, and dynamic analysis in mandatory. However, since the type of the dynamic analysis is not specified, RSA is usually the preferred method.

In multi-story buildings studied in the current work, the lateral force resistance in buildings studied was solely provided by an RC core wall. Each floor consisted of five equal spans in both horizontal directions, resulting in approximate outside-to-outside plan dimension of 25 m (8-story building) and 30 m (12-story and 16-story buildings). Considering the penthouse on the roof, the total heights of the structures were 34.05 m, 48.65 m and 63.25 m for 8, 12 and 16-story building respectively; consisted of a 4.85 m high first story and typical story height equal to 3.65 m. The 3D view and the plan of the 12-story building, as well as the seismic load direction, are presented in Fig. 5.9. The core wall system consisted of two C-shaped walls located at the centre of the building. The direction of the excitations for the nonlinear response of the building was solely considered to be in the cantilever direction of the walls (Fig. 5.9). The gravity-resisting system consists of 200-mm-thick flat plate slabs supported by square columns. The main characteristics of the buildings such as the height, the walls thickness and outside to outside dimensions are summarized in Table 5.3. The building was designed to be built using 30 MPa strength concrete and 400 MPa strength steel reinforcement.

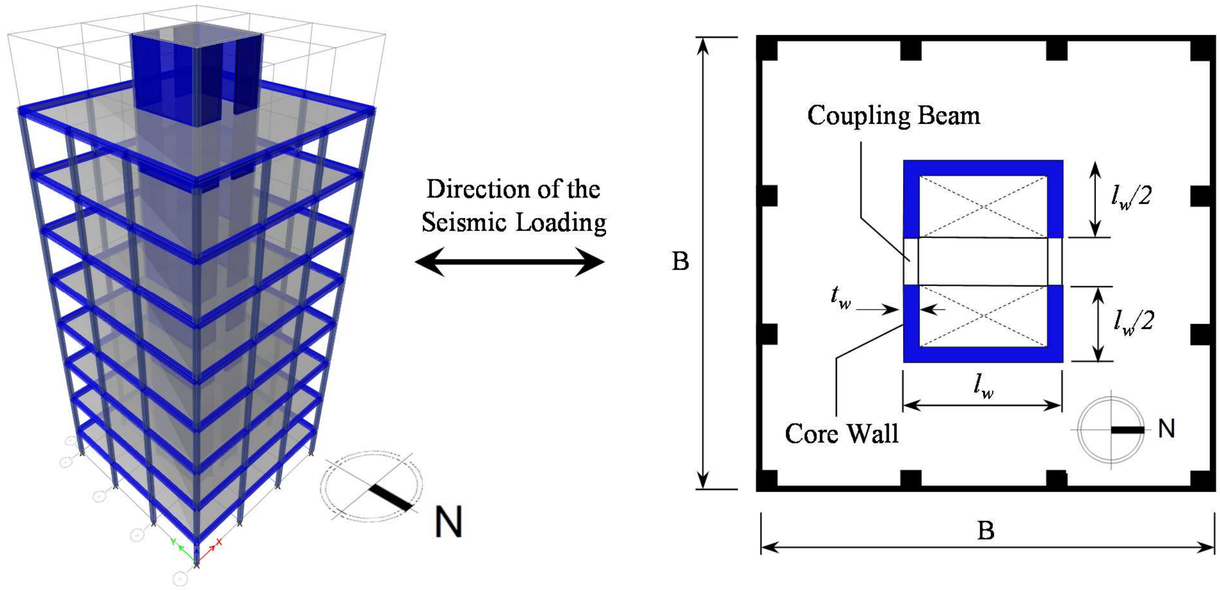

Fig. 5.9. 3D view and the floor plan of the studied buildings

As for the structural model of the buildings, Boivin and Paultre (2010) observed that the cantilever wall model can reasonably represent the behaviour of a complete building model and the stiffness from other structural components rather than the seismic resisting system has no considerable effect on the wall response predictions. Hence, the isolated core wall models could be employed for the investigations together with a gravity frame to capture the nonlinear P-Δ effects. In the current work, however, full 3D models of the buildings including the gravity columns and story floors were developed to increase the reliability of the modelling approach in capturing the P-Δ effects when the structure is subjected to torsional effects (Fig. 5.9). Hence, OpenSEES built-in feature for geometric transformation from the basic system to the global coordinate system was employed. A similar approach was used for the gravity columns. This approach was formerly supported by other researchers (e.g. Chae et al., 2012). Structural responses were controlled to avoid any code violation.

Table 5.3. Main characteristics of the studied buildings

Characteristic	8-story	12-story	16-story
Typical floor height (m)	3.65	3.65	3.65
Building height (m)	34.05	48.65	63.25
Plan dimension (m)	25	30	30
Core wall length (m)	4x5	5x6	5x6
Core wall thickness (m)	0.3	0.4	0.4
Fundamental natural period of vibration (s) (regular building, B=1.3)	1.34	1.81	2.76
Longitudinal reinforcement ratio at the base of the wall (%)	1.13	1.19	1.33
Transverse reinforcement ratio at the base of the wall (%)	0.46	0.56	0.58
Longitudinal reinforcement ratio at the mid-height of the DPH wall (%)	0.54	0.63	0.67
Transverse reinforcement ratio at the mid-height of the DPH wall (%)	0.36	0.34	0.42

The core wall in the original building was designed to have a single plastic hinge (SPH) at the base of the wall. Thus, the RC wall in the first two stories of the 8-story and 12-story buildings and the first three stories of the 16-story building were detailed as a plastic hinge region. The height of the plastic hinge was determined based on clause 21.5.2.1.2 of CSA, which prescribes the plastic hinge length of $0.5l_w+0.1h_w$. However, The CSA necessitates the extension of plastic hinge detailing up to 1.5 l_w, where l_w is the length of the wall in the direction considered and h_w is the height of the wall above the critical section. Flexural reinforcement was provided according to the CSA bending moment design envelope to satisfy the plastic hinge requirements. This was extended to provide the resisting moment prescribed by CSA.

The shear reinforcement in the assumed plastic hinging region was designed according to CSA, which was corresponding to the shear strength required to develop the probable flexural capacity of the wall. The shear detailing assigned for the base plastic hinge was extended in all the buildings to meet the factored shear strength above plastic hinge height, prescribed by CSA, and was lowered to the minimum required reinforcement in the upper floors.

5.5.2 Ground motion selection and scaling

The numerical analyses performed in this study follows the FEMA P695 (FEMA, 2009) guideline for seismic assessment of building structures, in which a group of 44 ground motions was prescribed to achieve reliable results. In the current work, due to the lack of records from earthquakes in Eastern Canada, a group of 48 artificial ground motion records (4x12 records), developed by Atkinson (2009), was used for time history analysis of the structure due to the lack of records from real earthquakes in Eastern Canada. Even though the applied method is acceptable, there are some limitations that need to be acknowledged as compare to using historical records or spectrally matched records. For instance, synthetic accelerograms often do not include wave propagation (path effects) or the near-source effects such as rupture propagations. Moreover, for multi-directional excitations, the simulated three components of ground motions are not physically consistent. Thus, time history analyses using artificial records should be done carefully, because of the influence of parameter variability on simulated earthquake results. Hence, it is advisable to use more number of records and take into account the results within a limited margin of the mean value. These accelerograms were including far field and near field records both with two different magnitudes of M=6 and M=7 Richter. Fig. 5.10 shows the plot of sample near-field M=6 and M=7 accelerograms used for the NTHA. The selected ground motions characteristics are summarized in Table 5.4.

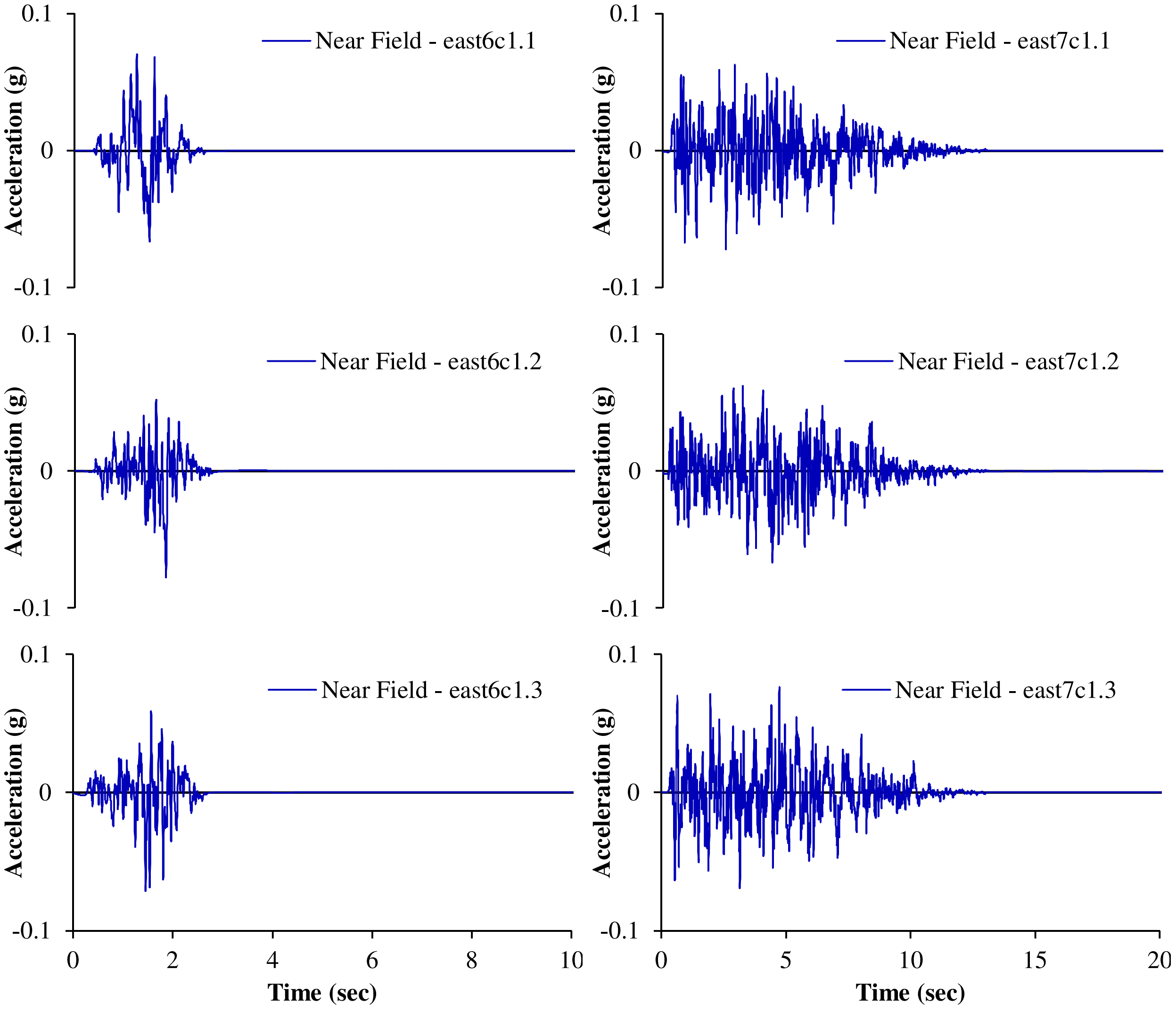

(a) (b)

Fig. 5.10. Sample time histories of selected near-filed ground motions: a) M=6; b) M = 7.

Table 5.4. Characteristics of selected ground motions (unscaled)

Near-field ground motions					Far-field ground motions				
Event	M[i]	R_{fault}[ii]	PGA[iii]	v/a[iv]	Event	M	R_{fault}	PGA	v/a
east6c1.1	6	12.8	0.756	0.0467	east6c2.1	6	20.8	0.277	0.0458
east6c1.2	6	12.8	0.768	0.0406	east6c2.2	6	20.8	0.268	0.0266
east6c1.3	6	12.8	0.717	0.0253	east6c2.3	6	20.8	0.295	0.0397
east6c1.4	6	12.5	0.646	0.0455	east6c2.4	6	21.5	0.311	0.0298
east6c1.5	6	12.5	0.597	0.0398	east6c2.5	6	21.5	0.279	0.0295
east6c1.6	6	12.5	0.661	0.0337	east6c2.6	6	21.5	0.192	0.0555
east6c1.7	6	12.8	0.523	0.0573	east6c2.7	6	16.9	0.267	0.0387
east6c1.8	6	12.8	0.565	0.0355	east6c2.8	6	16.9	0.315	0.0404
east6c1.9	6	12.8	0.411	0.0359	east6c2.9	6	16.9	0.287	0.0480
east6c1.10	6	12.8	0.431	0.0363	east6c2.10	6	21.1	0.232	0.0430
east6c1.11	6	12.8	0.405	0.0447	east6c2.11	6	21.1	0.296	0.0361
east6c1.12	6	12.8	0.533	0.0314	east6c2.12	6	21.1	0.218	0.0336
east7c1.1	7	13.8	0.727	0.0525	east7c2.1	7	41.6	0.229	0.0647
east7c1.2	7	13.8	0.598	0.0856	east7c2.2	7	41.6	0.203	0.0567
east7c1.3	7	13.8	0.770	0.0437	east7c2.3	7	41.6	0.229	0.0602
east7c1.4	7	15.3	0.806	0.0570	east7c2.4	7	50.3	0.151	0.0504
east7c1.5	7	15.3	1.162	0.0562	east7c2.5	7	50.3	0.148	0.0759
east7c1.6	7	15.3	0.871	0.0384	east7c2.6	7	50.3	0.122	0.0789
east7c1.7	7	14.2	0.922	0.0738	east7c2.7	7	45.2	0.204	0.0522
east7c1.8	7	14.2	0.764	0.0534	east7c2.8	7	45.2	0.184	0.0539
east7c1.9	7	14.2	1.085	0.0642	east7c2.9	7	45.2	0.180	0.0730
east7c1.10	7	14.9	0.971	0.0551	east7c2.10	7	50.3	0.125	0.0949
east7c1.11	7	14.9	0.971	0.0385	east7c2.11	7	50.3	0.127	0.0610
east7c1.12	7	14.9	0.844	0.0828	east7c2.12	7	50.3	0.122	0.0643

[i] M: magnitude,

[ii] R_{fault}: closest distance to fault

Each ground motion was scaled using the ASCE/SEI method (ASCE, 2010) such that within the range of $0.2T_1$ and $1.5T_1$, where T_1 is the fundamental period of vibration of the structure, the integration of response spectral accelerations matches or be above the integration of target spectral acceleration (i.e. Uniform Hazard Spectrum). The studied buildings were considered for Montreal, Canada only and no seismic hazard variation was considered which can be noted as a limitation of the current work. The structural damping was considered by means of mass and stiffness proportional Rayleigh damping. A damping ratio of 5% was assigned which is a typical value for RC buildings. Although the Rayleigh damping feature in OpenSEES can formulate the damping matrix using the initial, current, or last committed stiffness matrix, only the initial stiffness matrix was used in the current work. Fig. 5.11 presents the 5%-damped acceleration response spectra of the ground motions.

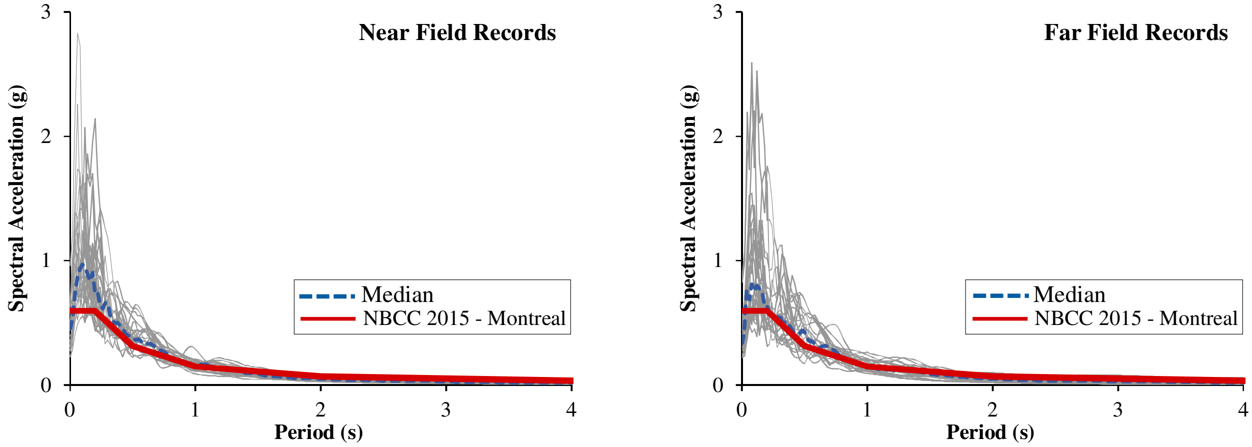

(a) (b)

Fig. 5.11. The 5%-damped acceleration response spectra of selected ground motions for Montreal

5.5.3 Results of time history analyses

The effect of the torsional sensitivity on the performance of the structures designed based on the Canadian codes (CSA A23.3-14 and NBCC 2015) was investigated using NTHA. After post-processing the data, time history response plots were created. A comparison has been made afterward between the results of NTHA and the design envelope obtained from the response spectrum analysis of the structure.

Shear force envelope of the studied buildings was developed to evaluate the effect of torsional sensitivity variation of the structure on the story shear demand. Results of the NTHA of 12-story buildings are shown as a sample in Fig. 5.12, in which the story shear demands fluctuated significantly for different ground motion records. As it was expected, a considerable increase in the shear force demand was observed by increasing the torsional sensitivity of the structure. Moreover, a wider range of variation of the shear force for each story was observed in building with higher torsional sensitivity.

Fig. 5.13 presents the summary of the results for 8, 12 and 16-story buildings, in all of which the story shear is normalized by the base shear resistance, V_r, specified according to the CSA A23.3-14. Comparison of the results showed that by increasing the torsional irregularity of the building, shear demand in some stories of all the structures exceeded the shear capacity. This trend continued until the point that at $B = 2.5$, almost all ground motions led to a shear envelope beyond what was predicted by the CSA capacity design method. Though exceeding the demand because of few artificial ground motion records (i.e. lower torsional sensitivity levels) might not be considered as code contravention, this could be a considerable issue when the capacity design based on the response spectrum analysis fails to resist the shear forces from a major part of the selected earthquakes at higher torsional sensitivity levels.

Comparison of the results from the analysis of buildings with different heights showed that, for a low torsional sensitivity level, the code predictions is more consistent for shorter wall height (i.e. 8-story building). However, an increase of the torsional sensitivity of the building has more significant effects on the shorter buildings rather than the taller ones. An increase of 65% in the peak normalized shear of the 8-story buildings was observed, while the amount of increases were 46% and 40% for 12-story and 16-story buildings respectively.

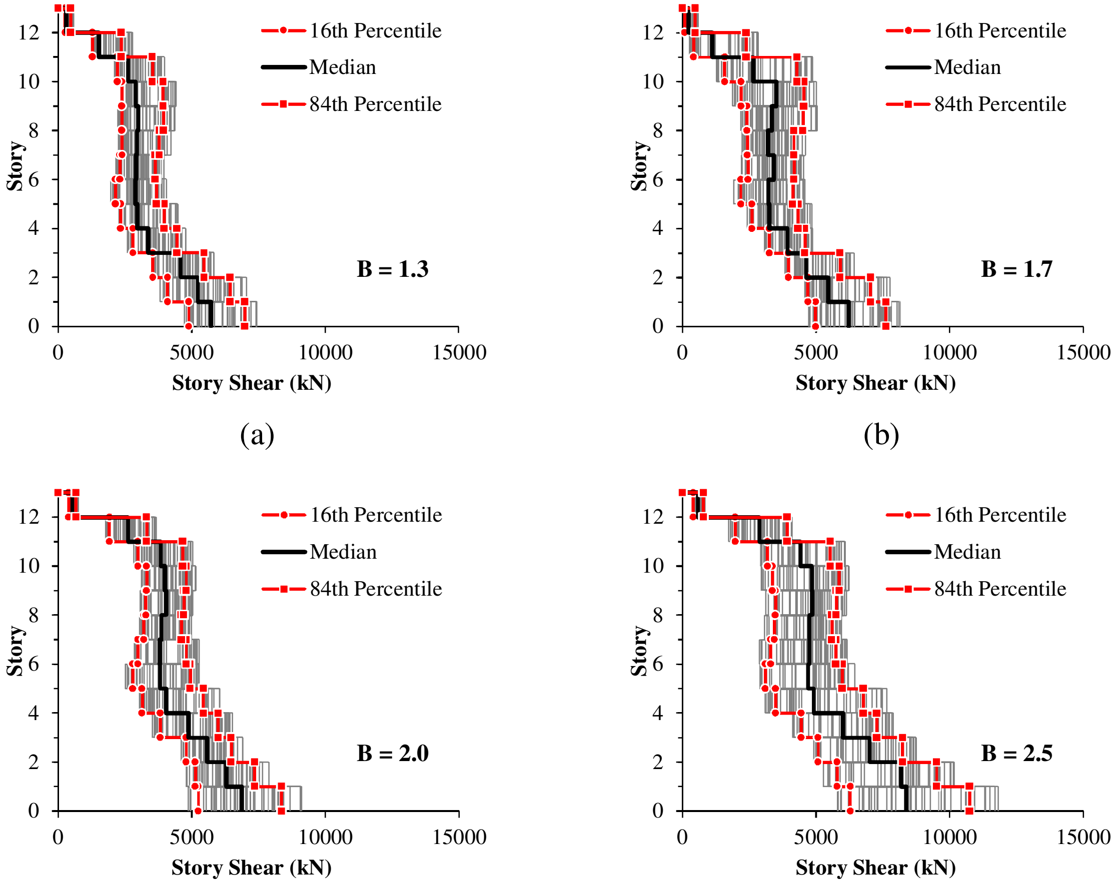

(a)

(b)

(c)

(d)

Fig. 5.12. Sample shear envelopes of the 12-story building subjected to individual ground motions

The scope of this study was limited to the buildings in which noticeable contribution of shear deformations in the seismic response of structure is expected. The lateral response of taller buildings is mainly controlled by flexural deformations. Hence, buildings over 16 stories were excluded from the study. It is worth mentioning that a study by Adebar et al. (2014) compared different proposed methods to consider the contribution of higher modes in the story force demands. Thirteen building structures in different heights up to 50 stories were studied, and the presented results in terms of the required shear amplification factor showed that almost all the proposed methods result in similar amplification factors for buildings with more than 16 stories.

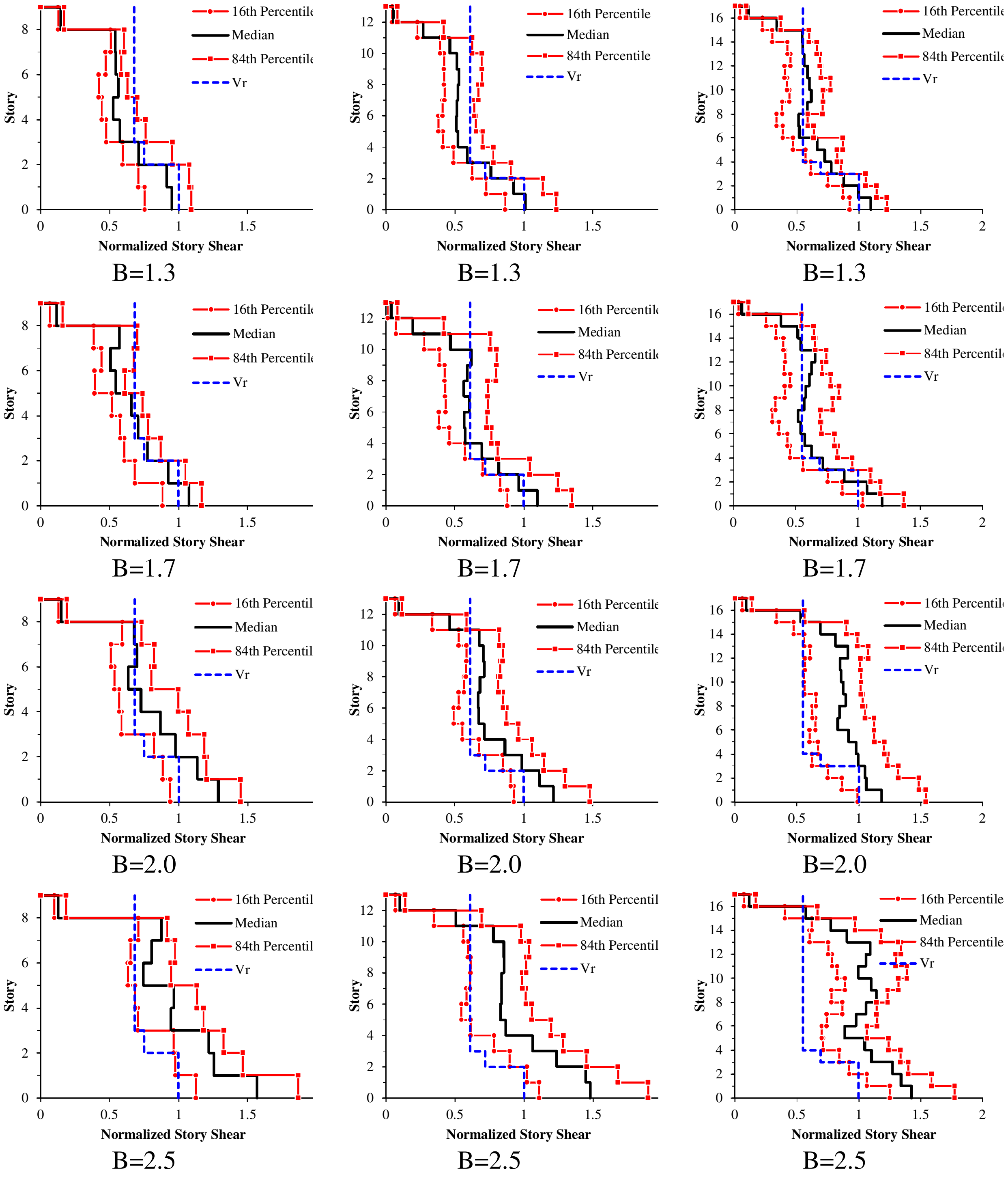

(a) 8-story (b) 12-story (c) 16-story

Fig. 5.13. Evaluation of shear force demand along the height of the building (NTHA)

Moment envelopes along the height of the buildings were also developed to investigate the effect of torsional irregularity of the structure on bending moment demands in the structure. A sample comparison of the median moment envelopes for the 12-story building subjected to the selected ground motions is presented in Fig. 5.14. Though shear force demands were highly affected by changing the torsional sensitivity, it was found to have no major effect on the moment envelope of the building. A similar observation was recently reported by Pelletier and Léger (2017).

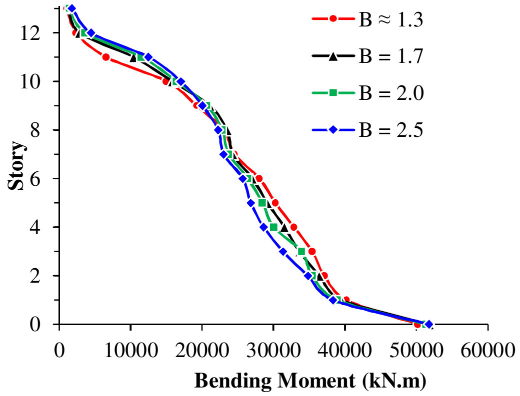

Fig. 5.14. Median moment envelopes of building structures (NTHA)

5.6 Seismic Performance of Core Walls with Dual Plastic Hinge

Panagiotou and Restrepo (2009) introduced a DPH concept for the design of RC shear walls, to overcome the disadvantages of extended plasticity and SPH methods such as special reinforcement detailing. DPH was proved to be an optimized method, since it provides the same control on the performance of the structure as the SPH does, while releases a significant portion of the height of the wall from special reinforcement detailing. Moreover, it was found that DPH could result in lower shear force demand in the structure in comparison with what was obtained from the buildings with SPH (Panagiotou and Restrepo, 2009). Hence, the DPH method was employed as a solution for controlling the shear force demand in torsionally sensitive structures studied in the current work. All the buildings were designed again according to the DPH concept, and the second plastic hinge was considered at the mid-height of the building as it was proposed by Panagiotou and Restrepo (2009). Longitudinal and transverse reinforcement ratios for the base and mid-height plastic hinges are presented in Table 5.2. Same equation from the CSA was used to determine the height of the plastic hinge at the mid-height of the wall, and h_w was considered as the height above the second plastic hinge level which is equal to half of the total height. However, the plastic hinge detailing was only extended up to the next story level. Moreover, no amplification was applied on the design shear forces for the buildings with DPH; amplification of story shear forces due to the inelastic effects of higher modes was neglected in this case. A sample distribution of reinforcement along the height of the 12-story RC wall with Dual Plastic Hinge is presented in the Fig. 5.15. As a comparison, the buildings with SPH has less longitudinal reinforcement ratio at mid-height of the wall (i.e. zone 4 in the Fig. 5.15) than the DPH walls, which is due to the minimum longitudinal reinforcement required for the plastic hinge zones. Regarding the horizontal reinforcement ratio, the design of SPH walls based on CSA A23.3-14 considers the shear forces amplified because of the inelastic effects of higher modes. Hence, the ratio of the horizontal reinforcement at mid-height of the wall (i.e. minimum reinforcement according to CSA A23.3-14) to the corresponding value at the base is again smaller in the SPH walls.

5.6.1 Shear envelopes of buildings with DPH

Fig. 5.16 shows the shear force envelopes obtained from NTHA for buildings with DPH. As it can be seen from the figure, DPH system performed well in controlling the story shear demand along the height of the structure. Though there are still stories in which the shear demand exceeded the shear resistance provided based on the capacity design method, the enhancement of the performance even in torsionally irregular buildings is noticeable. Considering the median of the results from the 48 selected ground motions, all the buildings were found to provide capacities higher than the shear force demand except in stories 3 to 4 and 3 to 5 for the 12-story and 16-story buildings respectively. However, the demand over capacity ratios were limited to 1.12 and 1.11 respectively.

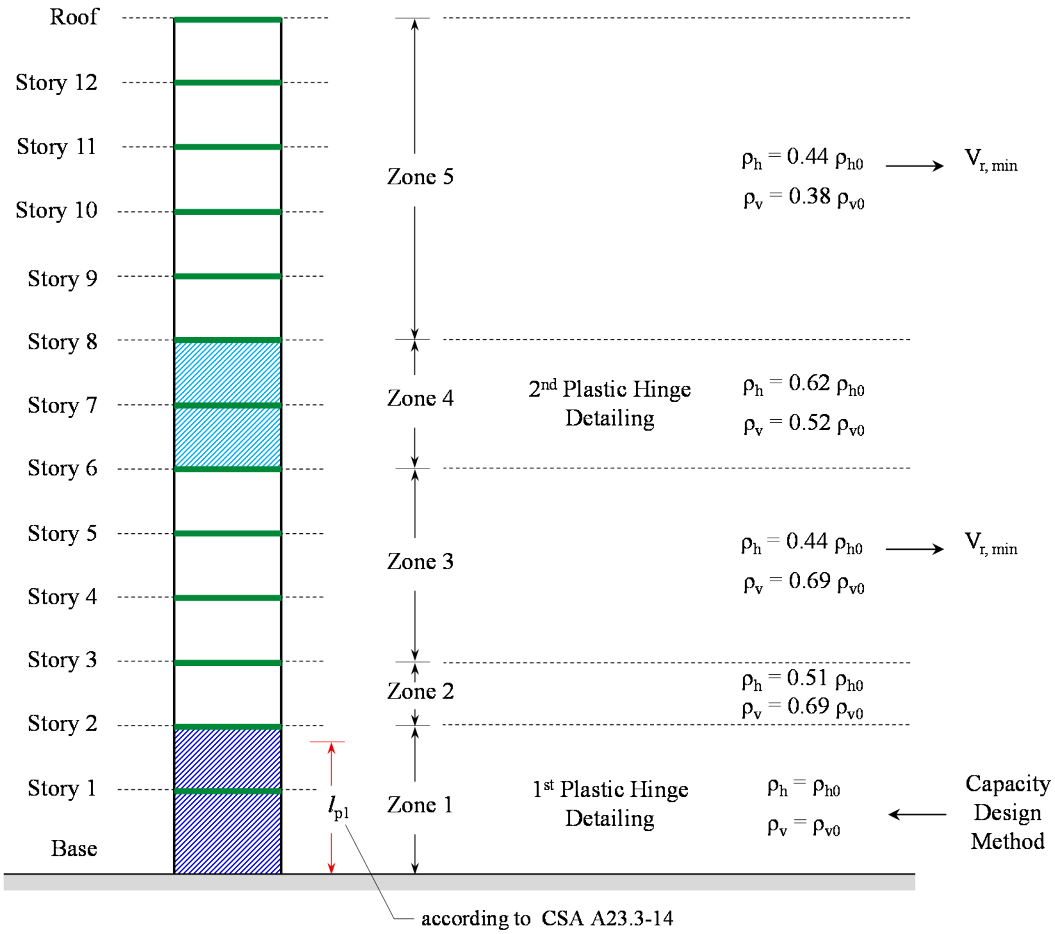

Fig. 5.15. Sample reinforcement ratios along the height of the 12-story RC wall with Dual Plastic Hinge

By increasing the torsional sensitivity of the building, the excessive demand predicted for the 8-story structure was ranged from 5% to 11%. This range was predicted from 6% to 17% and 6% to 15% on average for the 12-story and 16-story buildings respectively. Despite the buildings with SPH system in which excessive shear demand was predicted to happen even in the top stories, especially when the torsional sensitivity of the structure goes beyond the $B = 2.0$, none of the buildings with DPH system was experienced a demand over capacity ratio more than 1.0 in the upper half of the building. Results of DPH buildings, however, showed shear demands beyond the shear resistance in torsionally sensitive buildings ($B \geq 1.7$), but quite limited (within 6% to 15% average in 4 to 6 mid-height stories) in comparison with the average of 9% to 53%

which was observed in the buildings with SPH (i.e. averagely 3% to 38% smaller shear demand over capacity ratio).

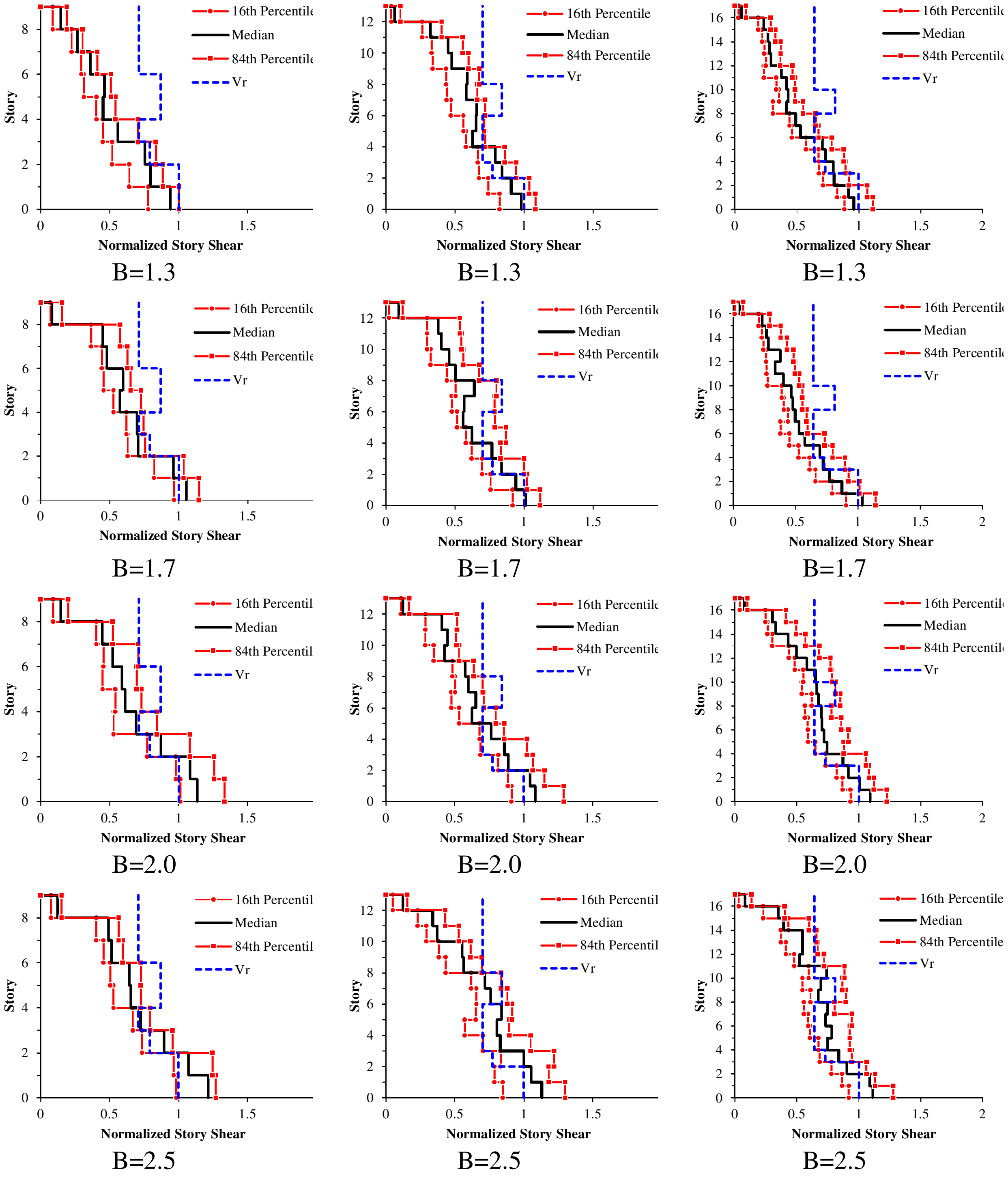

B=1.3 B=1.3 B=1.3

B=1.7 B=1.7 B=1.7

B=2.0 B=2.0 B=2.0

B=2.5 B=2.5 B=2.5

(a) 8-story (b) 12-story (c) 16-story

Fig. 5.16. Shear force demand along the height of the building with DPH (NTHA)

5.6.2 Response comparison for SPH and DPH core wall buildings

As it was observed in the previous section, the overall performance of DPH design in controlling the shear force demand along the height of the structures was significant. A comparison was made between the two design concepts, SPH and DPH, in terms of shear demand over capacity ratio of each floor.

Results of the comparison for the 12-story buildings are presented in Fig. 5.17. As it is depicted in the figure, NTHA of structures designed based on DPH concept resulted in shear demand/capacity ratio of less than 1.0 in most stories, and only a few stories in the irregular structures (mainly at $B \geq 2.0$) suffered from underestimation of the shear demand by the RSA. Moreover, developed box plots showed that the fluctuation of results of NTHA of buildings with DPH subjected to 48 individual records was considerably less than that of buildings with SPH.

Although not shown in detail herein, similar results were observed for 8-story and 16-story buildings. The summary of seismic assessment results for RC cores is presented in Table 5.5, in which the normalized shear demand/capacity at the base of the walls in all the buildings are compared. As it can be seen, the same trends of results are captured in 8-story and 16-story structures. This promotes the DPH concept as an efficient alternative for the design of torsionally sensitive buildings. A quantitative comparison also showed up to 65%, 47% and 30% increase in the normalized base shear demand (normalize to V_r) by increasing the torsional sensitivity in 8, 12 and 16-story SPH buildings respectively. The corresponding increases in DPH buildings were up 29%, 15% and 16% respectively.

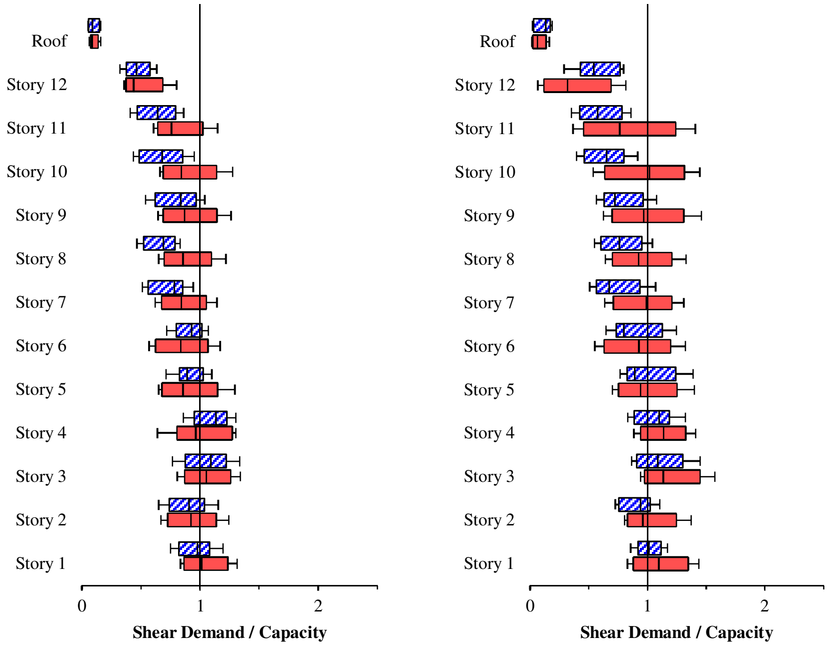

(a) B = 1.3 (b) B = 1.7

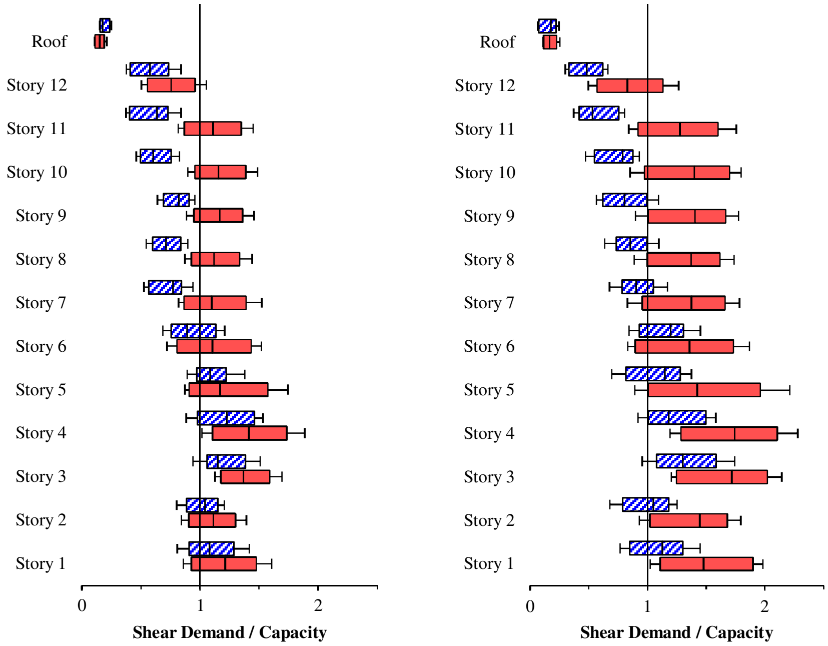

(c) B = 2.0 (d) B = 2.5

🟥 SPH ▨ DPH

Fig. 5.17. Shear demand-over-capacity ratios for 12-story buildings with SPH and DPH

Generally, taller SPH buildings showed larger normalized shear demand, while had less discrepancies because of torsional sensitivity variations. This was quite expected as the shorter buildings were subjected to higher levels of T/M ratios along the height of the structure, and torsional effects were more effective in these buildings. Buildings with DPH showed opposite responses by increasing the height of the structures, which is because of the influence of the second plastic hinge on the higher modes of vibration of the structure. In fact, DPH has more mitigation effects on the higher modes of taller buildings, and hence results in limited contribution of higher modes in increasing the story shear force demand in the structure.

Table 5.5. Summary of seismic assessment results for RC cores

Torsional Sensitivity	V_{base}^{i} / V_r (SPH)			V_{base}^{i} / V_r (DPH)		
	8-story	12-story	16-story	8-story	12-story	16-story
B = 1.3	0.95	1.01	1.09	0.94	0.98	0.96
B = 1.7	1.07	1.10	1.19	1.05	1.01	1.03
B = 2.0	1.29	1.21	1.18	1.13	1.08	1.09
B = 2.5	1.57	1.48	1.42	1.21	1.13	1.11

[i] median value of 48 ground motions

5.7 Discussion

Subject to the limitations imposed by the underlying assumptions, results of the study in the previous sections showed that the shear force demand predicted by the capacity design method is inadequate in some cases even after DSA prescribed by CSA A23.3-14 is used. As a result, the shear demand envelope obtained needs to be enhanced further to address the issue. It is worth mentioning that, in the explanatory notes, the CAC Concrete Design Handbook (2016) explicitly states that the shear amplification factors adopted in the 2014 version of CSA A23.3 are a lowerbound value compared to the other recommendations by Ambroise et al. (2013). The shear amplification prescribed was adjusted for spectral shapes in eastern Canada based on the work of Paultre (Ambroise et al., 2013). Table 5.6 shows the required enhancement in terms of a percentage of the code amplification factor for different building configurations studied here. Excepting the torsionally regular buildings (*B* < 1.7), in most of which the DSA prescribed by the CSA 23.3-14 performed well by reasonable estimation of shear force demand, NTHA of torsionally sensitive buildings resulted in shear envelopes that were exceeding the amplified envelope predicted through RSA by 3% to 64% and 3% to 75% for SPH and DPH buildings respectively. Results are presented in Fig. 5.18, and show that there is no constant trend between the results for lightly irregular buildings (*B* ≈ 1.7).

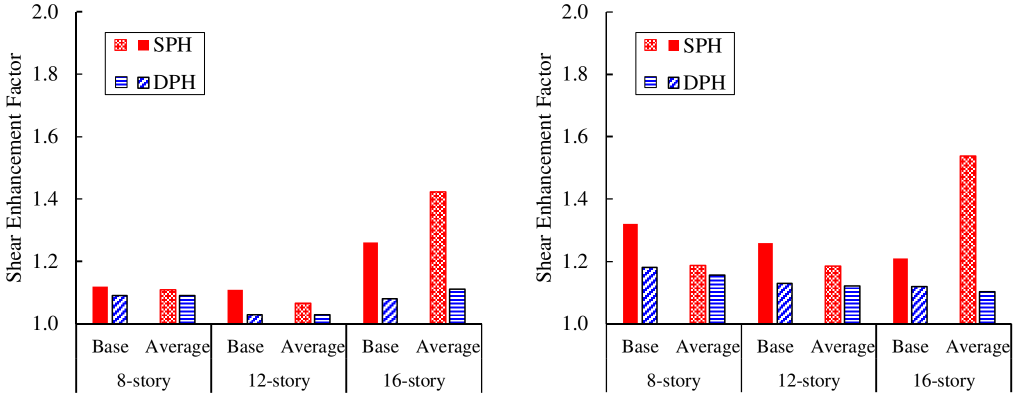

(a) B=1.7

(b) B=2.0

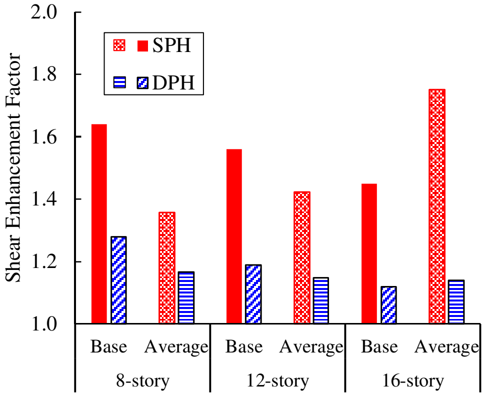

(c) B=2.5

Fig. 5.18. Required enhancements in the shear amplification factor

As for the buildings with $B \geq 2.0$, however, it can be clearly seen that the base shear enhancement factor decreased by about 10% by increasing the height of the SPH structures. Moreover, an ascending trend was observed for the average stories shear enhancement factor when the number of stories increases, resulted in up to 29% increase. Results of the DPH buildings, however, showed a descending trend for both the base and average stories shear enhancement factor; 9% and 4% decrease respectively. Hence, DPH concept was found to be an efficient alternative when high torsionally sensitivity in the structural response is expected.

Table 5.6. Required enhancement in the dynamic shear amplification factor

Torsional Sensitivity	Flexural Yielding	8-story		12-story		16-story	
		Base	Average	Base	Average	Base	Average
B = 1.3	SPH	---	---	1.04	1.04	1.12	1.18
	DPH	---	---	---	---	---	1.15
B = 1.7	SPH	1.12	1.11	1.11	1.07	1.26	1.42
	DPH	1.09	1.09	1.03	1.03	1.08	1.11
B = 2.0	SPH	1.32	1.19	1.26	1.19	1.35	1.55
	DPH	1.18	1.16	1.13	1.12	1.12	1.10
B = 2.5	SPH	1.64	1.36	1.56	1.42	1.45	1.75
	DPH	1.28	1.17	1.19	1.15	1.12	1.14

5.8 Conclusions

This study provides results from nonlinear time history analysis of C-shaped RC walls to investigate the performance of response spectrum analysis for the design of RC building structures with an RC core wall. A macro-modelling approach using the wide column analogy was employed to develop and calibrate a numerical model.

A total of 1152 nonlinear time history analyses were conducted on 8, 12 and 16-story buildings using a group of 48 artificial ground motion records. The buildings were designed for Montreal, Canada, using the response spectrum analysis method and according to the Canadian design codes, NBCC 2015 and CSA A23.3-14. Results showed that:

- Though RSA is known as a robust and practical dynamic analysis method, results of NTHA of torsionally sensitive buildings showed notably larger story shear demand than what was predicted by RSA using the NBCC 2015 provisions. The predictions were more consistent for regular low rise walls ($B < 1.7$) because of lower T/M ratio, however, a substantial increase of up to 65% was observed in the peak base shear when the torsional sensitivity of the structure reached B = 2.5. Results are in agreement with some previous findings in the literature (Tso and Yao, 1993; Pelletier and Léger, 2017).
- A significant contribution of higher modes noticeably affects the story force demand in the buildings as torsional irregularity of the building increases, especially in shorter buildings. This is expected because usually in torsionally irregular buildings, even third and fourth modes of vibration substantially affect the seismic response, while the seismic response of regular buildings would usually be controlled by only the first and second modes. It was also shown that the range of variations extends by the increase of torsional sensitivity of the structure.
- More effective mitigation of higher mode effects was observed in DPH buildings, which resulted in lower shear force demands in comparison with SPH buildings. DPH method was found to be an efficient alternative for controlling the shear force demand in torsionally sensitive buildings. Using the DPH method, the extra shear demands

observed in the torsionally irregular SPH buildings was controlled by a range of 14% to 36%, corresponding to 16 and 8-story buildings respectively. However, the shear demand envelopes were still beyond the RSA predictions in high torsionally irregular buildings ($B > 2.0$). Moreover, the fluctuation of the shear force demands was lower than the corresponding values in the SPH buildings.

- The new “dynamic shear amplification factor” in CSA A23.3-14 provisions performed well in predicting the shear force demand required for the design of torsionally regular RC walls ($B < 1.7$) using capacity design method and RSA analysis. However, results of RSA analysis based on the response spectrum prescribed by NBCC 2015 need to be further amplified as the torsional irregularity increases. Shear force enhancement factors were proposed in the current work, and showed that 3% to 64% and 3% to 75% increase is required for SPH and DPH buildings respectively.
- By increasing the torsional sensitivity of SPH structures, the required shear enhancement factor was decreased for base shear force while it was increased for the average story shear force. In DPH structures, however, a descending trend was observed for both the base and average story shear forces.

CHAPTER 6

Experimental Test on C-Shaped RC Walls

6.1 Abstract

This chapter presents results of a series of tests on a large-scale C-shaped reinforced concrete (RC) wall retrofitted with carbon fibre-reinforced polymer (CFRP) sheets and subjected to multi-directional excitations. The C-shaped wall was the main seismic force resisting system (SFRS) of a 5-story building, the base story of which was only constructed physically and the upper floors of the building were simulated numerically, and tested in a hybrid 6 degrees of freedom system using OpenSEES (2013) and OpenFresco (2013). The C-shaped wall was designed and detailed according to the seismic provisions of the NBCC 2010 and CSA-A23.3-04 standards. The objectives were to validate both qualitatively and quantitatively the efficiency of CFRP in retrofitting of damaged C-shaped RC walls. The Original C-shaped wall specimen was tested by Mechmachi and Bouaanani (2018) under two records of Nahanni earthquake, namely mainshock and aftershock. The Original tested wall was significantly damaged at the end of the hybrid tests and characterization tests. The wall was then removed from the test setup for FRP retrofitting. The retrofitted wall was then subjected to the same hybrid and characterization tests. Subsequently, a multi-directional cyclic loading protocol was applied in the test specimen. Based on the test results, the CFRP retrofitting scheme used in the current work successfully enhanced the structural performance of the wall. Strength degradation was efficiently controlled, and by conducting characterization tests at the end of hybrid tests, larger strength, yet with similar stiffness, was measured compared to the results from the Original wall.

6.2 Testing program

The description of the experimental work concerning the geometry, properties of constituent materials and testing of the C-shaped RC walls under multi-axial excitation is presented in this section. The work was done as a joint research team project by Concordia University and École Polytechnique de Montréal University, and supported by le Fonds de Recherche du Québec - Nature et Technologies (FRQNT) through an Èquipe (Team) grant.

6.2.1 RC Building with C-shaped Core Wall

Mechmachi and Bouaanani (2018) conducted a series of hybrid experimental tests on a large scale RC C-shaped core wall specimen, hereafter referred to as “Original wall”. The studied building was a 5-story building in Montreal, Canada with class C soil condition. The building was designed according to the National Building Code of Canada (NBCC, 2010) and the CSA A23.3-04 (2010 edition). Each floor consisted of three equal spans in both directions, with span lengths equal to 6 m and 5 m in X and Y directions, respectively. The total height of the building was 16.94 m; consisting of a 4.14 m high first story and a typical story height of 3.2 m.

The plan view of the studied building is shown in Fig. 6.1. The C-shaped RC core wall measured 2.52 m by 2.52 m in the plan, outside to outside of the walls with 165 mm thickness, which was positioned at the centre of the plan of the building. The reinforcement layout at the end of flanges and at the web-flange junctions were 4-20M bars, whereas 10M vertical and horizontal bars with 200 mm spacing were used as the distributed reinforcement. Geometrical details of the RC core wall is shown in Fig. 6.1. The building was designed using a 37 MPa concrete compressive strength and 400 MPa yield strength steel reinforcement (Mechmachi and Bouaanani, 2018).

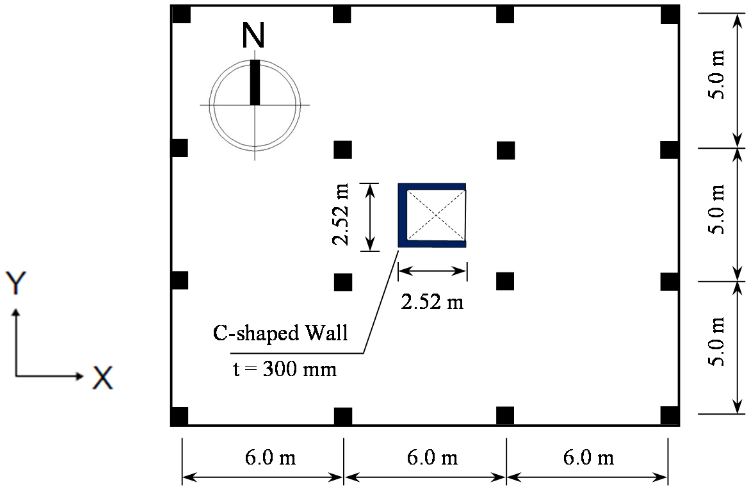

Fig. 6.1. Plan of the building studied using the hybrid test system (Mechmachi and Bouaanani, 2018)

6.2.2 Construction of the Test Specimen

Considering the available maximum space and dimensions of the C-shaped RC core wall, a large-scale (scale factor 0.56) RC specimen was constructed for the hybrid tests. The geometry of the C-shaped RC wall is shown in the Fig. 6.2. The RC wall was integrally cast with a 1.25 m high rigid concrete footing (that is fixed to the lab's rigid floor), and a 0.75 m top concrete collar (that is rigidly connected to the actuators' loading system). The height of the tested wall is 2.3 m, and considering the scale factor of 0.56 for the specimen, it was representing the first story of a building in the hybrid tests, where upper floors were simulated in the numerical model. Figures 6.2 and 6.3 show the geometry of the RC wall specimen.

The experimental testing program for investigating the 3D seismic effects on C-shaped walls was conducted at the Structures Laboratory of Polytechnique Montréal. A High-Performance Multiaxial Loading System available at the Structures Laboratory of Polytechnique was used for this purpose, to conduct the hybrid tests on the C-shaped RC walls (Fig. 6.4).

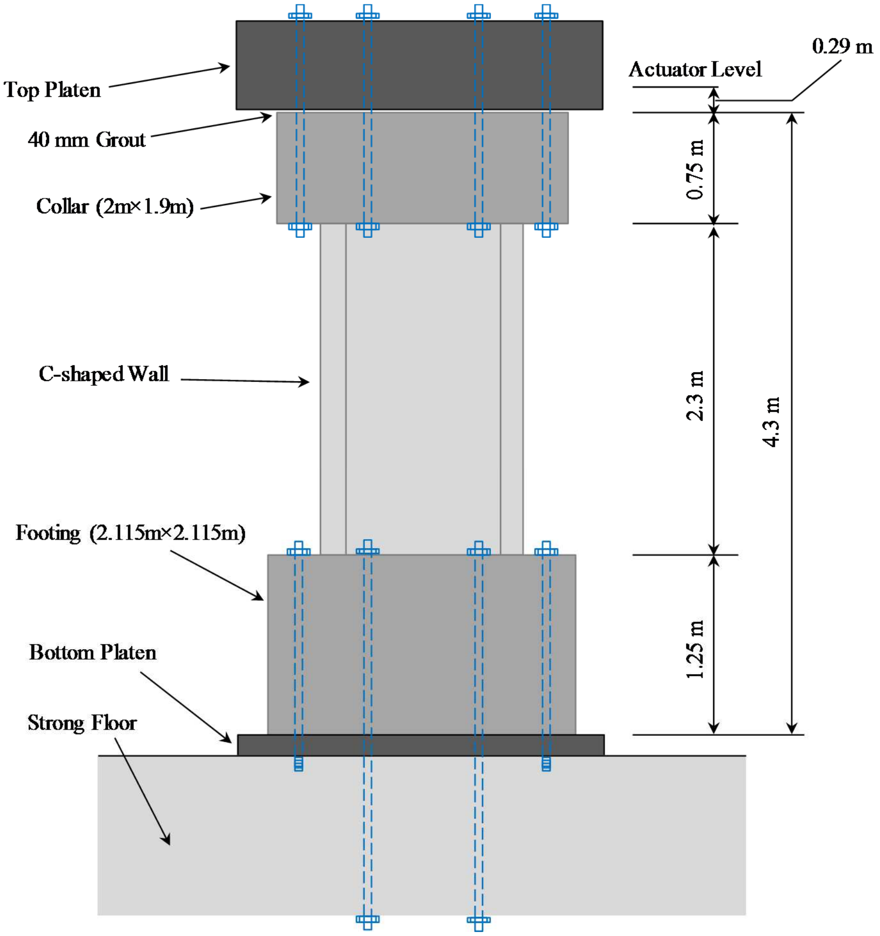

Fig. 6.2. Elevation view of the C-shaped wall in the 6DOF system (Mechmachi and Bouaanani, 2018)

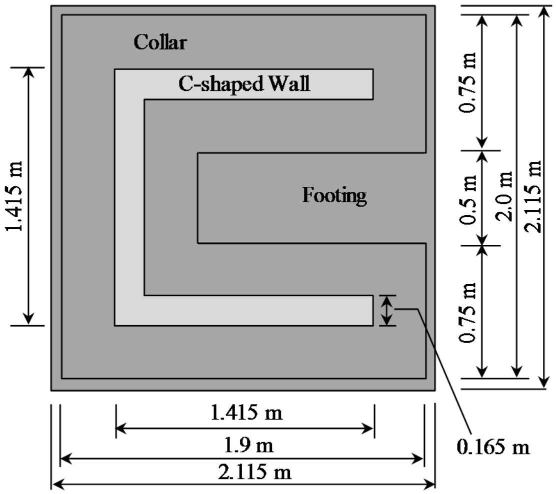

Fig. 6.3. Plan view and C-shaped wall dimensions (Mechmachi and Bouaanani, 2018)

Fig. 6.4. Experimental testing program: C-shaped shear wall tested using the Multiaxial Loading System at Polytechnique Montreal (Mechmachi and Bouaanani, 2018)

A numerical model in SeismoStruct was developed to predict the response of the Original wall, and to control whether the wall will reach the targeted performance point when it is subjected to the selected loading protocol. A Wide Column Model (WCM) modelling approach was used to model the C-shaped RC wall in SeismoStruct. Fig. 6.5 shows the numerical model developed for simulating the RC wall response. However, the numerical models for the hybrid tests were developed using OpenSEES. This model was linked to the hybrid test system using OpenFrasco.

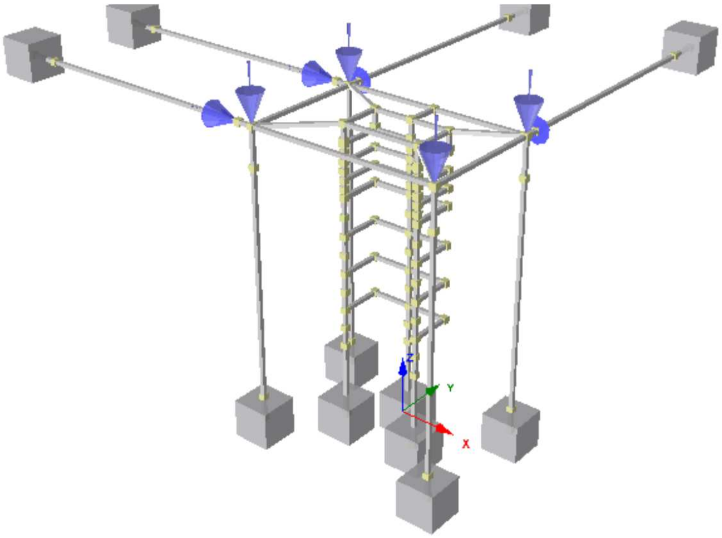

Fig. 6.5. Simulation of the tests using Seismostruct.

The Original wall specimen was tested under Nahanni ground motion in different steps, mainly called “mainshock” (steps 1 and 2) and “aftershock” (step 3). Accelerograms of both the mainshock and aftershock are shown in the section 6.2.6. Severe cracks were observed at the end of the hybrid tests (Fig. 6.6).

6.2.3 FRP Retrofitting of C-shaped RC Wall

6.2.3.1 FRP scheme for the C-shaped Section

The tested Original wall was retrofitted using CFRP (Carbon Fibre-Reinforced Polymer) sheets, and then re-tested under multi-axial cyclic loads. The goal of the retrofit was to enhance the seismic behaviour of the Original wall at the locations that experienced nonlinear response; i.e. at the critical locations that the applied moment exceeds the design bending moment for the RC wall. The retrofitting scheme was selected based on the expected failure mode of the wall in these critical regions. Based on the observed crack patterns after the Original wall was tested (Fig. 6.6), the planned CFRP retrofitting was re-evaluated for probable modifications needed, and verified to have enough efficacy in retrofitting the damaged RC core wall.

Fig. 6.6. Crack patterns observed at the end of test on Original wall specimen by Mechmachi and Bouaanani (2018): General view

The following figures show the observed crack patterns and compressive crushing of the C-shaped RC core wall at the end of the series of tests of Mechmachi and Bouaanani (2018).

(a) (b)

Fig. 6.7. Crack patterns observed at the end of test on Original wall specimen: a) Inside the core wall, b) North-East corner (Mechmachi and Bouaanani, 2018)

(a) (b) (c)

Fig. 6.8. Crack patterns observed at the end of the tests on Original wall specimen: Top of the core wall (Mechmachi and Bouaanani, 2018)

The capacity design philosophy of the wall necessitates that the RC wall should not fail in shear before reaching its flexural capacity; which has to be also respected for FRP Retrofitted walls. To respect this design philosophy, the retrofit strategy was designed to increase the flexural capacity of the C-shaped wall while providing the corresponding increase in shear capacity. The former will be achieved by applying vertical CFRP sheets at the boundary zones (i.e. corner zones) of the C-shaped RC wall, whereas, horizontal CFRP wraps will be applied to increase the shear capacity of the C-shaped wall. Table 6.1 shows the mechanical properties of the FRP and epoxy materials used in the current work.

Table 6.1. Mechanical properties of FRP and epoxy materials (Fyfe Co., 2017)

Properties	FRP sheets	Epoxy
Tensile Strength	834.3 MPa	72.4 MPa
Tensile Modulus	82 GPa	3.18 GPa
Ultimate Elongation	0.85%	5.0%
Density	1.8 g/cm^3	1.16 g/cm^3 (liquid)
Thickness	0.51 mm	---

The vertical FRP retrofitting was designed to theoretically provide approximately 30% increase in the nominal flexural strength of the Original RC wall using the strain compatibility method. The maximum concrete compressive strain for the unconfined concrete was limited to ε_{cu} = 0.0035 according to the CSA S806 (2012), whereas ε_{cu} = 0.01 was considered for the confined concrete at boundaries of the wall. The latter was according to the findings of Wallace (1995), and it is referenced by ACI 440.2R (2017). The maximum tensile strain (i.e. ultimate elongation) at the outermost fibre of the FRP strip was considered as ε_{fd} = 0.0085 according to the manufacturer's specifications. This was controlled and found to be lower than the debonding strain of ε_{fd} = 0.01 according to the ACI 440.2R (2017). Hence, considering the mechanical properties of the FRP materials shown in Table 6.1, vertical strips with a width of 250 mm were considered for both sides of the flange ends and on the outer faces of the conjunctions of the web and the flanges. Moreover, the shear capacity needed to be increased accordingly. The added shear capacity of the wall due to FRP wrapping was calculated based on the findings of Haroun et al. (2005), considering an FRP material reduction factor ψ_f = 0.85. However, as it was proposed by Haroun et al. (2005), and referenced by ACI 440.2R (2017), the effective strain for calculating the shear strength in the FRP sheets was limited to ε_{fe} = 0.004. Hence, two layers of horizontal FRP wrapping was found to be necessary to prevent premature shear failure of the wall, considering the added flexural capacity.

This rehabilitation scheme will thus increase the wall's flexural and shear strengths. The horizontal CFRP wrapping also helps to reduce the tendency of premature debonding of the vertical CFRP strips under compression during the cyclic loading, identified by Lombard et al. (2000) as an unfavourable response that needs to be avoided. Fig. 6.9 shows the elevation view FRP retrofitting scheme designed for the C-shaped RC wall specimen. A plan view is shown in Fig. 6.10.

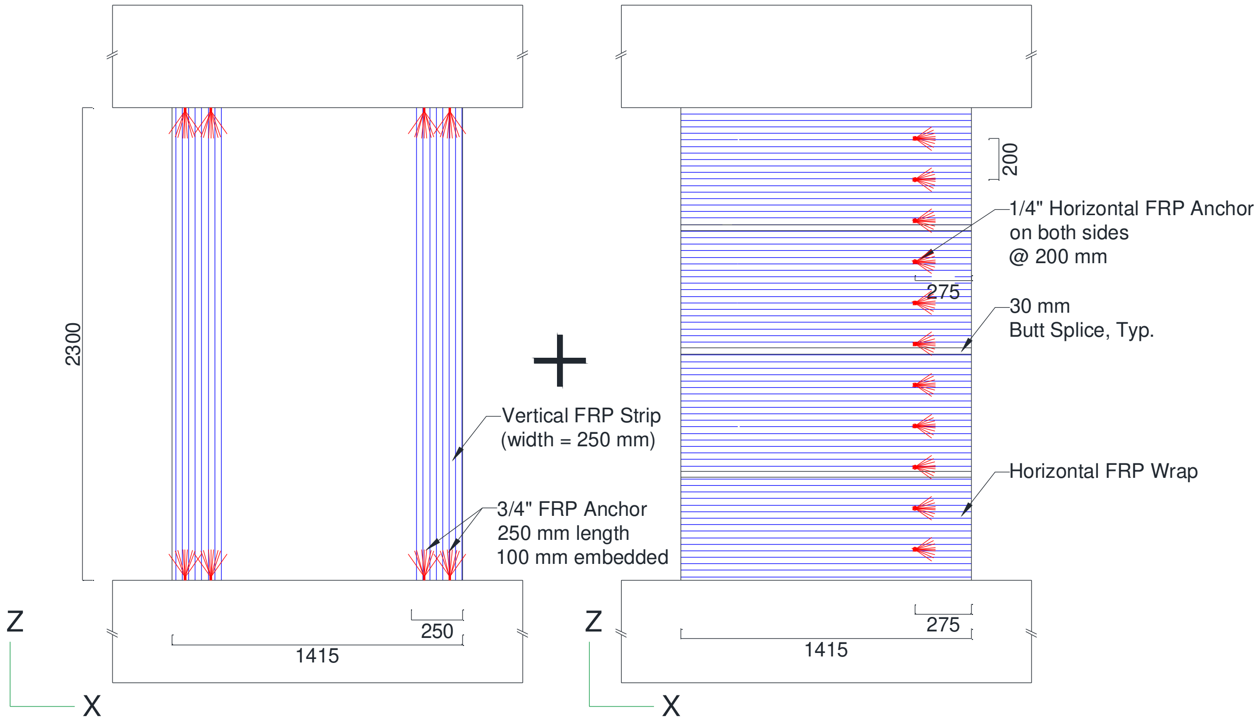

Fig. 6.9. Elevation view of the retrofitting scheme of the C-shaped wall

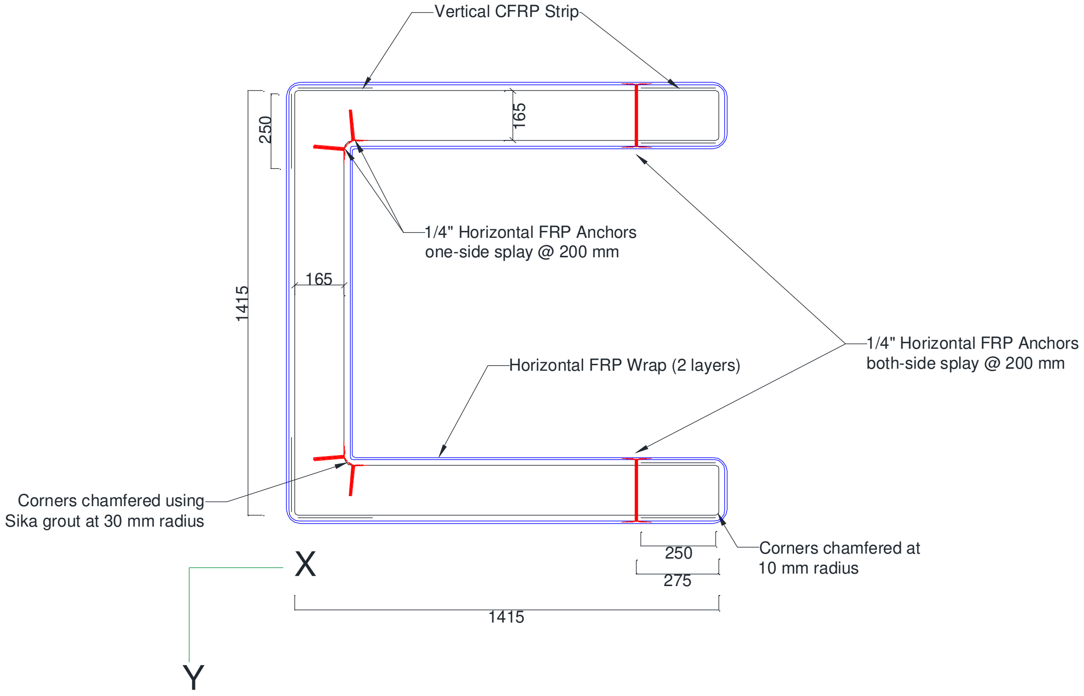

Fig. 6.10. Plan view of the retrofitting scheme of C-shaped wall

The CFRP retrofit scheme for the C-shaped RC wall, considering the severe cracks observed at the end of the series of tests on the Original wall by Mechamachi and Boanani (2018), needed several horizontal and vertical anchoring of FRP layers into both wall and footing/collar respectively. The vertical FRP anchors were designed to have higher capacity than the vertical FRP strips that they anchor to. This ensures that the FRP anchors will not fail before the vertical FRP strips. Two types of horizontal FRP anchors were used. Single-sided splay (fan type) FRP anchors were used along the height of the two re-entrant corners of the C-shaped wall in order to avoid peeling off of the horizontal FRP layers because the resultant force is away from the concrete. Double-sided splay through FRP anchors were used at the discontinuous ends of the C-shaped wall in order to form a four-sided confinement for the boundary element zone. The horizontal FRP anchors were equally spaced at 200mm along the height of the wall. The diameter of holes for FRP anchors needed to be at least 1/4" larger than the anchor diameter.

6.2.3.2 Surface Preparation

Before applying the CFRP sheets on the RC wall, the wall surface needed to be prepared based on the manufacturer instructions (provided by Fyfe Co). It follows ICRI guide No. 310.2R-2013 for concrete surface preparation, which transforms the surface to achieve a specific concrete surface profile (CSP) rating. The minimum CSP rating for installing composites onto most surfaces is a CSP-2 (Fyfe Co., 2017). This rating is based on independent research and testing from universities, governing bodies, and industry practice, to provide enough roughness for the surface such that the applied epoxy materials can provide enough bonding between the CFRP layers and the concrete surface.

Fig. 6.11 shows CSP Ratings based on ICRI guide. Moreover, recommended surface preparation methods are summarized in Table 6.2. Considering the safety concerns coming from people working on other projects in parallel, space limitations and the expensive facilities in the structural labs, surface grinding was selected and used for the current work.

ICRI 310.2R (2013) specifies that surface preparation is critical in: (i) flexural or shear applications, or element where FRP cannot be wrapped back onto itself, and (ii) typical bond critical elements such as beams, walls, and slabs. Surface must be cleaned and be free of any dust, laitance, grease, oil, or any other bond-inhibiting material. However, considering the sensitive devices, hydraulics, etc., a plastic curtain was made to keep the dust created because of grinding the surfaces by full isolation of the specimen (Fig. 6.12). A heavy-duty extraction system was then connected to a corner of the plastic curtain to exhaust concrete dust and circulate fresh air for breathing.

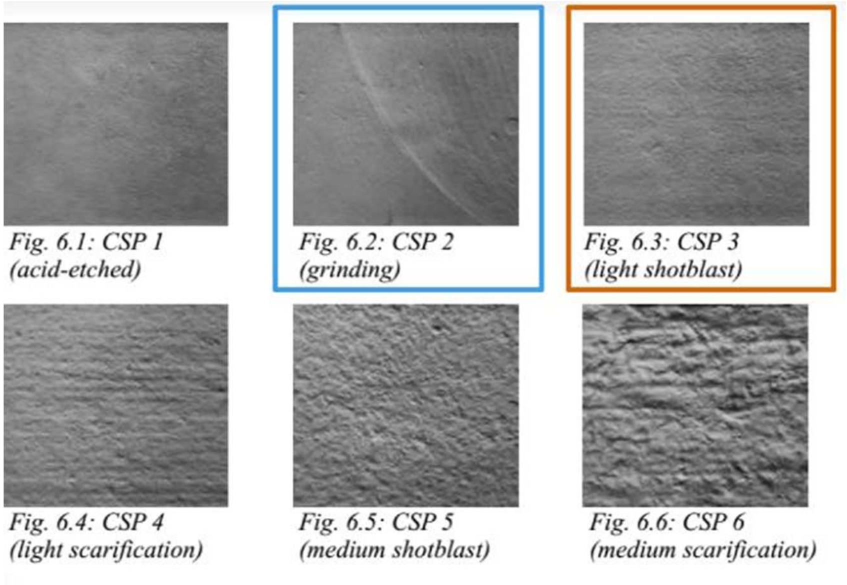
Fig. 6.1: CSP 1 (acid-etched)
Fig. 6.2: CSP 2 (grinding)
Fig. 6.3: CSP 3 (light shotblast)
Fig. 6.4: CSP 4 (light scarification)
Fig. 6.5: CSP 5 (medium shotblast)
Fig. 6.6: CSP 6 (medium scarification)

Fig. 6.11. CSP Ratings based on ICRI guide No. 310.2R-2013

Table 6.2. Recommended surface preparation method (Fyfe Co., 2017)

Surface Preparation Method	**Concrete Surface Profile**									
	CSP 1	CSP 2	CSP 3	CSP 4	CSP 5	CSP 6	CSP 7	CSP 8	CSP 9	CSP 10
Detergent scrubbing	■									
Low-pressure water cleaning	■									
Grinding	■	☒								
Acid etching	■	■	■							
Needle scaling		■	■	■						
Abrasive blasting		■	■	■	■	■	■			
Shotblasting		■	■	■	■	■	■	■	■	
High- and ultra-high-pressure water jetting			■	■	■	■	■	■	■	■

Fig. 6.12. Extraction system used for suction of air and dust during concrete surface preparation

Special preparation at the wall corners is needed in order to avoid stress concentration in the FRP sheets. The C-shaped wall section has 6 exterior and 2 re-entrant corners. The exterior corners were rounded to a radius of 1" (Fig. 6.13). The re-entrant corners were filled with a Sika grout to a radius of 30 mm. Moreover, it was ensured that the composite sheet makes smooth, uniform transitions during application.

6.2.3.3 Applying the FRP materials on the wall

Application of FRP materials (Fig. 6.14) on the RC wall includes the following steps:

a) Preparing FRP cuts
b) Mixing the epoxy components
c) Manual saturation (Fig. 6.15)
d) Installation of FRP layers and anchors

Epoxy resin components need to be mixed directly before the application, considering the 1.5 to 3 hours of pot life (based on the structures lab ambient temperature), and less than an hour for thickened epoxy mixes. Each FRP piece was manually saturated by applying epoxy resin on both sides of the layers/anchors before installation.

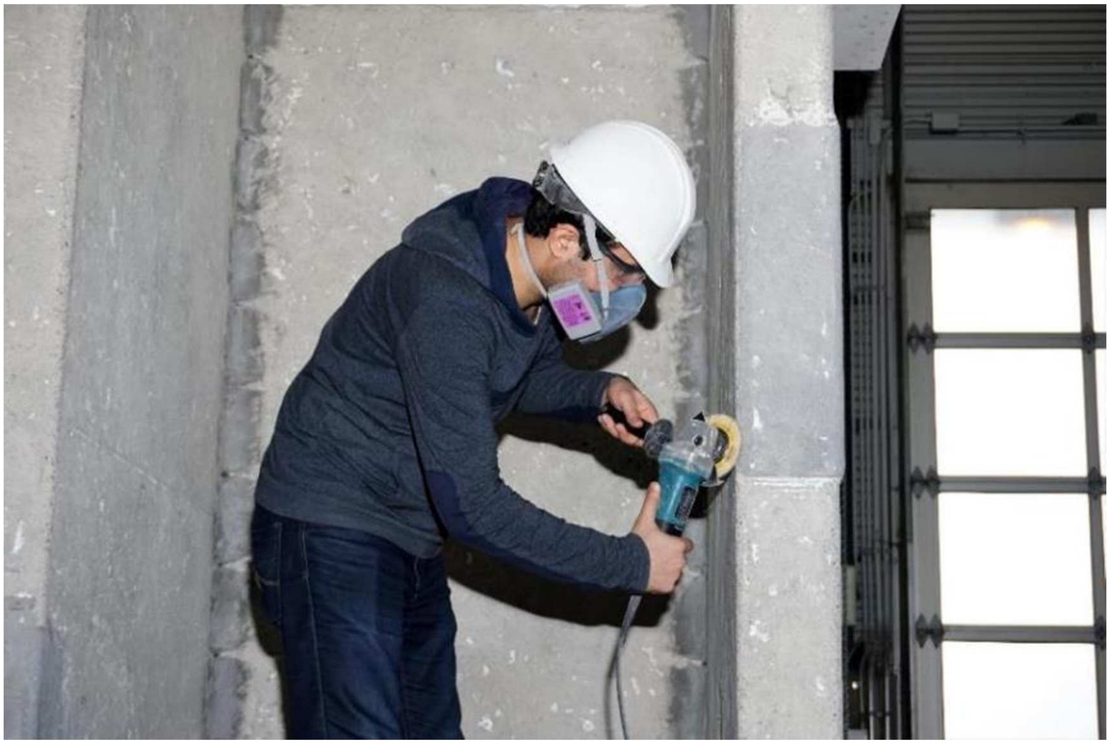

Fig. 6.13. Rounding exterior corners to avoid stress concentration in FRP sheets

Fig. 6.14. FRP roll (Tyfo SCH 11UP) and FRP anchor (Tyfo SCH Composite Anchors)

The concrete wall surface was primed with Tyfo Epoxy using a roller, and then, the first FRP layer was applied, be it vertical strip at the corners or horizontal layers in other regions. The order of the installations was as followings:

- Step 1: Vertical strips
- Step 2: Vertical anchors (for the vertical strip)
- Step 3: First horizontal layer
- Step 4: Horizontal anchors
- Step 5: Second horizontal layer

As for installation of FRP anchors, corners of holes was previously rounded to a ¾" minimum radius at the exit point of the hole to allow for a smooth transition for the anchor, and the holes were cleaned out from any dust inside the anchor hole. Then, the hole was filled half ways with Tyfo epoxy, before applying the first layer of fabric to structural RC wall. Finally, the FRP anchor was inserted through the fabric and into the hole.

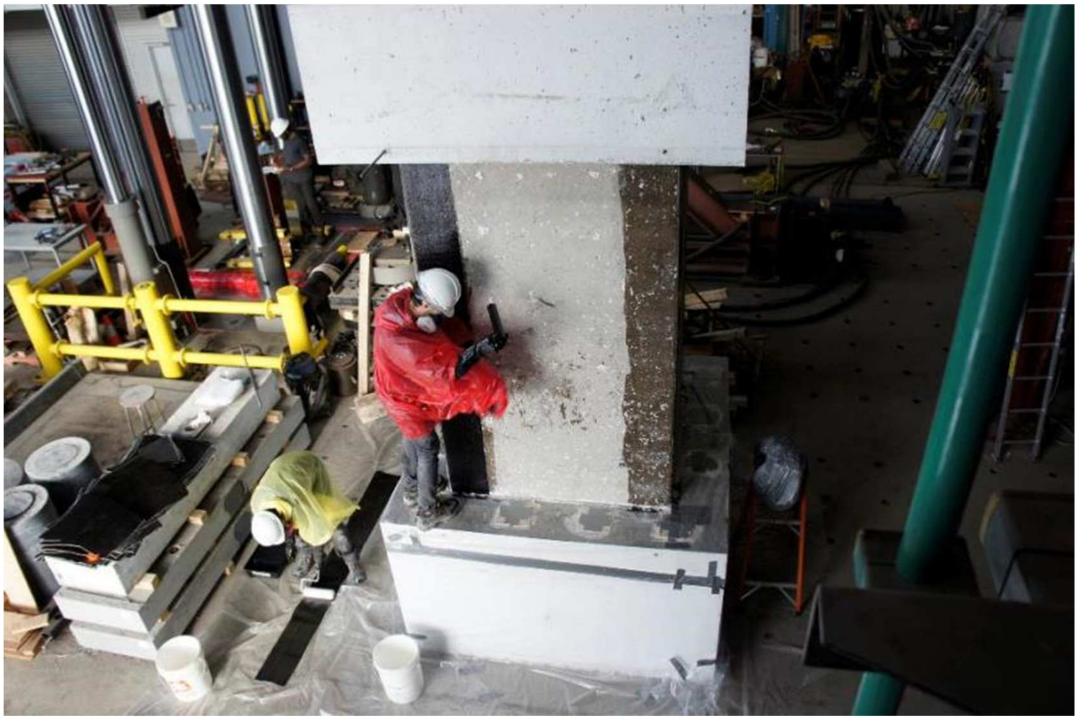

Fig. 6.15. Manual saturation and installation of vertical strips

The vertical FRP strips were anchored to the top collar and bottom footing using 3/4" diameter FRP fan anchors as shown in Fig. 6.14. Horizontal FRP anchors were used to anchor the horizontal wraps inside the corners and to enhance the confinement effects around the corner zones at the end of flanges of the C-shaped RC wall. FRP anchors width 1/4" diameter was selected for anchoring the horizontal wraps since they were expected to be subjected to the lower level of loads in comparison with the vertical FRP strips.


(a) (b)

Fig. 6.16. FRP layers after installation: a) Vertical FRP strips, b) Horizontal FRP layers

6.2.4 The 6DOF Test Setup

The tests on the FRP retrofitted RC C-shaped wall were conducted at École Polytechnique's structures lab. The six degree of freedom system (6DOF) used for the current work included eight actuators in total. The four vertical actuators, 1.8 MN each, were placed at the four corners and the four horizontal actuators, 1.0 MN each, were connected to perpendicular strong structural walls at the South-West corner of École Polytechnique's structures lab (two in each horizontal direction). A rectangular upper platen with 2.5 m x 3.5 m dimensions and 0.625 m thickness, formed from stiff multicellular steel plates, was connected to the actuators and could be displaced along 6DOF using the actuators control machine. A lower platen with the same dimensions was anchored to the laboratory's strong floor, and the RC C-shaped core wall specimen was placed between the two platens (Fig. 6.17).

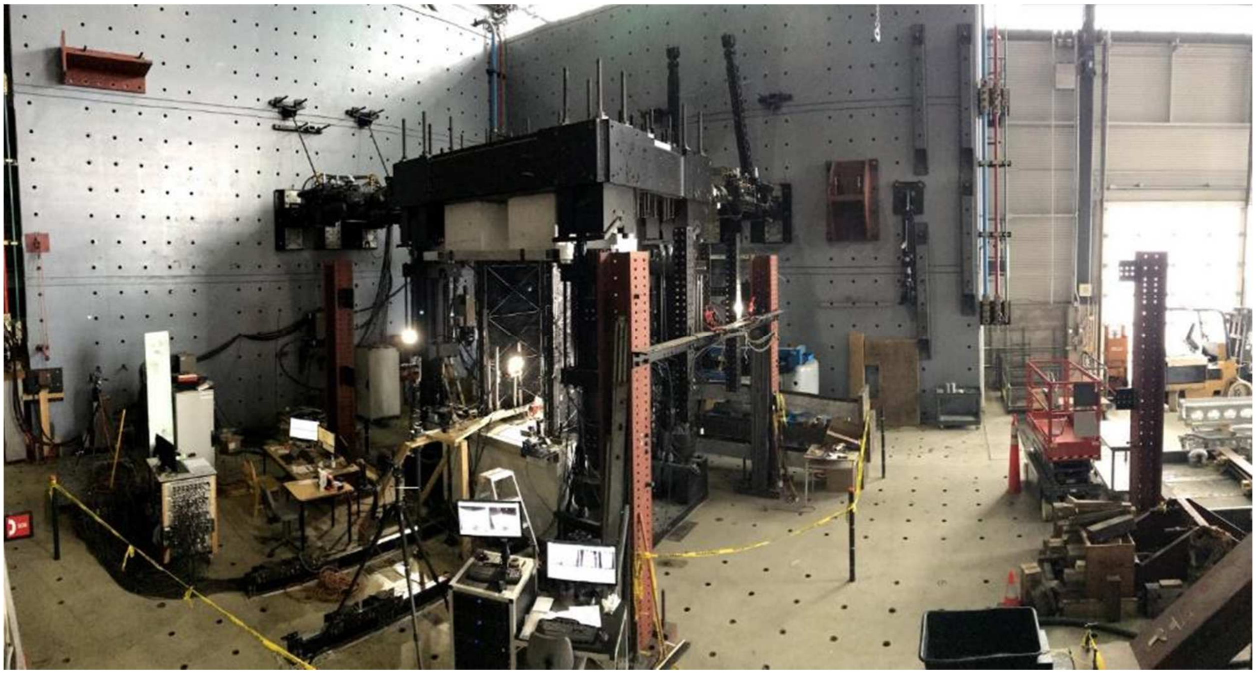

Fig. 6.17. General view of the 6DOF system at École Polytechnique's structures lab and the test setup of the FRP Retrofitted wall

Using a dedicated routine implemented in the MTS machine control system, the system exports the displacements/forces along six translational and rotational DOF at a control point by transforming the displacements/forces monitored in individual actuators. The control point was located at the centre of the bottom surface of the upper platen, which is rigidly anchored to the top centroid of the collar.

In the current work, the RC C-shaped wall was representing the bottom story of the main SFRS of a 5-story building; hence, the bottom end of the wall was fully fixed to the support while the 6DOF at the top end was interactively controlled by the controller machine during the test.

6.2.5 Instrumentations

Different instrumentations were used in order to measure the deformations, forces and strains as shown in Fig. 6.18. A data acquisition system featuring synchronous signal measurement was recording all data at a sampling rate of 20 and 100 Hz depending on the test step. Moreover, a Digital Image Correlation (DIC) system was used in order to capture the targeted surfaces with a frame rate of 5 FPS. The plan view of the installed instrumentations is shown in Fig. 6.19, whereas the elevation views of inner and outer faces are shown in Fig. 6.20.

As shown in the figure, the specimen was heavily instrumented to be able to capture possible deformations and reaction forces in an efficient yet extensive way. A total of 86 linear potentiometers and 62 strain gauges were used to record the deformations in the RC wall specimen during the test. Moreover, force-displacement data monitored for the 6DOF by the controller machine were set to be recorded at the same sampling rate as the data acquisition system.

A block of linear potentiometers was used on each segment of the C-shaped wall, in vertical, horizontal and diagonal directions to record the local deformations along the height of the wall (see Fig. 6.21). The purpose of these instrumentations was to capture the flexural and shear deformations in both flanges and web of the RC wall, results of which are explained in the Section 6.3.3.4. Fig. 6.21 shows the installed potentiometers on the flanges.

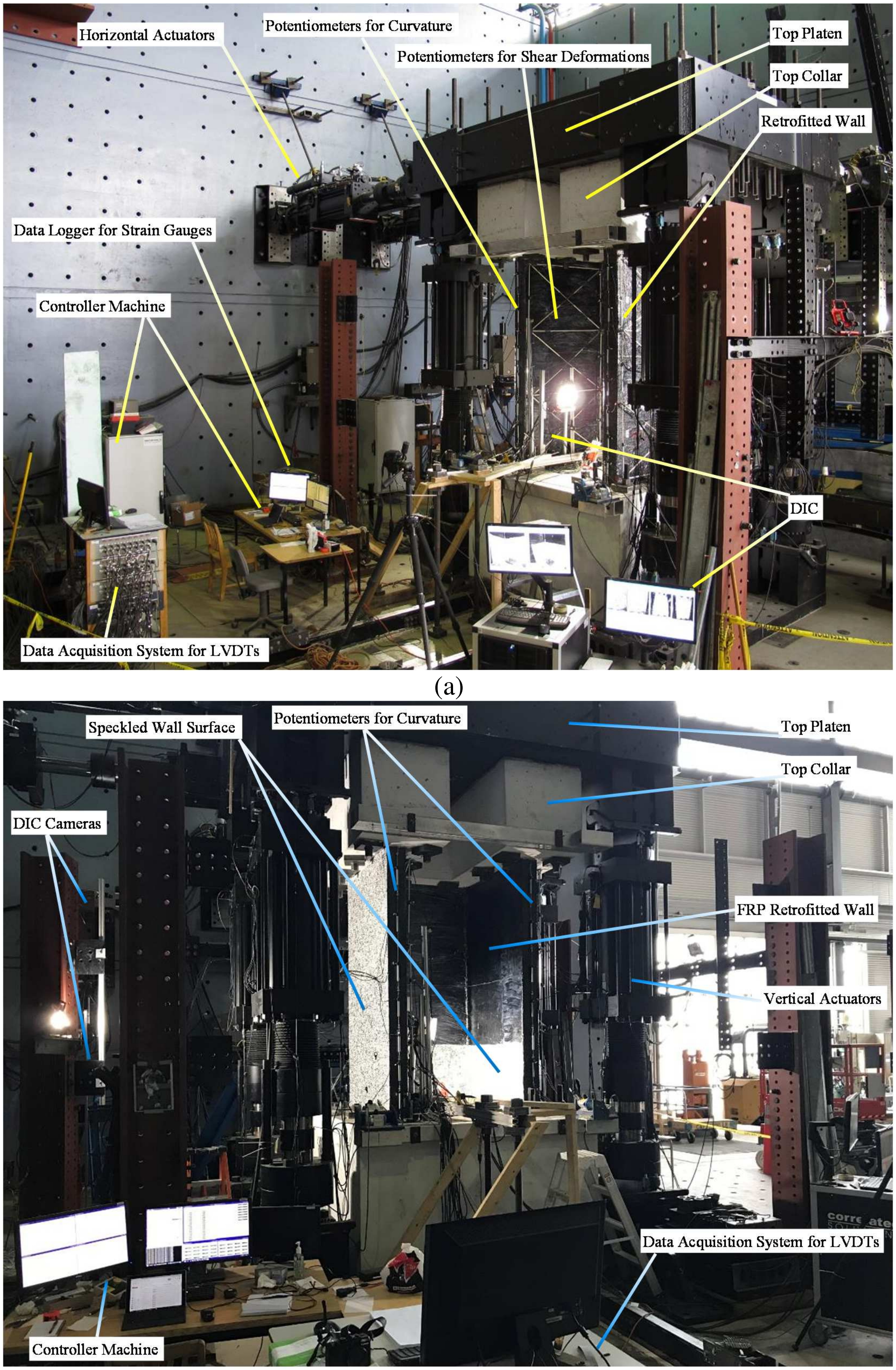

(a)

(b)

Fig. 6.18. General view of the installed instrumentations

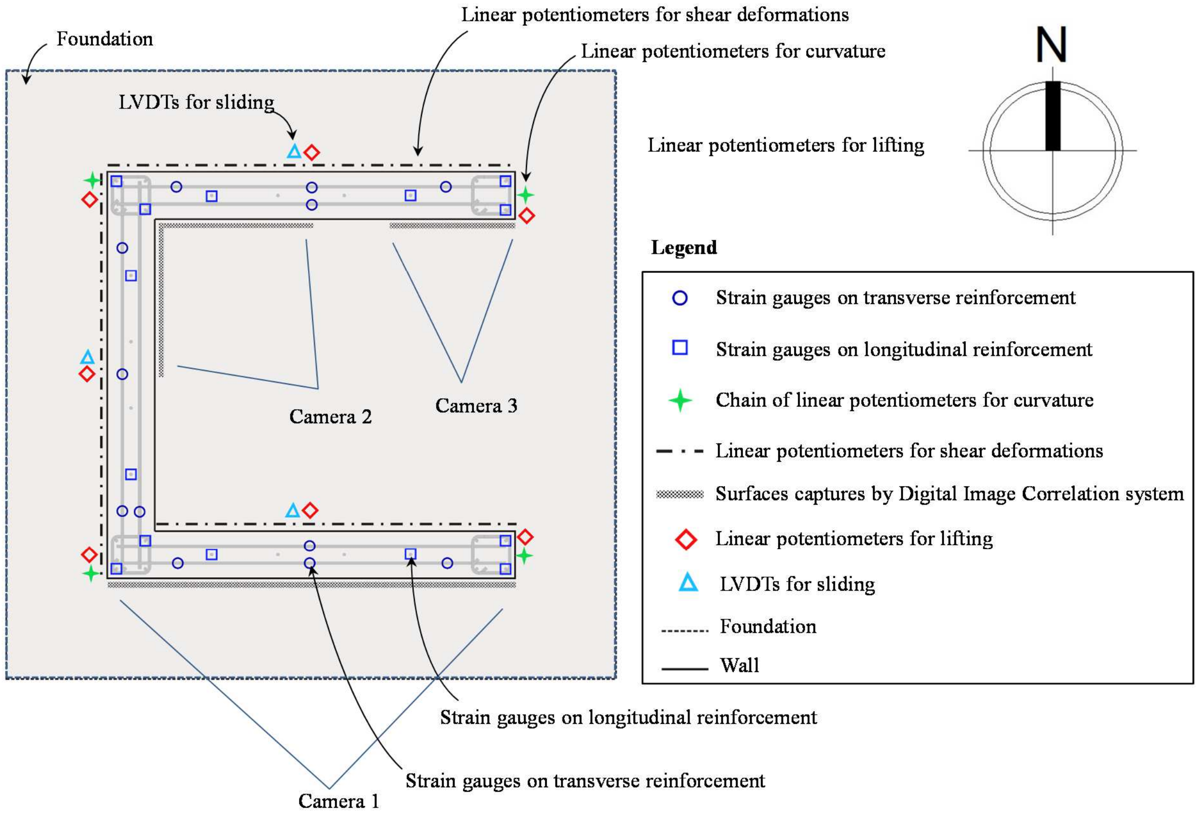

Fig. 6.19. Instrumentations of the test: Plan view

Moreover, a vertical chain of linear potentiometers was installed on each corner of the wall as indicated in the previous figures to capture the deformations along the height of the wall. These data were used to measure the curvature of the specimen at different levels during the test. Results of the variation of curvature along the height of the wall are presented in Section 6.3.3.5. Different spacing (length of potentiometers) was used; smaller spacing toward the bottom end where larger local deformations will occur at the expected plastic hinge location (Fig. 6.21).

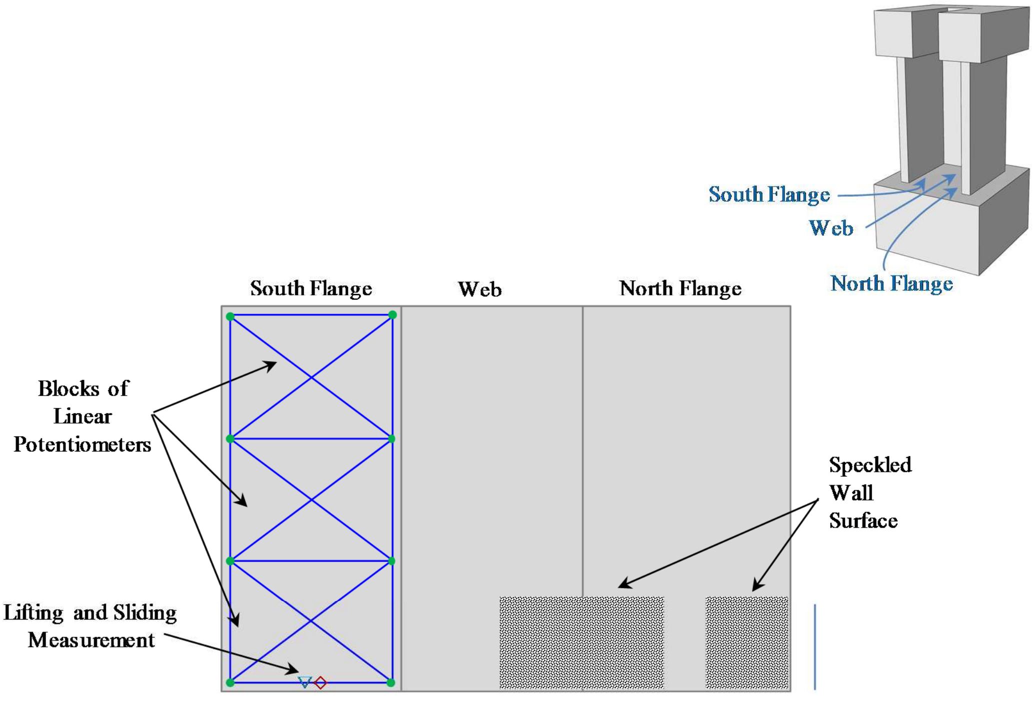

Inner Faces

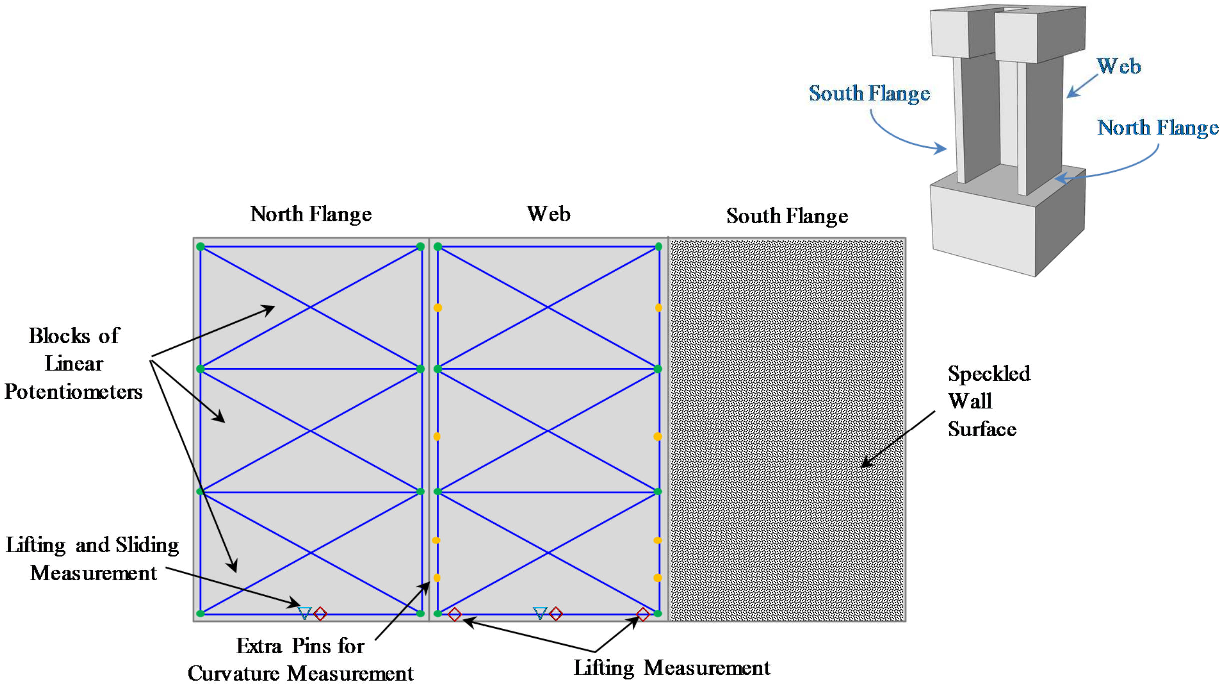

Outer Faces

Fig. 6.20. Instrumentations of the test: Elevation view

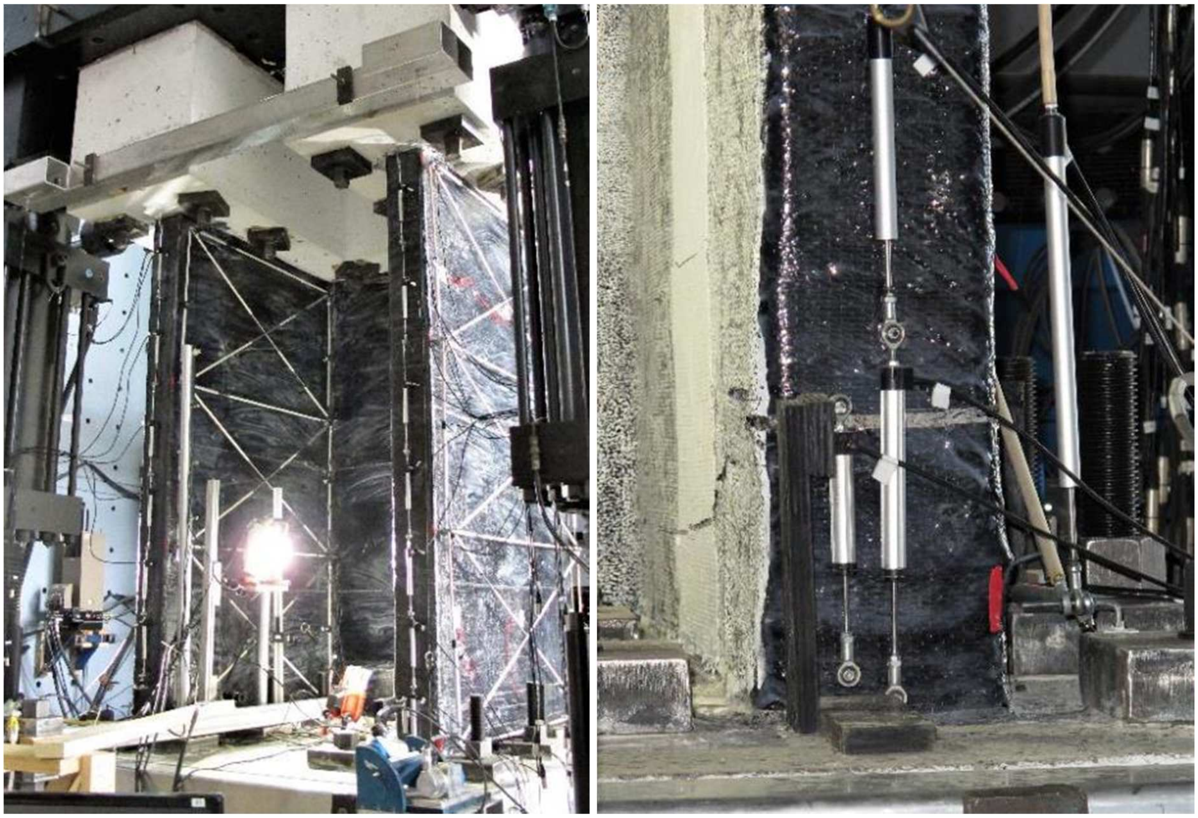

Fig. 6.21. Groups of linear potentiometers for capturing the deformations and curvature of the wall

A set of potentiometers installed to record the lifting of the wall from the support (i.e. flexural cracks at the wall-footing interface), as well as the shear sliding deformations (i.e. relative horizontal movement of the wall base with respect to the footing). A stiff wooden support was made to install the potentiometer such that it can measure the deformations between the footing and a point 1 inch away from the footing on the wall. This was done due to the limitation of the length of potentiometers. All the 148 channels connected to the sensors were checked and verified by the data acquisition system to have both the consistency of signal and acceptable initial value. The latter was verified to be close to half of the maximum extension length of each potentiometer, and then, was taken as the relative zero point. This was to ensure that the potentiometers will not reach to either of compressive/tensile ends during the tests.

As mentioned before, a DIC system was used to measure the deformations on one of the flanges and two selected regions on the inner corners during the test. Fig. 6.22 shows the digital image correlation (DIC) system.

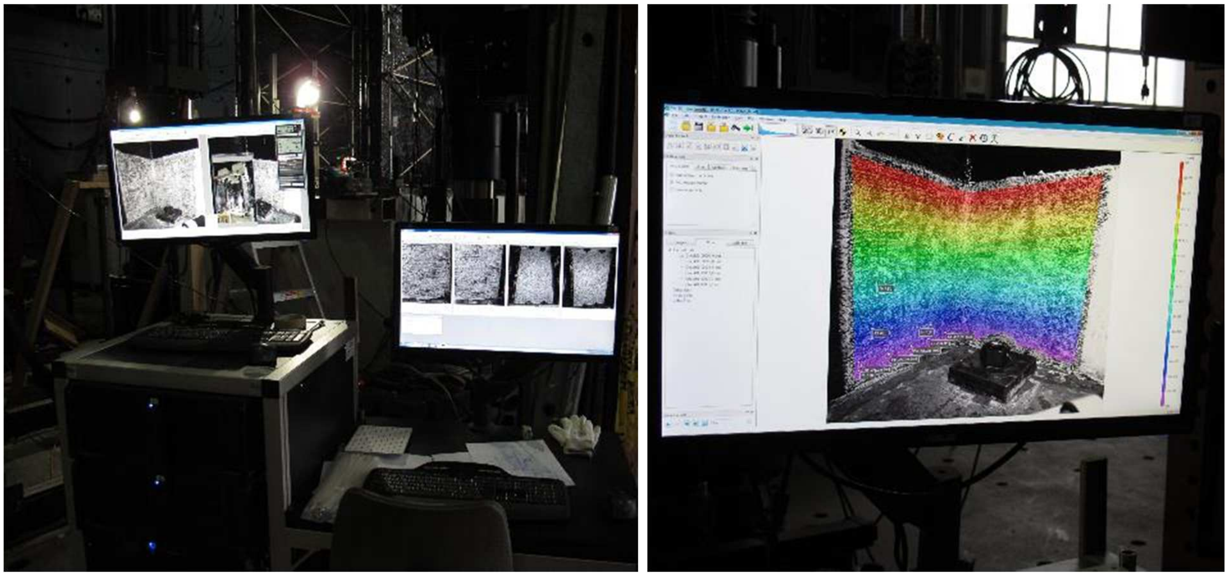

Fig. 6.22. Digital Image Correlation system

A group of 3D encoders was used as the 3D relative system for the 6DOF system to determine the relative deformations of the top collar from the footing (Fig. 6.23). Consistency and accuracy of these encoders are vital since their signals will be directly used as benchmarks by the controller machine using a transformation algorithm. Hence, a 3D laser scanner system was employed to create an accurate 3D model of the system, and the relative system was precisely calibrated accordingly before conducting the test (Fig. 6.24).

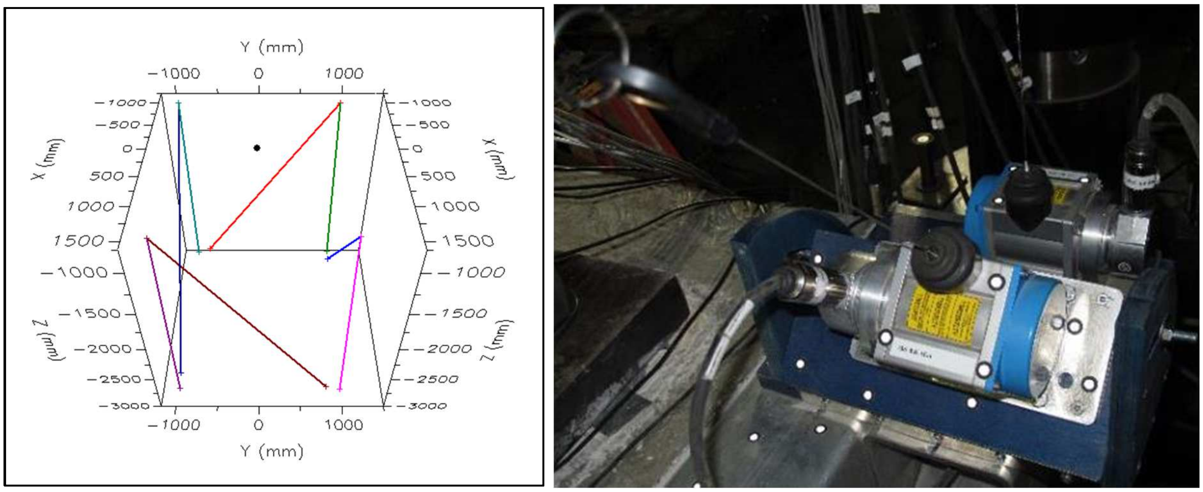

Fig. 6.23. 3D Encoders used for measuring the relative deformations in the 6DOF system

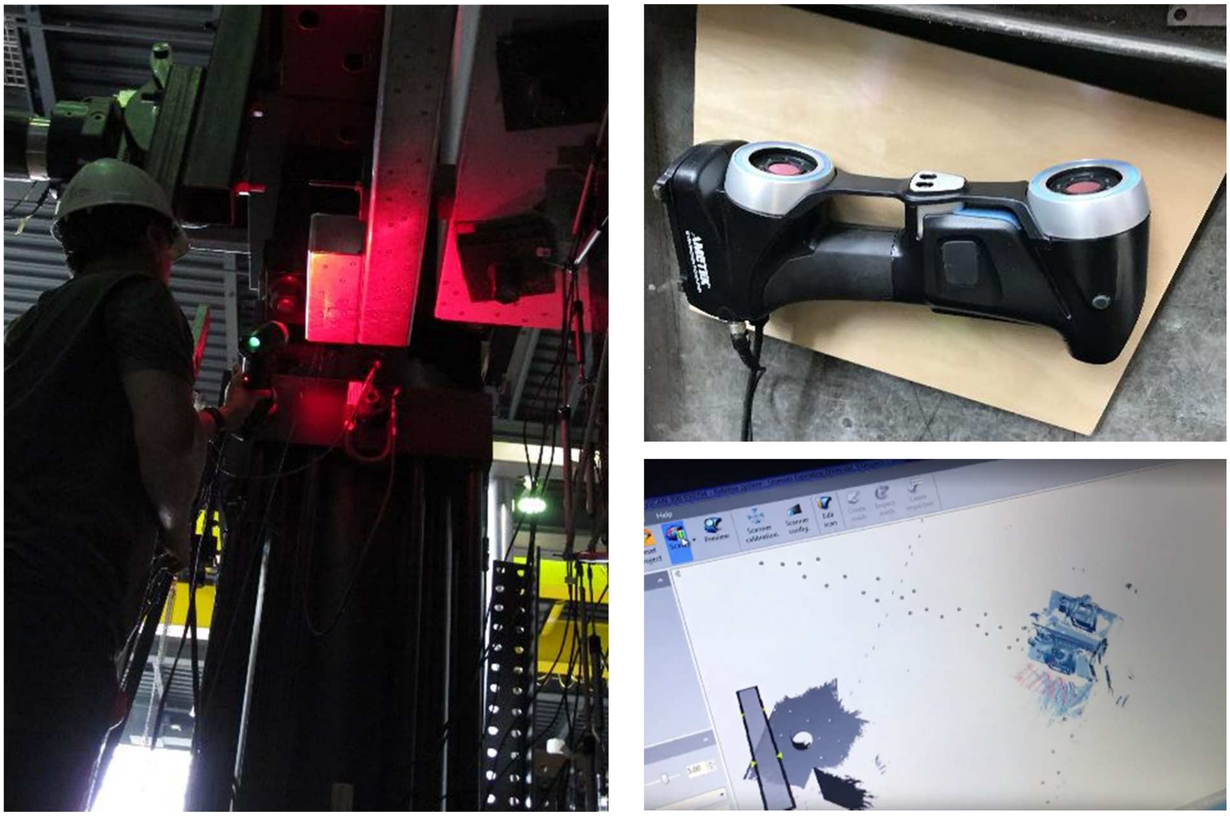

Fig. 6.24. 3D laser scanner used for calibration of the relative system

6.2.6 Loading Protocol

As mentioned earlier, the purpose of the experimental tests was to investigate the effectiveness of the proposed CFRP retrofit scheme on the seismic performance of the tested C-shaped RC core wall.

The loading protocol for the FRP retrofitted RC C-shaped wall included three phases, all of which were applied together with a constant 520 kN axial load (i.e. gravity load):

- Three hybrid tests of the FRP-retrofitted core wall at the base of a 5-story building when subjected to earthquake ground motion excitations,
- Characterization tests of the wall after the hybrid tests, then
- Increasing cyclic multi-directional displacement-control test

As mentioned in the section 6.2.2, the bi-directional acceleration records used for the hybrid tests were the recorded accelerograms of the 1985 Nahanni ground motion. Nahanni earthquake was one of the most significant earthquakes in Canada during the 20th century, with the moment magnitude scale (M_w) of 6.9. The hybrid tests were conducted in three steps including two respective records of 4.2 and 7.8 seconds as the mainshock, followed by an 8.8 seconds record representing an aftershock excitation. Fig. 6.25 shows the acceleration record for both the mainshock and aftershock steps.

After completing the hybrid time history tests, similar to what was done on the Original wall by Mechmachi and Bouaanani (2018), characterization tests were conducted to determine the core wall characteristics at the end of hybrid tests. The loading protocol applied at this stage of the test is presented in Fig. 6.26. As can be seen from the figure, small amplitude displacements were applied in both X and Y directions (flange and web direction, respectively). A torsional moment was applied afterwards to measure the walls response against twisting excitation. A full cycle test was conducted for each direction (i.e. positive and negative displacements/rotation) to ensure that the asymmetry of the geometry is considered.

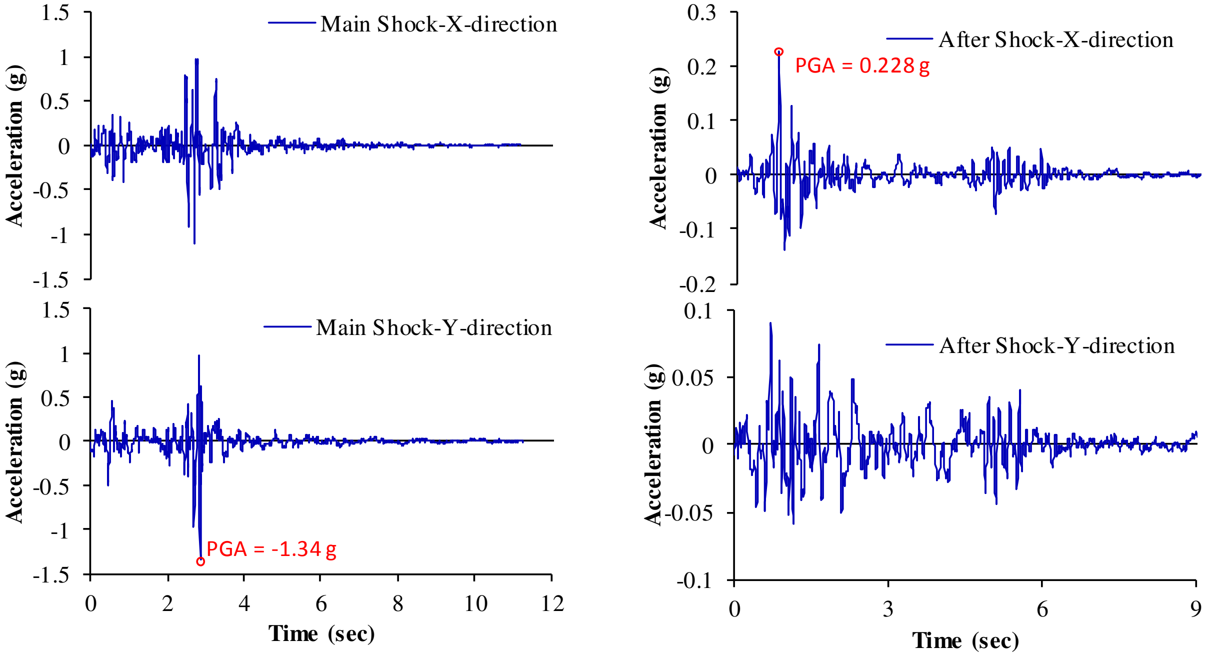

(a) (b)

Fig. 6.25. Acceleration record of the 1985 Nahanni earthquake: a) Mainshock, b) Aftershock

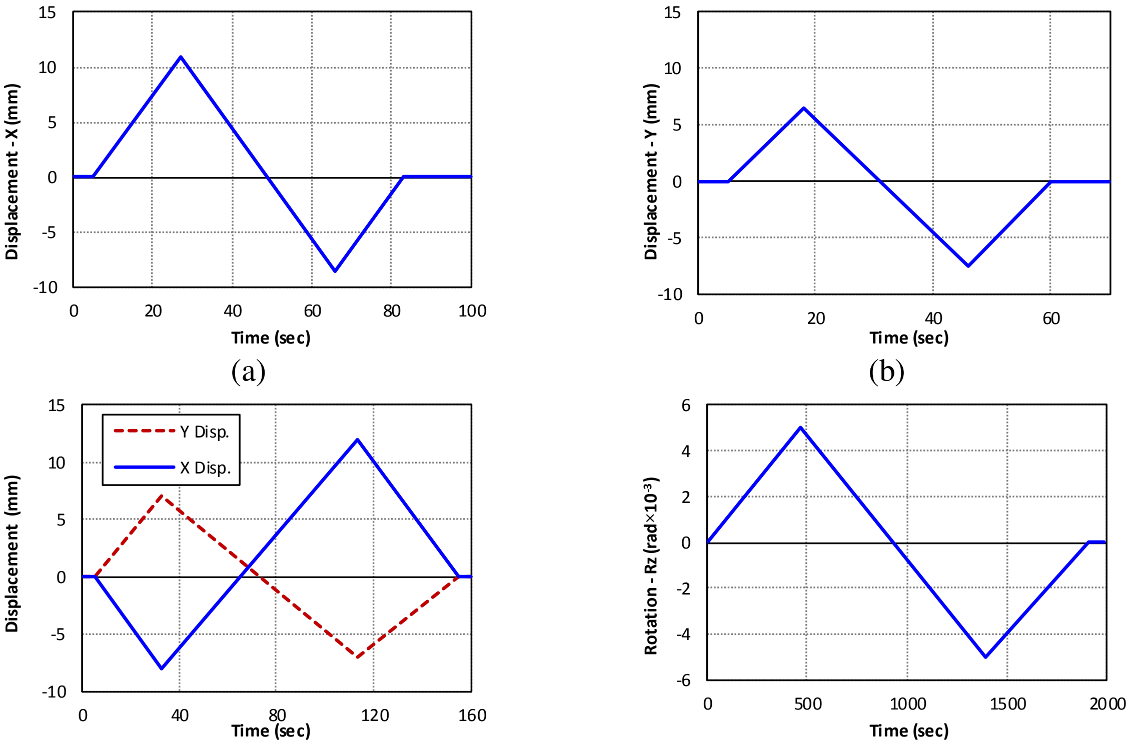

(a) (b)

(c) (d)

Fig. 6.26. Sequence of loading protocol applied to determine the wall characteristics at the end of hybrid tests

Last, the increasing cyclic displacement-controlled loading protocol applied to the C-shaped RC core wall in the third phase of the tests was the loading protocol proposed by Beyer et al. (2008-a). As it was proposed by Beyer et al. (2008-a), five different directions of loading were considered and labelled with different letters (Fig. 6.27):

- Parallel to the web (Positions A and B),
- Parallel to the flanges, flange ends in compression (Position C),
- Parallel to the flanges, web in compression (Position D),
- In the diagonal direction, one flange end in compression (Position E and H),
- In the diagonal direction, one corner in compression (Position F and G).

The diagonal direction was defined as the axis with 45 degrees inclination from the horizontal axis. Considering that only one specimen was tested, and since the objective of the tests was to assess the response of the FRP-retrofitted C-shaped walls in different loading directions, a bi-directional loading protocol was applied on the test specimen. The chosen loading history was based on a pattern developed by Hines et al. (2002) who proposed a history comprising a "sweep" and a diagonal at each level. The loading protocol is summarized in four steps for each level as follows:

- NS cycle: Full cycle parallel to the web (O→A→B→O),
- EW cycle: Full cycle parallel to the flanges (O→C→D→O),
- Diagonal cycle: Full cycle in the diagonal direction (O→E→F→O),.
- Sweep cycle: (O→A→G→D→C→H→B→O).

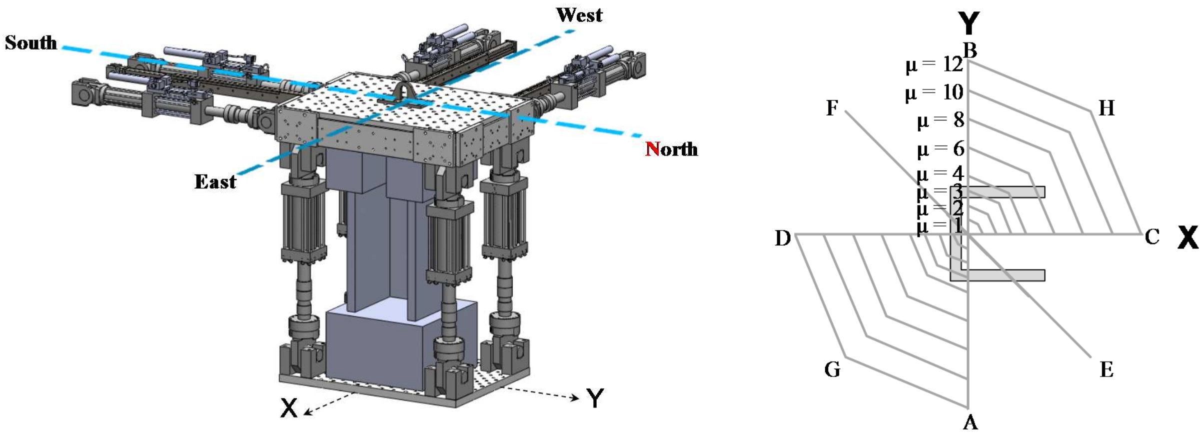

(a) (b)

Fig. 6.27. Displacement-based loading protocol applied on the FRP-retrofitted C-shaped wall specimen

In order to clarify the sequence of the experimental tests as well as the results presented in Section 6.3, a summary of the conducted tests, as well as the numerical analyses on the C-shaped RC wall specimen, is shown in Fig. 6.28.

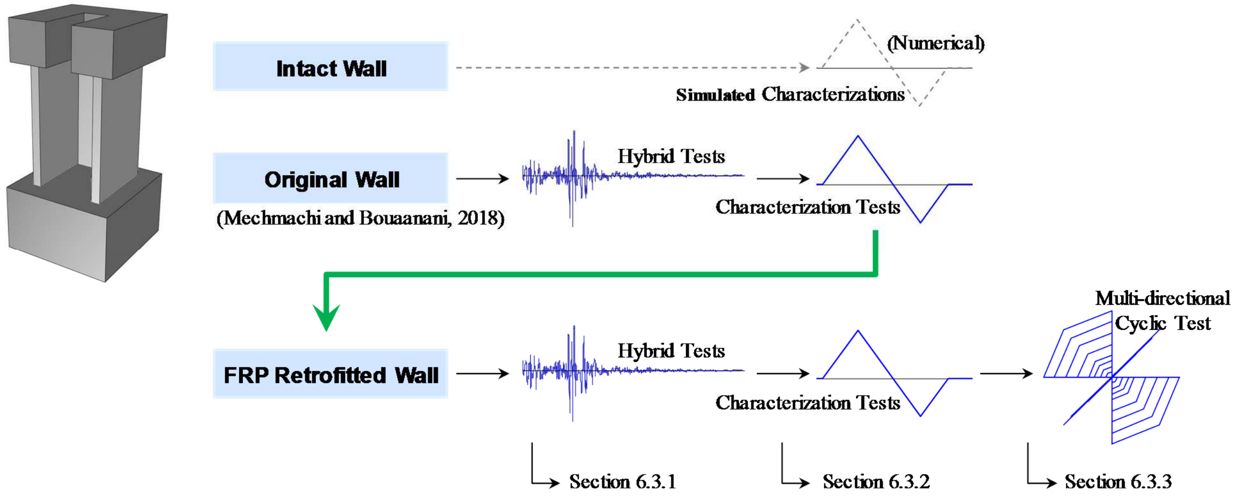

Fig. 6.28. Summary of the conducted experimental tests as well as the numerical analyses on the C-shaped RC wall specimen

6.3 Test Results of CFRP-Retrofitted C-shaped RC Wall

Results of the aforementioned experimental tests on the large-scale FRP-retrofitted C-shaped RC core wall are presented in this section. Results are presented in three steps, namely, hybrid tests, characterization tests and cyclic test. As mentioned in the Section 6.2.6, the hybrid tests included three time-history tests where the CFRP retrofitted C-shaped wall was tested as the core wall at the base of a 5-story building when subjected to earthquake ground motion excitations. The characterization tests were a test in which small amplitude displacements/rotations in each direction was applied (diagonal direction included) on the test wall to identify the characteristics of the FRP Retrofitted wall before conducting the final cyclic test. At the end of characterization tests conducted by Mechmachi and Bouaanani (2018) on the Original wall, 25 out of 57 strain gauges reached yielding strain. These yielded strain gauges were mostly on the longitudinal bars at the corners of the C-shaped wall (Mechmachi and Bouaanani, 2018).

6.3.1 Results of the hybrid tests

Figures 6.29 to 6.34 present the time history results of the hybrid tests in three different steps. Responses in all the six degrees of freedom are presented in terms of both the displacement/rotation and the reaction force/torque. Maximum and minimum responses from the Original wall (Mechmachi and Bouaanani, 2018) are depicted in the figures for comparison purposes. It is worth mentioning that step 2 of the hybrid tests was stopped prematurely due to an interlock in the controller system at the very last stage of the applied record. This, however, was at 91% of the total time of the test where just very small excitations (damped) at the end of the accelerogram was remaining, and hence had no notable influence on the results of the test steps 2 and 3.

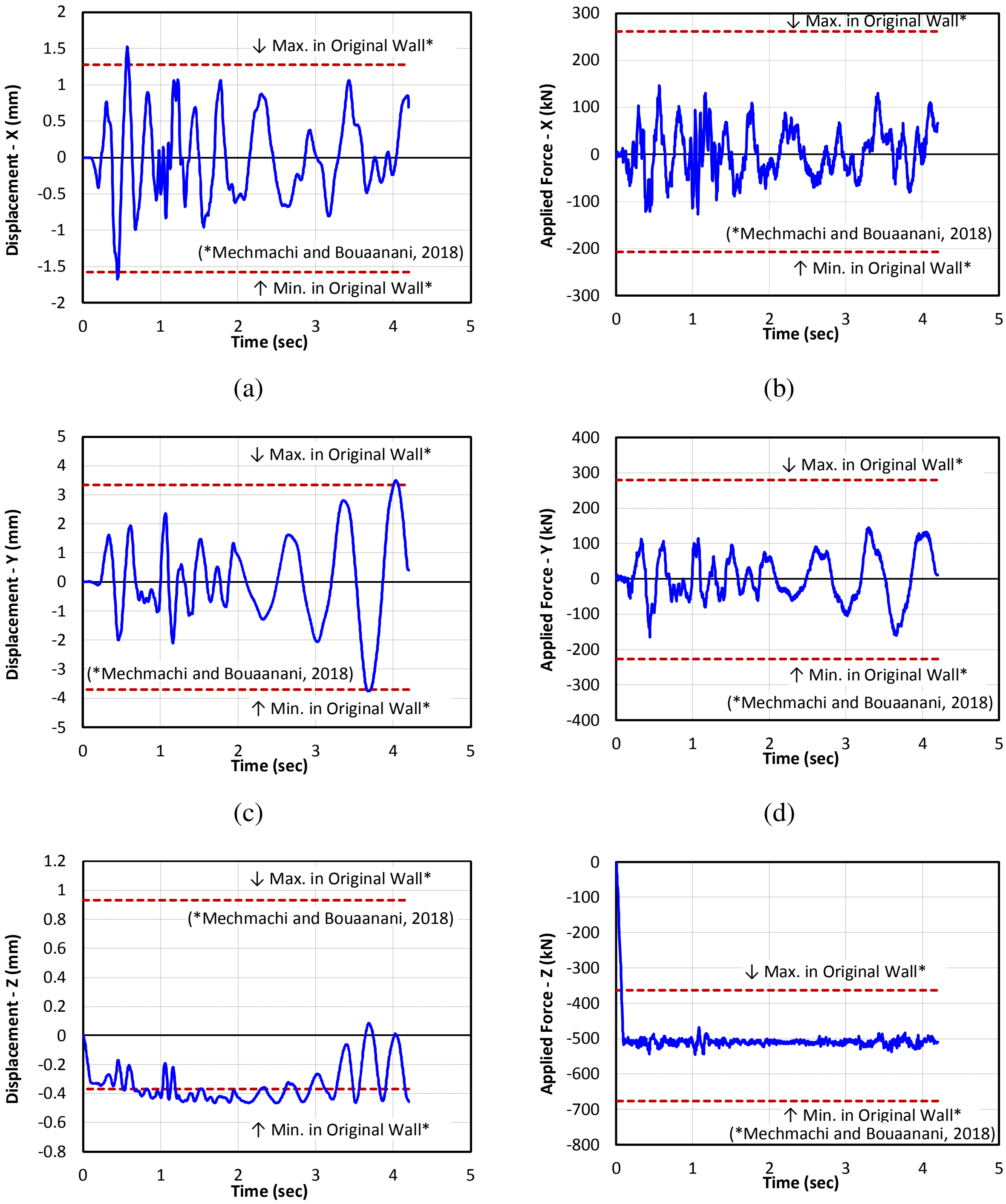

(a) (b)

(c) (d)

(e) (f)

Fig. 6.29. Time-history displacement and force results of the hybrid tests: Mainshock (Step 1)

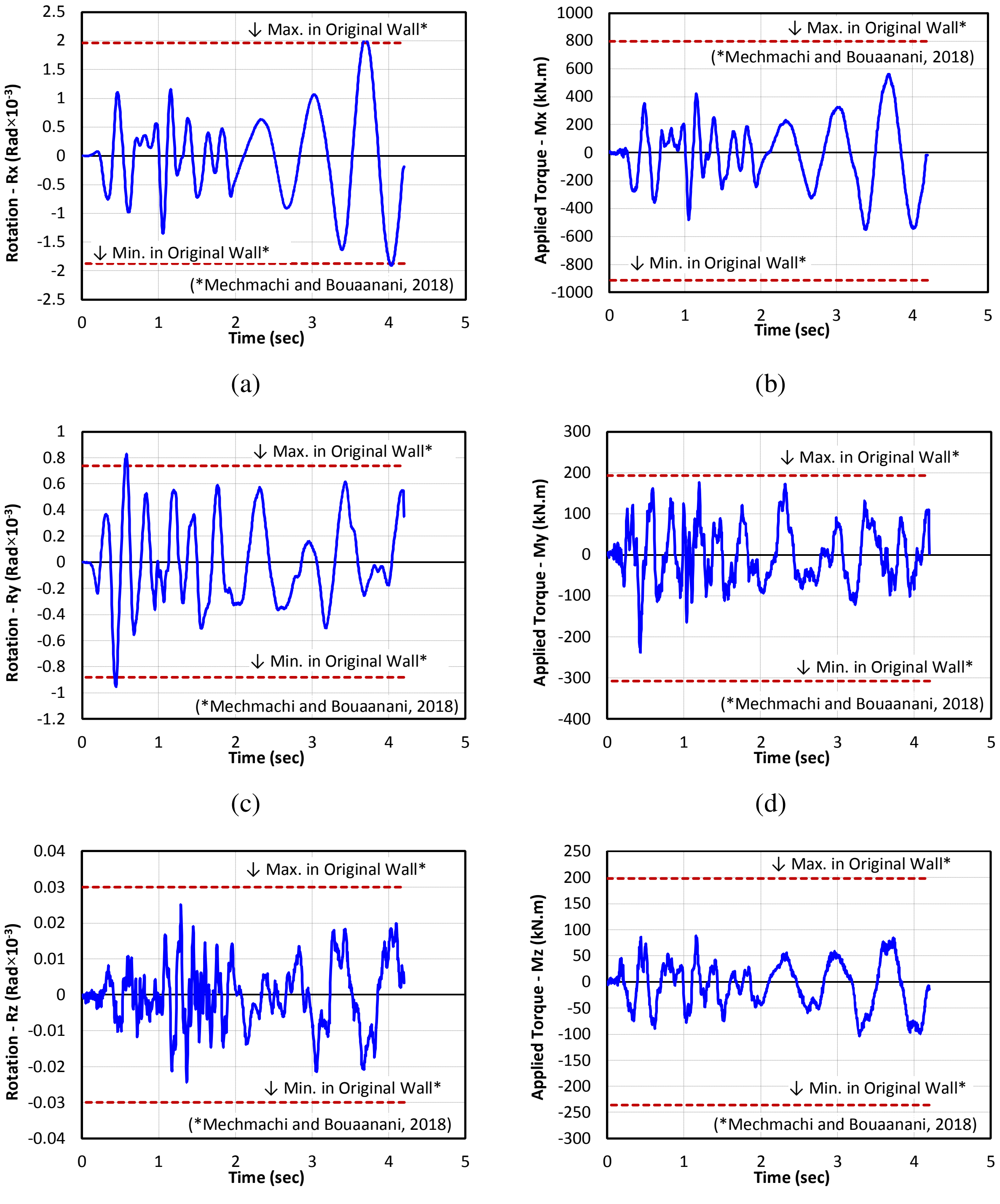

(a) (b)

(c) (d)

(e) (f)

Fig. 6.30. Time-history rotation and bending moment results of the hybrid tests: Mainshock (Step 1)

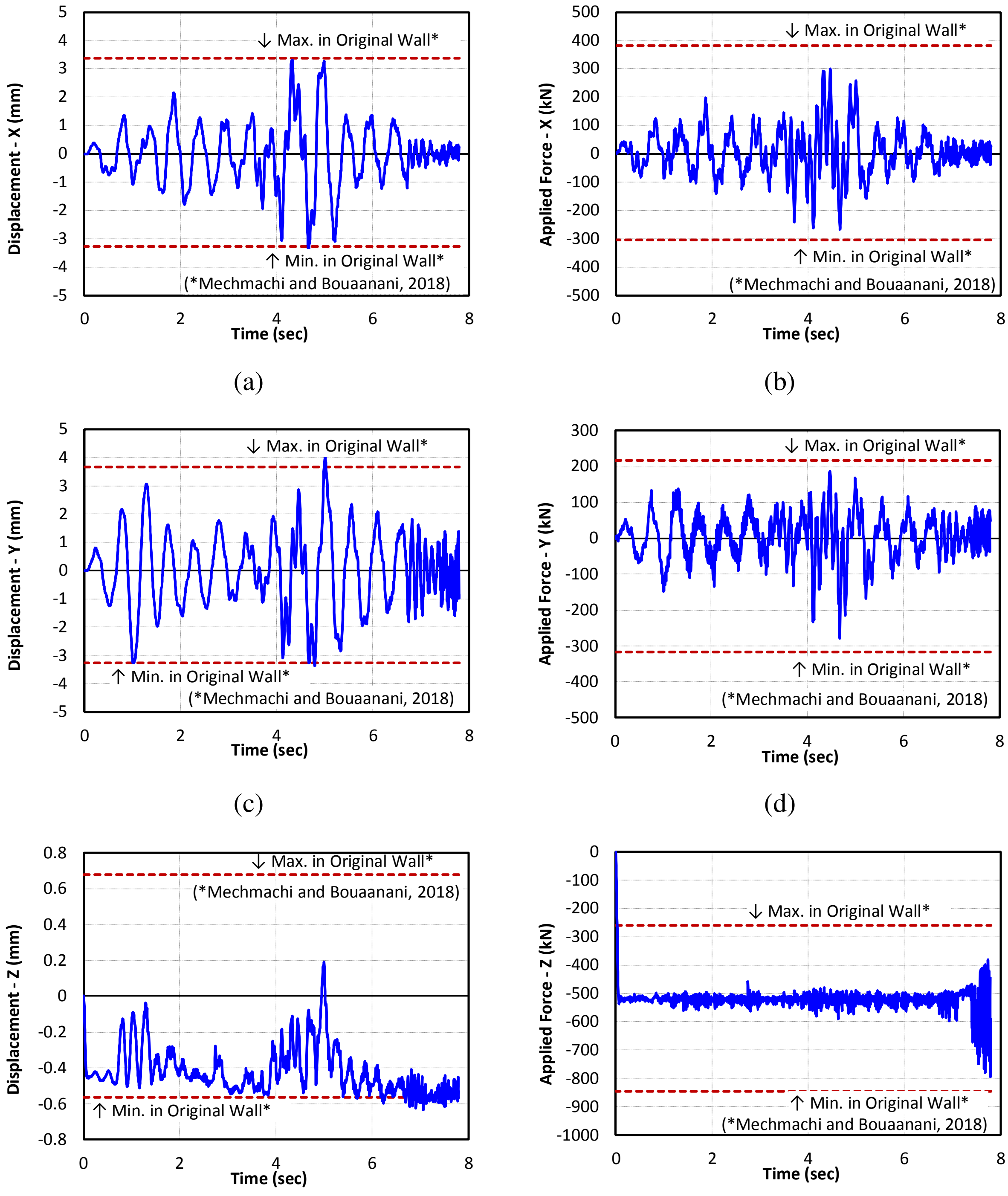

(a) (b)

(c) (d)

(e) (f)

Fig. 6.31. Time-history displacement and force results of the hybrid tests: Mainshock (Step 2)

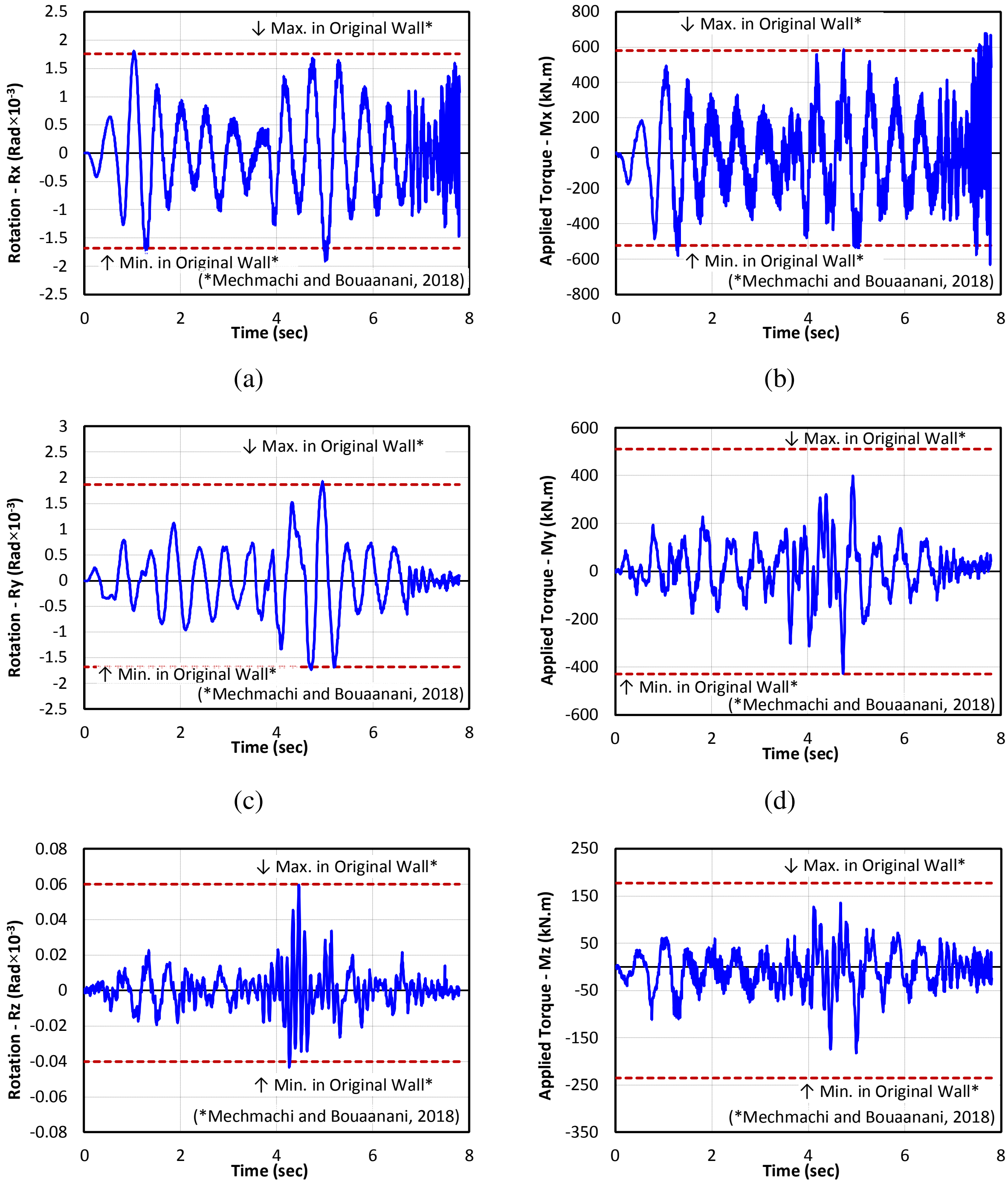

(a) (b)

(c) (d)

(e) (f)

Fig. 6.32. Time-history rotation and bending moment results of the hybrid tests: Mainshock (Step 2)

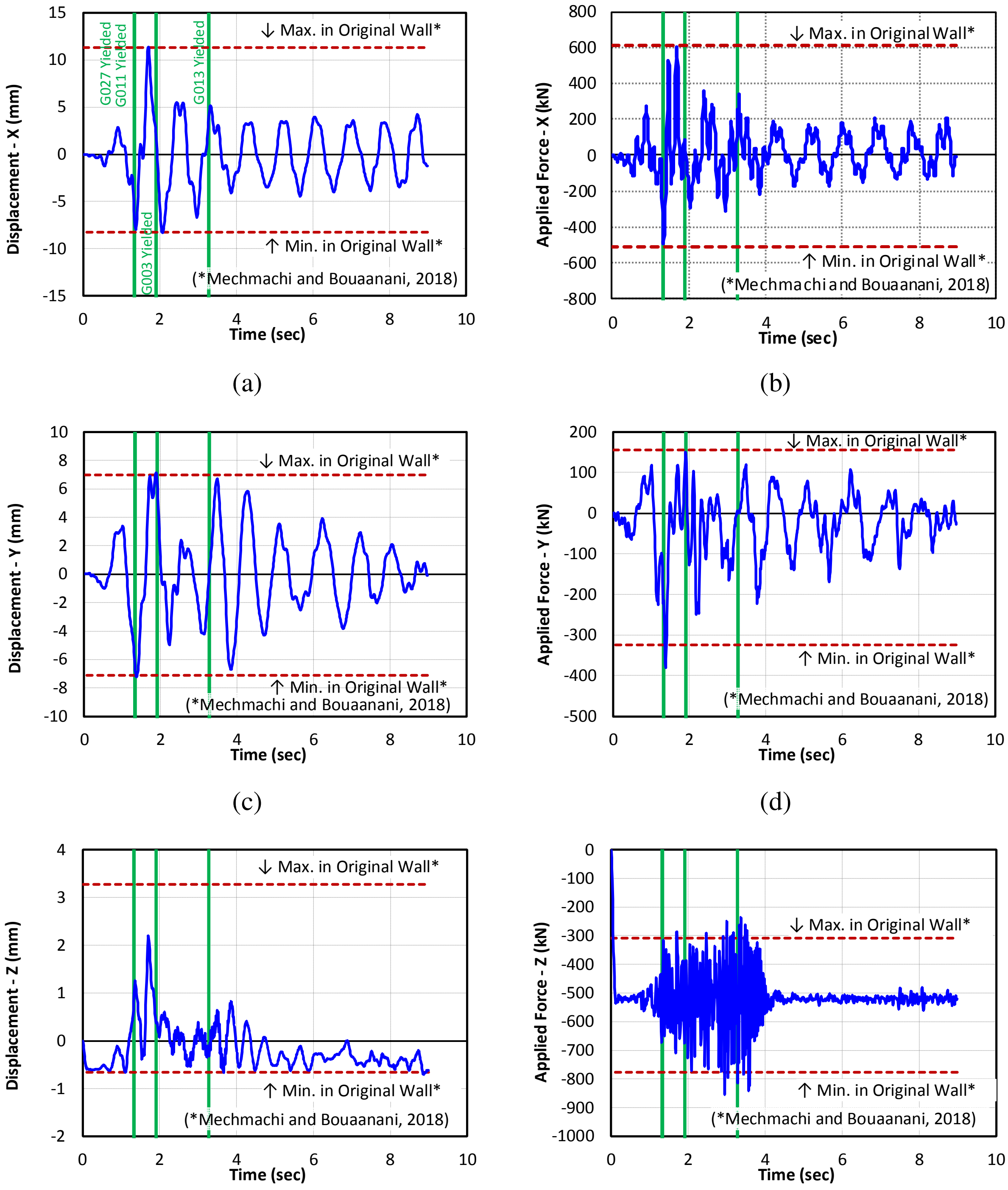
(a) (b) (c) (d) (e) (f)

Fig. 6.33. Time-history displacement and force results of the hybrid tests: Aftershock (Step 3)

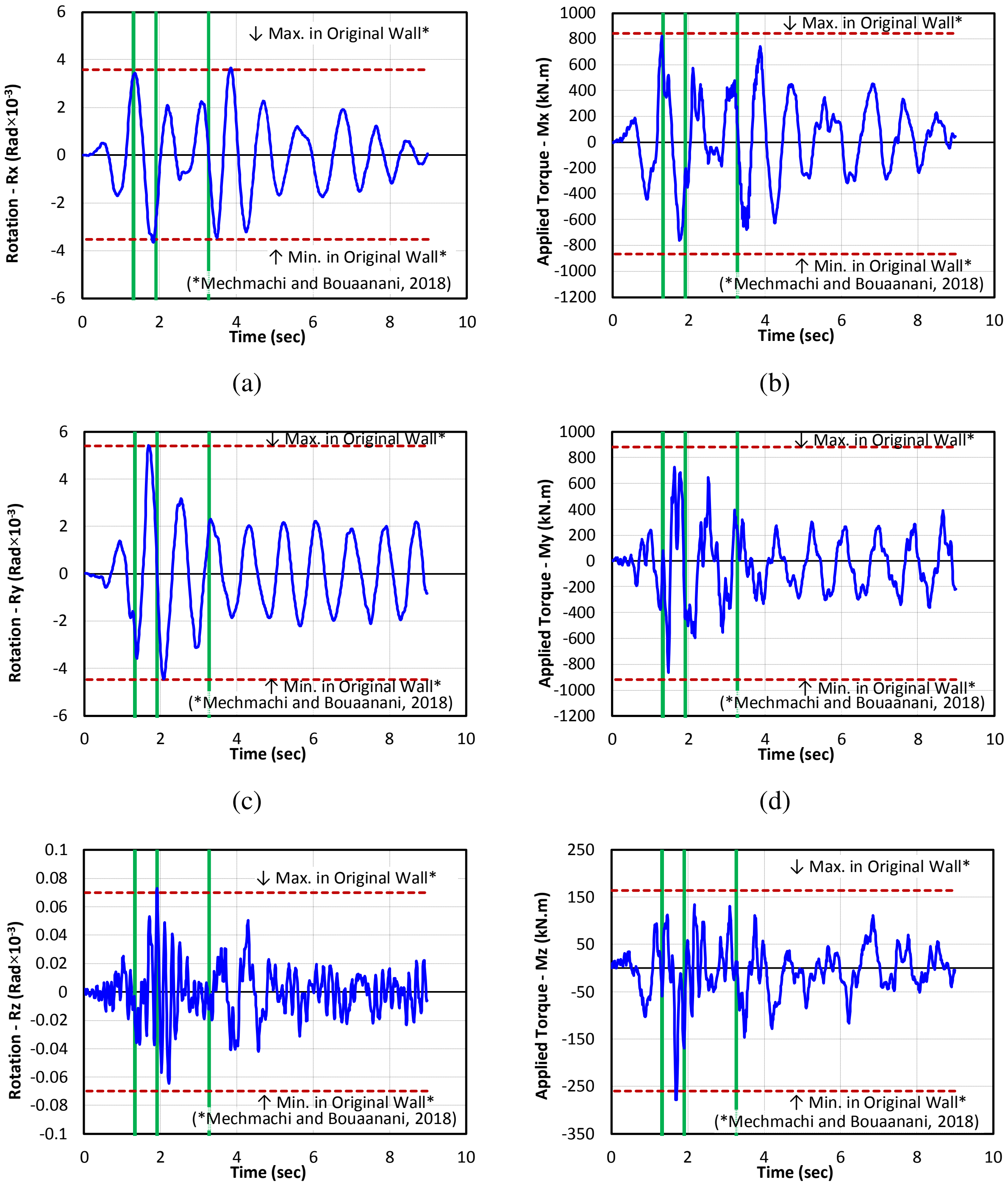

(a) (b)

(c) (d)

(e) (f)

Fig. 6.34. Time-history rotation and bending moment results of the hybrid tests: Aftershock (Step 3)

From the figures, it can be seen that the maximum/minimum displacement/rotation responses of the wall after being retrofitted with FRP materials were close to the displacement/rotation response of the Original wall, except for the Z direction (i.e. axial direction). According to Mechamchi and Bouaanani (2018), the controller machine was not able to stabilize the constant 520 kN axial force (Z direction) applied on the specimen during the hybrid tests of the Original wall. Hence, the axial load (and the axial displacement) of the C-shaped wall fluctuated during the hybrid tests. In testing of the FRP Retrofitted wall, however, these variations were relatively controlled by tuning the controller machine. Comparison of the results in other directions showed that peak displacements/rotations barely exceeded those of the Original wall, whereas the reaction forces/torques were significantly smaller during the mainshock (steps 1 and 2). The results from the aftershock record (step 3) of the Retrofitted wall were quite close to the data obtained from the Original wall, both in terms of excitations (displacement/rotation) and the applied force/torque. Step 3 of the hybrid tests, namely aftershock, included more severe excitations in comparison with the first two steps. Four strain gauges on the longitudinal steel reinforcement reached the yield strain during this step, as indicated in the Fig. 6.35. Strain gauge G003 yielded in tension at the drift levels of $\delta_x = 0.04\%$ and $\delta_y = 0.21\%$, while the tip of the wall was heading to the North (+Y) direction. Strain gauges G011 and G027 yielded in tension at the drift levels of $\delta_x = 0.20\%$ and $\delta_y = 0.21\%$, while the wall was moving toward the South-West direction (Fig. 6.33.a&c). As a reference, the theoretical yield drift of the C-shaped was calculated approximately to be equal to $\delta_y = 0.10\%$. The strain gauge G013 yielded in compression at the drift levels of $\delta_x = 0.13\%$ and $\delta_y = 0.01\%$, while the wall was load in the East (+X) direction.

A comparison of the displacements/rotations and the corresponding forces/torques between the Original and FRP Retrofitted wall shows that the initial stiffness of the wall which comes into action in relatively small amplitudes of the excitations was not enhanced by the applied FRP retrofitting approach. This is expected since the RC wall was under no axial load during the FRP retrofitting phase. Hence, the vertical FRP strips were somehow compressed by the 520 kN axial load applied at the beginning of each test. This prevented the FRP layers from increasing the initial stiffness of the wall and notably affected the response of the wall against the mainshock excitations.

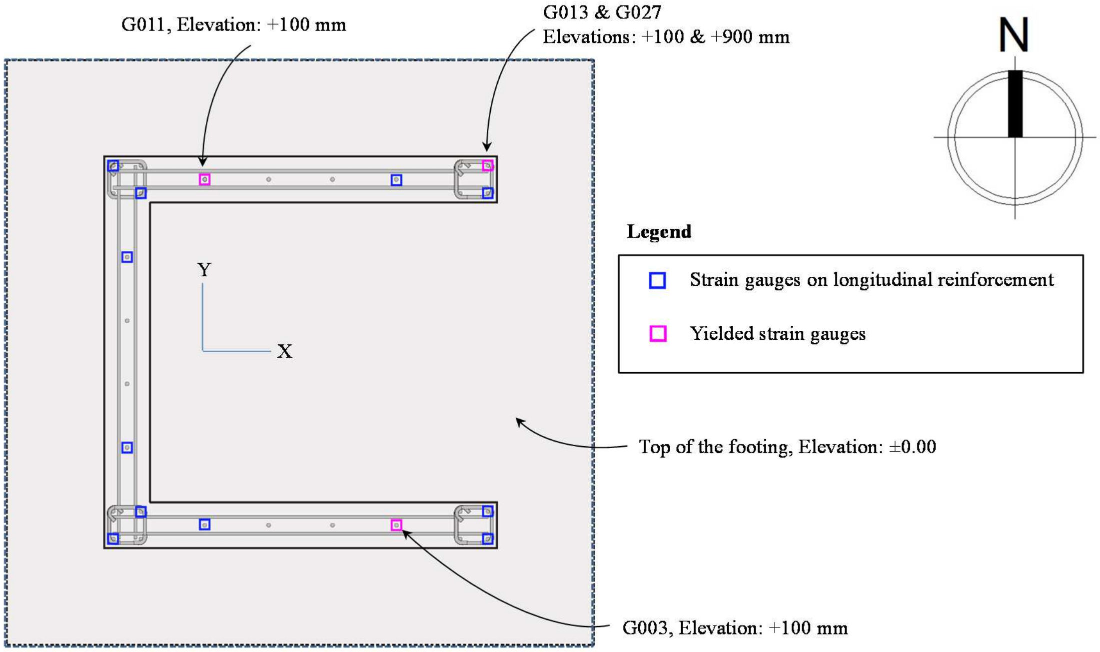

Fig. 6.35. Strain gauges yielded during the step 3 (aftershock) of the hybrid tests

In step 3 of the hybrid tests, where larger excitations were applied on the wall, larger vertical strains were measured by the DIC system on the FRP layers at the corners of the C-shaped wall (i.e. boundary zones). For instance, once the C-shaped wall hit the peak displacement of -7.2 mm in the Y direction (Fig. 6.33.c), the average vertical strains on the FRP layer at the inner side of the North-East corner was measured equal to 0.0034. This measured strain is compatible with the strain measured in the longitudinal corner bar that exceeded the yield strain at this moment. The measured strain in vertical FRP strip mounted on the inner side is equal to 41.5 kN force, and is equal to more than 85 kN total force resisted by the vertical FRP strip mounted on both sides. As a reference, the total yielding force for the 4-20M longitudinal corner bars is equal to 480 kN. Stretching of the FRP layers and the internal forces resisted by the vertical strips contributed to the tensile resistance of the corner zones of the cracked wall against the applied excitations. Hence, responses of the damaged wall after FRP retrofitting were found to be close to those of the Original wall. The results indicate the efficiency of the employed FRP retrofitting scheme in improving the performance of the damaged RC wall.

6.3.2 Results of the characterization tests

Characterizations of the wall in different directions (i.e. X, Y, diagonal and torsional direction) were tested by applying small amplitude cycles in low displacement rate of 0.1 mm/s. For comparison purposes with the Original wall, same fixed-fixed end boundary conditions were considered for both top and bottom ends of the FRP Retrofitted wall at this step, and the results were compared to the corresponding data from the Original wall tested by Mechmachi and Bouaanani (2018). Moreover, a numerical model was developed for the "Intact" undamaged Original C-shaped RC wall, using the modeling approach presented in Chapter 4. Characterization loading protocol was applied to the numerical model, and the results are shown in this section as a reference in order to quantify the level of damage in the C-shaped wall at the end of the characterization tests on the Original wall.

Fig. 6.36 shows the experimental results of characterization tests on the Original and Retrofitted walls, together with the results of numerical analysis of the Intact wall. As it can be seen from the figure, the Original wall showed a softer response at the high level of loading during the characterization tests, compared to the Intact wall. This can be attributed to the damage that the Original wall experienced in the hybrid tests. In fact, the difference between the resistance of the numerical Intact model of the wall and the measured resistance of the Original wall can be a quantification of the damage that the wall experienced during the hybrid tests. Results showed that the peak strength of the Original wall in the X direction decreased by 15% and 8% for the push and pull cycles (at $\Delta_X = +11.38$ mm and $\Delta_X = -8.15$ mm), respectively. A reduction of 4% and 9% was observed in the peak resistance in the Y direction for the push and pull cycles ($\Delta_Y = +6.71$ mm and $\Delta_Y = -7.31$ mm), respectively. In the diagonal direction, the reduction in the peak resistance was 12% and 18% for the push and pull cycles ($\Delta_{Diag.} = +10.48$ mm and $\Delta_{Diag.} = -13.24$ mm), respectively. The torsional cycles showed a reduction of 12% and

17% in the peak torsional moment for counter-clockwise and clockwise cycles (R_z = +0.0049 Rad and R_z = -0.0044), respectively. According to Fig. 6.36, the FRP retrofitting scheme used in the current work has higher peak reaction force/moment, while the initial stiffness of the wall in almost all loading directions remained close, compared to that of the Original wall. The latter, i.e. minimal change in the initial stiffness due to the FRP retrofitting scheme, is an important achievement since changing the initial stiffness would affect the dynamic characteristics of the structure. Moreover, the hysteretic loops of the Retrofitted wall were found to be very close to those of the Intact wall.

Comparison of the results shows that retrofitting with FRP restored the response of the damaged wall to be reasonably comparable to that of the Intact wall, while being better than that of the Original wall, knowing that it experienced additional damage due to the hybrid tests (which can be quantified when comparing the responses of the Intact and the Original walls). In the X cycle (flange direction) presented in the Fig. 6.36.a, the peak resisting force by the wall in the push cycle was improved by up to 27% (5% increase compared to the intact wall) at the displacement Δ_X = +10.73 mm, while the peak resisting force in the pull cycle was slightly higher than the Original wall by only 1%. Comparison of the X cycle curves also showed that the stiffnesses of the Original wall and the FRP Retrofitted wall were similar for both loading and unloading stages. However, thinner hysteresis loop was observed at this cycle for the FRP Retrofitted wall, which resulted in 29% lower energy dissipation during the X cycle in the FRP Retrofitted wall compared to the Original wall. This reflects the fact that FRP is effective in increasing the lateral resistance of RC walls, but it has limited capability of energy dissipation. Moreover, smaller residual displacement was observed for the FRP Retrofitted wall. No major changes were observed in the stiffness of the Retrofitted wall compared to the Original wall in which clear significant reductions were measured. Moreover, the stiffness reduction was more remarkable in the push cycle. This was due to earlier yielding of longitudinal bars in the web as well as the conjunctions of the web and the flanges of the Original wall (Mechmachi and Bouaanani, 2018) compared to the FRP Retrofitted wall.

Fig. 6.36.b shows the lateral force-deformation relationship of the Original and FRP Retrofitted walls in the Y cycle. From the figure, it can be seen that the force-deformation relationship of the FRP Retrofitted wall is close to that of the Original wall. However, the peak negative resisting force of the FRP Retrofitted wall was 19% higher than the corresponding force in the Original wall, and 8% higher than that of the Intact wall. This was expected since, during the hybrid tests on the Original wall, wide flexural cracks occurred at the North-East corner of the north flange. During the pull cycle, this corner was under tension, and the tensile resistance of the vertical FRP strips mounted on two faces of this zone increased the force corresponding to the peak displacement of $\Delta_y = -7.31$ mm. Comparison of the hysteresis loops showed that the residual displacements in the Retrofitted wall were decreased by 41% and 52% in push and pull cycles, respectively, compared to the Original wall. The FRP Retrofitted wall showed 21% lower energy dissipation. No considerable variation in the stiffness of the specimen was observed in this direction.

Similar trends were observed for the results of diagonal displacement and twisting of the wall. The resisting force in the diagonal cycle (Fig. 6.36.c) was increased by 19% and 25% on the push and pull cycle ($\Delta_{Diag.} = +10.48$ mm and $\Delta_{Diag.} = -13.24$ mm), respectively. The latter showed a substantial increase in both the loading and unloading stiffness of the Retrofitted wall compared to the Original wall. Compared to those of the Intact wall, the peak resisting forces in the FRP Retrofitted wall increased by 5% and 2% in push and pull cycles, respectively. Moreover, no stiffness reduction was observed in the FRP Retrofitted wall during the push cycle of the diagonal direction, as opposed to the Original wall.

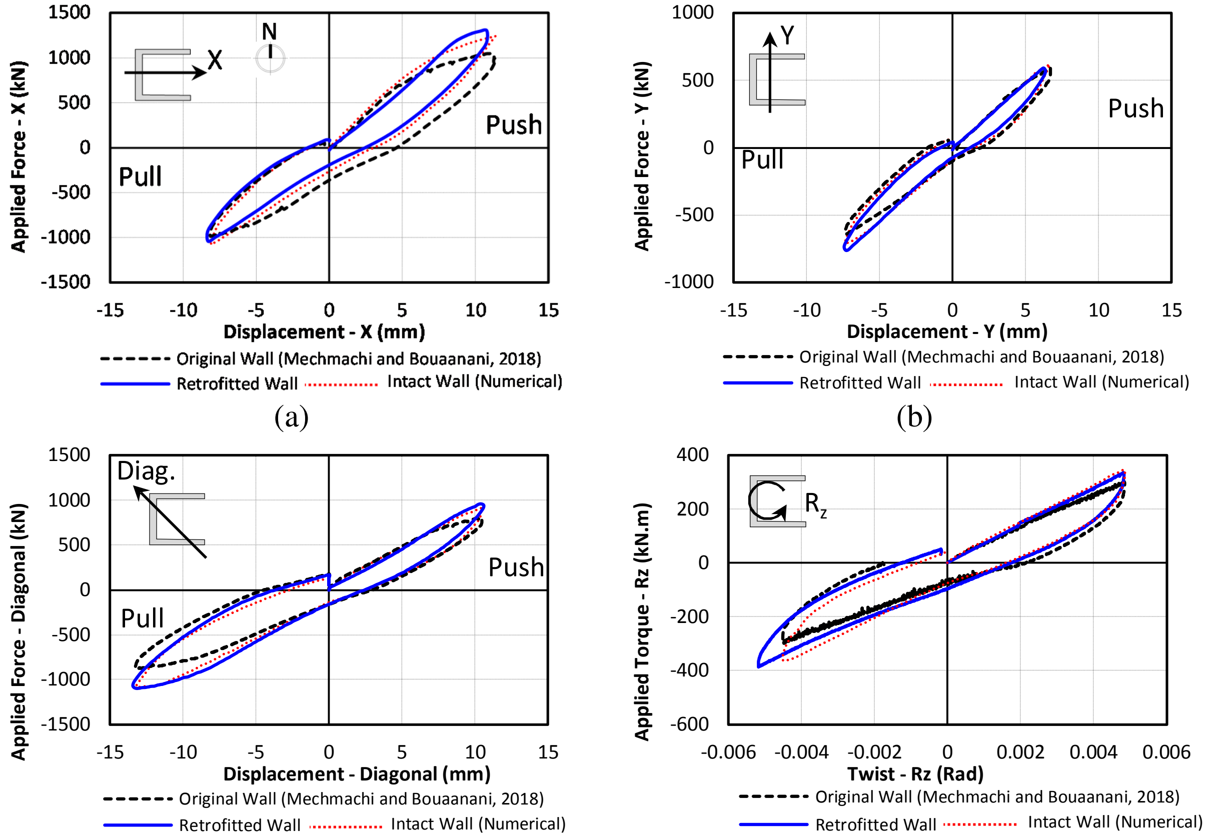

(a) (b) (c) (d)

Fig. 6.36. Characterization tests results: a) X-direction cycles, b) Y-direction cycles, c) Diagonal cycles, d) Torsional cycles

As for the torsional response of the wall (Fig. 6.36.d), the observed change in the stiffness of the wall was not significant, however, the resisting torques at R_z = 0.0049 Rad and R_z = -0.0044 Rad increased by 11% and 15% for the counter-clockwise and clockwise twists, respectively, and reached to approximately the same resisting torque as the Intact wall. During the torsional excitations, cross-section warping of the RC wall induces significant normal stresses at the base of the C-shaped RC wall, proportionate to the applied torque and the distance to the shear center of the section. Therefore, warping of the section results in excessive tensile/compressive forces at the corners of the C-shaped wall. In the FRP Retrofitted wall, the tensile forces at the corners will be partially resisted by the vertical FRP strips. Hence, larger torsional stiffness in the FRP Retrofitted wall is expected compared to the Original wall.

6.3.3 Results of the cyclic test

The cyclic loading protocol described in the Section 6.2.6 was applied at the top of the wall to measure the response of the C-shaped RC core wall when it is subjected to multi-directional loading. In order to evaluate the efficiency of the controller machine in controlling the target displacement pattern, Fig. 6.37 shows the actual imposed lateral displacement pattern as seen from the top. Comparing the measured displacement with the planned loading protocol plotted in the Fig. 6.27, the actuator control system was found to work very effectively.

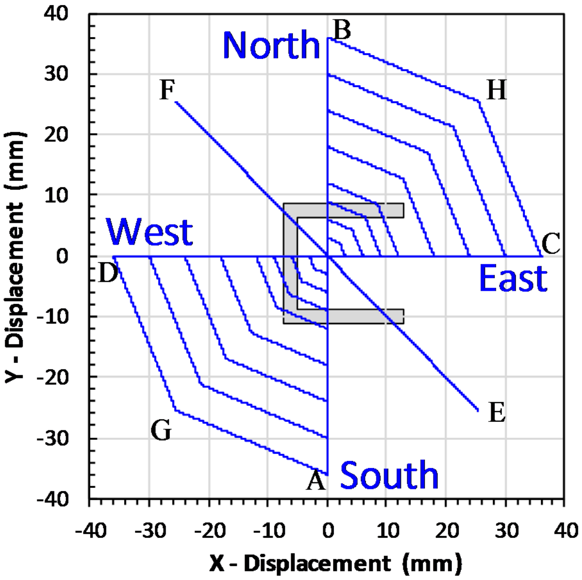

Fig. 6.37. Actual imposed displacement history

Results of the cyclic test in different directions of the loading are presented in Figures 6.38 and 6.39. The hysteresis loops are almost symmetric in Y cycles, whereas asymmetric load-deformation response was observed in the X and diagonal cycles. Moreover, the hysteresis load-displacement loops of the FRP retrofitted wall were fat and stable with no significant degradation up to the end of the cycle of $\mu_\Delta = 10$. The displacement ductility was defined as the displacement divided by the first yield displacement, considering that the wall has different yield displacements (i.e. different directions) due to the asymmetric geometry. During the last cycle of the test ($\mu_\Delta = 12$), however, maximum degradation of approximately 30% in the maximum resistance of the wall in the main directions was observed; more specifically, 28% in +X, 30% in –X, 22% in +Y, and 28% in –Y direction. The maximum degradations in the diagonal direction were equal to 21% and 23% in the push and pull cycles, respectively. During the sweeping cycles (i.e. O→A→G→D→C→H→B→O in Fig. 6.37), 28% degradation was observed in the +GH direction, whereas a maximum degradation of 44% was observed in the –GH direction. No significant pinching was observed in the hysteresis loops up to $\mu_\Delta = 10$, indicating that the wall did not experience shear-sliding deformations. However, during the cycle of $\mu_\Delta = 12$, slight sliding of the wall was observed due to the growth of cracks along the full length of the North flange and the web. For comparison purposes, results of pushover analysis of the Intact wall in the X, Y and diagonal directions are included in the Figures 6.38.a-b and 6.39.e. As it can be seen from the figures, the FRP retrofitted wall showed lower, yet close, stiffness compared to that of the Intact wall in all directions. This could be attributed to the damages that the Original wall experienced during the hybrid and characterization tests. The capacity of the wall, however, was notably improved by FRP retrofitting in all directions, both in push and pull cycles.

Table 6.3 shows a summary of the results of the multi-directional cyclic test together with the peak capacity of the Intact wall obtained from the numerical analysis. The FRP retrofitted wall showed 11% and 15% more capacity during the push and pull cycles, respectively, in the X direction. FRP retrofitting had more effect on the pull cycles, which is expected considering the geometry of the section. When the wall is loaded in the –X direction (O→D), the outer end of the flange will be under tension, which has to be resisted by the longitudinal steel reinforcements as well the vertical FRP strips. Hence, there is a considerable contribution by the vertical FRP strips in resisting the internal tensile forces. In the +X direction, however, the wall benefits from the longitudinal reinforcements along the web of the wall as well as the corner reinforcement and the vertical FRP strips. Hence, the contribution of the FRP strips in resisting the tensile forces will be less than that of the –X direction. In the +/-Y directions, FRP retrofitting increased the capacity of the wall by 8% and 10% during the push and pull cycles, respectively. Although the numerical model resulted in an identical capacity of the wall for loadings in the +Y and –Y directions due to the symmetry of the model, the cyclic test resulted in different capacities during the pull and push cycles in the Y direction. This was due to the fact that during the hybrid and characterizations tests, the flexural cracks and yielding of the steel reinforcement were started from the North-East end of the North flange and the specimen was no longer in a symmetric situation. In the diagonal direction, 5% and 8% increase in the wall capacity was observed during push and pull cycles, respectively.

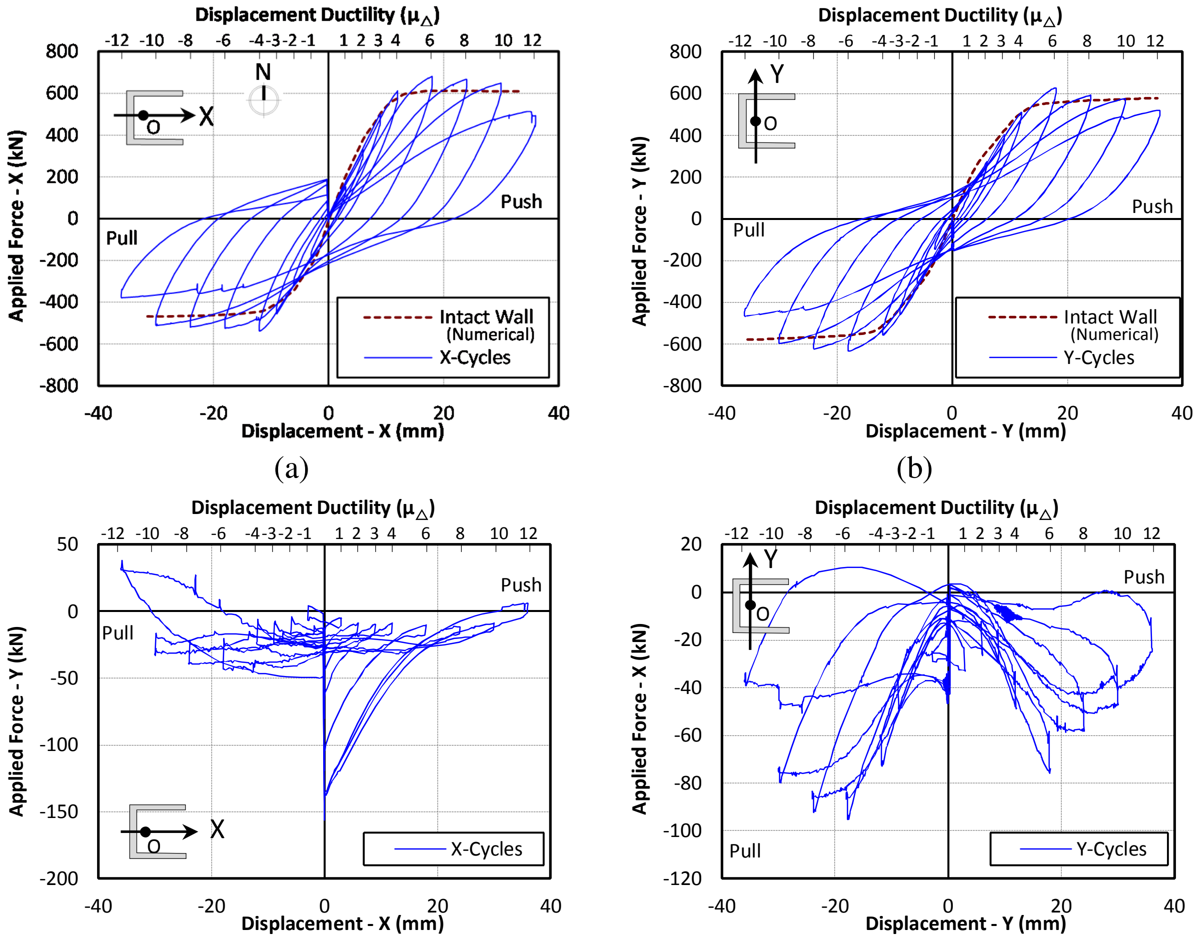

(a) (b)

(c) (d)

Fig. 6.38. Load-displacement results for the principal directions

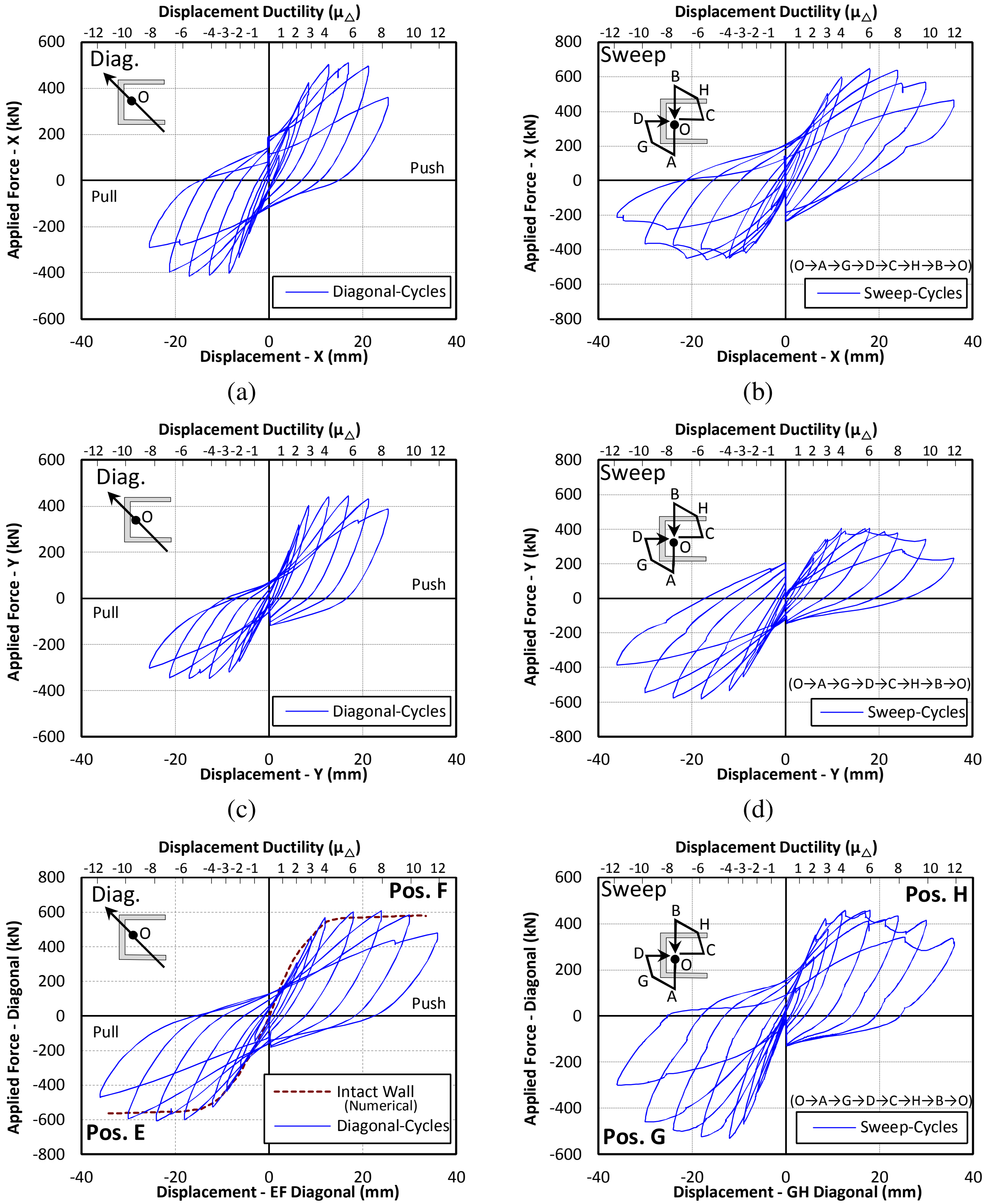

(a) (b)

(c) (d)

(e) (f)

Fig. 6.39. Load-displacement results for diagonal and sweeping cycles

Table 6.3. Summary of the multi-directional cyclic test results

Direction	Intact Wall (numerical)		FRP Retrofitted Wall (cyclic test)			
	Min. Force (kN)	Max. Force (kN)	Min. Force (kN)	$\delta_{@\min}$ (mm)	Max. Force (kN)	$\delta_{@\max}$ (mm)
X (C ↔ D)	-468.6	612.6	-538.7 (↑ 15%)	-11.9 ($\mu_\Delta = -3.98$)	681.4 (↑ 11%)	18.0 ($\mu_\Delta = 6.0$)
Y (A ↔ B)	-578.1	578.1	-635.7 (↑ 10%)	-17.9 ($\mu_\Delta = -5.98$)	626.3 (↑ 8%)	17.9 ($\mu_\Delta = 5.9$)
Diagonal (E ↔ F)	-565.4	580.0	-607.9 (↑ 8%)	-24.0 ($\mu_\Delta = -8.00$)	608.5 (↑ 5%)	24.0 ($\mu_\Delta = 7.99$)
Sweep	——	——	-531.2	-12.0 ($\mu_\Delta = -4.00$)	458.1	12.7 ($\mu_\Delta = 4.24$)

During the cycle of $\mu_\Delta = 6$ of the cyclic test, the first visible flexural crack (i.e. crack width of more than 3 mm) was observed at the interface between the outer side of the North flange when the wall was loaded in the –Y direction (O→A), where the North flange was in tension. Debonding of horizontal FRP wrapping was observed at small zones, mostly at the vicinity of the cracks, at this step. A fully extended crack in the north flange was observed once the wall reached to the position E during the cycle of $\mu_\Delta = 8$, followed by partial rupture of FRP vertical strips at the outer end of the northern flange by reaching the subsequent G position (Fig. 6.40). Full rupture of the external vertical FRP strip was detected at the outer end of the North flange when the wall was loaded in the –X direction (O→D), i.e. the flange outer end under tension (Fig. 6.41). The subsequent position H led to the partial rupture of vertical FRP strip in the external face of the web on the south-west end.

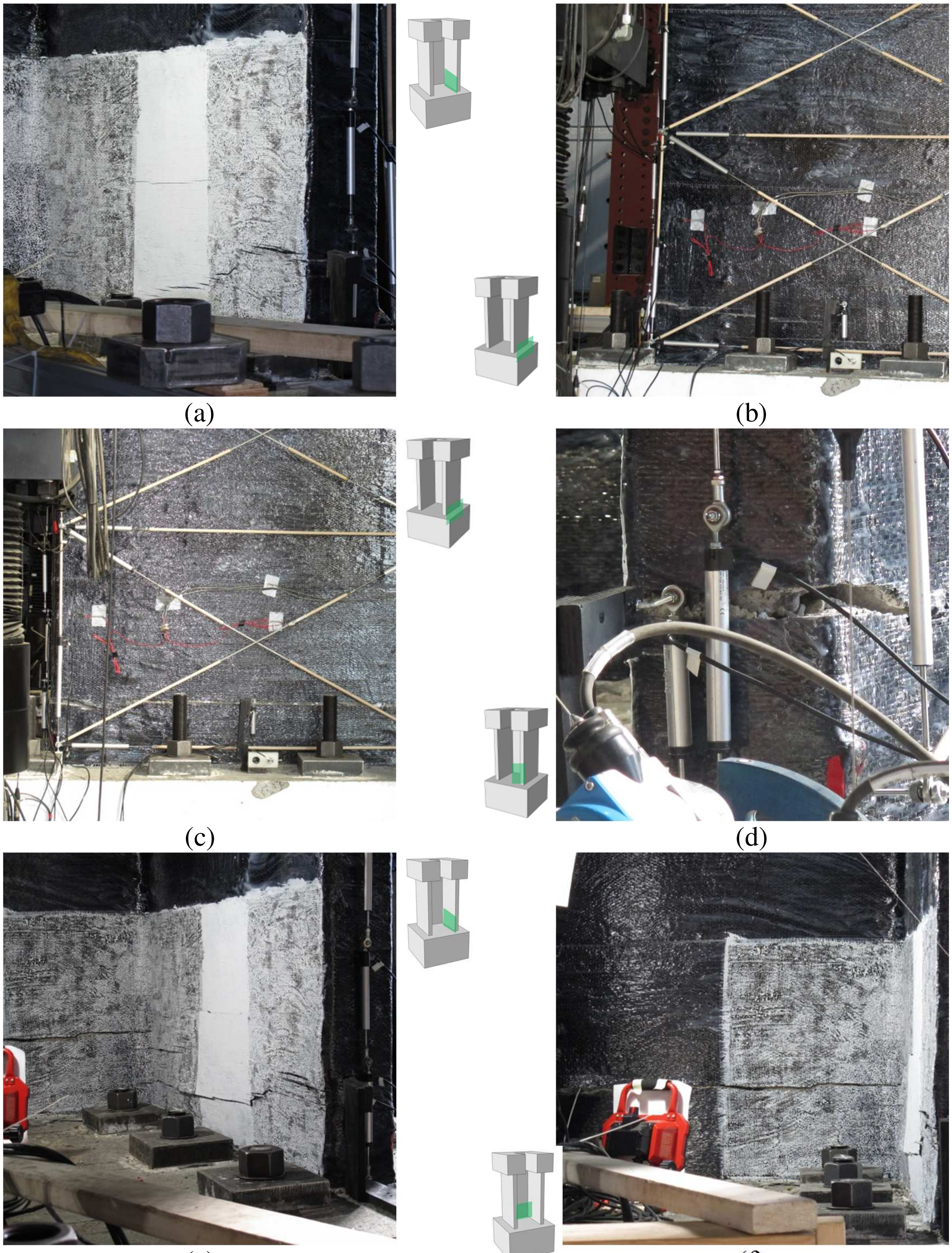
(a)
(b)
(c)
(d)
(e)
(f)

Fig. 6.40. Crack opening at: a) position D during the cycle of $\mu_\Delta = 8$, b) position D during the cycle of $\mu_\Delta = 10$, c) position D during the cycle of $\mu_\Delta = 12$; d) longitudinal bar rupture; e) full opening of crack in the North flange; f) crack opening along the web

The first step of loading (position A) of the cycle of $\mu_\Delta = 10$ led to the full rupture of both the external vertical FRP strip at the north-west corner (i.e. flange and web intersection), as well as the rupture of the internal vertical FRP strip at the outer end of the north flange. The external strip at the south-west end of the web was fully ruptured upon reaching the position C in this cycle. Crushing of the concrete under compression became visible during this cycle especially in the external face of the north flange and the web where debonding of FRP wraps occurred previously. However, despite the severe bulging of the FRP wraps, no large tearing was observed in the horizontal FRP wraps. The concrete materials stayed in place despite the compressive crushing, and hence, no buckling of the steel bars was served due to the provided lateral resistance. It, however, was hard to investigate and measure due to the lack of visibility because of the FRP wrapping.

During the cycle of $\mu_\Delta = 12$, a full growth of the crack along the flanges and the web was observed at the position C. The subsequent position D caused a rupture in longitudinal steel bar at the end of the north flange once the crack was opened by a width of almost half an inch (Fig. 6.41). The variation of the reaction force, as well as the longitudinal strain in steel rebar, is shown in Fig. 6.42. A severe degradation of more than 30% was observed at this stage and was deemed to be the highest ductility level for the cyclic test to be able to go through. Noticeable, yet local and without spalling, crushing of the concrete was observed at the north-west corner once the test specimen reached to the position B during the sweeping step of the loading in this cycle (H→B). The concrete in the confined regions (i.e. boundary elements) at the four corners of the wall stayed in a fairly good condition, while the unconfined regions along the flanges and the web seemed to quite suffer from the compressive stresses during the cycles of 10 and 12. The test was then stopped at the end of this cycle due to significant degradation in the capacity of the wall. The test specimen failed due to rupture of the longitudinal reinforcing bars.

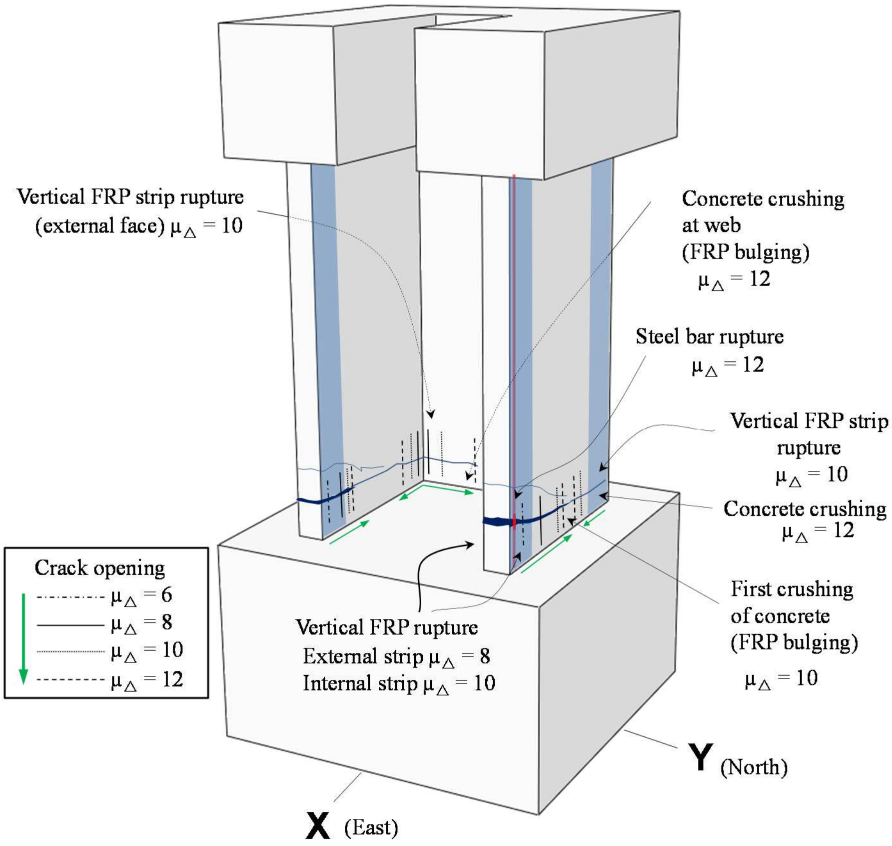

Fig. 6.41. Schematic of the failure of materials during the cyclic test

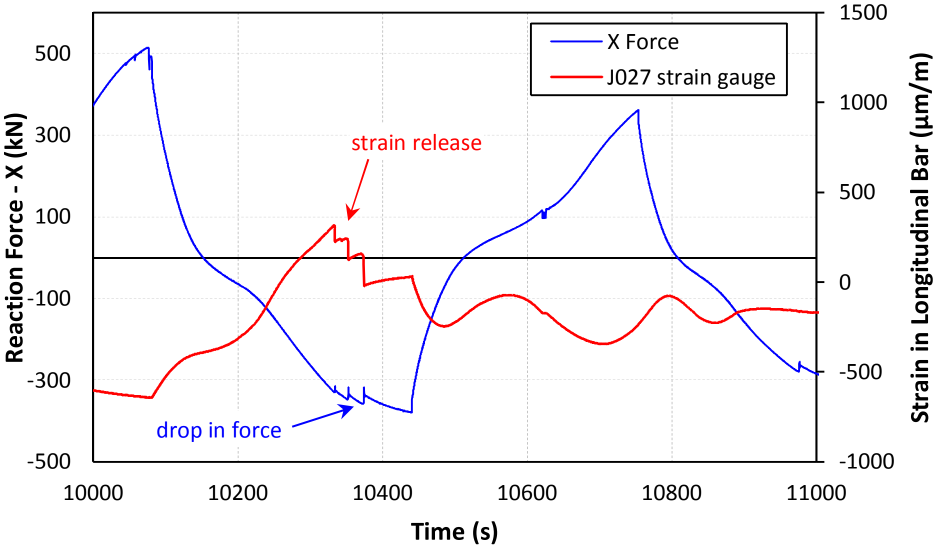

Fig. 6.42. Rupture of the longitudinal rebar during the cyclic multi-directional test

As mentioned in section 6.2.5, a DIC system was used to capture the deformations in three different zones of the C-shaped wall. The targeted zones, namely, the South flange, intersection of the web and the North flange and the North flange internal bottom corner, are shown in Fig. 6.43. Figures 6.44 to 6.46 present the strain distributions (ε_{yy}) in the targeted zones, as detected by the DIC system. In order to visualize the crack opening/closure during the cyclic test, for each displacement ductility level, the results were captured at peak points (positions A and B) in the Y direction. Distribution of vertical strain (ε_{yy}) on the bottom part of the South flange at different ductility levels are shown in Fig. 6.44. As expected, and visually observed qualitatively, flexural cracks mostly occurred at the bottom corners when the flange was under tension (position B).

During the cyclic test, no compressive crushing of concrete was observed in the South flange. This can be confirmed by the results of the DIC system. The compressive vertical strain did not reach to the crushing strain of concrete (ε_{cc}=0.0035). Moreover, at position A, the South flange was under compression, however, strain contours show regions of the wall with relatively large tensile strains. As it is marked in Fig. 6.44, these regions show the small zones of the FRP materials that were debonded from the concrete surface. These were initiated by opening of flexural cracks in the concrete, referred to as Intermediate Crack (IC) debonding. The first FRP debonding was captured at a compressive vertical strain of ε_{yy}= -0.0018, and was detected over 3% of the targeted zone area. By the end the cyclic test, FRP debonding was extended only in a minor portion of the south flange of the C-shaped RC wall (18% of the targeted zone area).

The strain distribution contours at the intersection of web and the North flange (internal face) are shown in Fig. 6.45, in which the FRP debonding at different ductility levels are marked. Results showed that FRP debonding at this zone was started at the cycles of μ_Δ=6 with a peak vertical compressive strain of ε_{yy}= -0.0051 (i.e. beyond the concrete crushing strain), and was detected over almost 6% of the targeted zone area. The FRP debonding was found to be concentrated around the crack openings, which shows the efficiency of the horizontal FRP anchors in supporting the FRP wraps. The anchors were mounted at the corner intersection (vertical spacing of 200 mm) to improve the bond between the FRP wraps and the wall surface. By the end of the cyclic test, FRP debonding was extended over 19% of the targeted zone area.

The bottom corner at the outer end of the North flange (Fig. 6.46) was considerably damaged due to the opening of flexural cracks started at the cycle of $\mu_{\Delta}=6$, and the FRP wraps were debonded consequently (position B in Fig. 6.46). The FRP debonding was first captured at the peak vertical compressive strain of $\varepsilon_{yy}= -0.0055$ (i.e. beyond the concrete crushing strain), and was detected over an area of about 6% of the targeted zone area. Delamination of FRP layers, however, led to the failure of the DIC system in processing a small zone of the speckled area. By the end of the cyclic test, FRP debonding was extended over 34% of the targeted zone area. Moreover, during the cyclic test, concrete crushing occurred at both bottom corners of the North flange during the cycle of $\mu_{\Delta}=6$. As it can be seen in figures 6.45 and 6.46, similar results were captured by the DIC system. A schematic of the FRP debonded area is shown in Fig. 6.47.

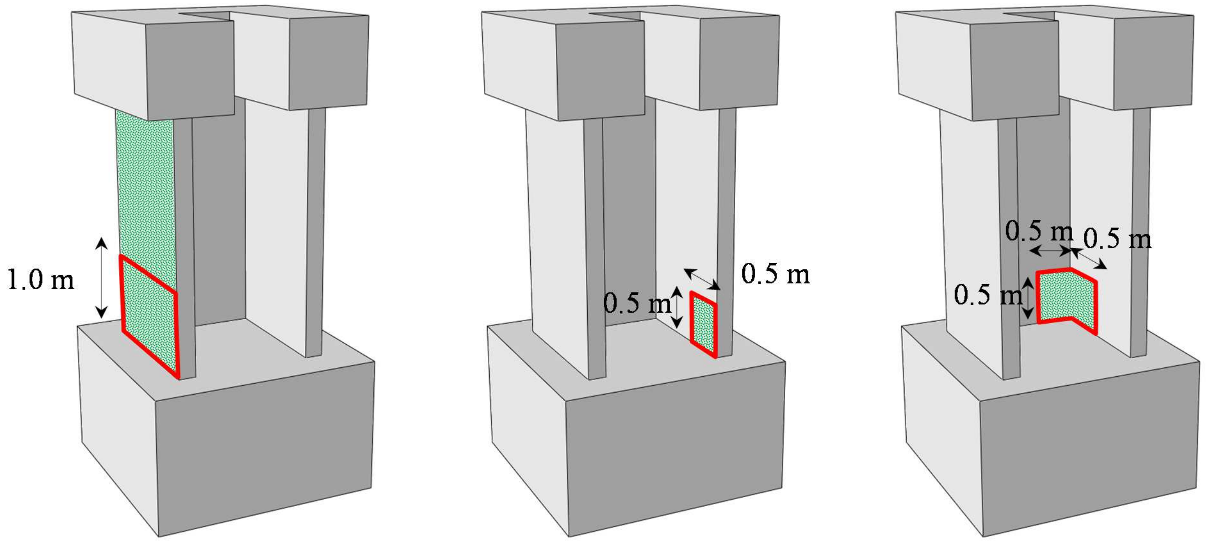

Camera 1 Camera 2 Camera 3

Fig. 6.43. Schematic of the speckled zones measured by DIC

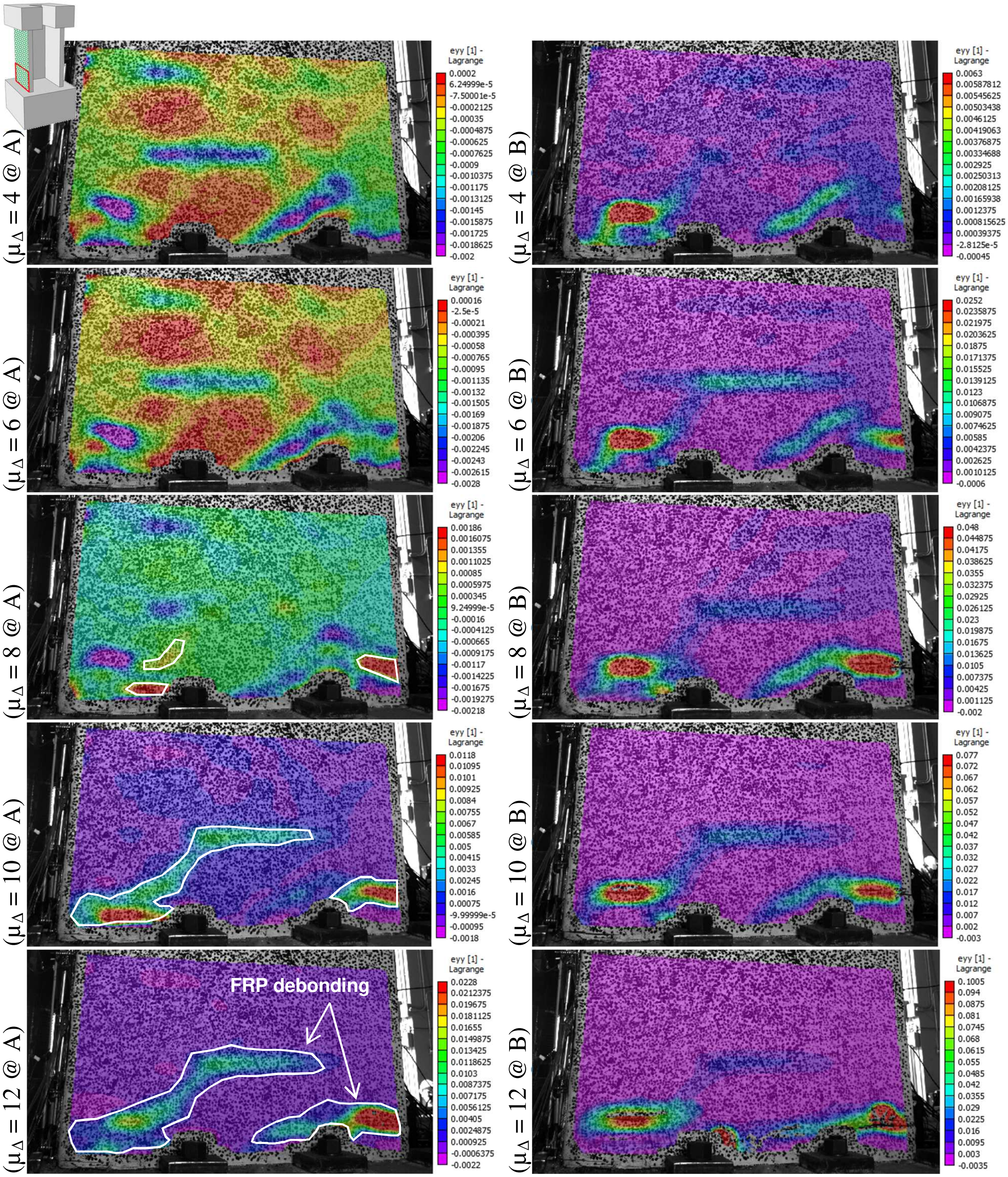

Fig. 6.44. Strain distribution (ε_{yy}) during the cyclic test at positions A and B: South flange (Camera 1)

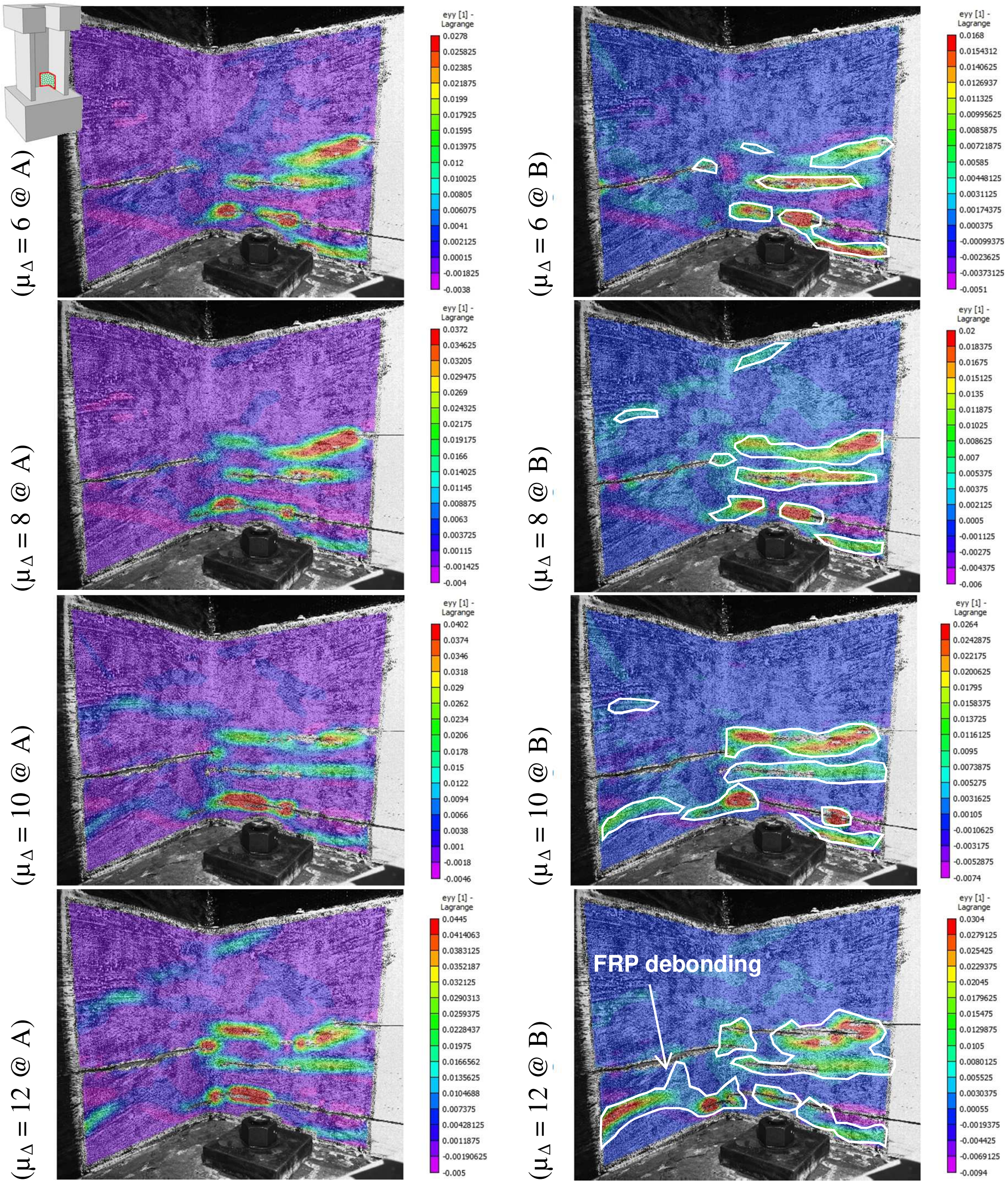

Fig. 6.45. Strain distribution (ε_{yy}) during the cyclic test at positions A and B: flange-web intersection (Camera 2)

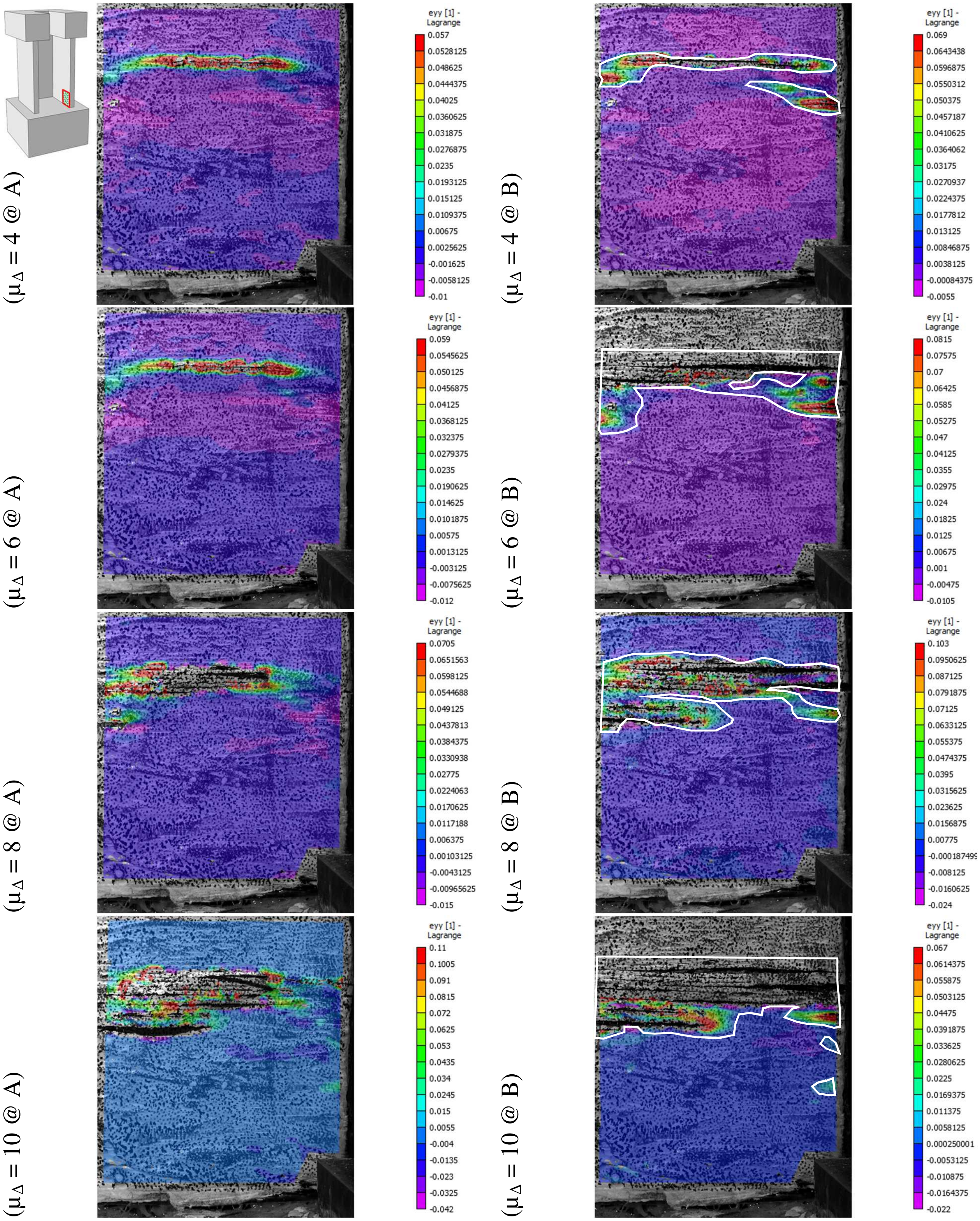

Fig. 6.46. Strain distribution (ε_{yy}) during the cyclic test at positions A and B: North flange outer end (Camera 3)

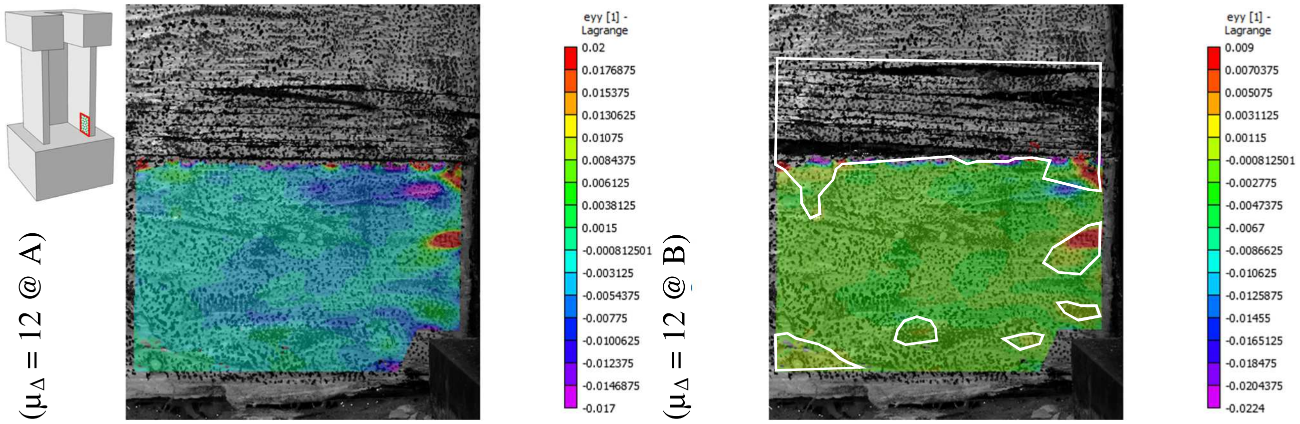

Fig. 6.46. Continue.

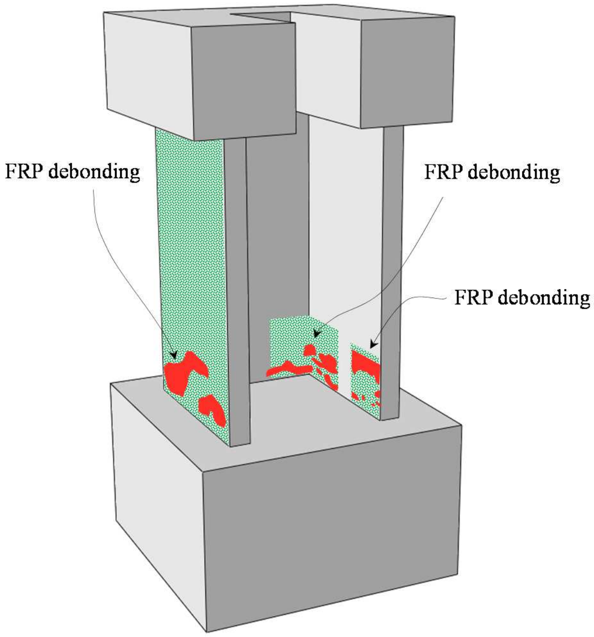

Fig. 6.47. Schematic of the FRP debonded area at the end of the cyclic test

6.3.3.1 Hysteretic behaviour in the main directions

Fig. 6.38 shows the force-displacement curves of the two main directions (i.e. X-direction in the East-West and Y-direction in the North-South). Despite the discontinuity of cycles for each of the curves depicted in the figure, due to the complexity of the loading history, the cyclic response of the wall looks quite similar to the reported responses of typical rectangular walls under pure uniaxial loading protocols. The Retrofitted wall showed a continued increase in lateral force resistance up to displacement ductility demand $\mu_\Delta = 6$, beyond which it started experiencing gradual post-peak degradation of its lateral load with larger displacement ductility levels. During each main loading direction, two horizontal actuators were pushing/pulling the test specimen to apply the targeted displacement while the other two were preventing the wall from out-of-axis displacements by applying a force couple (Fig. 6.38.c-d). This was due to the eccentricity of the load with respect to the shear centre of the C-shaped section located at the west, outside of the web of the wall. The magnitude of the force couple increased proportional to the applied cyclic force on the main load direction up to displacement ductility demand $\mu_\Delta = 6$. During the cycles with larger displacement ductility ($\mu_\Delta \geq 8$), the magnitude of the required force couple reduced since the shear center moved closer to the centre of the web of the wall (i.e. smaller eccentricity due to the gradual degradation at the free end of the two flanges). Similar behaviour was observed by Beyer et al. (2008-a) and Pégon et al. (2000). Moreover, as it is depicted in the Fig. 6.38.c-d, the variation of the force couple is not quite symmetric in both X and Y directions of the loading since different cracking states occurred in the two flanges led to different stress states attained during the preceding cycles. Besides, the push side of the Fig. 6.38.c (+X direction) shows a different large negative Y-force at the beginning of each cycle due to its previous cycle in which the wall was moving back to the origin (i.e. zero North-South displacement) before starting the new cycle on the East-West direction. Considering that X is an axis of symmetry of the C-shaped wall section, a zero Y-force would be expected theoretically if the wall had only been moved in the X direction.

6.3.3.2 Hysteretic behaviour in diagonal direction and sweeping cycles

Results from the diagonal excitations of the wall are the most complex part of the results mainly due to the asymmetry of the section, both in terms of the geometry and different effective stiffness of the flanges (i.e. flange is stiffer when subjected to compression rather than tension) in different cycles. Hysteretic force-displacement results of the FRP-Retrofitted wall in the diagonal and sweeping cycles are presented in Fig. 6.39.a-f. A clear, yet limited, difference was observed between the results of the diagonal and the sweep cycles in terms of lateral load capacity of the

Retrofitted wall. This was mainly because of the fact that the sweeping motions were the last stage of the loading protocol at each displacement ductility level, where strength degradation in the previous steps (i.e. Y, then X, then diagonal) was quite major. To validate this, a comparison of the results at low displacement ductility levels ($\mu_{\Delta}<6$), where strength degradation was not significant yet, showed a relatively good agreement between the lateral load resistance during the diagonal and sweeping cycles.

Results of a similar test by Beyer et el. (2008-a) on two C-shaped RC wall showed a considerable difference between the lateral load capacities (X and Y components) in main and diagonal directions, positions A and E in particular, where a smaller peak resistance was reported for the diagonal direction. Results of the FRP retrofitted test specimen in the current work, however, showed a relatively small difference between peak forces, 635 and 582 kN (9% difference) for positions A and E, respectively. Similar results were observed for positions F and B (X direction).

Considering that all the forces by the horizontal actuators in the test setup were acting at the same elevation level, it was possible to develop pure diagonal force-displacement plots through a geometrical transformation. The responses are presented in Fig. 6.39.e-f. As it can be seen from the plots as well as the summary results presented in Table 6.3, peak resisting forces measured in the diagonal direction are quite comparable to those of the two main axes. For example, higher wall resistance was measured at both positions E and F compared to that of the position D.

Although the magnitude of peak diagonal displacements in corresponding cycles are equal in EF and GH directions, comparison of the individual X and Y components of the load-displacement curves shows a noticeable difference (Fig. 6.39.a-d). This is partially due to the discontinuity of the hysteresis loops in both X and Y directions during the GH cycles compared to a single discontinuity at the end of each EF loop. Moreover, the EF diagonal cycles included two diagonal peak displacement points only, while during a sweeping motion, GH diagonal cycles included, the test specimen was moved toward six peak displacements (i.e. peak X, Y and diagonal displacements in push and pull cycle), four of which were repeated from the previous steps. For each displacement ductility level, this happened as the last step of a full loading cycle, where the wall was more prone to suffer from strength degradations in different segments.

6.3.3.3 Torsional reaction of the wall

During the tuning step of the cyclic test on the RC wall specimen, it was decided to restrain the torsional rotations of the wall. This was decided based on stability and sensitivity tests of the 6DOF testing system conducted by applying small amplitudes of excitations on the wall. Hence, the torsional actions imposed due to the eccentricity of the applied loads from the shear centre had to be resisted by force couples at the horizontal actuators. The resisting torsional moment (Rz torque) was recorded during the test. Fig. 6.48.a presents the variation of the resisting torsional moment solely for the smaller cycles ($\mu_\Delta \leq 4$) to provide better visibility, while a full plot of the results for all displacement ductility levels during the cyclic test is presented in Fig. 6.48.b.

While the results clearly show that the torsional moment (Rz), caused by eccentricity of the load with respect to the shear centre, peaked at North-South cycles (Y direction at positions A and B), the variation of Rz can be used as an indication of the strength degradation, especially in the flanges. During the cycles of $\mu_\Delta \leq 4$, there were slight decreases in the magnitude of Rz when the wall hits the same position for the second time (i.e. 5% and 15% variations at positions A and B, respectively). As the displacement ductility demand increased, however, the corresponding variations were found to be significantly larger (e.g. 15% and 72% decrease for positions A and B at the cycle of $\mu_\Delta=10$). At the last cycle ($\mu_\Delta=12$), extensive damages in the wall led to a decrease of 19% in the torsional resistance at two subsequent A positions. As for positions B, however, an opposite but smaller torsional resistance was recorded which indicates a significant shift of the shear centre because of severe damages in the wall.

No large torsional resistance was observed for excitations on the X direction (i.e. positions C and D) except at the very last cycles, where the wall considerably lost its symmetric configuration around X-axis. The peak torsional resistance was decreased dramatically during the cycles with larger displacement ductility demands ($\mu_\Delta \geq 8$).

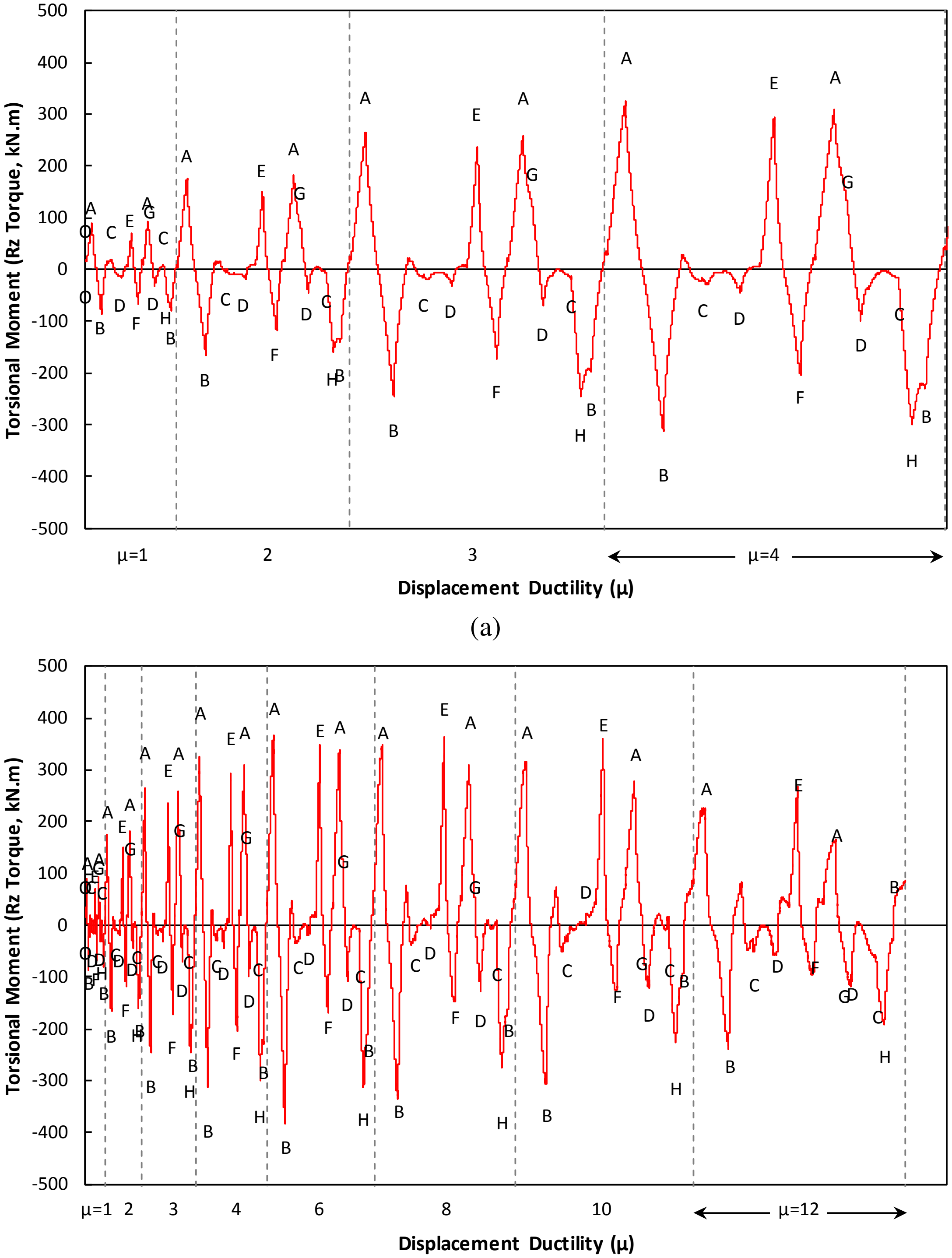

(a)

(b)

Fig. 6.48. Variation of torsional reaction of the wall during the cyclic test: a) Displacement ductility level 1~4, b) Full Test

6.3.3.4 RC Wall displacement components

Three main displacement components, namely sliding, flexural and shear displacements, result in the total lateral displacement of walls. In the current work, the sliding deformations at the base of the wall were directly measured at the centre of each segment of the C-shaped RC wall (i.e. web and flanges). Fig. 6.49 shows the variation of the base shear sliding displacement throughout the test. As it can be seen from the figure, sliding displacements at the base of the wall were fairly small, peaked at almost 2% of the total displacement during the cycles of μ_Δ = 1~6. As it was mentioned previously, during the cycles of μ_Δ = 8~12 severe bulging of the horizontal FRP wraps occurred due to the compressive crushing of the concrete. Hence, despite the un-interrupted readings recorded by the instruments measuring the sliding displacements, the sliding measurements were not valid anymore. The drops in the curves, however, can explicitly present the point of bulging of FRP (i.e. severe crushing of the concrete at the mid-length of the flanges and the web).

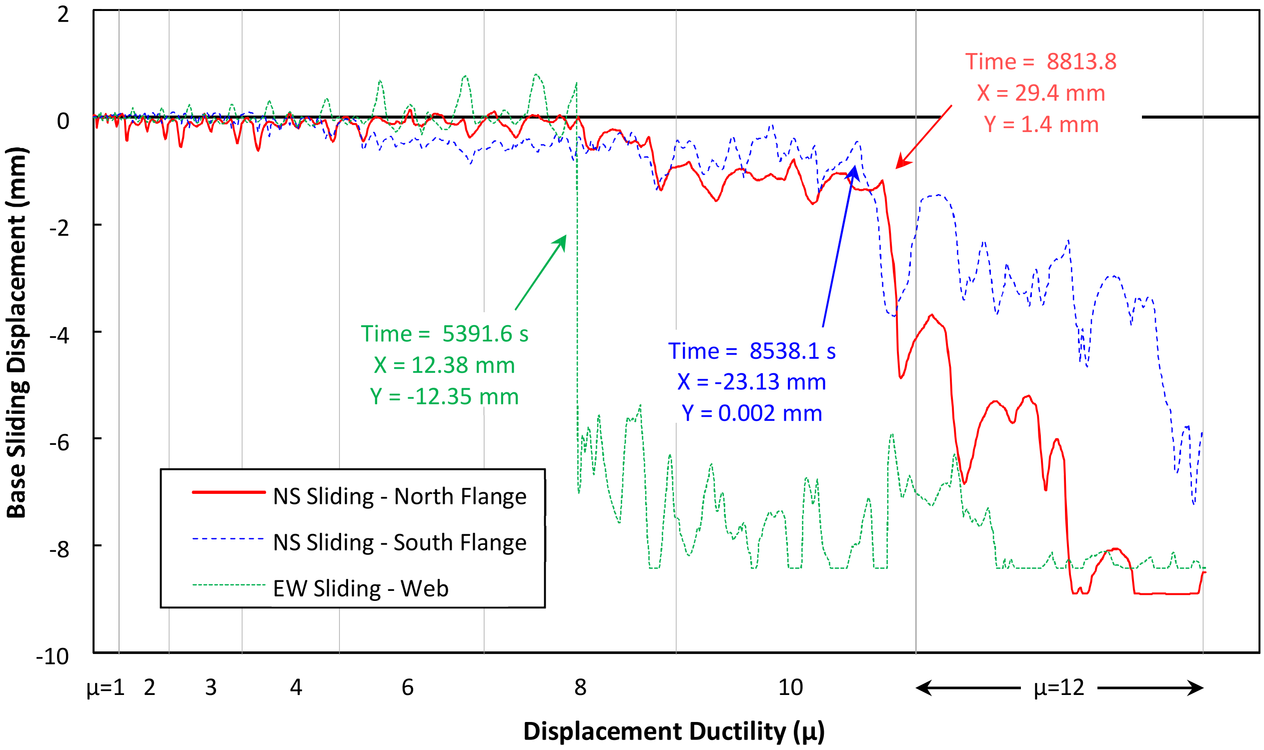

Fig. 6.49. Variation of the base shear sliding displacement throughout the test

In the current work, the method proposed by Massone and Wallace (2004) was used to evaluate the average shear and flexural deformations of the wall along the height of each segment using the data recorded by the linear potentiometers. Fig. 6.50 shows the theoretical model used to account for flexural/shear deformations. The height of the C-shaped RC wall was divided into three different levels, deformations in all of which were measured using the linear potentiometers. Displacements at the foundation level were set as the origin, and displacement components were accumulated along the height of the wall. Fig. 6.51 presents the variations of flexural/shear displacement components, base sliding excluded, in each segment of the wall during the cyclic test compared to the actual displacements measured at the top of the wall. As it can be seen from the figure, the total of flexural and shear displacements are in a very good agreement with the measured data at the top of the wall. The small discrepancies are mainly due to the inconsistent measurement levels. The actual displacements were measured by the controller machine at the top edge of the collar while the linear potentiometers were installed solely on the wall with a margin of almost two inches from the top and bottom edges.

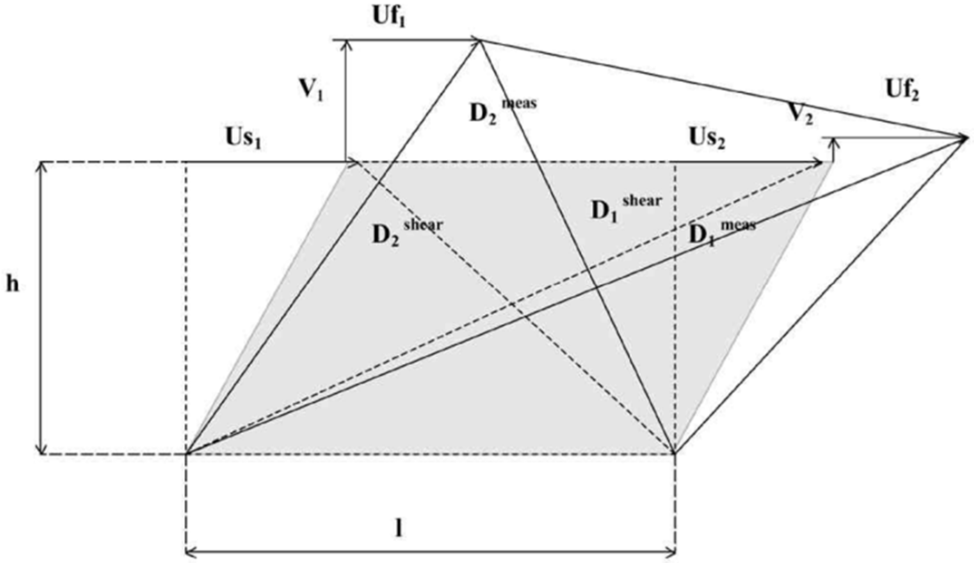

Fig. 6.50. The model used to evaluate the flexural/shear deformation (Massone and Wallace, 2004)

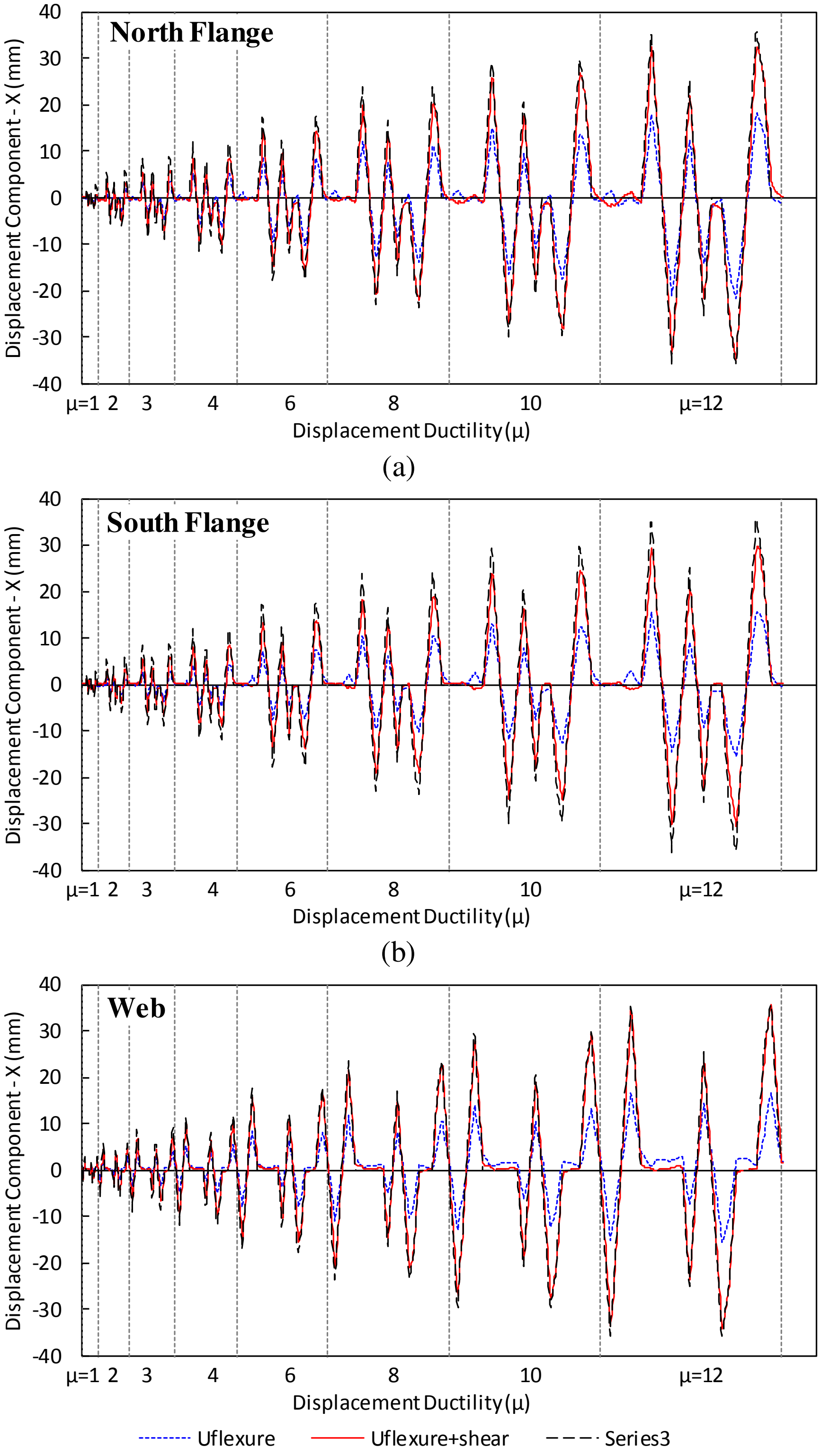

(a)

(b)

(c)

Fig. 6.51. Variation of flexural/shear displacement components during the multi-directional loading protocol

Contributions of main displacement components at peak displacements for each displacement ductility level are compared in Fig. 6.52 for main axes excitations (positions A, B, C and D). According to the results presented, on average, almost 60% of the flange total displacements were due to flexural deformations and the remaining 40% were from shear deformations in the wall's flanges (Fig. 6.52.a-b). As for the excitations on the web direction (Y-axis), however, the flexural displacements were found to be on par with shear deformations (Fig. 6.52.c-d).

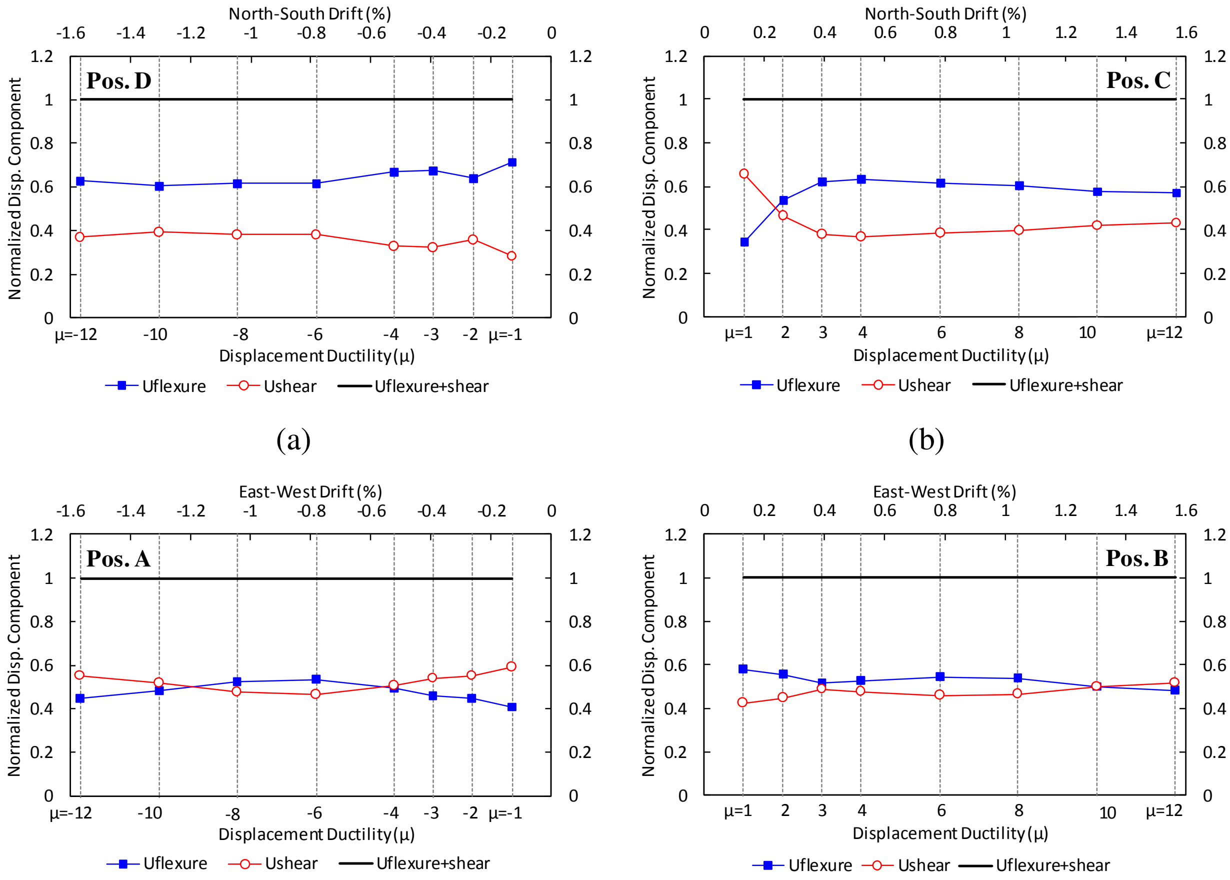

(a) (b)

(c) (d)

Fig. 6.52. Comparison of different displacement components along main directions of excitations

A similar comparison was performed for the EF diagonal direction, the results of which are presented in Fig. 6.53 for both the flanges and the web of the wall. In lower ductility levels

($\mu_\Delta \leq 3$), due to the complexity of the loading protocol, remarkable variations were observed in the curves and there was no consistent trend for contributions of flexural/shear deformations in different segments of the wall. However, by increasing the displacement ductility demand, less variations in both flexural and shear deformations were observed. In the flange direction, both flanges were found to have relatively close values for flexural and shear deformations when the wall was moved to position E (Fig. 6.53.a,c). Measurements showed 60% average flexural displacements in the North flange whereas the corresponding value for the South flange was only 44% of the total displacement. At position F, North flange deformed mostly due to the flexural deformations of 66% on average while only 42% flexural deformations were observed averagely. The South flange was found to have shear dominated deformations during the EF diagonal cycles while the North flange was deformed in a flexural dominant mode.

As for the web of the wall, deformations at cycles of $\mu_\Delta \geq 4$ were mainly shear dominant at position E resulted in 27% average flexural deformations, while at position F, the wall deformed mostly in flexure and resulted in 61% flexural deformations.

The large contribution of the shear deformation in total deformation of the wall seems a striking finding. However, observations can be justified by the fact that larger displacement ductility levels correspond to severe crack opening in the tension side of the wall section. This, in particular, is the situation at position F for the South flange and position E for the web. In both situations, the corresponding segment of the wall section is under tension, and it is likely that large crack widths led to a small shear stiffness and therefore to larger shear displacements. Similar observations were reported by Beyer et al. (2008-a).

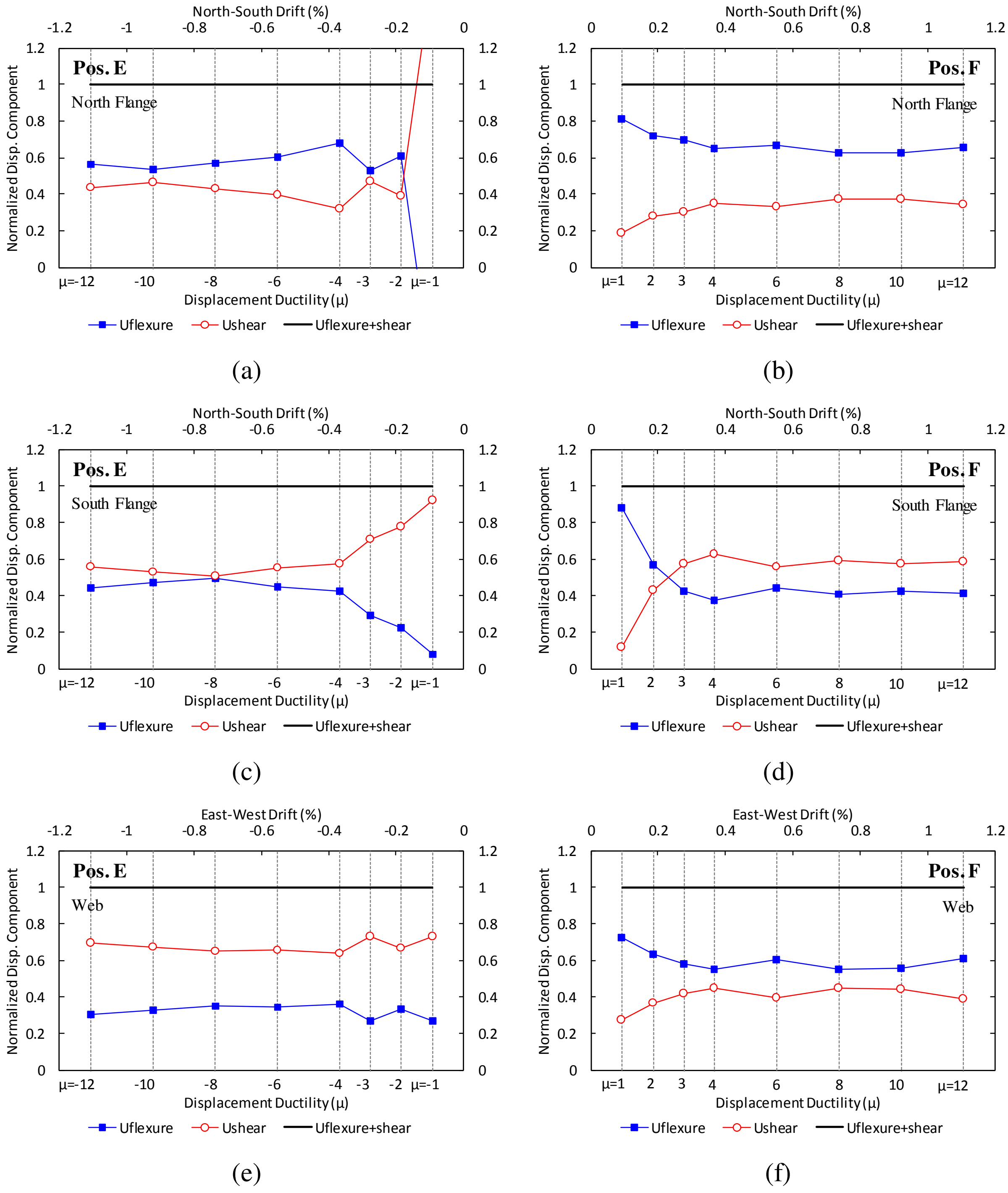

(a)

(b)

(c)

(d)

(e)

(f)

Fig. 6.53. Comparison of different displacement components along diagonal excitations

6.3.3.5 RC wall curvature profiles

Average curvature profile of the wall was developed using the measurements by a chain of linear potentiometers on each corner of the wall section. Fig. 6.54 shows the average curvature profiles of the wall in different directions of loading. As it can be seen from the plots, the curvature demands are concentrated at the bottom 20% height of the wall in all cases. Extension of the plastic hinge from the base of the wall was evaluated for different directions and at two loading stages, namely, “yield” and “20% degradation”. The former corresponds to the yield displacement of the wall, and the latter is the point that the wall’s capacity drops by 20% from the peak resistance in that direction. The length of the plastic hinge at each stage of the load was determined by finding the height of the wall at which the curvature profile exceeded the yield curvature.

According to Fig. 6.54, pushing the wall to the yield displacement in the Y direction (positions A and B) developed a plastic hinge up to 27% of the height of the wall (0.27h) while the plastic hinge was extended up to 0.44h at 20% degradation. The cyclic loop in the X direction (positions C and D) created a plastic hinge length of up to 0.17h in the North flange at yield displacement while this length was extended up to 0.45h at 20% degradation. In the South flange, these lengths were equal to 0.28h and 0.44h, respectively. A curvature profile was also developed for pure diagonal displacements in EF direction (Fig. 6.54.d). Results showed a plastic hinge developed length of up to 0.18h at yield and 0.34h at 20% degradation.

In the two main directions (i.e. X and Y), considering the wall height-to-length ratio of 1.63, the plastic hinge lengths measured at yield displacement were equal to $0.44l_w$, $0.27l_w$ and $0.46l_w$ in the web, North flange and South flange, respectively. As a reference, Thmosen and Wallace (2004) reported that the plastic hinge length varies between 0.33 to $0.5l_w$ in both rectangular and T-shaped slender RC walls.

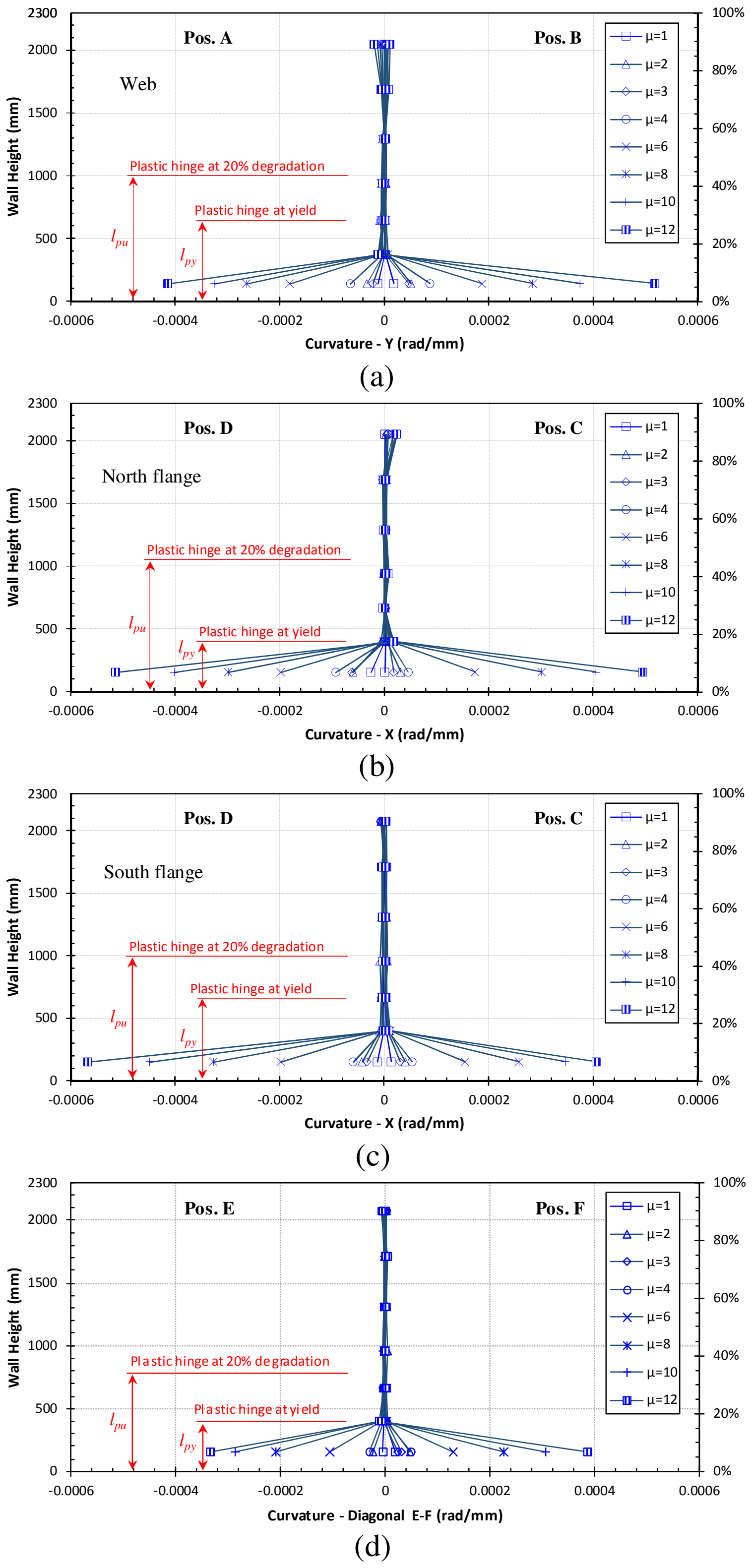

Fig. 6.54. Average curvature profiles of the wall in different directions of loading

CHAPTER 7

Summary, Conclusions, and Recommendations for Future Work

7.1 Summary

The purpose of the current study was to investigate the seismic response of C-shaped RC walls and the effectiveness of FRP retrofitting on enhancing the seismic performance of both intact and damaged C-shaped RC walls. To the best of the author's knowledge, the effects FRP retrofitting on the structural performance of C-shaped RC core walls have not been previously addressed by other researchers, especially by conducting experimental tests. This research enriches the knowledge in this area by providing numerical and experimental evidences of the structural response of FRP-retrofitted C-shaped RC walls.

This dissertation consists of numerical, analytical and experimental work. For the numerical part, a simplified method for modelling FRP retrofit systems is proposed and validated against experimental data. A collapse risk assessment for C-shaped walls subjected to an ensemble of ground motions was studied analytically. Lastly, a large-scale C-shaped RC shear wall was retrofitted using CFRP sheets and tested under multi-directional excitations to evaluate the effectiveness of the retrofit scheme.

The numerical and analytical studies included the followings:

- Evaluation of finite and fibre elements RC models for nonlinear cyclic analysis of C-shaped shear walls: Different available numerical tools were evaluated both at the level of micro and macro scale modelling. Modelling approaches were explained in details, and results from popular detailed solid finite element models (i.e. ANSYS, ABAQUS) and fibre elements (i.e. OpenSees, SeismoStruct, ETABS) were compared to the experimental test data reported in the literature to highlight the efficiency of each method. Macro modeling using fibre section elements was found to be an efficient modeling approach for engineering practice.

- Numerical investigation on the effectiveness of FRP wraps for retrofitting of existing RC shear walls: Finite element micro-scale models were developed, and shear walls with different geometries were evaluated numerically to study the effectiveness of FRP wraps with different configurations on the wall's behaviour in terms of strength and ductility. The FRP retrofitting was found to be capable of increasing the lateral load capacity, as well as the ductility, of RC walls.
- Seismic collapse risk assessment and FRP retrofitting of RC coupled C-shaped core walls using the FEMA P695 methodology: A detailed modelling approach was proposed and multi-story buildings before and after retrofitting with different FRP retrofitting schemes were assessed to evaluate, analytically, the efficiency of FRP retrofitting in reducing the collapse risk of the building according to the FEMA P695. Using FRP X-braces was found to be the most efficient retrofitting scheme for improving the collapse capacity of coupled C-shaped RC cores.
- Seismic response analysis of RC C-shaped core walls subjected to combined flexure, shear and torsion: Seismic force demand in C-shaped RC wall buildings with different levels of torsional sensitivity and effectiveness of using the dual plastic hinge method in controlling the seismic shear force demand were evaluated. It was found that though RSA is known as a robust and practical dynamic analysis method, the results are not conservative and notably larger story shear demands may be expected from nonlinear time history analyses. Enhancements were proposed for the new "dynamic shear amplification factor" in CSA A23.3-14 provisions.

The experimental program included retrofitting a previously tested large-scale C-shaped RC shear wall using CFRP wraps and conducting a series of tests to evaluate the effectiveness of FRP retrofitting on enhancing the structural performance of RC walls. The "Original wall" specimen was first tested as the bottom story of a multi-story building (hybrid tests) under three steps of time-history excitations (Mechmachi and Bouaanani, 2018). The studied building was a

5-story building in Montreal, Canada with class C subsoil condition. The building was designed according to the National Building Code of Canada (NBCC, 2010) and the CSA A23.3-04 (2010 edition). Each floor consisted of three equal spans in both directions, with span lengths equal to 6 m and 5 m in X and Y directions, respectively. The total height was 16.94 m; consisted of a 4.14 m high first story and typical story height was equal to 3.2 m. The test specimen outside-to-outside dimensions were 2.52 m by 2.52 m, and the thickness was equal to 165 mm. The RC wall specimen was reinforced by 4-20M bars at each corner, while 10M vertical and horizontal bars with 200 mm spacing were considered as the distributed reinforcement. The wall was built using 37 MPa strength concrete and 400 MPa strength steel reinforcement.

Mechmachi and Bouaanani (2018) conducted a series of hybrid tests followed by characterization tests on the Original wall specimen. Afterwards, the damaged C-shaped specimen was removed from the test setup for FRP retrofitting. The Retrofitted wall was subjected to the same series of tests for comparison purposes. Then, a cyclic multi-directional loading protocol was applied to the wall to measure the wall's response in each direction of loading (i.e. flange, web, diagonal and sweeping motions).

The FRP retrofitting scheme used for the C-shaped wall performed very well by enhancing both the strength and ductility of the damaged wall specimen, while keeping its stiffness very close to that of the Original wall. The study concluded that the FRP retrofitting scheme was efficient in retrofitting the damaged C-shaped RC wall.

7.2 Conclusions

The following points were concluded based on the numerical, analytical, and experimental results:

7.2.1 Conclusions based on the numerical and analytical results

This section presents the conclusions drawn from the numerical results:

- In numerical modelling of C-shaped RC walls; while the lumped plasticity models have the advantage of simplicity, it can be at the cost of precision (i.e. warping and shear deformations are not captured). Distributed plasticity models combined with the WCM analogy are relatively simple to use including features to enhance precision such as shear flexibility.
- FE modelling (e.g. ANSYS and ABAQUS) could provide detailed response of micro elements (e.g. local strains and deformations); however, calibration/validation of the numerical model is vital to account for probable uncertainties in its parameters in order to obtain an accurate global response. For instance, the shear reduction feature provided by ANSYS can perform well in predicting the cyclic behaviour, while the Concrete Damage Plasticity model in ABAQUS can only capture the cyclic response of RC elements in well-detailed concrete elements where no pinching behaviour is expected. In monotonic loading, however, the ABAQUS model can provide accurate predictions in both Implicit and Explicit analyses.
- FRP retrofitting of RC walls is not only effective in enhancing the lateral capacity of the wall, it also can improve the ductility and energy dissipation capability of the wall in different performance levels (e.g. IO and LS).
- The macro-modelling approach adopted in chapter 4 of this thesis proved to be capable of accurately simulating the behaviour of C-shaped RC walls under cyclic loading, with a reasonable error in predictions (7% on average of peak responses and the stiffness).
- By using a proper strengthening scheme with FRP material, the collapse margin ratio of the C-shaped RC wall buildings can be improved by a factor of more than two. The results, however, could be significantly affected (up to 36% decrease by increasing the torsional sensitivity to 2.5) by the level of torsional sensitivity of the building. Besides, FRP retrofitting leads to a considerable reduction in the inter-story drifts (decreased by 14% to 31%). FRP X-bracing was found to be the most effective FRP retrofitting scheme, however, this might be subject to applicability concerns depending on the

geometry of the wall. Shear/flexural failure was the most common failure mode, especially in higher torsional sensitivities and the steel rebar failure was the least common one.

- Though response spectrum analysis (RSA) provides consistent predictions for story shear demand in regular low rise buildings, results are not as reliable as time history analysis for torsionally sensitive buildings. Significant underestimation of design forces might be developed for buildings with a torsional sensitivity of B ≥ 2.0. Results also showed that significant contribution of higher modes of vibration, including third and fourth modes, noticeably affects the story force demand in the buildings as torsional irregularity of the building increases, especially in shorter buildings.
- Dual Plastic Hinge (DPH) method was found to be an efficient alternative for controlling the shear force demand in torsionally sensitive buildings because of its efficiency in mitigation of higher mode effects compared to Single Plastic Hinge (SPH).
- As the torsional irregularity increases, it is necessary to further amplify the results of RSA analysis based on the response spectrum prescribed by NBCC 2015. Base shear force enhancement factors of 3% to 64% and 3% to 75% were proposed for SPH and DPH buildings respectively. The average shear enhancement factor for DPH, however, was constantly decreased by increasing the torsional sensitivity.

7.2.2 Conclusions based on the experimental results

Results from the experimental tests on the FRP retrofitted RC C-shaped wall showed that:

- During the first two steps of the hybrid time-history tests (i.e. mainshock), the displacement/rotation responses of the FRP retrofitted wall were similar to those of the Original wall. Peak displacements/rotations barely exceeded those of the Original wall, while the reaction forces/torques were noticeably smaller. It was found that the FRP Retrofitted wall had lower initial stiffness compared to the Original wall at the start of the test.

- The results from the step 3 of the hybrid tests (i.e. aftershock) were close to those of the Original wall, both in terms of excitations (displacement/rotation) and the reaction (force/torque). The intensity of the excitations during this step was higher and resulted in yielding of four longitudinal steel reinforcements at the corners of the FRP retrofitted wall. Overall, results proved the efficiency of the used FRP retrofitting scheme in restoring the stiffness of the damaged RC wall.
- Results of the characterization tests showed that the FRP retrofitting scheme used in the current work notably improved the peak reaction force/moment of the wall specimen, compared to the Original wall. The stiffness of the wall, however, remained the same in almost all loading directions. This is quite important since changing the stiffness can significantly affect the dynamic characteristics of the structure.
- FRP retrofitting successfully restored the response of the damaged wall to be reasonably comparable to that of the Original wall. Characterization tests showed that the peak resisting force by the wall in almost all directions (flange, web, diagonal) was improved by 19 to 27% at certain displacements.
- During the characterization tests, the wall stiffness was quite similar in both loading and unloading stages, however, thinner hysteresis loops were observed from the FRP Retrofitted wall. No major changes were observed in the lateral stiffness of the Retrofitted wall as opposed to the Original wall in which clear significant reductions were measured. Moreover, no noticeable change was observed in the stiffness of the wall when subjected to torsional moment, while the peak resisting torque was increased by 11% and 15% for the counterclockwise and clockwise twists, respectively.
- Despite the bulging of the FRP wraps, horizontal wrapping is able to provide lateral support for the crushed concrete materials to stay in place, and hence, prevent the steel bars from buckling even in high levels of displacement ductility (i.e. μ_Δ=12).
- In general, during the diagonal excitations, resisting forces in a C-shaped RC wall will be distributed unevenly between the two flanges because of different cracking states,

which lead to different stress states attained during the cycles. This was observed in the response of the FRP retrofitted wall, and needs to be addressed in the design of new C-shaped RC core walls.

- Though results of a similar test by Beyer et el. (2008) on two C-shaped RC wall showed a considerably smaller peak resistance in diagonal direction compared to those of the main directions, the FRP retrofitted RC C-shaped wall in the current work was found to have close peak forces in all the directions (i.e. within 9% difference).
- A relatively large contribution of shear displacements was observed during the cyclic test of the FRP retrofitted C-shaped wall. In the flange direction, almost 60% of the flange total displacements were due to flexural deformations and the remaining 40% were from shear deformations in the wall. In the web direction, however, the flexural displacements were found to be on a par with shear deformations. Similar results were observed in the diagonal directions, except for the web during the larger cycles, in which the contribution of shear deformations was raised up to 73% of the total deformations.
- The developed plastic hinge of the wall in web direction at yield was up to 27% of the height of the wall ($0.27h = 0.44l_w$) while the plastic hinge was extended up to 0.44h at 20% degradation. The cyclic loop in the X direction (positions C and D) created a plastic hinge length of up to 0.17h ($0.27l_w$) in the North flange at yield displacement while this length was extended up to 0.45h at 20% degradation. In the South flange, these lengths were equal to 0.28h ($0.46l_w$) and 0.44h, respectively. As a reference, Thmosen and Wallace (2004) reported that the plastic hinge length varies between 0.33 to $0.5l_w$ in both rectangular and T-shaped slender RC walls. The Canadian Design Handbook (CSA A23.3-14) prescribes the plastic hinge length of $0.5Lw + 0.1h$ for RC walls. As for pure diagonal displacements, the plastic hinge was developed up to 0.18h and 0.34h at yield and 20% degradation, respectively.

7.3 Recommendations for Future Research

The conclusions of the current study were limited to the parameters that were being analyzed and tested. However, to further expand the knowledge in this field, other parameters may be considered. Hence, some recommendations for future research works are listed as followings:

- Experimental tests on coupled original and FRP retrofitted C-shaped RC walls
- Experimental parametric study on the effectiveness of different FRP retrofitting schemes on the seismic response of C-shaped RC walls
- Seismic response assessment of C-shaped RC walls with boundary elements
- Extending the experimental and numerical methodology developed in this study to investigate the effects of design variables, such as the compressive strength of the concrete, yield strength of reinforcement, detailing of reinforcement, and the geometry of the C-shaped.
- Calibration/validation of numerical and analytical models using the test data reported in the current dissertation.
- Most popular section-analysis programs are limited to analyzing a C-shaped section, RC sections in particular, in main directions only. Hence, for diagonal directions, it is vital to develop robust analytical tools capable of handling the analysis of these sections to be used in the engineering practice.

References

ACI 374.2R-13 (2013): Guide for Testing Reinforced Concrete Structural Elements under Slowly Applied Simulated Seismic Loads. American Concrete Institute.

ACI, American Concrete Institute. (2008). Guide for the design and construction of externally bonded FRP systems for strengthening concrete structures, ACI Committee 440, Technical Committee Document 440.2R-08

Adebar, P., Dezhdar, E., Yathon, J. (2014). Accounting for higher mode shear forces in concrete wall buildings: 2014 CSA A23. 3. The 11th Canadian Conference on Earthquake Engineering.

ANSYS Inc. (2010): Theory Reference for the Mechanical APDL and Mechanical Applications. Canonsburg, PA.

Antoniades, K., Thomas, K., Salonikios, N. and Kappos, A. J. (2003). Cyclic Tests on Seismically Damaged Reinforced Concrete Walls Strengthened Using Fiber-Reinforced Polymer Reinforcement. ACI Structural Journal, 100(4), 510-518

APPLIED TECHNOLOGY COUNCIL. (2009) FEMA P440A : Effects of Strength and Stiffness Degradation on Seismic Response, Prestandard, Federal Emergeny Management Agency (FEMA), Washington, D.C.

Arabzadeh, H., Galal, K. (2017). Seismic Collapse Risk Assessment and FRP Retrofitting of RC Coupled C-Shaped Core Walls Using the FEMA P695 Methodology. Journal of Structural Engineering, 143(9), 04017096.

ASCE/SEI 41–13. (2014). Seismic evaluation and retrofit of existing buildings, American Society of Civil Engineers, Reston, Virginia, USA.

ASCE/SEI 7-10. (2010). Minimum design loads for buildings and other structures. Reston, VA: American Society of Civil Engineers.

Askarizadeh, N., & Mohammadizadeh, M. R. (2017). Numerical Analysis of Carbon Fiber Reinforced Plastic (CFRP) Shear Walls and Steel Strips under Cyclic Loads Using Finite Element Method. Engineering, Technology & Applied Science Research, 7(6), 2147-2155.

Aslani, K., & Kohnehpooshi, O. (2018). Structural behavior of FRP-strengthened reinforced concrete shear walls with openings using finite element method. Advances in Structural Engineering, 21(7), 1072-1087.

Atkinson, G. (2009). Earthquake time histories compatible with the 2005 National Building Code of Canada uniform hazard spectrum., Canadian Journal of Civil Engineering, 36(6), 991–1000.

Bae, S., Bayrak, O. (2008). Plastic hinge length of reinforced concrete columns. ACI Structural Journal, 105(3), 290.

Baker, J. W. (2015). Efficient analytical fragility function fitting using dynamic structural analysis. Earthquake Spectra. 31(1): 579-599.

Behfarnia, K., & Shirneshana, A. (2017). A numerical study on behavior of CFRP strengthened shear wall with opening. COMPUTERS AND CONCRETE, 19(2), 179-189.

Beyer K., Dazio A., Priestley M.J.N. (2008-a). Quasi-static cyclic tests of two U-shaped reinforced concrete walls, Journal of Earthquake Engineering 12 (7), 1023-1053.

Beyer K., Dazio A., Priestley, M. J. N. (2011). Shear Deformations of Slender Reinforced Concrete Walls under Seismic Loading, ACI Structural Journal, 108(2), 167-177.

Beyer, K., Dazio, A., Priestley, M. J. N. (2008-b). Inelastic wide-column models for U-shaped reinforced concrete walls. Journal of Earthquake Engineering, 12(S1), 1-33.

Blakeley, R. W. G., Cooney, R. C., Megget, L. M. (1975). Seismic shear loading at flexural capacity in cantilever wall structures. Bulletin of the New Zealand National Society for Earthquake Engineering, 8(4), 278-290.

Boivin Y. Paultre P. (2012). Seismic force demand on ductile reinforced concrete shear walls subjected to western North American ground motions: Part 2 — new capacity design methods. Canadian Journal of Civil Engineering 39(7), 738-750.

Boivin, Y., Paultre, P. (2010). Seismic performance of a 12-storey ductile concrete shear wall system designed according to the 2005 National building code of Canada and the 2004 Canadian Standard Association standard A23. 3. Canadian Journal of Civil Engineering, 37(1), 1-16.

Burgueño, R., Liu, X., Hines, E. M. (2014). Web Crushing Capacity of High-Strength Concrete Structural Walls: Experimental Study. ACI Structural Journal, 111(1), 37.

CAC. (2010). Concrete Design Handbook. 3 ed. Ottawa, ON: Cement Association of Canada.

CAC. (2016), Concrete Design Handbook, fourth edition, Cement Association of Canada, Ottawa, ON, Canada

Calabrese, A., Almeida, J. P., Pinho, R. (2010). Numerical issues in distributed inelasticity modeling of RC frame elements for seismic analysis. Journal of Earthquake Engineering, 14(S1), 38-68.

Calabrese, A., Almeida, J.P. Pinho, R. (2010). Numerical issues in distributed inelasticity modeling of RC frame elements for seismic analysis, J. Struct. Eng., 14(S1), 38-68.

Calugaru, V. (2013). Earthquake resilient tall reinforced concrete buildings at near-fault sites using base isolation and rocking core walls. University of California, Berkeley.

Calugaru, V., Panagiotou, M. (2012). Response of tall cantilever wall buildings to strong pulse type seismic excitation. Earthquake Engineering & Structural Dynamics, 41(9), 1301-1318.

CAN, C. S. (2012). CSA-S806-12. Design and construction of building components with fiber-reinforced polymers. Mississauga, Ontario, Canada: Canadian Standards Association.

Carrillo, J. Alcocer, S. (2012). Acceptance limits for performance-based seismic design of RC walls for low-rise housing, Journal of Earthquake Engineering and Structural Dynamics, 41(15), 2273-2288.

Carrillo, Julian, Gonzalez, Giovanni, Rubiano, Astrid (2014). Displacement ductility for seismic design of RC walls for low-rise housing, Latin American J. of Solids Structure, Vol. 11, pp.725–37.

CEN EC8 (2006). Design of Structures for Earthquake Resistance. European Committee for Standardization: Brussels, Belgium.

Chae, Y., Ricles, J. M., Sause, R. (2012). Large-scale experimental studies of structural control algorithms for structures with magnetorheological dampers using real-time hybrid simulation. Journal of Structural Engineering, 139(7), 1215-1226.

Chang, G. A., J. B. Mander. (1994). Seismic energy based fatigue damage analysis of bridge columns: Part I — evaluation of seismic capacity. NCEER Technical Report No. NCEER–94–0006. State University of New York. Buffalo, New York.

Chen, S., Diao, B., Guo, Q., Cheng, S., Ye, Y. (2016). Experiments and calculation of U-shaped thin-walled RC members under pure torsion. Engineering Structures, 106, 1-14.

Clough RW, Benuska KL, Wilson EL (1965): Inelastic Earthquake Response of Tall Buildings. Proceeding of 3rd World Conference on Earthquake Engineering, Auckland and Wellington, New Zealand.

Colotti V. (1993). Shear Behavior of RC Structural Walls, ASCE Journal of Structural Engineering, Vol. 119, No. 3, p.p. 728-746.

Constantin R. Beyer K. (2012). Modelling of Reinforced Concrete Core Walls Under Bi-directional Loading, 15th World Conference on Earthquake Engineering, Lisbon, Portugal

Constantin, R., Beyer, K. (2016). Behaviour of U-shaped RC walls under quasi-static cyclic diagonal loading. Engineering Structures, 106, 36-52.

Cortés-Puentes, W. L., & Palermo, D. (2011). Modeling of RC shear walls retrofitted with steel plates or FRP sheets. Journal of Structural Engineering, 138(5), 602-612.

Cortes-Puentes, W. L., & Palermo, D. (2011). Modelling seismically repaired and retrofitted reinforced concrete shear walls. Computers & Concrete, 8(5), 541-561.

CSA. (2004). Design of concrete structures. Rexdale, ON: Canadian Standards Association.

CSA. (2014). Design of concrete structures. Rexdale, ON: Canadian Standards Association.

CSI, C. (2015). SAP2000 (version 18) Integrated Solution for Structural Analysis and Design – CSI Analysis Reference Manual, Computers and Structures, Inc., California, USA.

Dey, S. (2014). Seismic performance of Composite Plate Shear Walls, PhD Thesis, Concordia University Montreal, Canada.

Dhanasekar, M., Haider, W. (2008). Explicit finite element analysis of lightly reinforced masonry shear walls, Computers and Structures, Vol. 86, pp. 15–26.

Di Luccio, G., Michel, L., Ferrier, E., & Martinelli, E. (2017). Seismic retrofitting of RC walls externally strengthened by flax–FRP strips. Composites Part B: Engineering, 127, 133-149.

Dizhur, D., Ingham, J., Moon, L., Griffith, M., Schultz, A., Senaldi, I., Magenes, G., Dickie, J., Lissel, S., Centeno, J. and Ventura, C. (2011). Performance of Masonry Buildings and Churches in the 22 February 2011 Christchurch Earthquake (Vol. 44): Bulletin of the New Zealand Society for Earthquake Engineering.

Dubey, S. K., Sangamnerkar, P. D. (2011). Seismic behaviour of assymetric RC buildings. International journal of advanced engineering technology, 2(4), 296-301.

Elkady A., Lignos D. G. (2014). Modeling of the composite action in fully restrained beam-to-column connections: implications in the seismic design and collapse capacity of steel special moment frames, Earthquake Engineering & Structural Dynamics, 43, 1935–1954.

El-Khoriby, S., Sakr, M. A., Khalefa, T. M., & Nagiub, M. T. (2016). Numerical analysis of RC Shear Wall Retrofitted using CFRP. International Conference on Advances in Civil, Environmental, and Materials Research (ACEM15), Korea.

Elnady, M. M. (2008). Seismic Rehabilitation of RC Structural Walls, PhD Thesis, McMaster University, Hamilton, Canada.

El-Sokkary, H., and Galal, K. (2013). Seismic Behavior of FRP-Strengthened RC Shear Walls, Journal of Composites for Construction, ASCE, 17(5). 603–613.

El-Sokkary, H., Galal, K., Ghorbanirenani, I., Léger, P., Tremblay, R. (2012). Shake table tests on FRP-rehabilitated RC shear walls, Journal of Composites for Construction, ASCE, 17(1), 79-90.

El-Tawil, S. , Harries, K. A. , Fortney, P. J. , Shahrooz, B. M. , and Kurama, Y. (2010). Seismic design of hybrid coupled wall systems: State-of-the-art. J. Struct. Eng. , 136 (7), 755–769.

Elwood K. J. (2002). Shake Table Tests and Analytical Studies on the Gravity Load Collapse of Reinforced Concrete Frames, PhD Dissertation, University of California, Berkeley.

Esteva, L. (1987). Earthquake engineering research and practice in Mexico after 1985 earthquake (Vol. 20, pp. 159-200): Bulletin of the New Zealand National Society of Earthquake Engineering.

Fajfar, P., Marušić, D., Peruš, I. (2005). Torsional effects in the pushover-based seismic analysis of buildings. Journal of Earthquake Engineering, 9(06), 831-854.

Farhidzadeh, A. , Salamone, S. , Luna, B., Whittaker, A. (2013). Acoustic emission monitoring of a reinforced concrete shear wall by bb-value based outlier analysis. Struct. Health Monit., 12 (1), 3–13.

Federation International De Beton (fib). (2013). Model Code for Concrete Structures 2010, Lausanne, Switzerland, Ernst & Sohn.

FEMA 356. (2000). Prestandard and Commentary for the Seismic Rehabilitation of Buildings, Federal Emergency Management Agency , Washington, DC.

FEMA P58-1. (2012). Seismic performance assessment of buildings, Volume 1 - Methodology, Prepared by Applied Technology Council (ATC), Redwood City, USA.

FEMA P695. (2009). Quantification of Building Seismic Performance Factors, Federal Emergency Management Agency, Washington, District of Columbia, USA

Filippou, F. C., Popov, E. P., Bertero, V. V. (1983). Effects of Bond Deterioration on Hysteretic Behavior of Reinforced Concrete Joints. Report EERC 83-19, Earthquake Engineering Research Center, University of California, Berkeley.

Fintel, M. (1995). Performance of Buildings With Shear Walls in Earthquakes of The Last Thirty Years. PCI Journal, 40(3), 62-80.

Fischinger M., Rejec K. and Isakovic T. (2012). Modeling Inelastic Shear Response of RC Walls, Proceedings of 15th World Conference on Earthquake Engineering, Lisbon, Portugal.

Fyfe Co. LLC. (2017). Tyfo® Fibrwrap® Systems, San Diego.

Ghobara, A., Khalil, A. (2004). Seismic Rehabilitation of Reinforced Concrete Walls using Fibre Composites, 13th World Conference on Earthquake Engineering (WCEE, 3316), Vancouver, Canada.

Ghorbanirenani, I., Tremblay, R., Léger, P., and Leclerc, M. (2012). Shake table testing of slender RC shear walls subjected to eastern North America seismic ground motions. J. Struct. Eng., 1 , 492.

Gogus A. Wallace J. W. (2015). Seismic Safety Evaluation of Reinforced Concrete Walls through FEMA P695 Methodology, Journal of Structural Engineering, 141(10), 04015002.

Haroun, M. A., Mosallam, A. S., Allam, K. H. (2005). Cyclic in-plane shear of concrete masonry walls strengthened by FRP laminates. ACI Specia l Publication, 230(19), 327-340.

Hart, G. C. (1975). Torsional response of high-rise buildings. Journal of Structural Engineering ASCE, 101(2), 397-416.

Herrera, R. I., Vielma, J. C., Ugel, R., Alfaro, A., Barbat, A. H., Pujades, L. (2013). Seismic response and torsional effects of RC structure with irregular plant and variations in diaphragms, designed with Venezuelan codes. WIT Transactions on the Built Environment, 132, 85-96.

Hibbitt, Karlsson and Sorensen Inc. (2007): ABAQUS theory manual, user manual and example Manual. Version 6.7.

Hilber, H. M., Hughes, T. J., Taylor, R. L. (1977). Improved numerical dissipation for time integration algorithms in structural dynamics. Earthquake Engineering & Structural Dynamics, 5(3), 283-292.

Hiotakis, S., Lau, D. T., and Londono, N. (2004). Research on Seismic Retrofit and Rehabilitation of Reinforced Concrete Shear Walls using FRP Materials. Ottawa, ON, Canada: Carlton University

Honarparas S., Challal O. (2015). Seismic Upgrading of RC Coupled Shear Walls: State of the Art and Research Needs, Global Journal of Advanced Eng. Technologies and Sciences, 2(12).

Huang X. (2012). Applicability criteria of fiber-section elements for the modelling of RC columns subjected to cyclic loading. University of Toronto.

Hwang, S. J., Chiou, T. C. and Tu, Y. S. (2004). Reinforced Concrete Squat Walls Retrofitted With Carbon Fiber Reinforced Polymer. Proceedings of 2nd International Conference on Frp Composites in Civil Engineering - CICE. Adelaide, Australia, 47-56

Ibarra L, Medina R, Krawinkler H. (2002). Collapse assessment of deteriorating SDOF systems. Proceedings of the 12th European Conference on Earthquake Engineering, London, Elsevier Science Ltd. Paper #665. 9–13 Sept. 2002.

ICRI Guide No. 310.2R, (2013), Selecting and Specifying Concrete Surface Preparation for Sealers, Coatings, Polymer Overlays, and Concrete Repair. International Concrete Repair Institute. http://www.ardexamericas.com/fr/Documents/ICRI%20310-2R-2013.pdf

Ile, N. Reynouard, J. M. (2005). Behaviour of U-shaped walls subjected to uniaxial loading and biaxial cyclic lateral loading. Journal of Earthquake Engineering 9(1), 67-94.

Jiang H. Kurama Y. (2010). Analytical Modeling of Medium-Rise Reinforced Concrete Shear Walls, ACI Structural Journal, 107(4), 400-410.

Kezmane, A., Hamizi, M., Boukais, S., Eddine, H. N., (2012). Numerical Simulation of RC Shear Wall Strengthened by External Bonding of a Composite Material, 15th International Conference on Experimental Mechanics, Porto, Portugal.

Khalil, A., Ghobara A. (2005). Behaviour of Rehabilitated Structural Walls, Journal of Earthquake Engineering, Vol. 9(3), pp. 371-391

Kheyroddin, A., Naderpour, H. (2008). Nonlinear Finite Element Analysis of Composite RC Shear Walls, Iranian Journal of Science & Technology, Transaction B, Engineering, Vol. 32, pp. 79-89.

Kim, T. W., Foutch, D. A., LaFave, J. M., Wilcoski, J. (2004). Performance assessment of reinforced concrete structural walls for seismic loads. University of Illinois Engineering Experiment Station. College of Engineering. University of Illinois at Urbana-Champaign.

Klemencic, R., Fry, A., Hooper, J.D., Morgen, B.G. (2007). Performance-based design of ductile concrete core wall buildings – issues to consider before detailed analysis. Structural Design of Tall and Special Buildings, 16, 599-614.

Kobayashi, K. (2005). Innovative application of FRPs for seismic strengthening of RC shear wall. Fiber-Reinforced Polymer (FRP) Reinforcement for Concrete Structures. Framington Hills, Mi, USA, ACI, 1269-1288

Kolozvari K. (2013). Analytical Modeling of Cyclic Shear-Flexure Interaction in Reinforced Concrete Structural Walls, PhD Dissertation, University of California, Los Angeles.

Kowalsky, M. J., Priestley, M. J. N., Seible, F. (1999). Shear and Flexure Behavior of Lightweight Concrete Bridge Columns in Seismic Regions, ACI Structural Journal, 96(1), 136-148.

Krpan, P., Collins, M. P. (1981). Testing thin-walled open RC structure in torsion. Journal of the Structural Division, 107(6), 1129-1140.

Le Nguyen, K., Brun, M., Limam, A., Ferrier, E., Michel, L. (2014). Pushover experiment and numerical analyses on CFRP-retrofit concrete shear walls with different aspect ratios. Composite Structures, 113, 403-418.

Lefas, I. D., Kotsovos, M. D., Ambraseys, N. N. (1990). Behavior of Reinforced Concrete Structural Walls: Strength, Deformation Characteristics, and Failure Mechanism, ACI Structural Journal, Vol. 87(1), pp. 23-31.

Li, B., and Lim, C. L. (2010). Tests on Seismically Damaged Reinforced Concrete Structural Walls Repaired Using Fiber-Reinforced Polymers. ASCE Journal of Composites for Construction, 10.1061 ASCE CC.1943-5614.0000110, 597-608

Lombard, J., Lau, D. T., Humar, J. L., Foo, S., Cheung, M. S. (2000). Seismic strengthening and repair of reinforced concrete shear walls. In Proc., 12th World Conf. on Earthquake Engineering (pp. 1-8).

Lopes, S. M. R., Bernardo, L. F. A. (2009). Twist behavior of high-strength concrete hollow beams–Formation of plastic hinges along the length. Engineering Structures, 31(1), 138-149.

Lowes L., Lehman D., Kuchma D., Mock A., Behrouzi A. (2013). Large scale tests of C-shaped reinforced concrete walls. Summary report, NEES project warehouse; https://nees.org/warehouse/project/104

Lu, X. Z., Teng, J. G., Ye, L. P., Jiang, J. J. (2005)., Bond-slip models for FRP sheets/plates bonded to concrete, Journal of Engineering Structures, 27(6), 920-937.

Lu, Y. J. (2014). Three-dimensional Seismic Analysis of Reinforced Concrete Wall Buildings at Near-fault Sites. University of California, Berkeley.

Lu, Y. Panagiotou, M. (2013). Three-Dimensional Nonlinear Cyclic Beam-Truss Model for Reinforced Concrete Non-Planar Walls. Journal of Structural Engineering, 140 (3).

Lubliner, J., Oliver, J., Oller, S., And Onate, E. (1989). A Plastic-Damage Model for Concrete, International Journal of Solids and Structures, Vol. 25, No. 3, pp. 299-326.

Luu, H., Léger, P., Tremblay, R. (2013). Seismic demand of moderately ductile reinforced concrete shear walls subjected to high-frequency ground motions. Canadian journal of civil engineering, 41(2), 125-135.

Mander, J. B., Priestley M. J. N., Park R. (1988). Theoretical stress-strain model for confined concrete. ASCE Journal of Structural Engineering 114(8): 1804–1826.

Massone L. M., Orakcal K., Wallace J. W. (2006). Modeling Flexural/Shear Interaction in RC Walls, ACI-SP-236, Deformation Capacity and Shear Strength of Reinforced Concrete

Members under Cyclic Loadings, American Concrete Institute, Farmington Hills, MI, Paper 7, p.p. 127-150.

Massone, L. M., Orakcal K., Wallace J. W. (2009). Modeling of Squat Structural Walls Controlled by Shear, ACI Structural Journal, 106(5), 646-655.

Mazzoni, S., McKenna, F., Scott, M. H., Fenves, G. L. (2006). OpenSees command language manual. Pacific Earthquake Engineering Research (PEER) Center.

McKenna, F., Fenves, G., Scott, M. (2013). Computer Program OpenSees: Open system for earthquake engineering simulation, Pacific Earthquake Engineering Center, University of California, Berkeley, CA.

Mechmachi, Y., and Bouaanani, N. (2018). Hybrid Experimental Test on the Seismic Response of C-Shaped RC Walls, Internal report, Dept. of Civil, Geological and Mining Engineering, École Polytechnique de Montréal, Montréal, Quebec, Canada.

Meier U. (1987). Bridge Repair with High Performance Composite Materials, Material und Technik, Vol. 15, pp. 125-128.

Menegotto, M., Pinto, P. E. (1973). Method of Analysis for Cyclically Loaded RC Frames Including Changes in Geometry and Non-elastic Behaviour of Elements Under Combined Normal Force and Bending. In IABSE Congress Reports of the Working Commission (Vol. 13).

Michaud D., Léger P. (2014). Ground motions selection and scaling for nonlinear dynamic analysis of structures located in Eastern North America, Canadian Journal of Civil Eng., 41, 232-244.

Millard A. (1993). CEA-LAMBS Report No. 93/007 (Saclay, France, 1993) p. 186.

Miranda E. Taghavi S. (2005). Approximate Floor Acceleration Demands in Multistory Buildings. I: Formulation, Journal of Structural Engineering, vol. 131, no. 2, pp. 203-211.

Mohamed N. A. (2013). Strength and Drift Capacity of GFRP-Reinforced Concrete Shear Walls. PhD thesis, Sherbrooke University, QC, Canada.

Mostofinejad, D., Mohammadi Anaei, M. (2012). Effect of confining of boundary elements of slender RC shear wall by FRP composites and stirrups, Engineering Structures, Vol. 41, pp. 1–13.

Mousavi A. K., Shahaboddin, A. (2008). Seismic Performance Evaluation of Reinforced Concrete Shear Wall Seismic Force Resisting Systems, Master Thesis, Concordia University, Montreal, Canada.

Mullapudi R.T. Ayuob A.S. (2009). Fiber Beam Element Formulation Using the Softened Membrane Model, ACI Special Publication, Vol. 265, p.p. 283-308.

NBCC. (2005). National Research Council of Canada. National Building Code of Canada. Ottawa, ON.

NBCC. (2015). National Research Council of Canada. National Building Code of Canada. Ottawa, ON.

Neuenhofer, A., Filippou, F. C. (1997). Evaluation of nonlinear frame finite-element models. Journal of structural engineering, 123(7), 958-966.

Ngo D, Scordelis AC (1967). Finite Element Analysis of Reinforced Concrete Beams. Journal of ACI, 64(3), 153-163.

Nguyen K. Le, Brun M., Limam A., Ferrier E., Miche L. (2014). Pushover experiment and numerical analyses on CFRP-retrofit concrete shear walls with different aspect ratios, Composite Structures, Vol. 113, pp. 403–418.

NIST. (2010). Evaluation of the FEMA P695 methodology for quantification of building seismic performance factors. NIST GCR 10-917-8, Gaithersburg, MD.

NZS 3101 (2006). New Zealand Standard, Part 1: The Design of Concrete Structures. Standards New Zealand, Wellington, New Zealand.

Oesterle, R. G., Fiorato, A. E., Johal, L. S., Carpenter, J. E., Russell, H. G., Corley, W. G. (1976). Earthquake resistant structural walls-tests of isolated walls. Report to National Science Foundation.

Orakcal K., Massone L. M., Wallace J. W. (2006). Analytical Modeling of Reinforced Concrete Walls for Predicting Flexural and Coupled–Shear-Flexural Responses, University of California, Los Angeles, PEER Report 2006/07.

Orakcal, K., Wallace, J. W., Conte, J. P. (2004). Flexural modeling of reinforced concrete walls-model attributes. ACI Structural Journal, 101(5), 688-698.

Panagiotou, M. Restrepo, J. I. (2011). Nonlinear Cyclic Truss Model for Strength Degrading Reinforced Concrete Plane Stress Elements, Report No. UCB/SEMM-2011/01, Structural Engineering, Mechanics and Materials, Department of Civil and Environmental Engineering University of California, Berkeley, 37 pp., February 2011.

Panagiotou, M., Restrepo, J. I. (2009). Dual-plastic hinge design concept for reducing higher-mode effects on high-rise cantilever wall buildings. Earthquake Engineering & Structural Dynamics, 38(12), 1359.

Panneton, M., Léger, P., Tremblay, R. (2006). Inelastic analysis of a reinforced concrete shear wall building according to the National Building Code of Canada 2005. Canadian Journal of Civil Engineering, 33(7), 854-871.

Paulay T., and Priestley M. J. N. (1992). Seismic Design of Reinforced Concrete and Masonry Buildings. John Wiley and Sons, Inc.

Paulay, T. (1988). Seismic Design in Reinforced Concrete – the State of the Art in New Zealand. Bulletin of the New Zealand National Society for Earthquake Engineering, 21(3), 208-232.

Pelletier, K., Léger, P. (2017). Nonlinear seismic modeling of reinforced concrete cores including torsion. Engineering Structures, 136, 380-392.

Peterson, J. and Mitchell, D. (2003). Seismic Retrofit of Shear Walls with Headed Bars and Carbon Fiber Wrap. ASCE Journal of Structural Engineering, 129(5), 606-614

Priestley, M.J.N., Calvi, G.M., Kowalsky, MJ. (2007). Displacement Based Seismic Design of Structures. IUSS Press: Pavia, Italy.

Rafiei, Sh. (2011). Behaviour of Double Skin Profiled Composite Shear Wall System under In-plane Monotonic, Cyclic and Impact Loadings, PhD Thesis, Ryerson University, Toronto, Canada.

Reynouard J. M. Fardis M. N. (1993). Shear wall structures, ECOEST/ICONS Thematic Report No5, LNEC-National Laboratory of Civil Engineering, Lisbon, Portugal.

Rezaiefar, A. (2013). Finite Element Modeling of Cyclically Loaded FRP-Retrofitted RC Squat Shear Walls, Master Thesis, Concordia University.

Schellenberg, A., Kim, H. K., Takahashi, Y., Fenves, G. L., & Mahin, S. A. (2013). Open framework for experimental setup and control (OpenFresco).

Scott B. D., Park R., Priestley M. J. N. (1982). Stress-strain behavior of concrete confined by overlapping hoops at low and high strain rates. Journal of the American Concrete Institute 79(1): 13–27.

Scott, M. H., Fenves, G. L. (2010). Krylov subspace accelerated Newton algorithm: application to dynamic progressive collapse simulation of frames. Journal of structural engineering, 136(5), 473-480.

Scott, M., and Fenves, G. (2006). Plastic-Hinge Integration Methods for Force-Based Beam-Column Elements. Journal of Structural Engineering, ASCE, 132(2), 244-252.

Sedgh RE, Dhakal RP, Carr AJ (2015): State of the Art: Challenges in analytical modelling of multi-storey shear wall buildings. New Zealand Society for Earthquake Eng. (NZSEE) Annual Technical Conference, Rotorua, New Zealand.

SeismoSoft. (2014). SeismoStruct – User Manual For version 7.0. www.seismosoft.com, Pavia, Italy

Soleimani, D., Popov, E.P. and Bertero, V.V. (1979). Nonlinear Beam Model for R/C Frame Analysis. 7th ASCE Conference on Electronic Computation, St. Louis

Stafford-Smith, B. and Girgis, A. (1986). Deficiencies in the wide column analogy for shear wall analysis, Concrete International, pp. 58–61.

Standard, N. Z. (1982). Code of Practice for the Design of Concrete Structures, NZS 3101, Part 1: 1982. Standard Association of New Zealand, Wellington.

Takeda, T., Sozen, M. A., Nielsen, N. N. (1970). Reinforced concrete response to simulated earthquakes. Journal of the Structural Division, 96(12), 2557-2573.

Thomsen, J. H., Wallace, J. W. (1995). Displacement-based design of reinforced concrete structural walls: An experimental investigation of walls with rectangular and T-shaped cross sections. Rep. No. CU/CEE-95/06, Dept. of Civil Engineering, Clarkson Univ., Potsdam, NY.

Thomsen IV, J. H., Wallace, J. W. (2004). Displacement-based design of slender reinforced concrete structural walls-experimental verification. Journal of Structural Engineering, 130(4), 618-630.

Todut, C., Dan, D., Stoian, V. (2015). Numerical and experimental investigation on seismically damaged reinforced concrete wall panels retrofitted with FRP composites. Composite Structures, 119, 648-665.

Todut, C., Dan, D., Stoian, V. (2014). Theoretical and experimental study on precast reinforced concrete wall panels subjected to shear force, Engineering Structures, Vol. 80, pp. 323–338.

Tremblay, R., Ghorbanirenani, I., Velev, N., Léger, P., Leclerc, M., Koboevic, S., Bouaanani N., Galal K., Palermo, D. (2008). Seismic response of multi-storey reinforced concrete walls subjected to Eastern North America high frequency ground motions. In 14th World Conference on Earthquake Engineering, Beijing.

Tso, W. K., Yao, S. (1994). Seismic load distribution in buildings with eccentric setback. Canadian Journal of Civil Engineering, 21(1), 50-62.

Vamvatsikos, D. Cornell, A. (2002). Incremental dynamic analysis. Earthq. Eng. Struct. Dyn., 31(3), 491-514.

Vecchio, F. J. Collins M. P. (1986). The modified compressional-field theory for reinforced concrete elements subjected to shear. Journal of the American Concrete Institute 83(22): 219– 231.

Vulcano, A., Bertero, V. V., Colotti, V. (1988). Analytical modeling of RC structural walls. In Proceedings of the 9th World Conference on Earthquake Engineering (Vol. 6, pp. 41-46). Tokyo-Kyoto, Japan.

Wallace, J. W., Elwood, K. J., Massone, L. M. (2008). An axial load capacity model for shear critical RC wall piers. J. Struct. Eng., 134(9), 1548–1557.

Wiebe, L., Christopoulos, C. (2009). Mitigation of higher mode effects in base-rocking systems by using multiple rocking sections. Journal of Earthquake Engineering, 13(S1), 83-108.

Wong, R. S. Y. Vecchio, F. J. (2003). Towards Modeling of Reinforced Concrete Members with Externally-Bonded FRP Composites, ACI Structural Journal, Vol. 100, No. 1, pp. 47-55

Woods, J. E. (2014). Seismic Retrofit of Deficient Reinforced Concrete Shear Walls using Fibre-reinforced Polymer Sheets: Experimental Study and Anchor Design, Master Thesis, Carleton University.

Woods, J. E., Lau, D. T., Bao, X., Li, W. (2017). Measuring strain fields in FRP strengthened RC shear walls using a distributed fiber optic sensor. Engineering Structures, 152, 359-369.

Wyllie, L.A., Abrahamson, N., Bolt, B., Castro, G., and Durkin, M. E. (1986). The Chile Earthquake of March 3, 1985- Performance of Structures. Earthquake Spectra, 2(2), 93-371.

Xenidis H., Athanatopoulou A., Avramidis I. E. (1993). Modelling of shear wall cores under earthquake loading using equivalant frames, Structural Dynamics – EURODYN 93, eds T. Moan et al. (Balkema/Rotterdam/Brookfield), 901-910.

Yassin, M. H. M. (1994). Nonlinear analysis of pre-stressed concrete structures under monotonic and cyclic loads. Dissertation. University of California. Berkeley, California.

Yin, P. (2000). Building performance in the Taiwan Earthquake, A review of Nantou County, Los Angeles, Department of Public Works, Bureau of Engineering, page 40.

Zhang J. Xu S. Y. (2009). Seismic Response Simulations of Bridges Considering Shear–Flexural Interaction of Columns, Structural Engineering and Mechanics; Vol. 31, No. 5, p.p. 545–566.

Zhang, Y., Wang, Z. (2000). Seismic behavior of reinforced concrete shear walls subjected to high axial loading. ACI Structural Journal, 97(5), 739-750.

Zhao, J. Sritharan, S. (2007). Modeling of Strain Penetration Effects in Fiber-Based Analysis of Reinforced Concrete Structures. ACI Structural Journal, 104(2), 133-141.